The role of the inflammatory chemokine receptor CCR2 in immune responses to respiratory viral infection

The University of Adelaide

School of Biological Sciences

Todd Norton

July 2021

Declaration

I certify that this work contains no material which has been accepted for the award of any other degree or diploma in my name, in any university or other tertiary institution and, to the best of my knowledge and belief, contains no material previously published or written by another person, except where due reference has been made in the text. In addition, I certify that no part of this work will, in the future, be used in a submission in my name, for any other degree or diploma in any university or other tertiary institution without the prior approval of the University of Adelaide and where applicable, any partner institution responsible for the joint-award of this degree.

I give permission for the digital version of my thesis to be made available on the web, via the University's digital research repository, the Library Search and also through web search engines, unless permission has been granted by the University to restrict access for a period of time.

I acknowledge the support I have received for my research through the provision of an Australian Government Research Training Program Scholarship.

Signed,

Todd Simon Norton, B.Sc.

August 2021

"I hate a Barnacle as no man ever did before, not even a Sailor in a slow-sailing ship"

- Charles Darwin

Table of Contents

List of Figures

List of Tables

Abbreviations

APC	Antigen presenting cell
B6	C57Bl/6
BALF	Bronchoalveolar lavage fluid
BMDC	Bone marrow-derived dendritic cell
BFA	Brefeldin A
BrdU	5-bromo-2'-deoxyuridine
BSA	bovine serum albumin
cDC	conventional dendritic cell
CFP	Cyan fluorescent protein
cLN	cervical lymph node
CMP	Common Myeloid Progenitor
CNS	central nervous system
DPEC	Double positive effector cell
DMEM	Dublecco's modified essential medium
Dtx	Diptheria toxin
ESL-1	E-selectin ligand-1
EC	Endothelial cell
EEC	Early effector cell
ELISA	Enzyme-linked immunosorbent assay
Eomes	Eomesodermin
FACS	Fluorescence activated cell sorting
FCS	Fetal calf serum
FDC	follicular dendritic cell
FRC	fibroblastic reticular cell
GAG	glycosaminoglycans
GFP	Green fluorescent protein
gMFI	geometric mean fluorescence intesnsity
GPCR	G protein coupled receptor
HBSS	Hank's balanced salt solution
HEV	high endothelial venule
HSC	hematopoietic stem cell
HSV	herpes simplex virus
iBALT	induced bronchus-associated lymphoid tissues
IC	Immune complex
IFN-ɣ	Interferon-ɣ
iLN	inguinal lymph node
inf-cDC2	inflammatory cDC2
IV	Intravascular
IP	Intraperitoneal
L-selectin	CD62L
Ly5.1	B6.SJL-Ptprca
LCMV	lymphocytic choriomeningitis virus
mLN	mediastinal lymph node
MLN	Mesenteric lymph node
MNP	Mononuclear phagocyte
moDC	monocyte-derived dendritic cell
MPEC	Memory precursor effector cell
NALT	Nasal-associated mucosal tissue
nms	normal mouse serum
NP	Nucleoprotein
PBMC	Peripheral blood mononuclear cell
RFP	Red fluorescent protein
RP	Red pulp

NP	Influenza Nucleoprotein	SLO	Secondary Lymphoid organ
Ova	Ovalbumin	Tcm	Central memory T cell
PA	Viral polymerase	TCR	T cell receptor
PAMP	pathogen-associated molecular pattern	Tdn	Double negative memory T cell
pDC	plasmacytoid dendritic cell	Tem	Effector memory T cell
PRR	pattern recognition receptor	TEM	Transendothelial migration
PSGL-1	P-selectin glycoprotein-1	Tpm	Peripheral memory T cell
Ptx	Pertussis toxin	TRIM21	tripartite motif-containing protein 21
qPCR	quantitative PCR	Trm	Resident memory T cell
S1PR1	Sphingosine-1-phosphate receptor 1	VAT	viceral adipose tissue
SLEC	Short-lived effector cell	WP	White Pulp

Abstract

Effector and memory $CD8^+$ T cells are critical for the elimination of primary intracellular infections, and for providing rapid immunity upon re-infection. The T cells responding to an infection can take on disparate fates. Although many factors have been described that influence the generation of effector and memory cells, how T cells are polarised to a particular fate is poorly understood. One factor that is important for T cell fate decisions in the microanatomical localisation of activated T cells in specific niches that promote T cell differentiation, and this activity is regulated through the specific action of chemokines and chemokine receptors. However, the molecular mechanisms underlying these processes are unclear. Understanding the regulation of $CD8^+$ T cell trafficking should reveal key mechanisms in T cell differentiation and protective immunity, and this knowledge would have wide-ranging impacts on the development of vaccines against intracellular pathogens like influenza, where antibody responses provide only short-term protection, and against emerging intracellular pathogens. Thus, the regulation of $CD8^+$ T cell trafficking during infection was investigated by focusing on chemokine receptors, which orchestrate lymphocyte migration.

The expression of chemokine receptors was investigated in $CD8^+$ T cells responding to influenza infection. This revealed that the chemokine receptor CCR2 was highly expressed in $CD8^+$ T cells in the mLN, spleen, peripheral blood, and lung parenchyma. Further investigation revealed that CCR2 was expressed within the first T cell division in the mLN, and maintained broad and high expression across all effector and memory T cell subsets. Despite the high expression of CCR2 across $CD8^+$ T cell effector and memory subsets, the receptor was dispensable for $CD8^+$ T cell differentiation, acquisition of effector potential, and expansion and trafficking during viral challenge. Further investigation into the role of CCR2 on circulating memory T cells however, did uncover a potential role for CCR2 in the optimal immunosurveillance of damaged or stressed peripheral tissue during sterile inflammation.

Further investigation into the requirement for host CCR2 in protection from influenza infection revealed a cell-extrinsic requirement for CCR2 in optimal memory T cell function during influenza

challenge. Although host deficiency of *Ccr2* had no impact on the development of memory T cell populations after primary A/HK-x31 infection, these mice displayed increased morbidity during a lethal A/PR8-challenge and increased viral titres in the lungs relative to their WT counterparts. This was associated with a reduction in the re-expansion of influenza-specific memory $CD8^+$ T cells in the lungs. Concomitant with this reduction in T cell proliferation was a reduction in the number of monocytes and monocyte-derived cells, and an inflammatory cDC subset in the lungs.

This project demonstrates that the chemokine receptor CCR2 is dispensable for any cell-intrinsic role in $CD8^+$ T cell effector or memory cell differentiation and trafficking during viral infection. However, evidence for a cell-intrinsic role for CCR2 in the optimal immunosurveillance of peripheral tissue in certain contexts of sterile inflammation is provided. Additionally, this project demonstrates a cell-extrinsic role for CCR2 in shaping optimal re-call responses to a heterosubtypic influenza challenge. These findings provide a framework for the better understanding of memory T cell re-activation and immune protection at the site of infection and inflammation.

1 | Introduction

Given the potentially logarithmic growth of a pathogen during the early stages of infection it is critical for the immune system to generate efficient and appropriate immune responses to meet host needs [1]. As such, the immune system has evolved strategies for the optimal immunosurveillance of naïve T cells and the efficient recruitment of antigen-specific T cells to sites of infection. The events that lead from the activation of a naïve T cell, to it's differentiation into an effector cell, its localisation at infected peripheral tissue, and eventual development into a long-lived memory cell are regulated to a significant degree by chemokine receptor-mediated migration [2]. The same chemokine axes that guide T cell fate are also often co-opted by cells of the innate immune system to ensure the effective co-ordination of innate and adaptive cells within the same environment for antigen-presentation, and the provision of cytokines to drive T cell differentiation. The regulation of T cell fate and function by chemokine receptors has been subject to extensive investigation and is a complex system that requires the action of many chemokine receptors and their ligands which are differentially expressed across tissues, leukocyte populations, and activation states. Although the importance of the chemokine receptor system in $CD8^+$ T cell biology has been well established, the majority of studies have focused on the cell-intrinsic requirements for CXCR3 in T cell fate and function across a number of different infectious and disease models. While CXCR3 is well established as a key regulator of T cell fate and function, many other receptors have been investigated for cell-intrinsic and extrinsic effects in T cell biology and elimination of these receptors often has only minor, or context specific, impacts on T cell fate in comparison to CXCR3 [2–4]. The following section will focus on T cell responses to infection in the context of cell migration, with a particular focus on $CD8^+$ T cell responses during acute infections, and the myeloid cells that facilitate their activation and differentiation.

1.1 Chemokine receptors and lymphocyte trafficking

The chemokine receptor family consists of around 25 receptors in mice and humans, which co-ordinate the movement of immune cells through the sensing of their cognate ligands [5]. There are around 50 structurally related chemotactic cytokine ligands that are classified based on the configuration of a conserved N-terminal cystine motif, the CC family (no separation of the first two cysteines in the primary aa sequence) the CXC family (1 aa separation) CX3C family (3 aa separation) and the XC (with only the single cysteine residue) **(Table 1.1)**. Expression of these ligands can be broadly divided into homeostatic chemokines that are constitutively produced, inflammatory chemokines that are expressed during infection and disease, and dual-function chemokines that are active both at homeostasis and during inflammation. These chemokines and their receptors are differentially expressed across tissues

and leukocyte populations, and across differentiation states within specific leukocyte populations. Each chemokine receptor recognises a specific chemokine ligand, or set of ligands, and this sensing serves to recruit appropriate leukocyte populations into particular tissues or micro-anatomical niches to facilitate immune responses.

Table 1.1: Mouse chemokine receptors

Murine typical chemokine receptors		
Receptor	**Ligand(s)**	**Main function**
CCR1	CCL3, 5, 6, 7, 8, 9, 14, 16	Myeloid cell trafficking
CCR2	CCL2, 7, 12	Monocyte recruitment from bone marrow
CCR3	CCL5, 7, 9, 11, 24, 26, 28	Eosinophil recruitment
CCR4	CCL17, 22	T cell homing to lungs and skin
CCR5	CCL3, 4, 5, 11, 16	T cell activation
CCR6	CCL20	cDC and Treg recruitment
CCR7	CCL19, 21	Naive T cell migration, lymph node homing of mature cDCs
CCR8	CCL1, 8	T cell homing to the skin
CCR9	CCL25	T cell homing to the intestines
CCR10	CCL27, 28	T cell homing to skin
CXCR1	CXCL5, 7	Neutrophil recruitment
CXCR2	CXCL1, 2, 3, 5, 6, 7	Neutrophil recruitment
CXCR3	CXCL9, 10, 11	$CD8^+$ T cell and Th1 migration and activation
CXCR4	CXCL12	Hematopoiesis
CXCR5	CXCL13	T follicular helper responses
CXCR6	CXCL16	Natural killer cell responses
CX3CR1	CX3CL1	Non-classical monocyte patrolling of vasculature
XCR1	XCL1	$CD8^+$ T cell activation
Murine atypical chemokine receptors		
ACKR1	CCL2, 5, 7, 11, 13, 14, 17; CXCL5, 6, 8, 11	Chemokine scavenging & transport
ACKR2	CCL2, 3, 4, 5, 7, 8, 11, 12, 13, 17, 22	Chemokine scavenging

Continued on next page...

Table 1.1 – continued from previous page.

Receptor	Ligand(s)	Main function
ACKR3	CXCL11, 12	Chemokine scavenging
ACKR4	CCL19, 21, 25; CXCL13	Chemokine scavenging

1.1.1 Chemokine receptors and signalling

Chemokine receptors comprise a single polypeptide, folded and embedded in the cell membrane such that seven segments span the width of the membrane. The N-terminus and three loops on the extracellular component form a pocket for ligand binding, while the C-terminus and intracellular loops are coupled to a heterotrimeric G-protein unit comprised of an α-subunit (Gα) and a tightly associated β and γ-subunit. Signalling through chemokine receptors results in the dissociation of G-protein units and relay of the signal through phosphoinositide 3-kinases (PI3K) and members of the Rho family of small GTPases [6, 7]. These signalling events establish biochemical asymmetry within cells that produces a polarised myosin II–rich trailing edge and an F-actin rich leading edge that drives locomotion. This action, in combination with interaction between adhesion molecules on the cell and the extracellular matrix, enables navigation through tissues toward the source of the ligand. Regulation of chemokine receptor signaling and migration can target the dissociated G-protein units and secondary messengers [8], or through targeted-regulation of the membrane-anchored receptor [9]. Post-translational phosphorylation of GPCRs also enhances the binding of arrestins, uncoupling the receptor from its G-proteins to attenuate signalling. Arrestins link activated receptors to clathrin-coated pits to promote GPCR internalisation, desensitising receptors to further signalling [10, 11]. In addition, there is a sub-family of atypical-chemokine receptors which do not trigger canonical G-protein mediated signalling upon ligand binding [6] **(Table 1.1)**. These atypical receptors instead regulate the bio-availability of chemokines by sequestering them from the extracellular space, thereby facilitating the formation of chemokine-gradients [12], and in certain contexts can transport chemokines from tissue parenchyma to the lumen of blood vessels to promote leukocyte tissue infiltration [13–16].

Establishing chemokine gradients with glycosaminoglycans

Chemokines are soluble and will diffuse away from their source, however, most chemokines are capable of binding to glycosaminoglycans (GAGs) expressed on cells and the extracellular matrix [17]. Immobilisation of chemokines through GAG binding is thought to limit diffusion, establishing a gradient of chemokine that is highest at the source. The effective formation of these chemokine gradients is critical for the directed migration of immune cells, as altering the GAG-binding moieties on chemokines abrogates leukocyte migration *in vivo* [18]. Although chemokines can bind GAGs there is considerable disparity in their binding ability, which in turn affects their ability to form functional gradients in tissue [19]. This differential gradient formation may contribute to the formation of local chemokine gradients for chemokines with high GAG affinity, or tissue-drainage and the formation of intra-lymphatic and intra-organ gradients for chemokines with low GAG affinity [20, 21]. While most chemokine ligands are secreted to exert their function, CXCL16 and CX3CL1 can be expressed in a membrane-tethered form which, when membrane anchored, promote integrin-independent adhesion of leukocytes [22, 23]. These membrane-tethered chemokines can also be shed by enzymes in a constitutive or inducible manner to release them into the extra-cellular space [24], promoting dissociation of adhered cells, and the rapid formation of chemokine gradients. As well as forming stable gradients in tissue parenchyma, GAGs expressed on blood endothelial cells (BECs) immobilise chemokines on the luminal surface of BECs, a requirement for leukocyte adhesion on BECs [25]. This immobilisation on the surface of BECs enables the stable presentation of tissue chemokines in the presence of shear flow, when they would otherwise diffuse away, and broadcasts the inflammatory-state of the tissue to passing leukocytes.

1.1.2 "Once more unto the breach" Leukocyte transendothelial migration

Leukocyte recruitment into peripheral tissue is mediated through sequential capture, rolling, arrest, adhesion, crawling, and transendothelial migration, with each step conditional for the next. The initial events occur when circulating leukocytes establish weak and transient adhesive interactions with selectins expressed on endothelial cells (ECs)[26]. These initiating events occur in post-capillary venules, where physical changes restrict hemodynamic forces, enabling leukocytes to physically interact with the blood endothelium [27, 28]. Interactions between surface glycoproteins such as P-selectin glycoprotein ligand-1 (PSGL-1), E-selectin ligand-1 (ESL-1), CD44 and L-selectin (CD62L), expressed on leukocytes, and P and E-selectin, expressed on endothelial cells, promotes the initial capture and rolling of lymphocytes on endothelial cells, exposing them to chemokine signals that may be present on the

endothelial surface, bound to GAGs [29, 30]. Chemokine signalling triggers a conformational change in lymphocyte integrins such as VLA-4 and LFA-1, from a low-affinity, to high-affinity state. These high affinity integrin complexes allow leukocytes to firmly adhere to the vascular endothelium through interactions with VCAM-1 and ICAM-1 expressed on endothelial cells [28]. This activity can be enhanced during inflammation by cytokines produced by tissue-resident macrophages (Mϕ), such as IL-1β and TNFα, that increase expression of adhesion molecules on endothelial cells [31]. Leukocytes adhered to the vascular endothelium can then crawl along blood vessels to find a preferred site for transmigration which primarily occurs at the junctions between endothelial cells [32, 33]. The chemokines present on the luminal side of blood vessels that regulate the rolling to adhesion step can be derived from two sources. Cytokine-stimulated endothelial cells can secrete chemokines [34], or interstitial cells can produce chemokines that diffuse to the basal side of the blood endothelium and are transcytosed and presented on the luminal side to recruit cells [34, 35]. These secreted chemokines are immobilised by GAGs present on the apical surface of ECs [18], and sensing of these chemokines permits transcellular migration in the junctions between ECs.

1.1.3 Homeostatic trafficking of naïve lymphocytes

After mature, naïve, T and B cells exit primary lymphoid organs they enter a body-wide state of surveillance in search of their cognate antigen. The mucosal surfaces of the lungs, gastrointestinal and reproductive tracts, along with the skin, are all potential portals of entry for invading pathogens. As it has been estimated that only a few hundred $CD8^+$ T cells are specific for any particular antigen, and even less for $CD4^+$ T cells [36, 37], the probability of a naïve T cell encountering its cognate antigen across all this tissue is extremely low. To increase the chances of a naïve lymphocyte encountering its cognate antigen, secondary lymphoid organs (SLOs) (lymph nodes, spleen, Peyers patches) are spread throughout the body and serve to concentrate antigen in specific areas for lymphocytes to scan, massively reducing the total area a cell must patrol to potentially encounter its cognate antigen. The trafficking of immune cells to, and within, these SLOs is tightly regulated by chemokines and chemokine receptors. Entry of naïve lymphocytes into lymph nodes occurs mainly through transendothelial migration across specialised vascular endothelium called high endothelial venules (HEVs) [38, 39]. Unlike other ECs in peripheral tissues, HEVs express distinct lymphocyte trafficking molecules in a largely constitutive manner [40]. The main adhesion molecule on naïve cells that regulates lymph node entry is CD62L which binds GlyCAM-1 expressed on HEVs, and interactions between these two molecules regulates the initial tethering and rolling of lymphocytes. However, CD62L expression is not restricted to naïve lymphocytes,

so the rolling and tethering of cells on HEVs is common, but the ability to cross these endothelial barriers requires the expression of specific chemokine receptors, and this activity is primarily regulated through CCR7 expressed by T cells [41]. The chemokine ligands that entice T cells through HEVs are produced by lymph node stromal cells, follicular dendritic cells (FDCs), and fibroblastic reticular cells (FRCs), and are presented on the luminal side of HEVs to promote lymphocyte transendothelial migration in a CCR7-dependent manner. Once in the lymph node T and B cells are guided to specific niches through the cell-specific expression of chemokine receptors. In the follicles of lymph nodes network of FDCs constitutively produce CXCL13 which attracts, and temporarily retains, arriving B cells into the follicle via CXCR5 signalling. Within the paracortex of the lymph nodes FRCs constitutively produce the chemokines CCL19, CCL21 and CXCL12 which pulls arriving T cells into the paracortical regions of lymph nodes [42]. Recruitment of T cells into the white pulp of the spleen similarly occurs in a chemokine receptor-dependent manner, but does not require the action of selectins or HEVs. T cells that are deposited from arterioles into the red pulp sinuses attach to, and migrate along, perivascular pathways in a CCR7-integrin-dependent manner to enter the white pulp via bridging channels [43].

T cells present in SLOs undergo seemingly random migration with brief intermittent pauses to interact with stromal and other immune cells [44]. In the absence of activation, their exit from lymph nodes is regulated by a family of lipid-sensing GPCRs that demonstrate increasing responsiveness the longer an immune cell is present within an SLO. Sphingosine-1-phosphate receptor 1 (S1PR1) is the main receptor regulating T cell egress that senses the lipid molecule sphingosine-1-phosphate (S1P), the concentration of this ligand is high in the blood and lymph and, in lymph nodes, has an increasing gradient that runs from the paracortex to the lymph node cortex [45], directing cells into the draining efferent lymphatics. Without cognate antigen recognition T cells only transiently survey lymph nodes, and these dwell times are largely stochastic and result from the competition of retention signals through CCR7 and exit signals through S1PR1 [46], with $CD4^+$ T cells dwelling on average 10-12 hours, $CD8^+$ T cells 19-21 hours, and B cell 24 hours [47, 48]. These lymph node scanning behaviours are altered in the case of inflammation whereby CD69 expression, induced by T cell receptor (TCR) signalling and type I IFNs, antagonises S1PR1 function and mediates retention of T cells in the lymph node, increasing the likelihood that the cell will encounter an antigen-bearing conventional dendritic cells (cDCs) [49]. Cells that access the efferent lymphatics are eventually returned to the circulation via the thoracic duct where they may access another SLO.

1.1.4 Lymphocyte trafficking during inflammation

The shift from homeostasis to active infection is associated with a dramatic change in the expression of inflammatory chemokines that facilitates the rapid recruitment myeloid and adaptive cells to the infected tissue. Cells resident in peripheral tissues act as important early sources of chemokines through the action of a number of pattern recognition receptors (PRRs) that enable the detection of evolutionary conserved structures on invading pathogens (pathogen-associated molecular patterns, PAMPs) or endogenous stress signals (danger-associated molecular patterns, DAMPs). Ligand sensing through PRRs initiates inflammatory processes through the activation and secretion of pre-stored pro-inflammatory cytokines and chemokines, which promote immune cell recruitment from the circulation [50, 51]. Sustained recruitment relies on the action of cytokines such as IL-1, TNFα , and IFNs produced by activated cells, and these cytokines promote vascular permeability and the transcription of chemokines by local immune and stromal cells [52, 53]. The early stages of an inflammatory response are dominated by chemokines that, depending on the nature of the insult, primarily promote the recruitment of monocytes, neutrophils, and NK cells from the periphery [54]. Neutrophils are the first cell that is recruited to inflamed tissue, in a CXCR1/2-dependent manner. The deformable nature of neutrophils enables them to compress their nucleus to squeeze through the basement membrane post-transendothelial migration (TEM), which poses a physical barrier to most cells. Once neutrophils are within the basement membrane they secrete matrix metalloproteases that degrade the collagen IV network enabling other leukocyte populations to more rapidly, and efficiently, navigate this physical barrier. By the peak of a response chemokine expression is diversified to promote the recruitment and retention of adaptive immune cells. For example, at the peak of T cell responses to herpes simplex virus (HSV) infection in the mouse flank there is heightened expression of CXCL9/10, CCL1, CCL2, CCL8 and CCR5 ligands compared to naïve control mice [55]. At peak T cell infiltration into vesicular stomatitis virus (VSV) infected ear sheets there is heightened expression of the chemokines CXCL9 and CXCL10 as well as CCR2 and CCR5 ligands [56].

Chemokine-regulated peripheral tissue access

The migration of immune cells from the circulation into inflamed peripheral tissue has primarily derived from studies on neutrophils. The large numbers of these cells, combined with their rapid and predictable mobilisation from the blood, has enabled direct visualisation of their TEM in intimate detail via intravital microscopy [35, 57]. The migration of adaptive immune cells from the circulation has received far less attention, and publications that address the problem often rely on flow-based assays or *in vitro*

generated data [34, 58]. As mentioned, naïve $CD8^+$ T cells have migratory patterns that are restricted to the peripheral blood and SLOs, however, when naïve T cells are activated and differentiate they express additional adhesion molecules and chemokine receptors that enable them to infiltrate peripheral non-lymphoid tissue (NLT). Although $CD8^+$ T cells have been reported to express many chemokine receptors, the most thoroughly investigated in T cell trafficking into NLT from the circulation is CXCR3. In HSV infection of the female reproductive tract (FRT) *Cxcr3*$^{-/-}$ $CD8^+$ T cells migrated less efficiently into the genital mucosa [59]. Additionally, $CD8^+$ T cell recruitment into the FRT can be promoted after subcutaneous infection through exogenous application of CXCR3 ligands to the FRT, which increases T cell trafficking into the uninflamed tissue and ultimately increases the formation of resident-memory cells [60]. CXCR3 has also been reported to be important for migration into the central nervous system (CNS) during bacterial [61], viral [62], and parasitic infections [63], and in T cell migration into the inflamed lung after respiratory viral infection [64, 65]. However, this CXCR3-dependent tissue infiltration may be context dependent as there was no cell-intrinsic requirement for CXCR3 in $CD8^+$ T cell migration into the inflamed ear pinna [56], flank skin [66], or tumour microenvironments [67]. It should also be noted that many of these experimental approaches utilize broad knockout mice that could have compromised T cell activation, which also has the potential to indirectly alter T cell migratory capacity in peripheral tissues.

In addition to a general peripheral tissue-homing role granted through expression of CXCR3, several reports have demonstrated that the expression of a specific set of chemokine receptors and integrins required for tissue-specific homing of T cells can be imprinted in specific lymph nodes, or by priming through tissue-specific cDCs. For example, lung-homing T cells can be primed by cDCs sorted from the lungs. In this setting lung-derived cDCs imprinted CCR4 expression on *in vitro* co-cultured $CD4^+$ T cells, which were more efficient at trafficking to the lung than $CD4^+$ T cells that were primed by cDCs sorted from the mesenteric lymph nodes (MLN) [58]. Conversely, cDCs sorted from the gut-draining MLN were more efficient at driving, or maintaining, CCR9 expression in naïve T cells which was required for their optimal homing to the intestine [68, 69]. Additionally, cDCs sorted from skin-draining lymph nodes were shown to imprint CCR10 expression and subsequent trafficking to the skin [70, 71]. Altogether, this demonstrates that cDCs derived from specific barrier tissues can induce the expression of a set of chemokine receptors and integrins in T cells that promote the efficient migration of those cells into the barrier tissue from whence the priming cDC originally came. Although some studies have demonstrated that individual chemokine receptors can mediate tissue-specific homing, others have shown that there is considerable redundancy in the use of chemokine receptors in tissue infiltration, and loss of any one chemokine receptor could be compensated for by another. For example, by using

multiple individual chemokine receptor knockout transgenic $CD4^+$ T cells in adoptive transfer models, the trafficking of T helper cells to the lungs during Mycobacterium tuberculosis infection has been extensively investigated [72, 73]. The authors found no contribution for the migratory receptors CCR1, CCR2, CCR6, CX3CR1, CXCR5, or EBI2 in T cell infiltration into the infected lung, and only minimal contributions from CCR5 and CXCR6, while deficiency in CXCR3 resulted in a 50% decrease in lung infiltrating $CD4^+$ T cells. In a recent publication the entire region of the genome containing the genes *Ccr1*, *Ccr2*, *Ccr3* and *Ccr5* was excised in mice, and the extent of redundancy in trafficking of myeloid cells in these multi-receptor knockout mice was compared to each of the individual chemokine receptor knockout mice [74]. In that report Dyer *et al.* demonstrated that while there were profound differences in tissue infiltration of myeloid cells in the multi-receptor knockout mice, none of the individual receptor knockout mice alone could reproduce those results. These studies show that within the chemokine receptor family there is considerable redundancy in immune cell recruitment into inflamed tissue, where loss of an individual receptor can be, if not entirely, at least partially compensated for by the others. Additionally, Hoft *et al.* [73] also found that treatment of cells with pertussis toxin, which prevents chemokine signalling through GPCRs, only partially reduced $CD4^+$ T cell access to the infected lung. Together, these studies suggest that multiple chemokine receptors can regulate tissue access, and that chemokine receptor-independent mechanisms of tissue access exist.

Chemokine regulated tissue navigation

At barrier tissues, T cells arriving from the vasculature are deposited into the tissue parenchyma where they further navigate the extracellular space to find sites of active infection, or additional clusters of peripheral immune cells to receive further signals for differentiation and division. While many chemokine receptors are seemingly dispensable for T cell tissue infiltration, these chemokine receptors may be more important for the positioning of cells within tissue post-TEM. T cells infiltrating the influenza-infected lungs have two distinct barriers that impede their migration. The first is the blood endothelium that must be breached, and the second is the airway epithelium, which must be crossed to gain access to the airways, a step that is required for optimal protection from certain respiratory infections [75]. It has been demonstrated that the receptors CCR5 and CXCR6 are not required for $CD8^+$ T cells to breach endothelial barriers but are required for positioning $CD8^+$ T cells in the airways after influenza challenge [76, 77], a step that is also required for optimal tissue resident memory cell (Trm) formation [77], a long-lived memory $CD8^+$ T cell subset that will be discussed in detail later. Additionally, in the skin and FRT, CXCR3 ligands position $CD8^+$ T cells in epidermal and mucosal layers

for efficient formation of Trm cells [60, 78]. In several infectious settings peripheral T cells can also be found in groups of lymphocyte clusters [60, 79–82]. The formation of these T cell clusters is important for optimal T cell activation in the periphery, the formation of resident-memory populations, and the recall function of circulating memory T cells. These clusters also rely on chemokine signalling, primarily from tissue Mϕ, to form, as depleting tissue Mϕ or neutralising the receptors CCR5 or CXCR3 on T cells disrupts their formation, compromising T cell activation and memory formation. Once $CD8^+$ T cells enter infected tissue they must also locate infected cells. This process, once thought to be mediated by chance through random Brownian motion, has been shown to be enhanced through the action of CXCR3 on T cells in the CNS [83], although the source of the CXCR3 ligands was not determined in that study. Another report demonstrated that $CD8^+$ T cells in the skin of Vaccinia Virus (VV)-infected mice used the chemokine receptor CXCR3 to locate and eliminate CXCL9/10-expressing VV-infected monocytes [56]. However, the same action was not observed for HSV flank infection [66], suggesting that the use of chemokine receptors by $CD8^+$ T cells participating in pathogen clearance may depend on the context of the infection.

1.2 The Mononuclear phagocyte system

Over the course of an infection a T cell will undergo multiple distinct interactions with numerous myeloid cells that will facilitate its activation, differentiation, and eventual death or development into a long-lived memory cell. The myeloid cells that provide the most critical interactions in determining T cell fate and function are cells of the mononuclear phagocyte (MNP) system, which consists of monocytes, Mϕ and conventional dendritic cells [84–86]. These cells have important roles in homeostasis and infection, both in their own regard, and for the optimal positioning and activation of cells of the adaptive immune system. The unifying theme in this classification system is the ability of these cells to engulf particulate matter, and present this to T cells to drive their activation and differentiation. The extent to which individual subsets of MNPs contribute to this process, however, is not fully clear, and much of the knowledge regarding the contributions of distinct MNP subsets to this process has come from deciphering the development of these cells. With the exception of many tissue Mϕ populations, MNPs develop in the bone marrow where they are derived from a common myeloid progenitor cell (CMP) that is shared with erythrocytes, platelets, cDC, and granulocytes. Historically, these MNP subsets were thought to be closely related, with circulating monocytes acting as a precursor for mature tissue Mϕ and cDCs. Over the last decade this concept has been overhauled, and it is now recognised that most tissue Mϕ are seeded during embryogenesis, first from the embryonic yolk sac, then later the fetal liver [87,

88], with little contribution from circulating adult bone marrow-derived monocytes **(Fig. 1.1)**, although there are exceptions to this model which will be mentioned later. It was also thought that monocytes could acquire antigen-presenting capabilities in inflammatory settings to drive the proliferation of αβT cells. However, recent evidence has demonstrated that these monocyte-derived antigen presenting cells are actually a subset of cDCs that derive from a pre-cDC precursor in a type-I interferon dependent process, and are not monocytic in origin [89, 90]. These advances over the last decade have greatly furthered the understanding of the functional roles of Mϕs and cDCs during homeostasis and infection, but have rendered the specific functions of monocytes even more enigmatic.

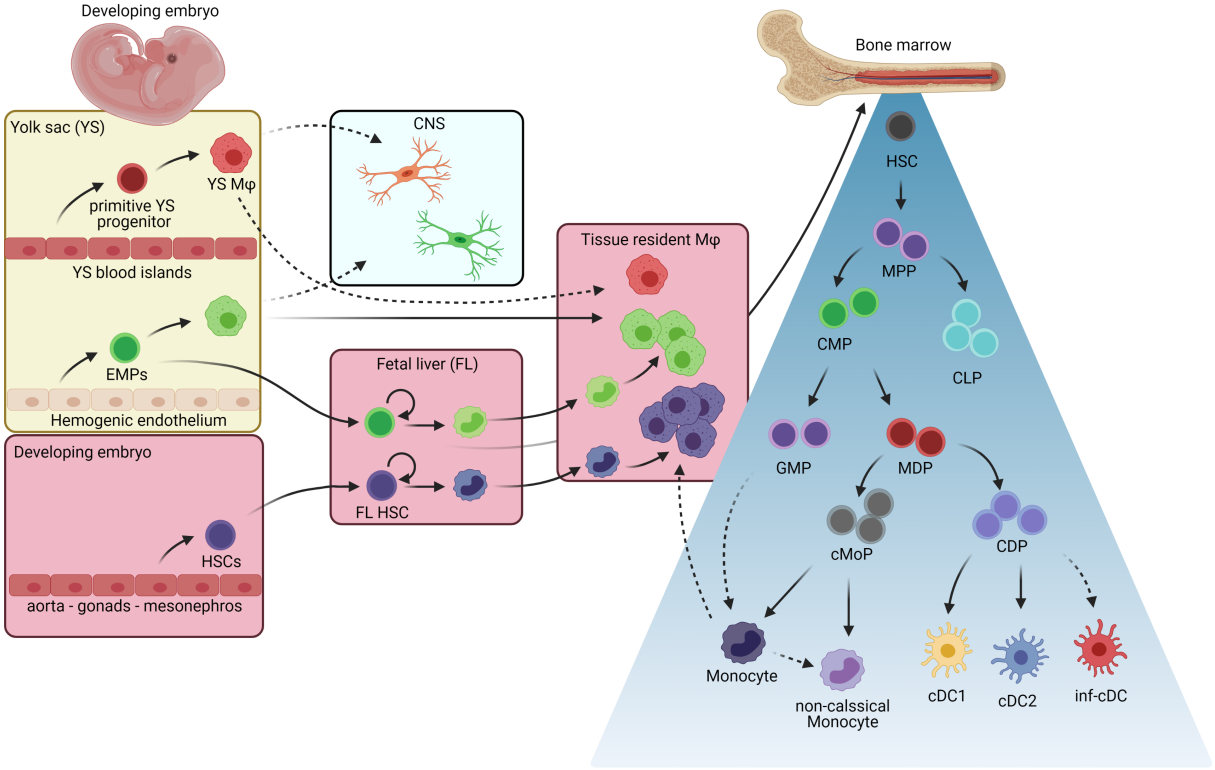

Figure 1.1: Development and seeding of the mouse MNP system
The discrete waves of hematopoiesis that establish the murine MNP system from extra-embryonic precursors to bone marrow-derived HSCs. Abbreviations: YS Mϕ, yolk sac macrophage; EMPs, erythro-myeloid precursors; HSC, hematopoietic stem cell; MPP, multipotent progenitor; CLP, common lymphoid progenitor; CMP, common myeloid progenitor; GMP, granulocyte Mϕ precursor; MDP, Mϕ dendritic cell precursors; cMoP, common monocyte progenitor; CDP, common dendritic cell precursor; cDC1, conventional dendritic cell type 1; cDC2, conventional dendritic cell type 2; inf-cDC, inflammatory conventional dendritic cell. Solid arrows indicate direct lineage relationship, dashed arrows indicate conditional or conflicting lineage relationship. [91–93]

1.2.1 Macrophages

Mϕ occupy all tissues of the body and, once inside a particular niche, the local environment instructs the final differentiation of the Mϕ which ultimately dictates its function [94]. Although it is now appreciated that tissue Mϕ are mostly derived from fetal-precursor cells, and not mature adult bone marrow monocytes, there are some exceptions to this. Mϕ in the intestine, dermis, heart and pancreas are continually replaced by bone-marrow monocytes [95], with these cells taking on a transcriptional program that is near identical to the fetal-derived Mϕ that they replace [95]. Inflammation induced death of tissue Mϕ can also trigger a transient replacement of fetal-derived Mϕ with bone marrow monocyte-derived Mϕ [96–98]. In one example, alveolar Mϕ death following influenza infection resulted in the formation of monocyte-derived alveolar Mϕ. Unlike tissue Mϕ that were replaced by bone-marrow monocytes at homeostasis, these cells were transcriptionally distinct from the resident alveolar Mϕ populations and provided short-term enhanced protection from secondary bacterial infections [96]. While tissue Mϕ were traditionally thought to act as cellular vacuum cleaners in most tissues, there has been an increasing appreciation for the roles that these cells play in the maintenance of tissue homeostasis [99, 100]. This is particularly well demonstrated in the genetic disease alveolar proteinosis, where humans that lack alveolar Mϕ have a build-up of material in the alveoli that causes shortness of breath [101]. These alveolar Mϕ have also been shown to rapidly migrate toward, and phagocytose, inhaled bacteria, a process that was required to sequester the antigen from neutrophils to prevent their recruitment, which can lead to inappropriate inflammation and injury [102], demonstrating dual roles for Mϕ in the regulation of both immune and physiological homeostasis.

Of relevance to T cell biology, evidence has shown that while Mϕ are not considered to be effective antigen-presenting cells (APCs), directly infected Mϕ can drive $CD8^+$ T cell proliferation and differentiation [103, 104], although there is evidence that this only appears to occur at very high infectious doses [105]. Many Mϕ populations are, however, remarkably permissive to pathogen infection, and can act as "middle-men" that shuttle antigen to cDCs for activation of adaptive immune cells [106, 107]. Tissue Mϕ have also been shown to regulate the homeostatic trafficking of memory T cells in peripheral tissue. A network of resident Mϕ in the FRT has been demonstrated to promote the retention of HSV-specific $CD4^+$ resident-memory T cells in a CCR5-dependent manner [79], with a similar mechanism recruiting, and retaining, $CD4^+$ T cells in the skin [55]. When this Mϕ-dependent retention is disrupted, the clustering of $CD4^+$ T cells is lost and host responses to HSV challenge are compromised [79]. Dermal Mϕ have also been shown to regulate the clustering of dendritic cells in the skin for the optimal activation and proliferation of effector T cells *in situ* in a CXCL2-dependent manner

[82]. Moreover, in the intestine of mice, resident Mϕ create inflammatory microenvironments that support the recruitment, and differentiation, of $CD8^+$ Trm cells following bacterial infection [81, 108]. Taken together, these previous reports all point to Mϕ being important mediators of tissue homeostasis and playing important roles in the positioning of immune cells at barrier tissues.

1.2.2 Monocytes

Historically, monocytes were thought to act as precursors for tissue Mϕ and cDCs, but recent advances in fate mapping and sequencing technologies have absolved them of this role [109, 110]. Monocytes are the dominant MNP subset found in the blood and are present in very small numbers in almost every tissue of mice, except the epidermis [111], alveolar space [87, 112], and the CNS [113]. In mice, at steady-state, two main subsets of monocytes are present, $Ly6C^+$ $CCR2^+$ $CX3CR1^{int}$ 'classical' monocytes, and $Ly6C^{low}$ $CX3CR1^+$ $CD43^+$ 'non-classical' monocytes [114]. The latter subset of monocytes represents a minority of total monocytes and patrols the vasculature, maintaining the integrity of the network [115], while the former subset has more important contributions to inflammation. At homeostasis classical monocytes, unlike non-classical monocytes, can enter uninflamed peripheral tissue where they may differentiate into tissue Mϕ, if the niche is vacant, or sample local antigen and migrate to draining lymph nodes [88]. Unlike other MNP subsets, large numbers of monocytes are rapidly recruited from peripheral sites to infiltrate inflamed or infected tissues. In these inflammatory contexts, monocytes represent a highly plastic cell subset, having been called monocyte-derived cells [90], monocyte-derived DCs (moDCs) [116, 117], inflammatory monocytes (IMs)[118], exudate Mϕ [119], and TNFα / iNOS producing (TIP) DCs [120], reflecting both their ability to adapt to diverse host needs, and the difficulty in adopting a consistent nomenclature for them. The major reservoir of monocytes is the bone marrow, although a large population is maintained in the spleen [121], and the mobilisation of these cells to the bloodstream is heavily dependent on the chemokine receptor CCR2 [74, 122]. Due to this observation, *Ccr2*$^{-/-}$ mice are commonly used as a model to study the functional role of monocytes during an immune response. Using these mice, monocytes have been shown to be important for the control of certain bacterial [123–125], fungal [126, 127], and viral infections [128]. In these settings monocytes play an accessory role, activating other cells via cytokine-dependent enhancement of cytokine production in other innate-like or adaptive cells *in situ*, to ensure the optimal control of pathogen spread, or through the provision of cytokines in SLOs to promote the differentiation of T helper subsets and optimal secretion of T cell-derived cytokines [128]. In the spleen during *Listeria monocytogenes* infection this activity occurs in discrete clusters that form in the red pulp [129, 130]. In these clusters, monocytes attract NK

and T cells in a CXCL9/10 dependent manner, with *Cxcr3*$^{-/-}$ cells failing to migrate into clusters and upregulate IFNγ expression. Similarly, in lymph nodes following protein immunisation, monocytes have been shown to form clusters in the paracortex, which concentrates inflammatory cytokines to microenvironments, promoting effector differentiation of T cells that localise in these areas[131].

Monocyte antigen presentation

The exact contributions of monocyte-derived cells to the development of a functional adaptive immune response are still unclear as reliable markers that can be used to distinguish these cells from cDC2s and tissue Mϕ have only recently been described [90, 132]. Despite their well documented activity as professional phagocytes, evidence of monocytes acting as professional antigen presenting cells is controversial given the ease with which *in vitro* generated, or FACS-sorted monocytes can be contaminated with cDCs [89, 90]. In infectious settings monocytes have been reported in large numbers lymph nodes draining inflamed tissue, with broad distribution throughout the paracortex and interfollicular areas [131, 133, 134], and are optimally positioned at these sites to influence both T cell activation, and differentiation. Some studies report that the monocytes present in lymph nodes access the tissue through draining lymph and thus, have the potential to bear tissue-associated antigen [88, 135–137], while other studies claim that they are poorly motile once in peripheral tissue and are unlikely to migrate into afferent lymph [90, 138–141]. Recent data suggest that nearly all monocytes present in inflamed lymph nodes during the early stages of inflammation arrive via the circulation, rather than tissue draining lymph, in a CD62L-dependent manner [131], as removing the inflamed tissue from which they would migrate (the ear) had no impact on monocyte accumulation in the ear-draining lymph node. These data would suggest that, unlike tissue-draining cDCs, monocytes in lymph nodes are not likely to be bearing foreign antigen and would rely on capture from the draining afferent lymph, or "cross-dressing" by other APCs, to acquire antigen [142]. Other studies suggest that monocytes that traffic to draining lymph nodes are ineffectual APCs [90, 143, 144], but may ‘shuttle’ antigen from peripheral tissues to lymph node resident cDCs, and provide cytokines to promote T cell differentiation [145, 146], while still other studies place them on par with cDC1s as effective APCs for $CD8^+$ T cells [136, 137, 147, 148]. As well as potentially presenting antigen to drive T cell proliferation, monocytes have been shown to influence T helper cell polarisation *in vivo*. During viral infection, monocytes in draining lymph nodes were identified as a potent source of IL-12 that drove Th1 differentiation and IFNγ secretion [128, 131]. The same role for monocytes has been demonstrated for Th1 polarisation during intracellular bacterial infection [137, 149] and for Th2 and Th17 polarisation during allergic

inflammation [136].

Unlike cDCs, Mϕ and monocytes both express a wide variety of Fc-receptors that enable the efficient phagocytosis of antibody-coated cells and particles [136, 141, 143, 150, 151]. B cell-derived antibodies that develop several days after the initiation of an adaptive response can bind to Fc-receptors for IgG, IgM, IgA, and IgE expressed on myeloid cells, altering their effector functions. Of particular importance to APCs is the binding of IgG to Fcγ receptors, which enhances the uptake of antigen and the antigen-presenting capability of the cell, leading to increased T and B cell responses [152–154]. The expression of these Fcγ receptors is increased in inflamed tissue through the action of effector cytokines such as IFNγ, IL-4, and type I interferons [90]. Although monocytes are considered as ineffectual antigen-presenters, most studies that have reached this conclusion use monocytes that have been FACS-sorted from peripheral tissue, and tissue-draining lymph nodes, around the peak of replicative infection. In such settings, antibodies against the invading pathogen would be minimal, as it usually takes up to a week before germinal centre B cells appear, and monocytes would primarily acquire antigen through phagocytosis of non-opsonised material, which is not as efficiently processed for antigen presentation [150]. Thus, while monocytes may be ineffectual at presenting antigen to naive T cells, they may have important roles in the ongoing expansion of T cells at sites of peripheral inflammation, and in the reactivation of memory T cells during secondary infections.

1.2.3 Conventional dendritic cells

With the exception of the CNS, cDC1s and cDC2s occupy all tissues throughout the body and can be distinguished through the surface markers XCR1, for cDC1s, and CD172α for cDC2s [89]. Plasmacytoid dendritic cells (pDCs) are also considered as cDCs because they derive from the same precursor cell, the common dendritic cell precursor, although they do not perform the hallmark role of cDCs, which is antigen presentation leading to T cell proliferation. These cells are instead recognised as potent producers of type-I interferons which have important roles for the optimal activation of other immune cells, and ultimately pathogen clearance [155, 156]. Whereas Mϕ are mostly sessile in peripheral tissues, cDCs are highly motile upon activation, rapidly migrating from peripheral tissues to local draining lymph nodes where they engage with T cells. Studies using *Batf3*$^{-/-}$ and XCR1-DTR mice have demonstrated that cDC1s are critical for the induction of CD8^{+} T cell responses [157, 158], as this subset has the constitutive *in vivo* capability of cross-presenting exogenously-derived antigen on MHC-I. The cDC1 subset also has distinct expression of DAMP receptors that enable them to phagocytose, and

present, dead cell associated antigen. For example, expression of CLEC9A enables cDC1s to redirect dead cell-associated antigen present in phagosomes for efficient cross-presentation on MHC-I, which is important for driving $CD8^+$ T cell responses to lytic infections, and against malignant cells [159–161]. Compared to cDC2s, the cDC1 subset also has superior capacity to secrete IL-12, a cytokine important for promoting the effector differentiation of $CD8^+$ T cells [162]. In contrast, cDC2s intrinsically lack the ability to drive $CD8^+$ T cell proliferation and instead primarily promote $CD4^+$ T cell activation and humoral immunity [163]. However, in the latter stages of an immune response activated, antigen-specific, $CD4^+$ T cells can 'licence' cDC2s in a CD40-CD40L dependent manner, permitting them to cross-present exogenously-derived antigen on MHC-I and further drive $CD8^+$ T cell responses [164–169]. In certain infectious settings, such as HSV and LCMV, this licensing of cDC2s is important for the primary $CD8^+$ T cell response, however, in other infections, such as influenza, absence of this cDC2 licensing has no negative impact on the development of effector $CD8^+$ T cell responses, or clearance of the virus. Despite this, in all infectious settings, cDC2 licensing is important for programming optimal memory $CD8^+$ T cell populations, as memory $CD8^+$ T cells that develop in $CD4^+$ T cell-deficient mice display suboptimal recall responses. This effect on memory programming occurs through the engagement of co-stimulatory receptors on $CD8^+$ T cells and licensed cDC2s, where absence of these co-stimulatory interactions leads to reduced proliferation and cytokine production in memory $CD8^+$ T cells upon reactivation [170]. Although $CD8^+$ T cells are spread throughout the paracortex of lymph node, activation of these cells primarily occurs in the outer regions of the paracortex, closer to the capsule [39, 155, 165, 171, 172]. This phenomenon occurs when a pathogen directly infects cells within the lymph node, when antigen must be transported to the lymph nodes via migratory cDCs [39, 155, 165, 171], and in non-infectious settings when soluble antigen drains to the lymph node [172]. Localisation to these inflammatory environments near the capsule and interfollicular regions of the lymph nodes provides access to cDCs bearing antigen, and inflammatory cytokines that are important for the effector differentiation of responding T cells.

Inflammatory cDC2s

As mentioned earlier, the ability of monocyte-derived cells to cross-present antigen to $CD8^+$ T cells is uncertain, given the ease with which these cells can be contaminated by cDC2s in flow-based assays. In the past, several studies had suggested that, when attempting to determine the function of cDC2s or monocytes and their derivatives, monocytes and Mϕ could be separated from bonafide cDC2s in FACS-based analyses using the markers CD64 and MAR-1 in mice, and CD14 and CD16 in humans, as these markers were predominately expressed by monocyte-derived cells or tissue Mϕ, but not cDC2s

[89, 95, 136, 143, 173]. By using these markers to FACS-purify monocytes from infected tissues many studies arrived at the conclusion that monocytes were an important APC when it came to the activation of naïve $CD8^+$ and $CD4^+$ T cells. However, experiments performed by Bosteels *et al.* [90] demonstrated that within this $CD64^+$ fraction of "monocyte-derived" cells are a population of cDC2s that are $CD64^{int}$ $MAR\text{-}1^+$ in inflammatory settings. These inflammatory-cDC2s (inf-cDC2) represented a pre-cDC-derived cDC subset that is absent during homeostasis, but dramatically increased in number after bacterial, viral, and allergen challenges. This inf-cDC subset was shown to be a proficient APC and a prolific IL-12 producing cell, driving both $CD8^+$ and $CD4^+$ T cell activation, proliferation and effector differentiation. An equivalent population of cDCs that share a similar surface phenotype to monocytes and Mϕ, but is derived from a cDC-restricted precursor cell, has also been identified in humans and is sometimes referred to as cDC3s [174–178].

Further characterisation of inf-cDCs also demonstrated shared tissue-homing mechanisms for monocytes and inf-cDCs. While monocytes are almost entirely dependent on CCR2 to exit the bone marrow during inflammation, inf-cDCs were also partially dependent on this axis for their migration into inflamed peripheral tissue, suggesting that studies using *Ccr2*$^{-/-}$ mice to determine monocyte function could have misattributed inf-cDC functions to monocytes [74, 122–124, 126–128, 179]. Unlike cDC1s and cDC2s, inf-cDCs express Fcγ receptors, enabling them to internalise antibody-complexed antigen and present it to T cells to drive their activation and proliferation. As stated above, antigen that is antibody-bound, rather than soluble, enable cDCs to activate T cells more efficiently, as uptake of immune-complexes by Fcγ receptors mainly enter cross-presentation pathways [180–182]. The presence of immune-complexes does not enhance the ability of cDC1s to cross-present antigen but does enhance the cross-presenting ability of inf-cDC2s [153], meaning these cells may have important functions in re-call settings where pre-existing antibodies and immune-complexes are more abundant. With the identification of inf-cDCs, it is possible that the confusion surrounding the antigen-presenting capacity of monocytes during infection had been due to the contaminating presence of this APC subset. As monocyte-derived cells, as identified by Bosteels *et al.*, were not capable of producing IL-12, it is also possible that reports of T cell polarisation by monocyte-derived IL-12 are actually measuring inf-cDC-dependent polarisation [128, 137, 149]. Together, these observations urge caution when interpreting data in studies regarding the role of monocytes as, depending on the gating strategy and animal models used, experimental methodologies could include inf-cDCs.

1.3 Naïve T cell activation and differentiation

$CD8^+$ T cells responding to infection are initially phenotypically homogeneous in their expression of surface molecules. As an immune response progresses, T cells begin to appear that are both phenotypically distinct from one another and bestowed with distinct effector and longevity potentials [183, 184]. As these cells often arise in the same tissue where the initial activation and clonal expansion of cells occurred, how the parallel development of short-lived effector cells and memory precursor effector cells occur at the same time, within the same general environment, is a key question in $CD8^+$ T cell biology. Activation of naïve T cells primarily occurs in tissue-draining lymph nodes and is driven by interactions with antigen-presenting cDCs that ultimately drive the proliferation, and differentiation of T cells. The success of these interactions requires the integration of three signals in the T cell: signalling through the T cell receptor (signal 1), engagement of costimulatory receptors (signal 2), and signalling through cytokine receptors (signal 3). Importantly, chemokines co-ordinate these signalling events, fine-tuning the localisation of T cells within appropriate micro-environments of lymph nodes.

1.3.1 Naïve $CD8^+$ T cell activation

Due to the unpredictable location and timing of pathogen infection, naïve $CD8^+$ T cells employ a body-wide state of immunosurveillance. To minimise the amount of tissue a cell must survey, and to maximise the chance a naïve T cell will encounter its cognate antigen, antigen once present in peripheral tissues is concentrated in organised lymphoid structures such as specific tissue/organ-draining lymph nodes, Peyer's patches, and the spleen. The migratory behaviour of naïve T cells within lymph nodes is primarily regulated by CCR7 ligands released by FRCs, and T cells use these signals to rapidly migrate along networks of FRCs where they make multiple contacts with DCs in the paracortex [185]. Once T cells find their cognate antigen and become activated they must localise to poorly-characterised inflammatory micro-environments that facilitate their differentiation into effector or memory T cell subsets. While it is not yet clear what these microenvironments are entirely composed of, they appear to involve inflammatory signals such as IL-12 and IL-2 [162, 183, 184, 186, 187], and CD4-licensed cDCs [164, 165], and develop in the peripheral interfollicular regions of lymph nodes [188–190]. T cells that are recently activated [190], or recently recruited to lymph nodes [189], upregulate several chemokines and chemokine receptors to optimise cDC interactions and differentiation. Within lymph nodes FRCs also downregulate CCL19/21 expression, and this, in combination with upregulation of certain chemokine

receptors, moves T cell migration patterns from 'random' surveying of LNs to active searching of APCs for further proliferation and differentiation [42, 191]. T cell-cDC interactions results in expression of CCR5 ligands by both T cells and cDCs, which promotes the recruitment of recently-activated and recently-recruited T cells to antigen-bearing DC clusters in both infectious and non-infectious settings [103, 155, 189]. $CD8^+$ T cells also rapidly express the chemokine XCL1, a ligand for XCR1-expressing cDC1s, downstream of TCR signalling which may serve to re-enforce T cell-DC interactions through the formation of T cell activation clusters observed in lymph nodes [39, 155]. The co-ordinated formation of these clusters concentrates antigen, costimulatory, and inflammatory cytokine signals in discrete areas that T cells can home to for their effective activation. Integration of all these signals results in the parallel development of short-lived effector cells, which are fated to die after resolution of the infection, and memory precursor effector cells, some of which are programmed for antigen-independent survival as long-lived memory cells [183].

1.3.2 Generation of effector T cell diversity

T cells developing within the same environment can differentiate into cells that have distinctly different fates during, and after, the clearance of pathogen. How exactly this diversity in fate specification is achieved is not completely understood, although it has been demonstrated that certain chemokine receptors have key roles in regulating this process [3, 192]. Thus, to establish a foundation for how chemokine receptors may regulate the development of discrete T cell fates, an explanation of the current leading models that explain this phenomenon is required **(Fig. 1.2)**. These models have been named i) the predetermined precursor model, ii) the signal strength model, iii) the decreasing potential model and iv) asymmetric cell division. These models are depicted in **figure 1.2** and described in detail below.

The predetermined precursor model: This model proposes that individual naïve T cell clones are pre-programmed to a specific effector or memory fate. However, this model has little support, with experiments using limiting dilution assays and DNA barcoding of $CD8^+$ T cells showing that a single naïve T cell can give rise to all possible effector and memory subsets [193–195]. However, some recent publications have provided support for this model, demonstrating that cDCs can provide TGFβ signalling to naïve T cells which pre-disposes them to a Trm fate later in life, as removing TGFβ signalling prior to, but not during or after, naïve T cell priming causes a reduction in the Trm compartment following antigen exposure [196]. Another report has shown that T cells that develop in the first few days of life are predisposed to be more effector like than those that develop during adulthood [197].

The decreasing potential model: This model suggests that the sustained exposure of T cells to antigen and inflammatory cytokines drives their proliferation and differentiation. As T cells go through successive rounds of division they gradually acquire more effector like traits and lose properties associated with memory cells, such as CD127 expression, longevity, and proliferation potential. This linear progression of T cell differentiation generates a spectrum of T cell states, reflective of their total signalling history, with a range of memory and effector properties. This model is supported by experiments showing that T cells that arrive in a lymph node during the late stages of infection, when viral antigen has dwindled and TCR stimulation is reduced, develop into more central memory-like cells [198]. Early cessation of inflammation also accelerates the generation of memory cells [184, 199], and insulating T cells from inflammatory signals through immuno-supressive cytokines promotes central memory fates [200].

The signal-strength model: This model suggests that heterogeneous populations of T cells are direct products of the overall signal strength delivered by antigen stimulation, co-stimulatory signals and cytokine signalling. This model differs from the decreasing potential model in that different cell fates can be programmed in the initial stages of T cell priming, rather than through successive rounds of antigen stimulation and cytokine signalling. This is supported by the observation that T cell clonal expansion and memory development can be programmed in the initial antigen encounters [201, 202]. The strength of TCR stimulation can also directly control the expression of cytokine receptors on T cells, influencing their downstream fate specification [203, 204]. *In vivo* TCR signalling strength has also been shown to be important for T cell division, but not acquisition of effector functions [205, 206]. Thus, intensity of signal strength during activation may regulate the stemness of the engaging cell.

Asymmetric cell division model: This model has derived from the observation that T cell division can be asymmetric, with daughter T cells resulting from a single division inheriting unequal amounts of various proteins, including transcription factors and cell surface and signalling molecules, from the initial mother T cell [207]. In this model a dividing T cell that is engaging an APC becomes a 'proximal' cell where the formation of the immunological synapse between the T cell and APC promotes clustering of certain proteins, some of which are associated with effector fates [207, 208]. As the T cell divides the distal daughter cell receives fewer effector fate proteins and retains a greater degree of stemness, whereas the proximal daughter cell becomes more differentiated [208–210]. This model is supported by the observation that the transcription factor T-bet shows asymmetrical inheritance. T-bet is known to regulate the formation of short-lived effectors and memory-precursor cells in a graded manner, and asymmetric cell division provides a mechanism through which that grade can be established

[183, 208, 210]. Many proteins cluster around the immunological synapse, including some chemokine receptors, and asymmetrical inheritance of CCR5 could promote retention in CCL5 expressing cDC clusters increasing antigen and cytokine exposure to the mother cell [211].

It is still unclear how each of these models of T cell differentiation contribute to T cell heterogeneity, and this is an area of active research [187, 212]. It is likely that these individual models are not mutually exclusive and that features of each model may be involved in a complex regulation of T cell differentiation. Investigations into the mechanisms that regulate T cell diversity are still required for a more complete understanding of how T cell activation, differentiation, and memory formation really proceed.

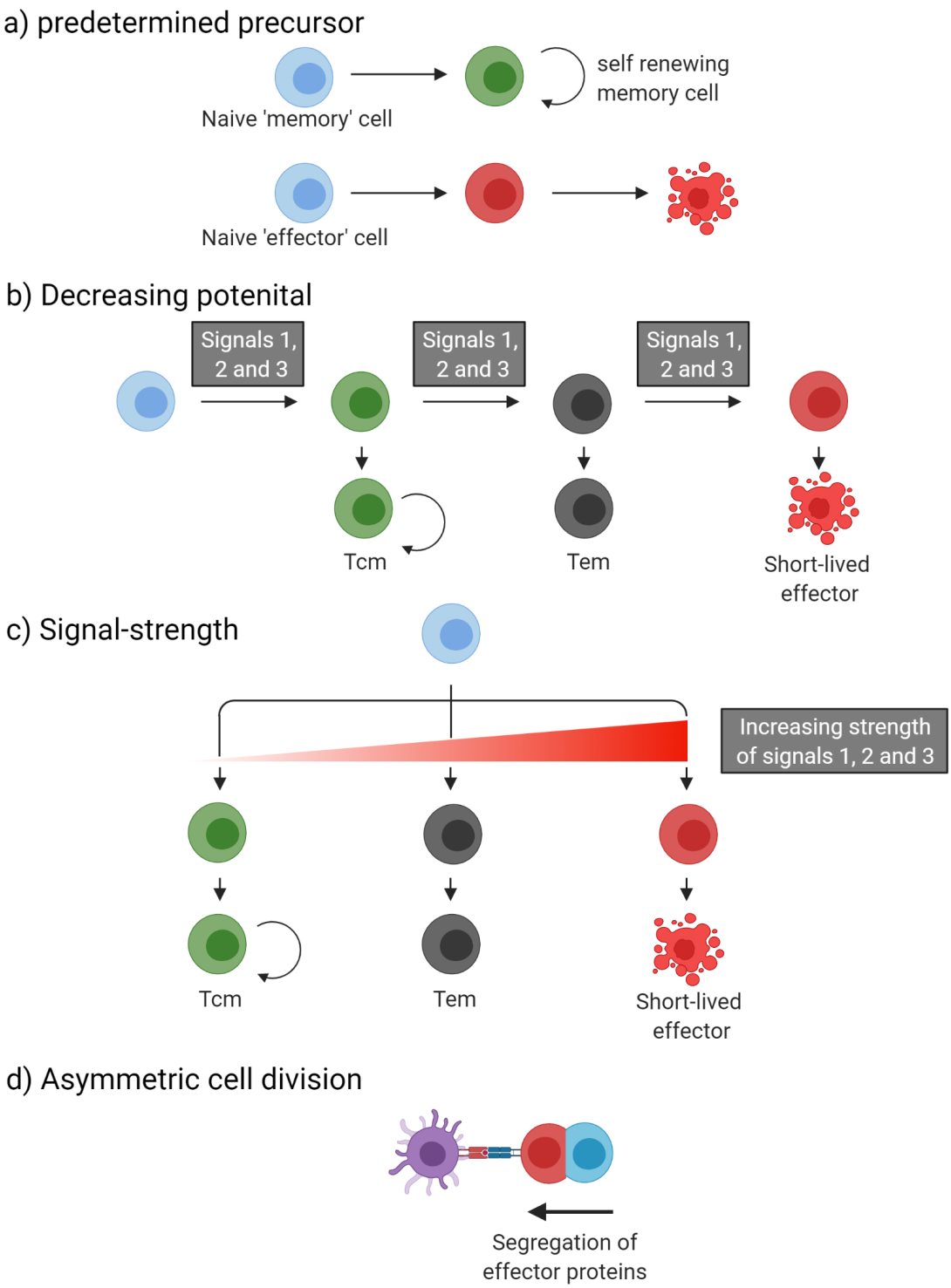

Figure 1.2: Models for generating effector and memory T cell heterogeneity
a) In the predetermined precursor model the fate of a T cell is pre-programmed into naive T cell prior to its activation. **b)** In the decreasing potential model T cells gradually lose their stem-like properties as they undergo successive divisions, eventually developing into a terminally differentiated effector T cell that will die after the resolution of infection. **c)** In the signal strength model the combined strengths of signals 1, 2 and 3 (antigen stimulation, co-stimulatory signalling and cytokine stimulation respectively) a T cell receives during its initial activation program the eventual fate of the cell, with combined strong signals promoting terminal effector fate, and weak signalling a memory cell fate. **d)** During asymmetric cell division effector-fate transcription factors and signalling molecules cluster with the dividing cell that forms the immunological synapse Tcm, central memory T cell; Tem, effector memory T cell. Adapted from [186].

1.3.3 $CD8^+$ T cell effector mechanisms

Upon arrival in inflamed tissue $CD8^+$ T cells can participate in the removal of virally-infected cells, and depletion of $CD8^+$ T cells during infection results in an increase in pathogen burden, and a delay in clearance [213–215]. For $CD8^+$ T cells to eliminate infected or malignant cells they require TCR-dependent detection, enabling the formation of an immunological synapse, which permits polarised secretion of effector molecules such as perforins and granzymes, and engagement of death receptors [213, 216]. In these cell-cell interactions, perforins secreted at the immunological synapse oligomerise and form pores in the target cell membrane, osmotic disparity promotes influx of Ca^{2+} and granzyme molecules from the synaptic space into the target cell cytoplasm [217]. The formation of perforin-pores in the target cell membrane triggers a Ca^{2+} cell-intrinsic membrane repair pathway that can quickly patch the pores [218], preventing osmotic death of the cells which would release cytosolic contents into the extracellular space. Granzymes that are now in the cell cytoplasm, however, trigger rapid caspase-dependent apoptotic cell death. Elimination of infected cells can also be delivered by extrinsic cues, these are delivered through transmembrane receptors expressed on the surface of target cells belonging to the TNFR superfamily, the main ligands of which, TNFα, TRAIL and FASL are expressed, or secreted, by $CD8^+$ T cells. Engagement of the receptors for these ligands on infected cells, either through direct cell contact (eg: membrane ligand expression on CD8+ T cell) or in soluble form (ligand secreted by CD8+ T cell) [219], engages the extrinsic cell death pathway which ultimately leads to caspase activation and cell death through apoptosis [220].

Aside from direct-killing of infected cells a second way in which $CD8^+$ T cells contribute to the control of infection is through the secretion of effector cytokines, primarily IFNγ and TNFα. The cytokine IFNγ can act on various myeloid and dendritic cell subsets, enhancing their antigen-presentation capacity and promoting further secretion of cytokines and chemokines [67]. $CD8^+$ T cells in influenza infected BALB/c mice are also major producers of the immuno suppressive cytokine IL-10 [221, 222], as well as conventional effector cytokines such as IFNγ. The ability of $CD8^+$ T cells to produce IL-10 was restricted to the effector site, and only present in cells that had recently migrated into the tissue [223]. When this cytokine is neutralised, influenza-infected mice suffer from enhanced pulmonary infiltration and lethal injury, indicating that T cells can have dual cytotoxic and regulatory roles in certain infectious settings.

1.4 Memory CD8$^+$ T cell formation and recall

After clearance of a pathogen, most effector cells enter a phase of contraction through apoptosis, and a small percentage of these cells survive this process to establish a heterogeneous pool of long-lived memory cells. This memory cell population is comprised of subsets of circulating memory cells that have distinct patterns of recirculation at homeostasis, and non-migratory resident memory cells that are retained at the initial site of infection **(Fig. 1.3)**. Through their combined efforts, these memory cells establish a body-wide state of immunosurveillance that extends far beyond the blood and SLO restricted re-circulation they offered as naïve T cells. These cells have an enhanced capacity for the production of effector molecules and cytokines, and can rapidly mobilise immune responses to peripheral tissues to provide rapid immunity in the case of re-infection.

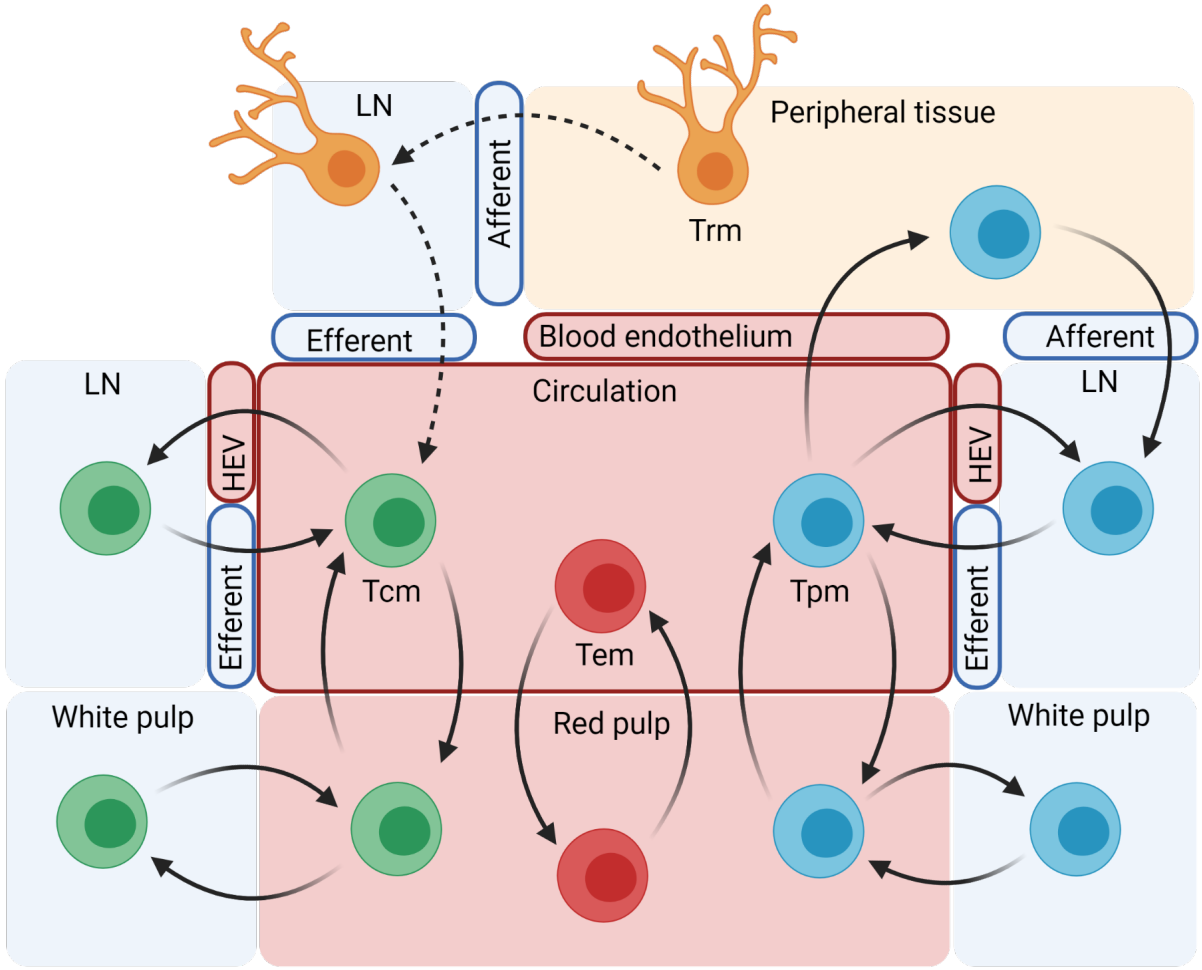

Figure 1.3: Memory T cell recirculation at homeostasis

Long after the resolution of an infection populations of long-lived memory $CD8^+$ T cells maintain a body-wide state of immunosurveillance. From the circulation Tcm cells can access lymph nodes via HEVs and are also capable of migrating into the white pulp of the spleen. Tpm cells have similar migratory properties to Tcm cells, but are also capable of entering uninflamed peripheral tissues, and accessing lymph nodes through the afferent lymphatics. Tem cells are the most restricted and are only capable of moving between the circulation and the red pulp. Tissue resident memory cells are typically restricted to the tissue in which the initial infection was present. In certain contexts however, resident memory T cells are able to access the afferent lymphatics and take up residence in tissue-draining lymph nodes, and are even capable of de-differentiating into ex-Trm Tcm cells. Abbreviations: Tcm, central memory T cell; Tem, effector memory T cell; Tpm, peripheral memory T cell; Trm, resident memory T cell, LN, lymph node; HEV, high endothelial venule.

1.4.1 Circulating memory CD8$^+$ T cells

Some of the earliest descriptions of naïve and memory T cells with distinct *in vivo* migratory properties came from studies in sheep. These early studies demonstrated that memory T cells, but not naïve, could be found in the afferent lymph that directly drained tissue. In contrast, naïve T cells were only found in efferent lymph downstream of lymph nodes, indicating that memory T cells could pass through peripheral tissue to access lymph nodes and lymphatics, whereas naïve T cells could only enter through lymph nodes [224]. The first description of functionally-distinct subsets of memory T cells came nearly a decade later when Sallusto *et al.* [225] described two populations of αβT cells in human blood based on the expression of CCR7 [225]. CCR7$^+$ central memory T cells (Tcm) displayed high expression of the lymph node homing marker CD62L and increased expression of proliferative cytokines upon re-stimulation. In contrast, CCR7$^-$ effector memory T cells (Tem) had higher expression of effector cytokines upon restimulation, lower lymph node homing capacity, and increased expression of chemokine receptors that were associated with homing to NLT [225]. Based on these observations Sallusto *et al.* [225] proposed a model of memory T cell immunosurveillance where Tcm cells would home to lymphoid tissue and rapidly proliferate upon reinfection to provide secondary effectors, while Tem cells would scan the blood and NLT, prepared to provide an immediate effector force at the site of infection, upon reinfection [225–227]. However, this model of NLT immunosurveillance by Tem cells was proposed based on observations made on human peripheral blood T cells, and subsequent studies in mice made the observation that Tem cells isolated from the blood and spleen did not resemble the diverse phenotypes of putative Tem cells recovered from a range of peripheral NLTs [228–230]. Additionally, it was demonstrated that CCR7 may regulate memory T cell egress from peripheral tissue by directing cell migration into draining lymph, challenging the notion that CCR7$^-$ Tem cells could recirculate through NLT [231, 232]. Some of these contradictions were eventually resolved with the discovery that the vast majority of Tem cells present in peripheral tissues were actually a functionally distinct population of non-recirculating resident memory cells [233–235]. Although these observations largely absolved Tem cells of the need to enter peripheral tissue, their designation as NLT-surveying cells remained [236–243]. While subsequent studies had developed other methods for the identification of circulating memory cells with distinct functions or potential [184, 244, 245], their capacity for recirculation through peripheral tissue had not been re-examined. More recently, work by Gerlach *et al.* [246] identified three distinct populations of circulating memory CD8$^+$ T cell subsets through the differential expression of CX3CR1, that have distinct patterns of immunosurveillance at homeostasis [246]. CX3CR1^{low} cells represented the classical Tcm cells while CX3CR1^{hi} cells represented the classical Tem cells with the caveat that these cells cannot enter peripheral tissue. A CX3CR1^{int} population represented a novel

subset of circulating memory cells, termed 'peripheral memory' T cells (Tpm), that had an enhanced capacity to migrate through peripheral NLT at homeostasis. These circulating memory cell subsets were shown to differentiate in a linear manner with Tcm cells appearing first, and with further stimulation differentiating into Tpm cells and finally into Tem cells. As these cells progress down the memory spectrum they acquire a more cytotoxic phenotype and progressively lose their ability to proliferate, with Tem cells being incapable of further division upon restimulation. Both Tcm and Tpm cells retained a high degree of stemness, with these cells able to produce high levels of IL-2 upon re-stimulation and undergo rapid proliferation and differentiation into secondary effector cells [246].

While the immunosurveillance of naïve T cells is restricted to SLOs via blood and lymphatic vessels, circulating memory cells extend their directed immunosurveillance beyond SLOs to include visceral and barrier organs [247, 248]. Yet the specific migratory signals that enable circulating memory cells to establish these homeostatic trafficking patterns are unclear. Central memory T cells retain their ability to enter SLOs from the circulation, as these cells either maintain expression of, or re-express, CCR7 and CD62L following activation, enabling continual trafficking across HEVs [249]. In contrast to naïve T cells, however, Tcm cells express CXCR3, which is important for their homing to peripheral interfollicular regions of lymph nodes, where they are optimally positioned to intercept tissue-draining cDCs for rapid reactivation in the case of re-infection [250, 251]. Unlike Tcm cells, Tem cells lose expression of lymph node homing markers and are unable to re-access SLOs or the white pulp of the spleen from the circulation and, under homeostatic conditions, these cells are found almost exclusively within the vascular-positive fractions of visceral and barrier organs [246]. Evidence of the reluctance of these cells to enter lymphoid or non-lymphoid tissues derives from the observation that circulating memory cells that enter lymphoid or non-lymphoid tissue eventually return to the circulation via the thoracic duct through S1PR1-mediated migration that directs cells into the efferent lymphatics [252]. As such, the immunomodulatory drug Fingolimod, which antagonises S1P-receptors, traps cells that are recirculating through lymph nodes, within lymph nodes. Administration of this antagonist to mice, or humans, results in the prolonged depletion of Tcm-like cells from the circulation, with little effect on the non-migratory Tem subsets, suggesting that these cells do not leave the circulation (or that they have S1PR-independent mechanisms of LN egress) [253]. Another feature that appears to be unique to the recirculation of this memory subset is its ability to form prolonged contacts with the blood endothelium enabling Tem cells to efficiently scan the vasculature [254], similar to the vascular patrolling behaviour that has been reported for non-classical monocytes [115], although the function of this patrolling behaviour in $CD8^+$ T cells is not known. The ability of some circulating memory cells to migrate through peripheral NLT is generally well accepted, however, exactly how this is achieved has

not been elucidated [246]. Effector-like memory cells lacking lymph node homing markers have been detected the efferent lymph through cannulation of the thoracic duct, suggesting that these cells have not accessed the lymphatics through HEVs. Additionally, in certain contexts, the maintenance of circulating memory cell populations at barrier tissues has been shown to be partially dependent on activation of latent TGFβ through $\alpha_v\beta_6$ and $\alpha_v\beta_8$ expressed by keratinocytes in the dermis [255], suggesting that active migration through peripheral NLT is required for the optimal maintenance of some circulating memory cells. While these studies suggest that circulating memory $CD8^+$ continuously migrate through NLT during homeostasis, and that this activity is required for their optimal maintenance, the specific migratory signals that regulate this process have not been determined.

1.4.2 Resident memory T cells

Trm cells represent a subset of peripheral, non-circulating, $CD8^+$ memory T cells that develop at the site of infection following clearance of the pathogen and are the memory subset predominately responsible for immunosurveillance of NLTs [234, 235]. These cells are present at all barrier surfaces, including the skin [78, 256], and the reproductive [79, 235], respiratory [257–259], and gastrointestinal tracts (GIT) [260, 261], as well as in non-barrier organs such as the liver [262], kidney [263], salivary glands [263], and CNS [264], in mice, as well as in humans [265, 266]. In most tissues Trm cells can be identified as cells that are protected from intravascular labelling and that express CD103 and CD69, and these two molecules also have important functions in Trm biology. CD69 antagonises S1PR1, which would otherwise promote tissue egress, and removing this surface molecule reduces the number of Trm cells that form in the skin after HSV infection [267]. CD103 is a ligand for E-cadherin, an adhesion molecule expressed on epithelial cells. However, in certain tissues, populations of $CD69^-$ or $CD103^-$ Trm cells can be found, indicating additional mechanisms of tissue-retention [108, 235, 268]. In fact, transcriptional comparisons of Trm cells from disparate tissues has revealed tissue-specific transcriptional profiles for lung, skin, and intestinal Trm cells, suggesting there may be tissue-specific residency programs and population redundancy. While Trm populations in most NLTs are stably maintained over time [269], Trm cells present in the lungs gradually decrease in number in the months following influenza infection [270]. Uniquely, this population gradually disappears in the months following resolution of infection and this loss is accelerated in the absence of circulating memory cells, suggesting that the short-term maintenance of this population requires constant input from circulating memory precursors [259].

The positioning of Trm cells at barrier surfaces enables them to act as a "first line of defence" in case

of secondary infection. Upon reactivation Trm cells rapidly produce IFNγ which enhances local cytokine and chemokine production and facilitates the rapid recruitment of circulating memory cells for optimal pathogen control [233]. Although these cells were originally thought to be terminally differentiated, due to high expression of co-inhibitory molecules [271], absence of turnover at homeostasis [78, 272], and expression of transcription factors similar to that seen in exhausted T cells [273, 274], they do retain a degree of stemness and are capable of *in situ* proliferation upon challenge [271, 275]. These proliferating Trm cells can shed their residency program and are able to re-gain a transcriptional program that resembles that of effector or central memory T cells and even re-enter the circulation [276, 277]. Additionally, some of these daughter Trm cells retain their Trm phenotype and can exit the tissue via the lymphatics to establish a secondary population of draining LN resident Trm cells [278]. Although SLO Trm cells arising from secondary infections have been described, primary influenza infection results in a population of Trm cells that can be detected in the lung-draining mLN [279–282]. Early parabiosis studies have shown that the majority of memory T cells within the mLN were resident cells, although at the time this was thought to be retention mediated by residual antigen present within the mLN [279, 281]. It was recently shown that these Trm cells were not generated in response to residual antigen, but rather are Trm cells that had left the lungs and made their way through the lymphatics to take up residency in the mLN [282]. How this occurs, and why it has only been described for influenza infection is unclear, but studies of 'free-living' mice and humans have shown large populations of $CD69^{+}CD62L^{-}$ putative Trm cells in LNs throughout the body [265, 266, 283], though the specific origins of these LN resident Trm cells is unclear.

1.4.3 Mechanisms of memory T cell protection

After the clearance of a primary infection the memory cells that develop far outnumber the original naïve precursors and are bestowed with enhanced effector function and distinct migratory capacity. These enhanced features of memory T cells enables them to rapidly respond in the case of re-infection and control infectious doses that would otherwise be lethal in a naïve mouse. In the case of re-infection, resident-memory cells present at barrier tissues are the first to come into contact with the pathogen. As Trm cells exist independent of the circulation, intravenous administration of depleting antibodies depletes circulating, but not resident-memory cells [78, 271]. Using such strategies it has been demonstrated that Trm cells can control secondary infections independently of a contribution from circulating memory cells [284]. Using an influenza model of re-challenge, mice primed by intra-peritoneal injection of inactivated influenza, which generates circulating but not resident-memory $CD8^{+}$ T cells, were less

efficiently protected from secondary infection than mice that had received intranasal vaccination with a live-attenuated virus [285]. Using parabiosis experiments with HSV-2-infected and naïve parabionts, where circulating memory cells are equilibrated between the two hosts but Trm cells are not, naïve parabionts that have circulating memory cells, but not resident memory cells, show reduced protection after secondary infection with HSV-2 [79].

Although these experiments demonstrate that either resident or circulating memory cells alone are sufficient for protection from lethal challenges, optimal host immunity requires the combined action of both circulating and resident cell subsets. This protective capacity also relies on the unhindered migration of memory T cells within the infected tissue, as disrupting migration by blocking integrin or chemokine binding decreases T cell velocities within infected tissue, and increases pathogen burden [83, 286]. Critically, this protection relies on IFNɣ signals derived from Trm cells, as IFNɣ receptor knockout mice, or mice seeded with IFNɣ-deficient Trm cells, are not protected during lethal challenges [79]. The production of IFNɣ by resident memory cells serves several functions; it enhances the anti-viral activity of local immune and stromal cells, promotes the secretion of CXCL9 and CXCL10, and increases expression of integrins in the nearby vasculature which promotes recruitment of pathogen-specific circulating memory cells that can further eliminate infected cells [287]. However, despite their demonstrated role in protection from re-infection resident memory cells express very high levels of co-inhibitory molecules [271], and Trm cells isolated from the lung airways have poor *ex vivo* cytotoxic capabilities [288, 289]. Although imaging experiments have shown that Trm cells move into infectious foci during HSV challenge [271], whether Trm cells simply serve as sentinels that rely upon recruited cells for effective viral control, or whether they are unshackled from their inhibited state by the inflammatory mileu and participate in elimination of infected cells, is unclear.

The current model for recall responses of circulating memory subsets is that central and peripheral-memory T cells re-encounter antigen in SLOs, where they undergo secondary expansion to provide further effector cells to curtail infection. In contrast, Tem cells, which have the highest effector potential but no proliferative or LN-homing capacity, traffic to inflamed NLT to mediate early pathogen clearance. While Tcm cells were thought to be reactivated and undergo secondary division primarily within lymph nodes, recent studies have demonstrated that these memory T cells are capable of infiltrating NLT, and that tissue infiltration can be antigen independent [235, 290]. This tissue infiltration was dependent on glycosylation of cell surface adhesion molecules that creates functional ligands for P and E-selectins present on vascular endothelial cells, enabling the initial tethering and rolling steps required for transendothelial migration. Interestingly the glycosylation of CD43 by core 2 β1,6 N-

acetylglucosaminyltransferase-I only occurs in Tcm cells and Tpm cells but not Tem cells, indicating that NLT infiltration may be a feature that is restricted to Tcm cells and Tpm cells [290]. These $CD62L^+$ NLT-homing Tcm cells were shown to migrate into the skin during Vaccinia virus (VacV) infection and lyse infected cells in a perforin-dependent manner [290]. It has also been observed that Tem cells, despite high expression of a number of different chemokine transcripts, have poor migratory capacity *in vivo* during infection and inflammation and are largely restricted to the vasculature, suggesting they may not have a major contribution to the elimination of infected cells in peripheral tissues during a recall response [254]. These observations suggest that Tem cells may be a memory subset that is "resident" in the vasculature and patrol the blood endothelium to search for infected cells, similar to how non-classical monocytes patrol the vasculature to perform their function [115].

1.5 The research project

The specific microanatomical localisation of T cells is critical for the formation and execution of primary and secondary immune responses. To achieve this, the movement of immune cells within, and between, tissues and organs is regulated through the action of chemokines and chemokine receptors. The specific chemokine receptors that regulate the discrete events involved in T cell activation, expansion and eventual memory formation are not completely understood, with only one chemokine receptor to date, CXCR3, being identified as a key receptor in this process. Therefore, the broad aims of this project were:

- To investigate the homing signals that drive $CD8^+$ T cell effector differentiation and responses
- To investigate the homing signals that promote $CD8^+$ memory T cell development and homeostatic maintenance

2 | Materials and Methods

2.1 Mice

C57Bl/6 (B6) and B6.SJL-Ptprca (Ly5.1) mice were purchased from the Animal Resource Centre (Western Australia) or bred in-house at the University of Adelaide animal house. OT-I mice were purchased from Kew Animal Facility at the Walter and Eliza Hall Institute of Medical Research (Victoria) and crossed to Ly5.1 mice to generate Ly5.1 OT-Is. *Ccr2*-deficient mice (*Ccr2*$^{-/-}$) mice were bred in house by crossing *Ccr2*$^{-/+}$ mice to generate *Ccr2*$^{-/-}$ and WT littermate controls. *Ccr2*$^{-/-}$ OT-I mice were generated by crossing *Ccr2*$^{-/-}$ mice with OT-I mice. *Ccr2*$^{-/-}$ OT-I Ly5.1 mice were generated by crossing *Ccr2*$^{-/-}$ OT-I mice with Ly5.1 mice. *Ccr2*-CFP-DTR mice were kindly provided by Prof. Andrew Lew (WEHI, Victoria). *ifng*$^{-/-}$ mice were provided by Dr. Geoff Hill (QIMR, Queensland). UBC-GFP-OT-I mice were generated by crossing UBC-GFP mice to OT-I mice. *Ccl2*-Red Fluorescent Protein (RFP)$^{fl/fl}$ mice, floxed mutant mice that contain loxP sites flanking exons 2-3 of the Ccl2 gene, which has been modified with a 2A cleavage site and a cleavable RFP at the 3' end of exon 3, were purchased from the Jackson Laboratory. Mice were maintained in a specific pathogen-free, temperature-controlled (22±1°C) mouse facility on a 12-h light, 12-h dark cycle. Stock Mice were fed a standard chow diet, breeder mice were fed a 10% high fat chow diet, with food and water provided *ad libitum*. Experiments using OT-I mice were performed with gender and aged matched mice between 6 to 14 weeks of age, unless otherwise specified. Experiments using all other mice were of mixed age and gender. All animal experiments were conducted in accordance with institutional and national regulations with the approval of the University of Adelaide Animal Ethics Committee.

2.2 Murine tissue processing

2.2.1 Lymphoid organs

Spleens were passed through 70µm filters (BD) and washed in phosphate buffered saline (PBS) before incubation in murine red cell lysis buffer (MRCLB) for 5 minutes at 37°C. Red blood cell lysed cell suspension were then washed again in PBS in preparation for cell counting. Lymph nodes were either (1) mashed through 70µm filters (2) minced in general digestion media and incubated at 37°C with gentle agitation to disrupt tissue (3) minced in PBS and disrupted using a pellet pestle (SigmaAlrdich). All cell suspensions were centrifuged at 300 rcf for 5-7 minutes unless otherwise specified.

2.2.2 Airways associated mucosa

Mice were dissected to expose the diaphragm which was punctured to induce pneumothorax. To perfuse the pulmonary vasculature the right aorta was cut and a 21 gauge needle was inserted into the right

ventricle to flush at least 10mL of cold PBS until lungs had blanched. BAL fluid was harvested by exposing the trachea and making a small incision in the pharyngeal cartilage. Using a syringe fitted with an Insyte Autoguard catheter (BD) the airways were washed 2-3 times using three sequential changes of PBS 5mM EDTA. Individual lung lobes were excised and minced into general digestion media, incubated at 37˚C with gentle agitation, and passed through a 1000µL pipette every 15 minutes until fine (30-45 minutes), filtered through a 70µM filter, washed, incubated in MRCLB for 5 minutes at 37˚C and washed for counting. Trachea was excised from just below the cricoid cartilage to just above the tracheal bifurcation, removed of excess fat, minced into 300uL of general digestion media, incubated at 37˚C with gentle agitation for 30 minutes with the tissue being passed through a 1000µL pipette after 15 minutes. Nasal-associated lymphoid tissue (NALT) was harvested by excising the upper palate using a razor then processed the same as the trachea.

2.2.3 Skin

Whole ears were removed, split into dorsal and ventral halves using forceps, minced into skin digestion media, and incubated for 1 hour at 37˚C with gentle agitation and with mixing every 20 minutes. Digested tissue was passed through a 50µM filter, incubated in MRCLB 5 minutes at 37˚C and washed in PBS for counting.

2.2.4 Peripheral blood

For endpoint experiments up to 500µl of blood was harvested from the right ventricle of mice via cardiac puncture with an insulin syringe and collected into BD Vacutainer heparin coated tubes. For timecourse experiments mice were bled through the submandibular vein and blood was collected into BD Vacutainer heparin coated tubes. Blood was lysed in 10mL of MRCLB for 20 minutes at 37˚C and washed 3 times in PBS before counting.

2.2.5 Peritoneal wash

Peritoneal cavity was washed three times through the peritoneum with 1ml PBS using a syringe fitted with a 19 gauge needle.

2.2.6 Visceral adipose tissue

In male mice, perigonadal visceral adipose tissue (VAT) was finely minced in adipose tissue digestion media, incubated at 37˚C for 45 minutes with gentle agitation, and passed through a 1000µL pipette every 15 minutes. After incubation the suspension was diluted 10 times with PBS + 2% fetal calf serum (FCS) and centrifuged at 800g for 15 min at 4˚C. The pellet was lysed with MRCLB for 5 minutes at 37˚C,

washed in PBS 2% FCS, and resuspended for counting.

2.2.7 Bone Marrow

Femurs were removed from mice and flushed twice with 3ml of PBS 5mM ETDA using a 3ml syringe fitted with a 19 gauge needle. Cells were lysed in 5mL MRCLB, washed in PBS and resuspended for counting.

2.2.8 Human peripheral blood

Peripheral blood mononuclear cells were isolated from human blood using Lympoprep™ (StemCell) per manufacturers instructions. In brief, Lympoprep™ was warmed to room temperature and 3-4 mL added to the bottom of a 14 mL conocal tube. Three to four mL of human blood was mixed at a 1:1 ratio with PBS 2% FCS and layered ontop of Lympoprep™. Tubes were centrifuged at 800g for 20 minutes at room temperature with no brake. The upper plasma layer was then removed and discarded and the underlying layer of mononuclear cells removed without disturbing the erythrocyte/granulocyte pellet. Recovered mononuclear cells were washed 3x in PBS and resuspended in PBS for downstream applications.

2.3 Ex vivo techniques

2.3.1 Flow cytometry

Single cell suspensions were stained in 96 well round bottom, or V bottom plates (Corning) at 1.5 – 2x10^6 cells per well using antibodies and reagents detailed in **table (2.1)**. Cells were washed in PBS and resuspended in a solution containing BD Horizon™ Fixable Viability Stain 780 (BD) and mouse γ-globulin (mγg) (200μg/ml) for 10-15 minutes at room temperature.

a) Purified antibodies

For stains with purified antibodies, cells were stained with the purified antibody for 40-60 minutes at 4°C. Secondary antibody was pre-incubated with 100μg/mL mγg and 1% normal mouse serum (NMS), added after washing cells in FACS buffer, and stained for 20–30 minutes. Cells were washed in FACS buffer and blocked with rat γ-globulin for 15 minutes and stained as below.

b) Standard flow cytometry

Cells were washed in FACS buffer and resuspended in a cocktail containing directly conjugated antibodies and incubated for 30 minutes at 4°C in the dark. For the use of biotinylated antibodies, cells were washed

in FACS buffer and resuspended in a solution containing FACS buffer with a streptavidin-fluorophore conjugate for 15 minutes. Cells were then washed in PBS 0.04% sodium azide.

c) Intracellular staining

For the staining of intracellular cytokines cells were first incubated in restimulation medium containing either 1µg/mL SIINFEKL or PMA for 4 hours at 37˚C. Surface antibodies were stained for as in **section 2.3.1 a-b** then cells were incubated in Cytofix/Cytoperm (BD) for 20–30 minutes at room temperature, washed twice in Permwash (BD) and stained with antibodies directed against cytoplasmic proteins for 20–30 minutes. For staining of nuclear factors and Bromodeoxyuridine (BrdU), cells were incubated in Foxp3 kit fixation & permeabilization buffer (eBioscience) for 30 minutes at room temperature then washed twice in Foxp3 kit permwash (eBioscience). For staining of nuclear factors, cells were incubated with a solution containing directly conjugated antibodies directed at nuclear factors in 2% NMS and normal rat serum (2%) for 20–30 minutes before washing in PBS 0.04% azide. For BrdU detection, after permeabilisation cells were incubated in PBS 50U/mL DNase for 1 hour at 37˚C. Cells were washed with Foxp3 kit permwash then stained with αBrdU antibodies for 20–30 minutes. Cells were washed in PBS 0.04% azide and acquired immediately. Stained cells were acquired on FACSAria and LSRFortessa flow cytometers and analysed in FlowJo (Treestar) after gating on live, single cells as outlined in **(Fig. 2.1)**, prior to the identification of immune cell subsets based on lineage markers, and markers of interest.

d) Tetramer staining

For the use of tetramers, cells were incubated in 50µL FACS buffer containing NP and PA tetramers at 4˚C for 15 minutes. Surface antibodies were then added directly to cells without washing and processed as in **section 2.3.1 a-c**.

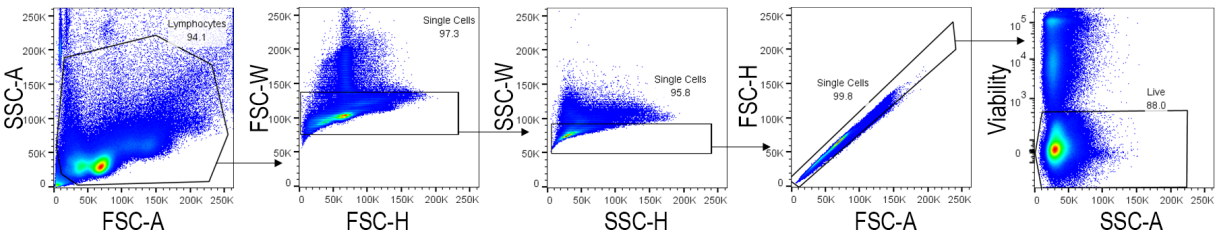

Figure 2.1: Gating strategy for the identification of live, single cells, by flow cytometry.
Representative flow cytometry of the gating strategy used throughout this thesis for the identification of live, single cells. Further gating proceeds as outlined in each figure throughout this thesis

2.3.2 Quantitative PCR

All procedures involving RNA were conducted with equipment and work spaces cleaned with RNaseZap (ThermoFisher). For qPCR on purified cells, cells were stained as described above and sorted on a FACSAriaII. For some OT-I sorts OT-I T cells were first enriched from SLOs using an active $CD8^+$ T cell negative isolation kit (Miltenyi Biotec). mRNA was prepared using RNeasy micro kit (Qiagen) with on-column DNase I treatment. Alternatively, snap-frozen tissues were ground into a fine powder and RNA isolated using Trizol reagents, followed by DNase treatment using TurboDNase (AppliedBiosystems). cDNA was prepared using High-Capacity cDNA Reverse Transcription Kit (Thermofischer). Quantitative polymerase chain reaction (qPCR) was performed using PowerUp SYBR Green Master Mix™ (ThermoFisher) on a LightCycler-480 instrument (Roche). Relative gene expression was calculated using the equation $2^{(\text{CT target} - \text{CT reference})}$ where the reference gene was *Rplp0*. Primer sequences listed in **(Table. 2.2)**.

2.3.3 Enzyme-linked immunosorbent assay (ELISA)

Harvest of supernatants

Lymph node supernatants were prepared by mincing lymph nodes in 300µL of PBS containing 1X protease inhibitor (Sigma) and incubating for 10 minutes at 37°C with gentle agitation to liberate proteins. BAL supernatants were collected by washing the airways with 500µL of PBS and supplementing the BALF with 1X protease inhibitor. Supernatnats were stored at -80°C and centrifuged at 5000RCF for 10 minutes prior to use.

ELISA

96 well high-binding plates (Corning) were coated with capture antibody diluted ELISA coating buffer overnight at 4°C. All further incubations were at RT, and all washes were performed 3 times with PBS 0.05% Tween-20. Plates were washed then blocked with PBS 3% bovine serum albumin (BSA) for 2 hr. Plates were washed and 50 to 80µL protein standards and samples were diluted in PBS 1% BSA and incubated for 2 hr. Plates were washed then incubated with detection antibody in PBS 1% BSA for 2 hr. Plates were washed and incubated with streptavidin-HRP (R&D) in PBS 1% BSA for 30 min. Plates were washed, developed with TMB (eBioscience), stopped with 1M orthophosphoric acid and read at 450nm on a Biotrak II spectrophotometer (Amersham Biosciences). Concentrations of protein in biological samples were determined by interpolation of the standard curve of log10(concentration) vs. Absorbance. Protein concentration was then used to determine the total amount of protein in the recovered sample.

2.3.4 Chemotaxis assay

Splenocytes were harvested and rested in chemotaxis buffer for 4 hours at 37°C. Chemokine ligands CCL2 and CXCL11 (from the late Prof. Ian Clark-Lewis) and CCL7 (Peprotech) were serially diluted in chemotaxis buffer and 200µL loaded into the bottom-chambers of 96 well transwell plates (Corning). Up to 5×10^5 splenocytes were loaded into the upper-chambers in 100µL of chemotaxis buffer, and transwell plates incubated at 37°C for 3 hours. Lower-chambers where then harvested and stained for flow-cytometric analysis of cells of interest. Before acquisition 2×10^4 count bright beads were added to each sample. Event counts were normalized to beads, then divided by no chemokine control to determine chemotaxis index.

2.4 In vivo assays

2.4.1 Adoptive cell transfer

Splenocytes were harvested from OT-I mice and naïve ($CD44^-$ $CD62L^+$) $CD8^+$ T cells were isolated using an EasySep naïve $CD8^+$ T cell negative isolation kit (Stem Cell Technologies). Purity and ratios (for competitive transfer experiments) of naïve OT-I cells was determined by flow cytometry prior to transfer. 1×10^4 Purified OT-I cells were injected into host mice via the lateral tail vein in 200µl of PBS.

2.4.2 Viral infections

For infections mice were anaesthetised with 6mg/Kg pentobarbitone (Ilium) via IP injection and 32µl of diluted A/HK-x31, x31-OVA, A/PR8 or PR8-OVA virus (detailed in **Table 2.3**) was applied to the nares of anaesthetised mice. Mice were left to recover on a 37°C heatpad until they regained consciousness. Infected mice were monitored daily over the course of infection for changes in weight and physical appearance.

2.4.3 BrdU labelling

Influenza infected mice were injected IP with 1mg BrdU (Sigma) in 100µl of a sterile 0.85% saline solution 24 and 14 hours prior to sacrifice.

2.4.4 In vivo cytotoxicity assay

Splenocytes were harvested from Ly5.1 mice and half of the recovered cells labelled with 1µM eBioscience™ Cell Proliferation Dye eFluor™ 670 as per the manufacturers instructions (Non-target cells). The other half of recovered splenocytes were pulsed with 10nM Influenza A $NP_{366\text{-}374}$ Strain A/PR8 peptide

(Anaspec) for 30 minutes at 37°C (Target cells). Both cells were washed three times in sterile endotoxin-free PBS, mixed at a 1:1 ratio and $5x10^6$ total cells ($2.5x10^6$ each of target and non-target) were injected intravenously into day 28 A/HK-x31 immunised WT and *Ccr2*$^{-/-}$ mice and WT naïve controls. Four hours post-injection spleens were harvested and stained with CD45.2 and CD45.1 antibodies to discriminate between host and transferred cells. The percent specific killing was calculated as: 100 (100 × [(% eFluor™ 670+/% eFluor™ 670-)/(%CFSE^{lo} in naïve group/%CFSE^{hi} in naïve group)].

2.4.5 Vascular labelling

For the labelling of vascular CD8$^+$ T cells 3µg of fluorescently conjugated antibody (detailed in **Table 2.1**) was injected into the lateral tail vein of mice in 200µL of sterile PBS 3 minutes prior to sacrifice.

2.4.6 In vivo depletion

For the depletion of CCR2-expressing cells *Ccr2*-DTR mice were injected IP with 10ng per gram of body weight of diptheria toxin in sterile PBS 1 day before influenza challenge and every 2 days thereafter until endpoint.

2.5 Solutions and buffers

2.5.1 PBS

1 X PBS was either purchased from the University of Adelaide technical services unit (TSU) or prepared by diluting 20 X PBS (TSU) in MilliQ water.

2.5.2 PBS + EDTA

PBS EDTA solutions were prepared by diluting 0.5M EDTA (v/v) (TSU) in 1 X PBS to the desired concentration.

2.5.3 MRCLB

9 parts 155mM NH_4Cl (AnalaR) solution and 1 part 170mM TRIS (Biochemicals) solution (pH 7.65) were mixed and adjusted to pH 7.2.

2.5.4 Paraformaldehyde solutions (PFA)

4% PFA (w/v) was prepared by dissolving paraformaldehyde (Sigma) in PBS and stored at -20°C to prevent degradation. 1% PFA was prepared by diluting 4% PFA in PBS.

2.5.5 Fluorescence-activated cell sorting (FACS) buffer

1 X PBS supplemented with 1% BSA (w/v) (Sigma) and 0.04% sodium azide (Ajax Finechem)

2.5.6 General digestion media

Dulbecco's Modified Eagle Medium (DMEM) (Life Technologies) supplemented with 10% FCS (Sigma), 1mM HEPES (ThermoFischer), 1 X penicillin/streptomycin (Gibco), 2.5mM $CaCl_2$ (TSU) and 2.5mM MgCl (TSU). 30U/mL DNase (SigmaAldrich) and 1mg/mL Collagenase IA (Sigma Aldrich) were added prior to tissue digestion.

2.5.7 Skin digestion media

Roswell Park Memorial Institute medium (RPMI) 1640 (Gibco) supplemented with 1% FCS (Sigma), 15 mM HEPES (SA Pathology). 85 µg/ml Liberase™ TM (Roche) and 30 U/ml DNase I (Sigma) were added prior to tissue digestion.

2.5.8 Adipose tissue digestion media

PBS supplemented with 0.5% FCS, 1mg/mL CollagenaseIV (Sigma), and 30 U/ml DNase I (Sigma) were added prior to tissue digestion.

2.5.9 BD Cytofix

BD Cytofix diluted 1:4 with 1× PBS

2.5.10 PBS-Tween

1 X PBS supplemented with 0.05% (v/v) Polyoxyethylene-sorbitan monolaurate (Tween20, SigmaAldrich).

2.5.11 Complete Iscoves Modified Dulbeccos Medium (cIMDM)

IMDM (Gibco) supplemented with 10% FCS (Sigma), 1 X penicillin/streptomycin (Gibco), 1 X Glutamax (Gibco), 54 pM β-mercaptoethanol (Sigma).

2.5.12 T cell re-stimulation media

cIMDM (**2.5.11**) supplemented with 1nM ionomycin (Life Technologies), 1/1500 GolgiStop™ (BD) 1/1000 GolgiPlug™ (BD) and either 20 pg/ml phorbol 12-myristate 13-acetate (PMA) (Life Technologies), for re-stimulation of all cells, or 1µg/mL SIINFEKL (Anaspec), for restimulation of OT-I cells.

2.5.13 Blocking solution

1 X PBS supplemented with 0.3% Triton-X100 (Sigma) and 1% normal mouse serum

2.5.14 ELISA coating buffer

3.03g of Na_2CO_3 and 6.0g of $NaHCO_3$ resuspended in 1L of MilliQ water and pH adjusted to 9.6.

2.5.15 Chemotaxis buffer

RPMI 1640 (Gibco) with 0.5% BSA (Sigma) and 20mM HEPES (SA Pathology)

2.5.16 Sorting buffer

1× PBS supplemented with 2% FCS (v/v) (Sigma) and 1mM EDTA (TSU).

2.5.17 Wash buffer

1× PBS supplemented with 0.3% Triton-X100 (Sigma)

2.5.18 FACS buffer

PBS 1% BSA (Sigma) 0.04% sodium azide (Ajax Finechem)

2.5.19 Tail tip lysis buffer

100mM Tris HCl (pH 8.5) (Biochemicals), 5mM EDTA (TSU), 0.2% SDS (TSU), 200nM NaCl (AnalaR) and 100µg/ml proteinase K (Roche).

Table 2.1: Antibodies and reagents

Antibodies			
Reagent or Resource	**Conjugate**	**Clone**	**Source**
B220	PECF594	RA3-6B2	BD
B220	UV496	RA3-6B2	BD
B220	AF700	RA3-6B2	BD
BrdU	AF488	3D4	Biolegend
BrdU	PerCP-Cy5.5	3D4	Biolegend
BrdU	PeCy7	RA3-6B2	Biolegend
CD103	PECF594	M290	BD
CD103	V421	M290	BD
CD103	FITC	2E7	BD
CD11b	V510	M1/70	Biolegend
CD11b	BB515	M1/70	BD
CD11b	PeCy7	M1/70	BD
CD11b	AF594	M1/70	BD
CD11c	V711	HL3	BD
CD172α	PeCy7	P84	BD
CD172α	UV395	P84	BD
CD19	PECF594	1D3	BD
CD19	UV395	1D3	BD
CD25	BV480	PC61	BD
CD27	V711	LG.3A10	BD
CD3	V421	145-2C11	BD
CD3	V711	145-2C11	BD
CD3	PeCy7	145-2C11	BD
CD3	PECF594	145-2C11	BD
CD3	UV805	145-2C11	BD
CD4	UV496	GK1.5	BD
CD4	UV805	GK1.5	BD
CD43	UV737	S7	BD
CD44	FITC	IM7	BD
CD44	V450	IM7	BD
CD44	BV480	IM7	BD
CD44	V711	IM7	BD
CD45	FITC	30F11	BD
CD45	AF700	30F11	BD
CD45	UV395	30F11	BD
CD45	UV805	30F11	BD
CD45.1	V421	A20	BD
CD45.1	V605	A20	BD
CD45.1	FITC	A20	BD
CD45.1	PE	A20	BD

Continued on next page...

Table 2.1 – continued from previous page.

Reagent or Resource	Conjugate	Clone	Source
CD45.1	AF594	A20	BD
CD45.1	AF647	A20	Biolegend
CD45.1	Biotin	A20	Biolegend
CD45.2	FITC	104	BD
CD45.2	PE	104	BD
CD45.2	APC	104	BD
CD45.2	V786	104	BD
CD45.2	Biotin	104	BD
CD49b	V786	HMα2	BD
CD62L	BB515	MEL-14	BD
CD64	AF647	X54-5/7.1	BD
CD64	PE	X54-5/7.1	BD
CD69	PeCy7	H1.2F3	BD
CD8α	BV480	53-6.7	BD
CD8α	AF647	53-6.7	BD
CD8α	PeCy7	53-6.7	BD
CD8α	UV395	53-6.7	BD
CD8α	UV805	53-6.7	BD
CD90	PECF594	53-2.1	BD
CX_3CR1	V421	SA011F11	BD
CX_3CR1	PE	SA011F11	BD
CX_3CR1	PeCy7	SA011F11	BD
CXCR3	Biotin	CXCR3-173	Invitrogen
F4-80	Biotin	BM8	Biolegend
γδTCR	V421	GL3	BD
Granzyme B	V421	GB11	BD
Granzyme B	AF647	GB11	BD
IFNγ	FITC	XMG1.2	BD
IFNγ	V480	XMG1.2	BD
IFNγ	PeCy7	XMG1.2	BD
IFNγ	PECF594	XMG1.2	BD
IL-17	V711	TC11-18H10.1	Biolegend
IL-2	FITC	JES6-5H4	BD
IL-2	PE	JES6-5H4	Invitrogen
Ki67	V450	SolA15	Invitrogen
Ki67	AF660	SolA15	Invitrogen
Ki67	PeCy7	SolA15	
KLRG1	V786	2F1	BD
KLRG1	APC	2F1	eBioscience
Ly6C	FITC	AL-21	BD
Ly6C	V510	HK1.4	Biolegend
Ly6C	V786	HK1.4	Biolegend
Ly6C	APC	AL-21	BD

Continued on next page...

Table 2.1 – continued from previous page.

Reagent or Resource	Conjugate	Clone	Source
Ly6C	AF700	Col3	BD
Ly6G	BB700	1A8	BD
Ly6G	V650	1A8	BD
MerTK	PeCy7	DS5MMER	eBioscience
MHC-II	BB515	M5/114.15.2	BD
MHC-II	V421	M5/114.15.2	BD
MHC-II	BV480	M5/114.15.2	BD
NK1.1	PECF594	PK136	BD
NK1.1	Biotin	PK136	BD
Siglec F	V605	E50-2440	BD
TCRβ	V786	H57-597	BD
TCRβ	PE	H57-597	BD
TER-119	PE	TER-119	BD
TNFα	V421	MP6-XT22	BD
TNFα	V510	MP6-XT22	BD
Vα2	APC	B20.1	BD
XCR1	V421	ZET	BD
XCR1	V650	ZET	BD
Purified antibodies			
CCR2	-	Col3	BD
MerTK	-	RA3-6B2	BD
Other flow cytometry reagents			
Streptavidin	PerCP-Cy5.5	N/A	BD
	V421		BD
	V510		BD
	AF647		BD
	PE		BD
	UV395		BD
	UV805		BD
αrat IgG	AF647	Polyclonal	BD
	AF488	Polyclonal	BD
	PE	Polyclonal	Jackson ImmunoResearch
Fixable viability dye	APC-Cy7	-	BD
Annexin V	V421	N/A	BD
	UV395		BD
Propridium iodide	PECF594	-	BD
***In vivo* antibodies**			
TCRβ	FITC	H57-597	Invitrogen
	PE	H57-597	BD
CD45	PE/Dazzle	30-F11	Biolegend
	FITC	30-F11	BD

Continued on next page...

Table 2.1 – continued from previous page.

Reagent or Resource	Conjugate	Clone	Source
Human antibodies			
CCR2	V421	LS132.1D9	BD
CD107α	PeCy7	H4A3	BD
CD27	V711	M-T271	BD
CD3	UV737	UCHT1	BD
CD4	UV496	SK3	BD
CD45RA	BB515	Hl100	BD
CD45RO	UV805	UCHL-1	BD
CD62L	647	DREG-56	BD
CD8	UV395	RPA-T8	BD
CX_3CR1	PeCy7	2A9-1	Biolegend
CXCR3	PE-CF594	1C6/CXCR3	BD
Granzyme B	AF647	GB11	Biolegend
IFNɣ	PE	B27	BD
IL-2	V711	5344.111	BD
Perforin	FITC	B-D48	Biolegend
TNFα	V510	MAb11	BD

Table 2.2: Primers

Primers used in qPCR		
Gene	**Forward primer (5' → 3')**	**Reverse primer (5' → 3')**
Rplp0	TGCAGATCGGGTACCCAACT	ACGCGCTTGTACCCATTGA
Chemokines		
Ccl1	TCCCCCAGCTGTGGTATTCAG	GGTTAGCAGGGGTTCACCTT
Ccl2	AGCTGTAGTTTTTGTCACCAAGC	GTGCTGAAGACCTTAGGGCA
Ccl3	CCATATGGAGCTGACACCCC	TCAGGAAAATGACACCTGGCT
Ccl4	GCCAGCTGTGGTATTCCTGA	TGAACGTGAGGAGCAAGGAC
Ccl5	TGCTGCTTTGCCTACCTCTC	TCCTTCGAGTGACAAACACGA
Ccl7	CCCTGGGAAGCTGTTATCTTCA	CTCGACCCACTTCTGATGGG
Ccl8	CTACGCAGTGCTTCTTTGCC	GGTGACTGGAGCCTTATCTGG
Ccl17	AGGGATGCCATCGTGTTTCT	AGGTCATGGCCTTGGGTTTT
Ccl20	GCAGAAGCAAGCAACTACGAC	CTTTGGATCAGCGCACACAG
Ccl25	AGTTCACTGATCCCATAGGCA	GGTTTAAGGGGGCCACCAAT
Ccl27	ATGAGTTACCCGAGGTCCAGTG	TACTCGTGTGACCGGATATTGC
Ccl28	AGTCATTGCCAGACTCAGTGG	CCATGGGAAGTATGGCTTCTGA
Cxcl1	ACCGAAGTCATAGCCACACTC	CTCCGTTACTTGGGGACACC
Cxcl2	TGAACAAAGGCAAGGCTAACTG	CAGGTACGATCCAGGCTTCC
Cxcl5	TGCCCTACGGTGGAAGTCAT	AGCTTTCTTTTTGTCACTGCCC
Cxcl9	TGTGGAGTTCGAGGAACCCT	AGTCCGGATCTAGGCAGGTT
Cxcl10	CCACGTGTTGAGATCATTGCC	GAGGCTCTCTGCTGTCCATC
Cxcl12	AAAGCTTTAAACAAGGGGCG	GCAGGAAGCGGGGAACTA
Cxcl16	CTTCTGGCACCCAGATACCG	AGTTCCACACTCTTTGCGCT
Xcl1	CATGGGTTGTGGAAGGTGTGG	AATTACAGCTCTCATGGCCCC
Cx_3cl1	GCGACAAGATGACCTCACGA	TGTCGTCTCCAGGACAATGG
Chemokine receptors		
Ccr1	ACTCTGGAAACACAGACTCAC	TCCTTTGCTGAGGAACTGGTC
Ccr2	AGGAGCCATACCTGTAAATGCC	TGTCTTCCATTTCCTTTGATTTGT
Ccr4	CTTTCAGAAGAGCAAGGCAGCTC	TCTGTGACCTCTGTGGCATTC
Ccr5	CCCTACAAGAGACTCTGGCTC	TTGGCAGGGTGCTGACATAC
Ccr7	CATGGACCCAGGTGTGCTT	CATGAGAGGCAGGAACCAGG
Ccr8	GCTCGCTCAGATAATTGGTCTT	GAGGAACTCTGCGTCACAGG
Ccr9	TGGAGGCTGGTCTGCATTATC	CATGCCAGGAATAAGGCTTGTG
Ccr10	AAGCCCACAGAGCAGGTCTC	GGGAGACACTGGGTTGGAAG
CX_3cr1	TCACCGTCATCAGCATCGAC	CGCCCAGACTAATGGTGACA
Xcr1	TCAAAGGAAGCACAAAGCGT	CAGGGATACTGAGAGCATCTGAC
Cxcr1	CCAGCTGGTGCCTCAGATCAA	AATAATCTCCAGTGGGCAGCA
Cxcr2	TCGTAGAACTACTGCAGGATTAAG	GGGACAGCATCTGGCAGAATA
Cxcr3	GCCATGTACCTTGAGGTTAGTGA	ATCGTAGGGAGAGGTGCTGT
Cxcr4	GAAGAGCAAGGCAGCTCAAC	GACCTCCCCAAATGCCTTGA
Cxcr5	AGGCACCAGCACAAACCTTC	AGGCCAGTTCCTTGTACAGGTC
Cxcr6	TACTGGGCTTCTCTTCTGATGC	TCGTAGTGCCCATCGTACAG

Continued on next page...

Table 2.2 – continued from previous page.

Gene	Forward primer (5' → 3')	Reverse primer (5' → 3')
S1pr1	TTCTCTTCTGCACCACCGTC	TGTTCTTGCGGAAGGTCAGG
S1pr5	CAGTCCTGGAGTAGCAACCG	GCGCTTATTTGGCGAGTCAG

Table 2.3: Virus strains

Strain	Stock concentration
A/HK-x31	2.4 x 10^4 $TCID_{50}$
A/PR8	1.8 x 10^5 $TCID_{50}$
x31-Ova	3.6 x 10^6 $TCID_{50}$
PR8-Ova	2 x 10^6 $TCID_{50}$

3 | The role of cell-intrinsic CCR2 in $CD8^+$ T cell fate and function

3.1 Introduction

The co-ordinated control of $CD8^+$ T cell movement by chemokine receptors during infection is critical for their interactions with antigen-presenting cells [39, 155, 165], homing to anatomical micro-environments to drive differentiation [291–294], infiltration of inflamed peripheral tissues [65, 76, 77], and execution of effector function [56, 66]. Although $CD8^+$ T cells responding to infection have been reported to express numerous chemokine receptors that could potentially regulate these responses, the majority of reports focus on just two of these receptors, CXCR3 and CCR5 [4]. However, inflamed lymph nodes and infected peripheral tissues express many different chemokines that have the potential to influence T cell responses [42, 56]. The extent to which these other chemokine axes influence $CD8^+$ T cell fate and function has not been fully explored. Thus, to address these gaps in knowledge and to better understand what other chemokine receptors could influence $CD8^+$ T cell responses to infection, the expression of chemokine receptors on antigen-specific $CD8^+$ T cells, and the function of novel chemokine receptor candidates, was investigated in a model of virus infection.

3.2 Chemokine receptor expression by antigen-experienced $CD8^+$ T cells

To study the chemokine-dependent regulation of T cell responses to infection, an influenza model of viral infection was used. Unlike infection models where pathogens are injected IV or IP, 'short-cutting' peripheral immune responses [295], influenza is delivered through the nasal passage and establishes a peripheral mucosal infection that develops over several days. The infection is entirely localised within the respiratory tract, with viral antigen only reaching the lung-draining mediastinal lymph node (mLN) via antigen-bearing cDCs [296]. Segregation of the site of infection, and the site of T cell priming, provides distinct locations, and processes, in which T cell migration can be assessed. T cells within the mLN must co-locate with antigen-bearing cDCs to undergo clonal expansion, and then home to inflammatory niches within SLOs for their effector differentiation [155, 165, 294]. In the periphery, effector T cells must transmigrate across the vascular endothelium and enter the lung parenchyma and airways where they must find, and eliminate, influenza-infected cells. As $CD8^+$ T cells can recognise internal viral proteins that are often more conserved across virus strains than surface proteins, memory $CD8^+$ T cell responses to heterosubtypic stains of influenza can also be assessed. Different strains of influenza are classified by expression of different surface hemagglutinin and neuraminidase proteins. As

these two surface proteins are the primary targets of the neutralising antibody response, infecting mice with one strain of influenza and then challenging with another minimises the contribution of B cells to the recall response, while still enabling the study of influenza-specific memory $CD8^+$ T cell responses during recall.

To determine which chemokine receptors are expressed by antigen-specific $CD8^+$ T cells during influenza infection, the transgenic OT-I system was used. In OT-I mice all $CD8^+$ T cells express a transgenic T cell receptor that is specific for the ovalbumin (Ova) peptide $Ova_{257\text{-}264}$, when presented in the context of the MHC-I variant H-$2K^d$ [297]. To determine the kinetics of OT-I T cell (hereafter called OT-I cells) responses to infection, 10^4 naïve OT-I cells were transferred intravenously (IV) into C57BL/6 (hereafter called B6) hosts. Twenty four hours after transfer, host mice were infected with $10TCID_{50}$ x31-Ova, a transgenic strain of the A/HK-x31 influenza virus engineered to express the $Ova_{257\text{-}264}$ peptide in the neuriminidase stalk [298], and OT-I responses to viral infection were tracked in the blood over the course of infection **(Fig. 3.1A)**. At this infectious dose mice show moderate weight loss with robust OT-I cell expansion and differentiation of effector subsets, and a sizeable memory population that enables easy quantification several weeks after infection. Responding OT-I cells were first identifiable in the blood in small numbers at day 6 post-infection, after which OT-I cell proportion and numbers steadily increased until numbers peaked at day 8 post-infection, and declined thereafter **(Fig. 3.1B-C)**.

Based on the kinetics of the response to infection, OT-I cells were FACS-sorted to high purity from the mLN (the site of priming), the blood and red pulp of the spleen (cells in transit, identified as being positive for an IV injected αTCRβ antibody), and the parenchyma of the lungs (the effector site, identified as being negative for an IV injected αTCRβ antibody), of infected mice on day 7 post-infection to screen cells for expression of chemokine receptors by qPCR **(Fig. 3.2A)**. Naïve splenic OT-I cells were used as a control to determine relative expression in activated cells. This day 7 timepoint would capture cells that are still undergoing expansion and differentiation in the mLN, as well as mature effector cells in the blood and spleen that are trafficking to the effector site, and cells that are already at the effector site, the lung parenchyma. Expression of chemokine and lipid-sensing receptors was mostly consistent across tissues, only varying in intensity of expression. Notable exceptions to this are *Cxcr4* and *Ccr8*, which had high expression in OT-I cells from the lungs but little to no expression in OT-I cells from other organs **(Fig. 3.2B-C)**. Relative to naïve OT-I cells, activated OT-I cells down-regulated *Ccr4*, *Ccr7*, *Ccr9*, *Cxcr4*, and *Cxcr5*, and transcripts encoding the lipid-sensing receptor *S1PR1*, which is important for tissue egress, while *S1PR5* was elevated in OT-I cells from all tissues, and highest in the OT-I cells in circulation. Compared to naïve OT-I cells, *Cxcr6* was elevated in OT-I cells from all tissues and highest

in OT-I cells in the lungs, where its expression may identify early Trm precursor cells [260]. *Ccr1*, *Ccr2*, *Ccr5*, *Xcr1*, and *Cxcr3* displayed strong upregulation in activated OT-I cells relative to naïve OT-I cells, with the most dramatic increase in *Ccr2*, which had a 10 $\log_2$ fold-increase in expression relative to naïve controls **(Fig. 3.2B-C)**.

3.3 Distinct patterns of chemokine ligand expression in influenza- infected lungs

Having determined which chemokine receptor transcripts were expressed by OT-I cells responding to influenza infection it was next determined which chemokines were expressed in the lungs of influenza-infected mice. A time-course was performed to screen for changes in chemokine expression in whole lung over the course of infection. Mice were infected intranasally with 10$TCID_{50}$ of x31-Ova and whole lungs from infected mice snap frozen at 0, 1, 3, 5, 7 and 9 days post-infection and processed for qPCR. Analysis of expression of transcripts encoding chemokines over the course of influenza infection revealed that the lungs of naïve mice displayed low expression of the majority of chemokines, with exceptions being *Ccl5*, *Cxcl12*, *Cxcl16* and *Cx3cl1* **(Fig. 3.3A)**, in infected mice these chemokines were either unchanged in their expression, or downregulated. Relative to naïve controls, influenza-infected mice displayed strong upregulation of chemokines commensing day 3 post-infection, with expression decreasing by day 7 post-infection **(Fig 3.3B)**. High levels of expression of chemokine mRNA in the infected lungs correlated with the presence of replicating virus as influenza nucleoprotein (NP) mRNA was detectable in the lungs only on days 1, 3 and 5 post-infection **(Fig 3.3C)**. Of the chemokines that were upregulated in the lungs following infection, genes encoding the CC-chemokines CCL2 and CCL7, and CCL3 and CCL4, ligands for the chemokine receptors CCR2 and CCR5, respectively, and the CXCR3 ligands CXCL9 and CXCL10, showed the highest extent of upregulation relative to naïve controls **(Fig. 3.3B)**. The genes encoding the CCR8 ligand CCL1 and the CCR6 ligand CCL20 also displayed intermediate expression. Because results in **Fig 3.2** indicated strong up-regulation of CCR2 on activated OT-I cells, expression of the CCR2 ligand CCL2 was investigated in more detail. CCL2 protein was detectable in the BALF from day 3 post-infection, peaking at days 7 post-infection, and elevated in mLN over the course of x31-Ova infection **(Fig. 3.3D-E))**.

3.4 CCR2 is expressed by antigen-experienced CD8$^+$ T cells in both mice and humans

The results from qPCR screens of influenza-infected mice identified a core "chemokine signature" of influenza infection in the lungs that involved upregulation of ligands for CCR2, CXCR3, CCR5, CCR8, and CXCR6, although CXCL16 was expressed only late in infection. Activated OT-I cells sorted from diverse tissues 7 days post influenza-infection were shown to express high levels of transcripts for all of these receptors. Though the receptor CCR8 had tissue-specific expression, with transcripts only elevated in OT-I cells in the lung parenchyma, there is currently no CCR8 antibody available for use in flow cytometry, complicating a comprehensive analysis of CCR8 expression and function on T cells. Transcripts for the receptor CXCR6 were also highly expressed in OT-I cells present in the lung parenchyma, however, CXCR6 has previously been shown to regulate CD8$^+$ T cell access to the airways after influenza infection [77], and so was not pursued further. Additionally, previous studies of CD8$^+$ T cells responding to infection had also demonstrated key roles for the chemokine receptors CXCR3 and CCR5 in both the formation and execution of CD8$^+$ T cell responses to infection [56, 76, 162, 291–294]. In contrast, the chemokine receptor CCR2 and its function on CD8$^+$ T cells has not been extensively investigated, despite numerous publications reporting its expression on T cells following a diverse range of infectious and non-infectious challenges [209, 299–304]. Thus, CCR2 was further investigated for a cell-intrinsic role in CD8$^+$ T cell biology, including the generation of CD8$^+$ T cell effector responses and formation of long-lived memory cells following influenza infection.

First, the earliest point of CCR2 expression on activated CD8 T cells was investigated following influenza infection. The CCR2 ligand CCL2 was present in mLN from day 4 post-infection **(Fig. 3.3E)**, which coincides with the initiation of clonal expansion for influenza-specific CD8$^+$ T cells [305]. To investigate a potential correlation between CCR2 expression and antigen-specific CD8$^+$ T cell division, and expression of activation markers, 10^6 naïve OT-I cells were labelled with a fluorescent proliferation dye and transferred into naïve host mice that were infected with 1TCID$_{50}$ PR8-Ova 24 hours later, an infection model which has well-defined T cell activation kinetics [305]. On day 4 post-PR8-Ova infection the lung-draining mLN was harvested for analysis of early-activation markers and CCR2 expression by responding T cells. By day 4 post-infection a substantial proportion of OT-I cells in the lung-draining mLN had been activated, and divided, with upregulation of the activation markers CD69, CD25, CD44 and downregulation of CD62L evident in all divided cells **(Fig. 3.4A)**. Relative to naïve, endogenous CD8$^+$ T cells, all T cells that had undergone proliferation, and a small percentage that had

not, had upregulated CCR2 **(Fig. 3.4B-D)**. The geometric mean fluorescence intensity (gMFI) for CCR2 expression in divided cells increased upon the first cell division, and by the third division OT-I cells maintained stable expression out to 5 cell divisions and beyond **(Fig. 3.4E)**. These results demonstrate that CCR2 expression increased as soon as the first division of antigen-activated OT-I cells and, therefore, has the potential to influence both their priming and effector differentiation in the mLN.

Next, CCR2 expression was assessed on $CD8^+$ T cells as they matured and exited the mLN. Mature, activated T cells begin to exit the mLN at days 5-6 post-infection and the earliest time-point at which influenza-specific T cells can be consistently detected in the blood is day 6 post-infection, with numbers peaking at around day 8 **(Fig. 3.1B)**. Thus, naïve OT-I cells were transferred into naïve host mice that were infected with $10TCID_{50}$ x31-Ova 24 hours later. Blood was taken from day 8 x31-Ova infected mice and transferred and endogenous T cells screened for expression of CCR2 by flow cytometry **(Fig. 3.5A-B)**. Of the host endogenous T cells, both $CD4^+$ and $CD8^+$ $CD44^{hi}$ T cells expressed CCR2, with the frequency of receptor-expressing cells slightly higher for $CD44^{hi}$ $CD8^+$ T cells **(Fig. 3.5B-C)**. In contrast, CCR2 expression was undetectable on naïve $CD44^-$ $CD4^+$ and $CD8^+$ T cells in the circulation **(Fig. 3.5B)**. Of the transferred OT-I cells 60% of cells in the circulation expressed CCR2 while, in contrast, both influenza nucleoprotein (NP)- and viral polymerase (PA)-specific endogenous $CD8^+$ T cells displayed the highest proportion of $CCR2^+$ cells, with 76% of NP-specific T cells expressing CCR2 and 68% of PA-specific T cells **(Fig. 3.5C)**. To assess functionality of CCR2 on $CD8^+$ T cells, cells from the spleens of influenza-infected mice were examined in *ex-vivo* chemotaxis assays with the CCR2 ligands CCL2 and CCL7 **(Fig. 3.5D-E)**. Both endogenous activated $CD8^+$ $CD44^{hi}$ T cells and OT-I cells migrated in response to CCL2 and CCL7, whereas naïve $CD8^+$ $CD44^{low}$ T cells did not. Thus, functional CCR2 is expressed on influenza-specific, and endogenous $CD44^{hi}$, but not naïve, T cells at the peak of the T cell response to influenza infection.

Having established that CCR2 is expressed by the majority of influenza-specific $CD8^+$ T cells it was next investigated if this expression during the acute phase of the response was biased to a particular $CD8^+$ effector T cell subset. Over the course of infection $CD8^+$ effector T cell subsets arise that have distinct fates upon resolution of infection, and these cells can be identified by expression of the surface markers CD127 and KLRG1 [183]. $KLRG1^+$ short-lived effector cells (SLECs) undergo complete contraction, and a portion of $CD127^+$ memory precursor effector cells (MPECs) survive to form long-lived memory cells after viral clearance [183, 306]. $KLRG1^-$ $CD127^-$ early effector cells (EECs) represent recently-activated cells that have not yet committed to an SLEC or MPEC fate, while the $KLRG1^+$ $CD127^+$ double-positive effector cells (DPECs) are a poorly understood subset that may contribute to the formation of effector-

like memory cells after resolution of the infection [307]. These cells were identified in the blood of influenza-infected mice on day 9 post-influenza infection **(Fig. 3.6A)**, as this location, and time point, has the best representation of these effector subsets. Expression of CCR2 was detectable on all of the effector subsets present in the blood, with the frequency of receptor-positive cells, and gMFI for CCR2, higher for the more effector-like CD127$^-$ KLRG1$^+$ SLEC and CD127$^+$ KLRG1$^+$ DPEC populations **(Fig. 3.6B)**. These results indicate that CCR2 expression is not restricted to a particular effector subset and may contribute to the biology of all these effector populations.

Recently, three subsets of circulating memory CD8$^+$ T cells have been characterised that have distinct patterns of re-circulation during homeostasis: central memory CD8$^+$ T cells (Tcm) that circulate through the blood and secondary lymphoid organs; effector memory CD8$^+$ T cells (Tem) that circulate through the blood and spleen; and the recently-identified peripheral memory CD8$^+$ T cells (Tpm) that circulate through the blood and secondary lymphoid organs but also have the capacity to enter uninflamed peripheral tissue [246]. These memory subsets can be identified by the co-expression pattern of the surface markers CD27 or CXCR3, with CX3CR1 [246]. A fourth, poorly-characterised, subset that lacks expression of these memory markers is also present in some models of infection [308], and may represent terminally differentiated exhausted cells [309]. As there is no nomenclature associated with this subset at the time of writing, these cells are referred to here as double-negative memory CD8$^+$ T cells (Tdn). To determine if these circulating memory cell subsets express CCR2, blood was taken from mice 35 days after influenza infection and expression of CCR2 was determined by flow cytometry **(Fig. 3.6C)**. Analysis of surface CCR2 expression on long-lived memory T cells showed that CCR2 was present on all circulating memory cell subsets with 60%-70% of CXCR3$^-$ CX3CR1$^+$ Tem and CXCR3$^+$ CX3CR1$^-$ Tcm cells expressing CCR2. The surface expression of CCR2 was highest on CXCR3$^+$ CX3CR1$^+$ Tpm cells where 80% of these cells expressed CCR2 **(Fig. 3.6D)**. Like those results seen in the effector subsets present at day 9 post-infection, CCR2 expression is present to some degree across all memory CD8$^+$ T cell subsets, and is higher on the more effector-like memory subset. In contrast to circulating memory cells, only 20% of CD69$^+$ CD103$^+$ tissue-resident memory T cells in the lungs, which do not recirculate throughout the body but are confined to the tissue in which they are generated, expressed CCR2. Taken together, these experiments demonstrate that CCR2 is expressed on all long-lived CD8$^+$ memory subsets with expression highest on circulating memory T cells that posses the capacity to migrate into peripheral tissue.

Data generated thus far indicated that murine CD8$^+$ effector and memory T cells expressed CCR2 in response to viral infection. To expand the relevance of these observations a limited number

of experiments were conducted to determine if humans also had an equivalent population of CCR2-expressing T cells. Blood was taken from healthy donors and processed to enrich for peripheral blood mononuclear cells (PBMCs) for use in flow cytometry. Live $CD3^+$, $CD4^+$ and $CD8^+$ T cells were gated based on CD45RA and CD45RO expression to identify naïve ($CD45RA^+$) and effector / memory ($CD45RO^+$) T cells **(Fig. 3.7A)**. Similar to those results seen in mice, naïve $CD45RA^+$ $CD4^+$ and $CD8^+$ T cells did not express CCR2, and both $CD4^+$ and $CD8^+$ antigen-experienced T cells expressed CCR2 with around 40% of $CD45RO^+$ $CD4^+$ and $CD8^+$ T cells expressing the receptor. The majority of the CCR2-expressing $CD8^+$ T cells were $CD45RA^+$ $CD45RO^+$ cells, and while this double-positive subset in the $CD4^+$ gate also expressed CCR2, its surface expression and gMFI was lower than the CD45RO single positive subset **(Fig. 3.7B-C)**.

Results from the flow cytometry screen of CCR2 expression on murine memory $CD8^+$ T cells demonstrated that all subsets of circulating memory $CD8^+$ T cells expressed CCR2, with expression highest on Tpm cells **(Fig. 3.6C-D)**. Next, human T cells were stained for CD27 and CX3CR1 to determine if the CCR2 expression pattern seen in mice also applied to human circulating memory T cells **(Fig. 3.7D)**. However, unlike the data observed in mice, surface expression for CCR2 was highest in Tcm cells and the poorly-defined Tdn cells, of which humans have a much larger population than in influenza-infected mice **(Fig. 3.7D-E)**. Around 60-70% of Tcm cells and Tdn cells expressed CCR2 while only 15% of Tpm cells and 5% of Tem cells expressed CCR2 **(Fig. 3.7D-E)**. These results suggest that, in humans, expression of CCR2 is lost as memory cells become more terminally-differentiated and effector-like in phenotype. However, further analysis of the lymph node homing markers CCR7 and CD62L on $CCR2^+$ and $CCR2^-$ Tcm cells revealed that cells expressing CCR2 had lower expression of these lymph node homing markers **(Fig. 3.8A-C)**. Additionally CCR2-expressing Tcm cells had lower expression of the chemokine receptor CXCR3 **(Fig. 3.8A-C)**, which is associated with memory cells that retain a higher degree of stemness [294]. Together, these results contrast to that observed in murine memory T cells, where generally the more terminally-differentiated a population of memory $CD8^+$ T cells is, the higher the level of expression of CCR2 observed in that population [310]. However, in both mice and humans CCR2 is expressed by Tcm cells and, to a lesser degree, in Tpm cells, and, similar to effector cells, CCR2-expressing Tcm cells had lower expression lymph node homing markers.

3.5 Monocytes and monocyte-derived cells are the major producers of CCL2

Results thus far demonstrated that CCR2 was highly expressed across $CD8^+$ T cell effector and memory subsets, that transcripts for the ligands were highly expressed in the influenza infected lungs, and that CCL2 protein is present in the airways and lung-draining mLN after influenza infection. Next, to better determine the cellular source of one of the main CCR2 ligands, CCL2, and identify cell types with which CCR2-expressing $CD8^+$ T cells may be interacting via this axis, CCL2-RFP mice, in which all CCL2-producing cells also express a red fluorescent protein (RFP) that accumulates in the cytoplasm, were infected with A/HK-x31. Lungs and mLNs were harvested from CCL2-RFP mice on days 0, 3, 5, 7, 9 and 11 post A/HK-x31 infection and single cell suspensions were analysed for expression of RFP. Initial investigations found that cells expressing the T cell lineage markers CD3 and TCRα, the pan T cell and ILC marker CD90, the B cell lineage marker CD19, and the natural killer cell marker NK1.1, did not express RFP during A/HK-x31 infection, and these cells were excluded from further analyses **(Fig. 3.9B)**. The remaining analysis focused on live, lineage-negative (CD3, TCRα, CD90, CD19, NK1.1), $CD45^+$ myeloid cells present in the lungs and mLN **(Fig. 3.9A)**. Of the cells analysed, eosinophils were identified as Siglec F^+ $CD11c^-$, alveolar Mϕ as Siglec F^+ $CD11c^+$ and neutrophils were gated as Siglec F^- $Ly6G^+$ $CD64^-$. Conventional dendritic cells were identified as $CD64^-$ $CD11c^+$ MHC-II^+ and $XCR1^+$ $CD11b^-$ for cDC1s and $XCR1^-$ $CD11b^+$ for cDC2s. Non-classical monocytes were identified as $Ly6G^-$ $CD64^+$ $Ly6C^{low}$ $CD43^+$ with the remaining cells a mixture of monocytes and Mϕ. Monocytes are highly plastic cells that are capable of differentiation into Mϕ after entering inflamed tissue, which involves upregulation of MHC-II and MerTK and gradual downregulation of Ly6C [311, 312]. These monocytes are defined here as: $Ly6C^+$, MHC-II^- monocytes, $Ly6C^+$, MHC-II^+ monocyte-derived Mϕ, and $Ly6C^-$, MHC-II^+ tissue Mϕ **(Fig.3.9A)**.

Alveolar Mϕ are highly autofluorescent and so were analysed separately based on Siglec F and CD11c expression **(Fig. 3.9A)**. Analysing this population separately, alveolar Mϕ did not display any expression of the reporter between days 0 and 5 post-infection **(Fig. 3.10A)**. However, a small percentage of alveolar Mϕ in the lungs were RFP positive on days 7 and 9 post-infection, and the majority of alveolar Mϕ at day 11 were RFP^+, timepoints at which the infection is resolving. These are likely monocyte-derived alveolar Mϕ that replace apoptotic alveolar Mϕ after influenza infection [96]. Analysing the remaining $lineage^-$, alveolar $M\phi^-$, $CD45^+$ and $CD45^-$ cells over the course of A/HK-x31 infection revealed that there was minimal RFP expression in the lungs on days 0, 1 and 3 post-infection

with a substantial population of $CD45^+$ cells in the lungs expressing RFP by day 5 post-infection **(Fig. 3.10B)**. This expression peaked at day 7 where approximately 36% of live, lineage-negative, cells were RFP^+, the frequency and total number of RFP^+ cells declined thereafter but were still apparent at 11 days post-infection **(Fig. 3.10B and D)**. In the lung-draining mLN there was a small increase in the frequency of $CD45^+$ RFP^+ cells on day 5 post-infection, but the expression did not reach the levels present in the lungs at any of the time-points analysed **(Fig. 3.10C)**. Unlike the RFP^+ cells in the lungs, which peaked on day 7 post-infection, the frequency and total number of RFP^+ cells in the mLN peaked at day 5 post-infection, after which the number and frequency of RFP^+ cells declined until day 11 post-infection where they showed a late resurgence in both frequency and number **(Fig. 3.10E)**.

A more detailed analysis of the reporter-positive cells in the lungs on days 5, 7, 9 and 11 post primary A/HK-x31 infection using the gating strategy outlined in **Fig. 3.9A** revealed that the overwhelming majority of reporter-positive cells were $CD64^+$ monocytes and monocyte-derived cells, with other cells, including cDCs, $CD45^-$ stromal cells and granulocytes compromising less than 5% of total RFP^+ cells **(Fig. 3.10F)**. Early in the A/HK-x31 response RFP^+ cells were mostly monocytes and monocyte-derived Mϕ and, as the response progressed and the virus was cleared, these monocytes likely differentiated into alveolar Mϕ and tissue macrophages that sustained expression of the reporter [96]. Analysis of RFP gMFI over the course of infection demonstrated that monocyte-derived Mϕ displayed the most intense expression of the reporter, peaking at day 7 post-infection, which would coincide with the arrival of T cells from the circulation, and the clearance of virus. The RFP gMFI declined in monocyte-derived Mϕ after day 7 post-infection, but was increased in alveolar Mϕ from day 7 through 11 post-infection **(Fig. 3.10G)**. Calculating the total number of RFP^+ cells revealed that on days 5 and 7 post-infection the dominant CCL2-producing cells were monocytes and monocyte-derived cells, however, after day 7 post-infection these RFP^+ cells decline in number while there was a concomitant increase in the number of RFP^+ tissue Mϕ, and at day 11 post-infection, an increase in the number of RFP^+ alveolar Mϕ **(Fig. 3.10H)**. Together, these data identify monocytes and monocyte-derived cells as the major CCL2-producing cell type in the influenza infected lungs.

3.6 Investigation of the cell-intrinsic requirement for CCR2 in the CD8$^+$ T cell effector response to influenza

Results thus far had shown that the chemokine receptor CCR2 was expressed on CD8$^+$ T cells that were responding to influenza infection. The receptor was expressed very early in T cell activation, within the first division, and maintained broad expression on effector and memory T cell subsets. To determine if there was any cell-intrinsic role for CCR2 in the development of antiviral effector CD8$^+$ T cell responses, *Ccr2*$^{-/-}$ mice were crossed with OT-I mice to generate *Ccr2*$^{-/-}$ OT-I mice and WT OT-I littermate controls for use in *in vivo* competitive transfer experiments. To confirm genetic deletion of CCR2 in OT-I cells, 10^4 WT and *Ccr2*$^{-/-}$ OT-I cells were co-transferred into B6 hosts that were infected with x31-Ova 24 hours later. On day 9 post x31-Ova infection, *Ccr2*$^{-/-}$ OT-I cells in the blood displayed no significant expression of the receptor CCR2 when stained with the monoclonal αCCR2 antibody MC-21, demonstrating both the faithful deletion of *Ccr2* and the specificity of the αCCR2 mAb **(Fig. 3.11A-B)**. *Ccr2*$^{-/-}$ OT-I cells taken from the spleens of day 14 x31-Ova-infected mice were also unable to migrate in response to the CCR2 ligand CCL7 in an *ex-vivo* chemotaxis assay **(Fig. 3.11C-D)**, but were as capable of migrating to the CXCR3 ligand CXCL11 **(Fig. 3.11E)**, confirming loss of CCR2 function.

To determine if the loss of CCR2 impacted the generation of OT-I effector responses, and the formation of long-lived memory populations, 10^4 WT (CD45.1$^+$) and *Ccr2*$^{-/-}$ (CD45.1$^+$ CD45.2$^+$) OT-I cells were co-transferred into naïve B6 hosts that were infected with 10TCID$_{50}$ x31-Ova 24 hours later **(Fig. 3.12A)**. Prior to sacrifice mice were injected with 3μg of αTCRβ IV to allow discrimination between OT-I cells that were present in the vasculature of the lung and the lung parenchyma [313], and the white and red pulp of the spleen [43]. WT and *Ccr2*$^{-/-}$ OT-I effector responses were assessed on day 9 post-infection, the peak of OT-I cell expansion, in lymphoid organs (mLN, splenic white pulp), effector sites (NALT, trachea, airways, lung parenchyma (lungs IV$^-$)), and in circulation (peripheral blood, lung vasculature (lungs IV$^+$), splenic red pulp) **(Fig. 3.12B)**. At day 9 post-infection OT-I cell numbers and frequencies were equal between WT and *Ccr2*$^{-/-}$ OT-I cells in all tissues analysed with the exception of the airways, where there was a slightly higher frequency of WT OT-I cells recovered from BAL washes compared to *Ccr2*$^{-/-}$ **(Fig. 3.12C)**, although this difference in frequency did not translate into a significant numerical difference **(Fig. 3.12D)**. These data suggest that CCR2 is not required for initial OT-I cell expansion after infection. These data also suggest that CCR2 is largely dispensable for OT-I cell recruitment to peripheral tissues, although the data suggest that CCR2 may contribute to CD8$^+$ T cell migration from the lung parenchyma into the airways.

During activation T cells can receive signals that predispose them to a terminal effector fate or prepare them to transition into long-lived memory cells [131, 183], and chemokine receptors have been shown to influence this process by regulating exposure to inflammatory signals [162, 291–294]. On day 9 post-influenza infection, a time point at which the different $CD8^+$ effector T cell subsets are all well represented, the differentiation of effector subsets was analysed for WT and *Ccr2*$^{-/-}$ OT-I cells using the gating strategy outlined in **(Fig. 3.13A)**. In the IV^+ fractions analysed (PB, lung vasculature and red pulp of the spleen), there was a slight increase in the frequency of SLECs at the expense of the MPEC population in *Ccr2*$^{-/-}$, compared to WT, OT-I cells **(Fig. 3.13B)**. This difference was not observed in the IV^- fractions (mLN, splenic white pulp, trachea, NALT, BALF), which have a much smaller population of SLECs and much higher frequency of MPECs. These differences in the IV^+ fraction did not translate into a numerical difference for any of these subsets, however, a small but statistically significant reduction in the number of EECs and MPECs present in the white pulp of the spleen and in the number of EECs present in the BALF was seen for *Ccr2*$^{-/-}$, compared to WT, OT-I effector cell populations **(Fig. 3.13B)**. Initial characterisation of CCR2 expression on OT-I effector subsets identified higher frequencies of CCR2-expressing SLECs compared to MPECs and EECs **(Fig. 3.6B)**. The increased frequency of *Ccr2*$^{-/-}$ OT-I SLECs detected in IV^+ fractions could reflect a defect in the ability of these cells to migrate from the circulation into the lungs in the absence of CCR2. To test this, the ratio of vascular-labelled to unlabelled cells was determined for WT and *Ccr2*$^{-/-}$ OT-I cells in the lungs and spleen **(Fig. 3.14A)**. A defect in migration would present as a lower ratio of IV^- to IV^+ *Ccr2*$^{-/-}$ OT-I cells relative to WT OT-I cells in these anatomical compartments. Vascular labeling of OT-I cells, however, did not identify a difference in the ratio of total labelled to unlabelled OT-I cells in either the spleen or lungs **(Fig. 3.14B)**. However, when comparing the ratios of IV-labelled effector subsets, there was an increase in the ratio of parenchymal OT-I MPECs in the lungs and a decrease in the ratio of IV-labelled SLECs in the spleen for *Ccr2*$^{-/-}$ OT-I cells **(Fig. 3.14C)**. These results indicate CCR2 expression may deter MPECs from accessing the lung parenchyma, and contribute to SLEC egress from the white pulp of the spleen.

Lastly, the effector potential of WT and *Ccr2*$^{-/-}$ OT-I cells was determined. Virus-specific T cells upregulate the effector cytokines IFNγ[314], IL-2 [315, 316], TNFα [317] and the cytotoxic molecule granzyme B [314] after activation and differentiation, enabling them to execute their effector function. To determine if CCR2-deficiency altered the acquisition of effector potential, single-cell suspensions from the lungs, spleen and mLN were restimulated *ex vivo* with SIINFEKL in the presence of protein transport inhibitors and screened for granzyme B and cytokine expression by flow cytometry **(Fig. 3.15A)**. OT-I cells present in the lungs displayed a lower frequency of cells expressing, and gMFI, of the effector cytokines IFNγ, TNFα and IL-2 compared to cells present in SLOs, although OT-I cells in the

lungs did exhibit a higher level of expression of the cytotoxic molecule granzyme B. However, there were no statistically significant differences in the percentage of cytokine expression between WT and *Ccr2*$^{-/-}$ OT-I cells or in the gMFI for each of those cytokines, indicating normal acquisition of effector potential **(Fig. 3.15B-C)**. Together, these data demonstrate that there is no cell-intrinsic role for CCR2 in the generation of primary effector OT-I responses to influenza infection.

3.7 Investigation of the cell-intrinsic requirement for CCR2 in the generation of memory populations

The data in the previous section indicated that the absence of CCR2 on antigen-specific CD8^{+} T cells had a minor impact on the acute phase of the response to x31-OVA, more specifically on the development of effector populations present in the spleen, vasculature and BALF, and in the distribution of some effector subsets within the vasculature and tissue parenchyma. Mice were subsequently analysed 35 days post-infection to determine if these minor differences observed on day 9 post-infection had any impact on the generation of long-lived memory populations **(Fig. 3.16A)**. Memory T cells have broad distribution following the resolution of infection, occupying both tissues that were affected by the initial infection, and seeding distal tissues that were not impacted [278, 318]. At the memory time point chosen (day 35 post-x31-Ova infection, mice at this timepoint are hereafter referred to as resting memory mice) the distribution of memory T cells was equivalent throughout the airways, circulation, proximal and distal SLOs, and the bone marrow **(Fig. 3.16B-C)**. Some peripheral tissues, such as the skin, skin draining lymph nodes, and visceral adipose tissue have been reported to express CCR2 ligands at homeostasis and were investigated as potential site of memory T cell homing [74, 133, 319]. However, the frequency and total number of OT-I cells recovered from these organs was also unaffected by the absence of T cell expression of CCR2 **(Fig. 3.16C-D)**.

As indicated in section **3.4**, long-lived memory cells that develop after infection can by classified based on their migratory properties at homeostasis, with subsets of circulating memory cells that have distinct patterns of re-circulation [246], and resident memory T cells that are restricted to peripheral tissues [235]. Resident memory cells can be identified in the IV^{-} fractions of peripheral tissues and typically express the markers CD69 and CD103, as outlines in the gating strategy in **Fig. 3.17A**. After influenza infection Trm cells were identified throughout the entirety of the respiratory tract: in the NALT, trachea, airways and lung tissue and can be found in the lung-draining mLN, but not distal lymph

nodes **(Fig. 3.17B)**. In resting memory mice, equivalent frequencies of WT and *Ccr2*$^{-/-}$ Trm cells were present in the NALT and trachea where, as a frequency of total OT-I cells, the highest percentage of Trm cells was detected. In the lower airways and lung parenchyma no difference was also observed in the frequency of Trm cells **(Fig. 3.17B-C)**. The frequency of mLN Trm cells was also equivalent between WT and *Ccr2*$^{-/-}$ OT-I cells, with these cells absent from the non-draining mesenteric lymph nodes (MLN) **(Fig. 3.17B-C)**. Moreover, the total number of Trm cells recovered from these organs was equivalent for WT and *Ccr2*$^{-/-}$ OT-I cells **(Fig. 3.17D)**. These data do not support a role for CCR2 in the development of resident memory T cells that populate the upper and lower respiratory tract, and lung-draining lymph nodes.

As stated in section **3.4**, The markers CD27 or CXCR3 alongside CX3CR1 can be used to identify distinct populations of circulating memory cells [246]. When staining total memory T cell populations, resident memory T cells appear as CD27^{+} CX3CR1^{-} central memory T cells and can be excluded from analyses by pre-gating on Ly6C^{+} cells in in all tissues [278], as outlined in the gating strategy in **Fig. 3.18A**. The majority of peripheral and effector memory cells were localised to tissues that are susceptible to intravascular labelling: the PB, splenic red pulp, lung vasculature and the bone marrow **(Fig. 3.18B)**. The mLN and white pulp of the spleen contained mostly Tcm cells and a small percentage of Tpm cells but were largely devoid of Tem cells, consistent with the notion that these cells are excluded from SLOs at homeostasis [246]. The parenchyma of the lungs contained mostly Tcm cells, with only a small frequency of the tissue-patrolling Tpm cells. Whether these Tcm cell are actively patrolling the lung tissue or are transiently present in tertiary lymphoid organs that persist in the lungs after influenza infection is not clear [320, 321]. Across all tissues there were equivalent frequencies and numbers of WT and *Ccr2*$^{-/-}$ circulating memory OT-I cells **(Fig. 3.18B)**. Taken together, these results show that there is no cell-intrinsic requirement for CCR2 in the establishment of resident or circulating memory T cells following influenza infection.

Next it was determined if resting memory populations retained equivalent effector potential. Single-cell suspensions from the lungs, spleen and mLN were restimulated *ex-vivo* with SIINFEKL in the presence of protein transport inhibitors to determine expression of effector cytokines and granzyme B **(Fig. 3.19A)**. The frequency of OT-I cells expressing, and gMFI for, effector cytokines and granzyme B was much lower in memory OT-I cells present in the lungs compared to those at peak T cell expansion **(Fig. 3.15)**. OT-I cells isolated from SLOs had the highest production of the effector cytokines IL-2, IFNγ and TNFα, but negligible expression of granzyme B **(Fig. 3.19B-C)**. However, in all these organs WT and *Ccr2*$^{-/-}$ resting memory OT-I cells had no significant differences in their ability to produce effector

cytokines after *ex vivo* restimulation.

3.8 Investigation of the requirement for CCR2 in tissue infiltrating memory CD8$^+$ T cells

Results thus far indicate that, under the conditions tested, the chemokine receptor CCR2 exerts only a minor influence on the development of the CD8$^+$ T cell effector response and had no impact on the development of memory. However, analysing the distribution of effector subsets 9 days after x31-Ova infection by intravascular labelling did reveal a potential role for CCR2 in the trafficking of effector cells during advanced inflammation **(Fig. 3.14C)**. Of relevance, CCR2 also displayed higher expression on all circulating memory T cell subsets relative to resident memory cells from the lung parenchyma **(Fig. 3.6D)**, suggesting it may have a more important function for the recruitment of highly-motile cells. These migration and CCR2 expression patterns led to the hypothesis that CCR2 is required for circulating memory CD8$^+$ T cells to access inflamed peripheral tissue during the early stages of inflammation. In support of this hypothesis, it has previously been demonstrated that CCR2 is required on human effector CD8$^+$ T cells to cross inflamed endothelial layers in an *in vitro* model of transendothelial migration [34]. In the present study, data obtained from the primary response to x31-OVA infection demonstrated that transcripts for the chemokines CCL7 and CCL2 were rapidly expressed in the lungs, and CCL2 protein was detected very early after infection, both in the BALF and lung-draining mLN **(Fig 3.3)**. In a recall setting, CCR2-expressing circulating memory cells could potentially exploit this axis to enter the lungs and airways as a means of rapidly accessing inflamed tissue. In addition, *in vivo* data has shown a role for CCL2 in early monocyte recruitment to inflamed lymph nodes, where ACKR1 expressed on HEVs is capable of transporting lymph-borne CCL2 to the lumen of blood vessels, which promotes monocyte infiltration into lymph nodes draining inflamed tissue [13, 14]. This represents a potential mechanism that could promote recruitment of CCR2-expressing Tcm and Tpm cells to inflamed lymph nodes. Thus, a potential role for CCR2 in the recruitment of circulating memory T cells into inflamed tissue upon influenza challenge was investigated.

First, the kinetics of CCL2-expression was determined during A/PR8 challenge of A/HK-x31 immunised CCL2-RFP mice. CCL2-RFP mice were challenged with 100TCID$_{50}$ A/PR8 35 days post-A/HK-x31 infection, and the frequency of RFP$^+$ cells in the lungs and mLN was assessed by flow cytometry. As alveolar Mϕ are highly autofluorescent, this population was analysed separately for

reporter expression, as previously in **Fig 3.10**. In contrast to that observed in primary A/HK-x31-infection, CCL2 was expressed much earlier in alveolar Mϕ, within 48 hours of A/PR8 challenge **(Fig. 3.20A)**. This expression increased through days 3 and 5 post-infection, a time point by which the majority of alveolar Mϕ were RFP^+. Analysis of the remaining $lineage^-$ alveolar $M\phi^-$ $CD45^+$ and $CD45^-$ cells in the lungs revealed that, unlike in primary A/HK-x31 infection, CCL2 was expressed within the first 48 hours of A/PR8 challenge. However, consistent with the primary infection, RFP in the lungs and mLN was exclusively expressed by $CD45^+$ cells **(Fig. 3.20B)**. In the lungs, expression of RFP was established early, and although the frequency of RFP^+ cells among live lineage-negative cells began to decline by day 5, a large but stable population of CCL2-reporting cells was seen from days 2 to 5 post challenge **(Fig. 3.20C)**. In the primary response there was minor expression of RFP in $CD45^+$ cells isolated from the mLN **(Fig. 3.10C)**, however, in the recall setting there was a substantial population of RFP^+ $CD45^+$ cells apparent on day 3 post-challenge that did not persist to day 5 **(Fig. 3.20D-E)**. A closer analysis of those cells in the mLN that were RFP^+ upon A/PR8 challenge revealed that the majority were $CD64^+$ $Ly6C^+$ monocyte-derived cells **(Fig. 3.20F)**. Though a large portion of these cells expressed the Mϕ marker MerTK, the high expression of Ly6C indicates that these cells are monocyte-derived infiltrating cells and not Mϕ resident within the mLN [322]. A more detailed analysis of the RFP^+ cells that were present in the lungs during A/PR8 challenge revealed that, similar to the primary response to A/HK-x31, the majority of the RFP^+ cells were monocytes and monocyte-derived cells **(Fig. 3.20G)**. Like the primary response, the majority of RFP^+ cells at the early stages of infection were monocytes however, as the response progressed, monocyte-derived Mϕ, tissue Mϕ, and alveolar Mϕ became the more dominant sources of CCL2, which was reflected in both the gMFI for RFP and the total number of RFP^+ cells present in the lungs **(Fig. 3.20H-I)**. Thus, these results demonstrate that CCL2 is expressed within 48 hours of A/PR8 challenge in both the lungs and mLN, though only transiently in the latter, and in both organs RFP was almost exclusively expressed by monocyte-derived cells.

To assess the requirement for CCR2 in the trafficking of memory T cells during infection, mice that had received WT and *Ccr2*$^{-/-}$ OT-I cells and had been infected with x31-Ova 35 days prior were challenged with A/PR8 and the movement of memory OT-I cells tracked over the course of A/PR8 challenge. Prior to the A/PR8 challenge experiments it was determined if CCR2 was involved in the homeostatic trafficking of circulating memory $CD8^+$ T cells through peripheral tissues. The surface protein Ly6C can be used as a surrogate marker to identify T cells that are transiently migrating through a tissue, from those that are resident [323]. Thus, memory OT-I cells in SLOs and peripheral tissue were stained for the putative resident-cell marker CD69 and for the circulating-cell marker Ly6C as represented in **Fig. 3.21A**. As expected, under homeostatic conditions nearly all the cells present in the

spleen, PB, bone marrow, MLN and lung vasculature expressed the marker Ly6C. Only half of the cells present in the mLN expressed Ly6C, with the remaning 50% likely resident memory cells that migrate into this organ after infection **(Fig. 3.17)**. In contrast, cells present in the NALT, trachea, airways, lung parenchyma and skin only had small populations of Ly6C$^+$ cells, where the majority of the cells in these tissue are resident memory. Comparison of Ly6C expression between WT and *Ccr2*$^{-/-}$ OT-I cells revealed no difference in the frequency of these cells in any of the tissues analysed **(Fig. 3.21B)**, indicating that CCR2 is not involved in the homeostatic trafficking of these cells.

As the homeostatic trafficking of circulating memory T cells was unaltered in the absence of CCR2 the kinetics of OT-I memory cell migration during influenza challenge was next determined. As the intention of these experiments was to measure the recruitment of memory T cells into inflamed tissue, the non-transgenic A/PR8 virus was used in challenge experiments. This method generates inflammation in the lung, without the confounding presence of OT-I cell cognate antigen. Thus, any increase in OT-I cell number in the lung is likely due to recruitment, rather than recruitment and *in-situ* proliferation. WT OT-I cells were transferred into B6 hosts that were infected with x31-Ova and left for 35 days to develop memory populations (hereafter referred to as OT-I-immune mice). OT-I-immune mice were challenged with A/PR8 and the number of OT-I cells in the respiratory tract, mLN, spleen, bone marrow and peripheral blood was determined on days 0 (no challenge), 2, 3 and 5 post-challenge **(Fig. 3.22A)**. By day 2 post-challenge there were statistically significant increases in the number of OT-I cells present in the lungs and lung-draining mLN, and by day 3 post-challenge there was significant infiltration of the airways. OT-I cell numbers in the lung parenchyma peaked by day 3 post-challenge, and by day 5 OT-I cell numbers in the lungs began to decline. In contrast, the spleen, which holds the largest reservoir of circulating memory T cells, BM and PB saw a major reduction in the number of OT-I cells present between 0 and 48 hours. The OT-I cells present in the lung parenchyma and airways from day 2 post challenge were mostly Ly6C$^+$, identifying them as tissue infiltrating cells **(Fig. 3.22B)**. Despite the increase in OT-I cell number in the mLN there was a reduction in the frequency of Ly6C$^+$ cells on day 3, which may be due Trm cells that had been dislodged from the lungs upon inflammation migrating into this SLO [276, 277]. To determine how these migration kinetics compared with the expression of inflammatory chemokines and the presence of replicating virus, lung tissue was collected over the course of A/PR8 challenge of A/HK-x31 immunised mice, and processed to obtain cDNA for use in qPCR. Screening for the expression of inflammatory chemokine transcripts in the lungs after A/PR8 challenge revealed acute expression of the chemokines CCL2 and 7 and CXCL9 and 10 that peaked by day 3 post challenge relative to un-challenged mice, and rapidly declined thereafter **(Fig. 3.22C)**. The expression of these chemokines was tightly coupled to the presence of replicating virus, as influenza

NP mRNA was only detectable on days 1 and 3 post-challenge **(Fig. 3.22D)**. The expression of these chemokine transcripts also correlated with the recruitment of circulating memory T cells, with numbers of lung-infiltrating T cells peaking at the same time as inflammatory chemokine transcripts **(Fig. 3.22A and C)**. Together, these data demonstrate that within 48 - 72 hours of non-anamnestic A/PR8 challenge memory OT-I cells are recruited into the inflamed lungs and lymph nodes.

To demonstrate that the migration of memory OT-I cells into inflamed tissue was dependent on the action of GPCRs, these receptors were inhibited with pertussis toxin (Ptx). Ptx inhibits the activation of the Giα protein subunit of GPCRs, including chemokine receptors. This prevents the signalling cascade that would normally result from GPCR ligand binding, leading to cell migration [324]. Memory OT-I cells were enriched from the spleens of OT-I-immune mice, these cells were labelled with different concentrations of eFluor 670 proliferation dye and treated with either Ptx, or control media **(Fig. 3.23A)**. Treated OT-I cells were washed extensively, mixed at a 1:1 ratio and transferred IV into day 6 A/PR8 infected host mice. Mice were left overnight before receiving 3μg of TCRβ IV to label vascular cells and the migration of Ptx-treated and untreated cells into the inflamed lungs and lymph nodes was assessed. Ptx-treated cells were completely absent from the airways, the lung parenchyma, and mLN of A/PR8-infected hosts **(Fig. 3.23A-B)**. There was also a significant reduction of Ptx-treated cells in the white pulp of the spleen, which requires chemokine receptor signalling to access [43]. In contrast, Ptx-treated cells were over-represented in the vasculature of the lungs, the red pulp of the spleen and the PB. These results demonstrate that the migration of circulating memory cells from the circulation into inflamed tissue and SLOs is almost entirely dependent on GPCR signalling.

Having determined the recall kinetics of memory OT-I cells and their reliance on Giα-dependent GPCR signalling to achieve this, the potential involvement of CCR2 in this process was next determined. Naïve WT and *Ccr2*$^{-/-}$ OT-I cells were co-transferred into naïve B6 hosts that were infected with x31-Ova 24 hours later and left for 35 days to develop resting memory populations. These x31-Ova immune mice were challenged with 100$TCID_{50}$ A/PR8 and the movement of WT and *Ccr2*$^{-/-}$ memory OT-I cells tracked on days 0, 2, 3 and 5 post-challenge. At all time points mice received 3μg of TCRβ IV prior to sacrifice to distinguish between cells in the vascualture and tissue parenchyma. The upper and lower respiratory tracts as well as the blood and distal and proximal peripheral SLOs were harvested and the frequency of WT and *Ccr2*$^{-/-}$ OT-I cells was quantified for each compartment **(Fig. 3.24A-B)**. To investigate a potential impact of CCR2 on migration, the ratio of WT to *Ccr2*$^{-/-}$ OT-I cells was determined for each organ on each of the days post-challenge and normalised to the ratio of WT to *Ccr2*$^{-/-}$ cells in un-challenged mice. Using this analysis, a role for CCR2 in regulating tissue-infiltration would present

as an increase in the ratio of WT to *Ccr2*$^{-/-}$ cells in inflamed tissue and a corresponding decrease in the ratio of WT to *Ccr2*$^{-/-}$ cells in the circulation and potentially distal, un-inflamed, tissue. In these recall experiments the ratio of WT to *Ccr2*$^{-/-}$ OT-I cells was mostly similar to those seen in un-challenged mice **(Fig. 3.24B)**. A notable exception was the vasculature of the lungs and the red pulp of the spleen where there was a statistically significant increase in the frequency of *Ccr2*$^{-/-}$ OT-I cells relative to WT at all timepoints post-challenge. This statistically significant difference was also seen in the bone marrrow, but only on day 5 post-challenge and was not observed in the peripheral blood of mice **(Fig. 3.24B)**. Cells recovered from the BALF also displayed a small but statistically significant increase in the ratio of WT to *Ccr2*$^{-/-}$ OT-I cells on day 3 post challenge. Based on the kinetics defined in **Fig 3.22A**, this supports a potential role for CCR2 in promoting migration of OT-I cells from the lung parenchyma into the airways, which was also apparent during at the peak of the OT-I response to primary x31-Ova **(Fig. 3.12)**. The lung parenchyma and mLN, which had significant infiltration of memory cells during recall, did not exhibit an increase in the ratio of WT to *Ccr2*$^{-/-}$ cells, suggesting that CCR2 was not required for memory cells to access these inflamed tissues. There was also no difference in the infiltration of WT and *Ccr2*$^{-/-}$ OT-I cells into the trachea and NALT, which had poor infiltration of circulating memory cells during initial kinetics experiments. These results provide further evidence for a CCR2-dependent role in CD8^{+} T cell recruitment to the airways, but suggest that the receptor CCR2 is dispensible for memory CD8^{+} T cell infiltration into inflamed lung parenchyma and mLN.

As the influenza challenge model represents a highly inflammatory infection, it was hypothesised that multiple redundant inflammatory chemokine axes were available to circulating memory CD8^{+} T cells that could promote tissue infiltration in the absence of CCR2. Thus, to determine if CCR2 had a more important role in CD8^{+} T cell migration in a less inflammatory setting, a model of cutaneous inflammation that produces transient inflammation with restricted production of chemokines was developed by injecting cytokines into ear pinna of mice. The cytokines IL-1α, IL-1β, and TNFα were chosen due to their known roles in initiating inflammatory responses in peripheral tissues. IL-1α and IL-1β can both be released by cells following PRR-dependent inflammasome activation, with IL-1α also released by damaged and stressed cells without the need for inflammasome-dependent pre-processing for its biological activity [325], while TNFα can be secreted by a number of tissue-resident myeloid cells in a cytokine- or PRR-dependent manner to amplify local immune responses. To determine if OT-I cell migration was dependent on CCR2 in this model of cytokine-induced inflammation, WT and *Ccr2*$^{-/-}$ OT-I cells were transferred into B6 hosts that were infected with x31-Ova 24 hours later. Influenza infected mice were left to generate populations of resting memory OT-I cells and, 35 days following x31-Ova infection, mice were injected in the ear pinna with combinations of the cytokines IL-1α, IL-1β,

and TNFα **(Fig. 3.25A)**. To determine if there was a requirement for CCR2 in OT-I cell infiltration into cytokine-injected ears, 48 hours after cytokine injection mice were injected with 3μg of αCD45 IV 3 minutes prior to sacrifice to label vascular cells, and the ratio of IV^- to IV^+ WT and *Ccr2*$^{-/-}$ OT-I cells present in the ear tissue was compared to the ratio in the blood to determine how efficiently these cells migrated from the circulation into cytokine-treated ears **(Fig. 3.25B)**. Injection of IL-1β alone did not drive sufficient OT-I cell migration into the ear to enable reliable quantification, however, injection of TNFα alone, or TNFα in combination with IL-1β, resulted in robust OT-I cell infiltration into the ears that was equivalent between WT and *Ccr2*$^{-/-}$ OT-I cells. In contrast, injection of IL-1α alone resulted in significantly higher infiltration of WT OT-I cells compared to *Ccr2*$^{-/-}$ OT-I cells. In addition, there was a statistically significant difference in the ratio of IV^+ to IV^- *Ccr2*$^{-/-}$ OT-I cells compared to WT OT-I cells in IL-1α treated ears **(Fig. 3.25C)**, indicating that *Ccr2*$^{-/-}$ cells are adhering to the blood endothelium, but are impaired in their ability to breach this barrier, consistent with published *in vitro* data [34]. Together, these data demonstrate that there is a cell-intrinsic requirement for CCR2 in the trafficking of memory OT-I cells into peripheral tissue stimulated with the alarmin IL-1α.

3.9 Conclusion

The data presented here identify the chemokine receptor CCR2 as a broadly expressed receptor on influenza-specific $CD8^+$ T cells. Initial qPCR screening of OT-I cells responding to influenza infection revealed high expression of transcripts for the receptor CCR2, and the receptor had broad and relatively consistent expression across both effector and memory subsets. However, despite the high levels of expression of the receptor on responding OT-I cells, genetic deletion of *Ccr2* in transgenic $CD8^+$ T cells had no major impact on the generation of either effector or memory populations, or in their acquisition of effector potential, in competitive transfer models. There were minor, but statistically significant, reductions in the infiltration of *Ccr2*$^{-/-}$ OT-I cells into the airways, and in the differentiation of effector subsets in the vascular fractions of B6 hosts at day 9 post x31-Ova infection, however, this did not translate into a long-term impact on the formation of memory populations. Additionally, CCR2 was expressed at higher levels on circulating memory cell subsets relative to resident memory cells. However, although migration of memory OT-I cells into inflamed tissue was dependent of the activity of GPCRs, CCR2 had no role in the migration of circulating memory cells into inflamed tissues during a non-anamnestic A/PR8 challenge. In contrast, there was a significant reduction in the recruitment of *Ccr2*$^{-/-}$ memory OT-I cells into IL-1α treated ears, and a concurrent accumulation of these in the vasculature, relative to WT OT-I cells. These results suggest that CCR2 is dispensable for cell-intrinsic

$CD8^+$ T cell effector and memory differentiation, and acquisition of effector functions, but support a potential role for CCR2 in $CD8^+$ T cell immunosurveillance of peripheral tissues.

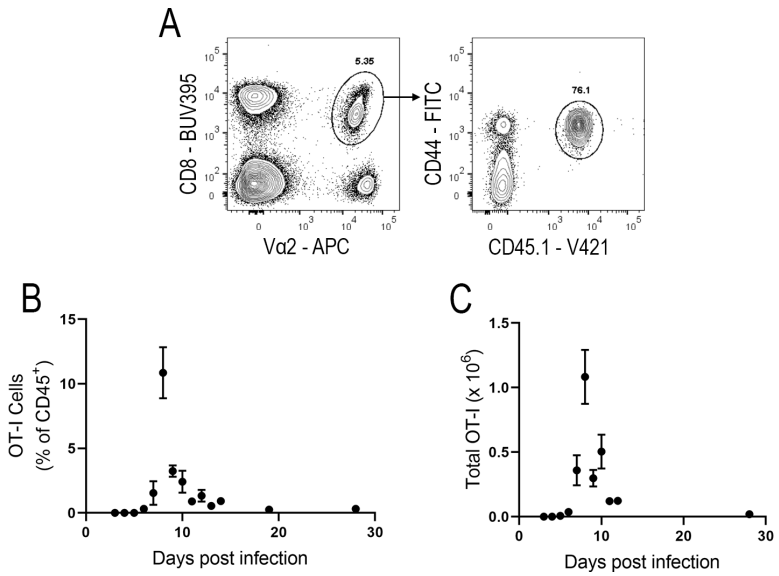

Figure 3.1: OT-I kinetics following x31-Ova infection.

Naïve CD45.1$^+$ OT-I cells (10^4) were transferred IV into C57BL/6 hosts that were infected with 10TCID$_{50}$ x31-OVA 24 hours later. **A)** Representative flow cytometry for the identification of transferred OT-I cells in the blood of day 8 x31-OVA infected mice. The frequency among live CD45$^+$ cells **B)** and total number per mL of peripheral blood **)** of transferred OT-I cells over the course of influenza infection. Data are presented as mean ± SEM (n=3-12 mice per timepoint), pooled from 3 independent experiments.

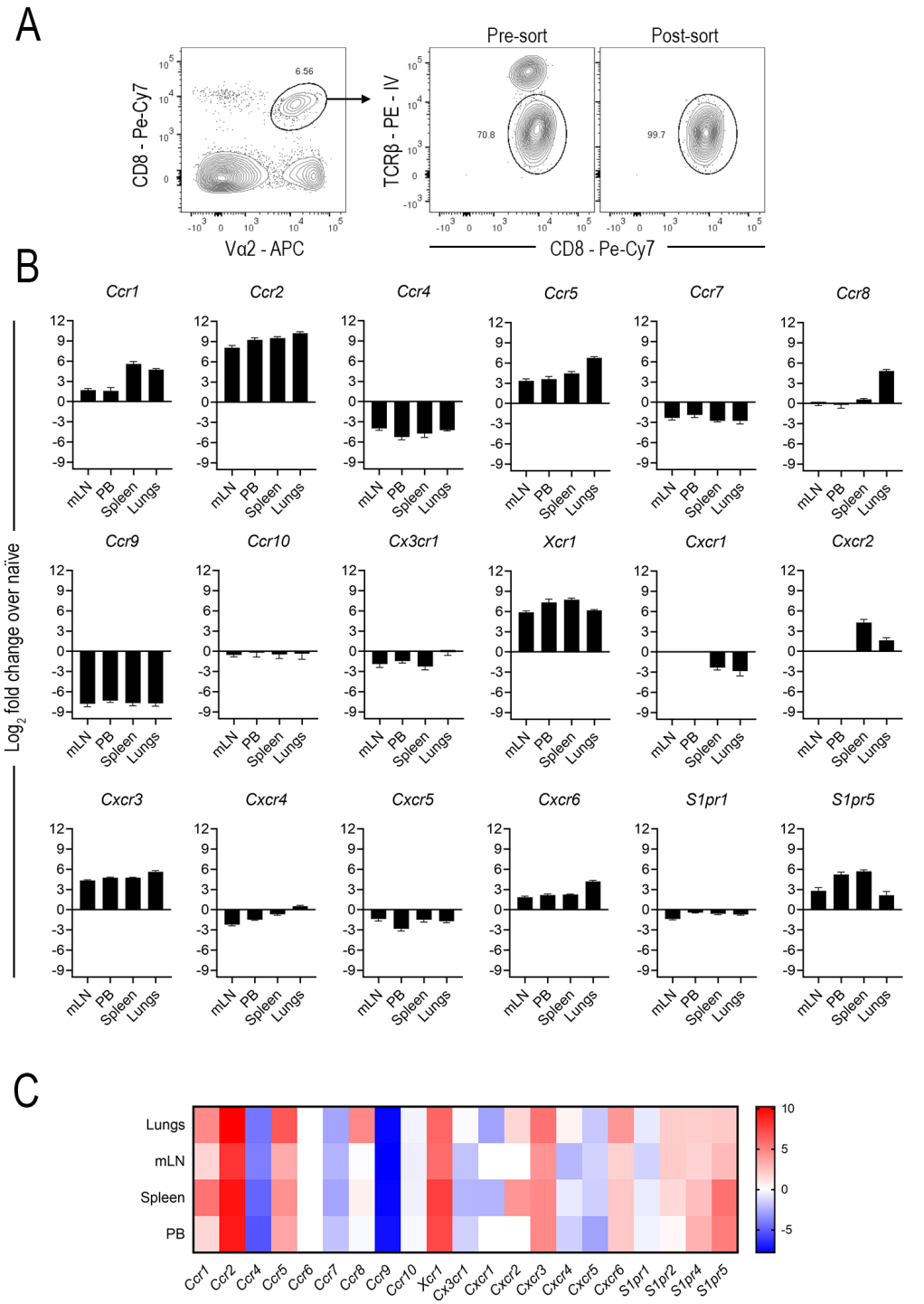

Figure 3.2: Chemokine receptor mRNA expression in antigen-experienced OT-I cells following x31-OVA infection.

OT-I cells were sorted from the lungs, spleen, mLN and peripheral blood on day 7 post x31-Ova infection, or from spleens of naïve OT-I mice, and screened for expression of migratory receptors by qPCR. **A)** Representative flow cytometry of pre-sorted and post-sorted OT-I cells from the lung parencyhma on day 7 post x31-Ova infection. **B)** Chemokine receptor and lipid-signalling GPCR mRNA expression in OT-I cells recovered from the lungs, mLN, spleen and PB, displayed as Log^2 fold-change over naïve splenic OT-I T cells. **C)** Heatmap of chemokine and sphingosine phosphate receptor expression on antigen-experienced OT-I cells. Data are presented as log2 fold-change over naïve OT-I, mean ± SEM (n=5 mice per organ).

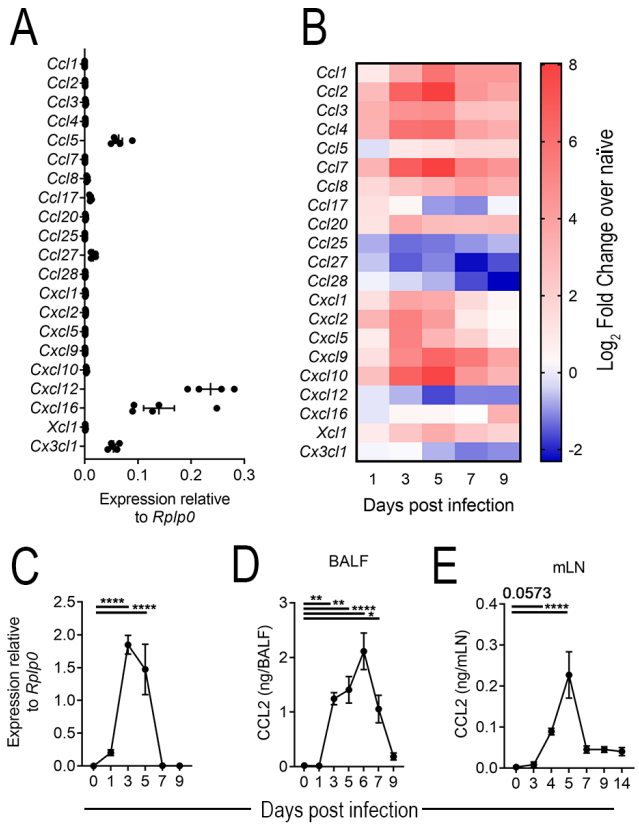

Figure 3.3: Inflammatory chemokines are expressed in the lungs and lung-draining mLN following influenza infection.

C57BL/6 mice were infected with 10TCID$_{50}$ x31-Ova and whole lungs of infected mice were processed to obtain cDNA on days 0, 1, 3, 5, 7 and 9 post-infection. **A)** Chemokine mRNA expression in the lungs of naïve mice. **B)** Expression of chemokine mRNA transcripts in the lungs of x31-Ova-infected mice on the indicated days post-infection, displayed as Log$_2$ fold-change over naïve. **C)** Influenza NP mRNA in the lungs of x31-Ova-infected mice on the indicated days post-infection, relative to *Rplp0*. CCL2 protein was analysed by ELISA in the BALF **D)** and in mLN supernatants **E)** on the indicated days post-infection. Data are presented as mean ± SEM (n=4-8 mice per time point). *p≤0.05, **p≤0.01, ***p≤0.001 One-way ANOVA.

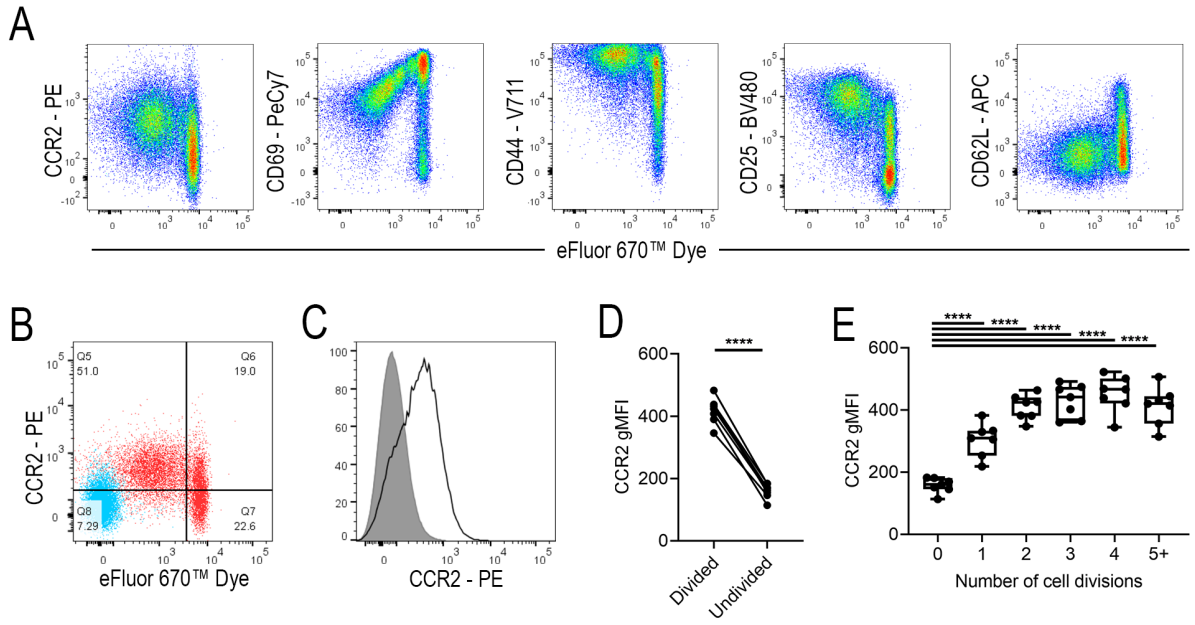

Figure 3.4: CCR2 is expressed on activated CD8⁺ T cells in the mLN within the first cell division.

Naïve OT-I cells (10^6) were labelled with proliferation dye and transferred into C57BL/6 hosts that were infected with PR8-Ova 24 hours later. Four days post-A/PR8-Ova infection, transferred $CD8^+$ $CD45.1^+$ OT-I cells in the mLN were screened for expression of CCR2, activation markers, and cell division. **A)** Representative flow cytometry of CCR2 and the activation markers CD69, CD44, CD25 and CD62L on transferred $CD8^+$ $CD45.1^+$ OT-I cells in the mLN. **B)** Representative flow cytometry of CCR2 expression on transferred OT-I cells (red) relative to endogenous naïve CD8 T cells ($CD8^+$ $CD3^+$ $CD44^{low}$, blue). **C)** Representative histograms of CCR2 expression on divided (black line) and undivided (shaded) OT-I cells. **D)** CCR2 gMFI on all divided and undivided OT-I cells. **E)** CCR2 GMFI on OT-I cells at the indicated number of cell divisions. Data are presented as mean ± SEM (n=7 mice), representative of two independent experiments. ****$p \leq 0.0001$ (**(D)** paired Students *t*-test. **(E)** One-way ANOVA).

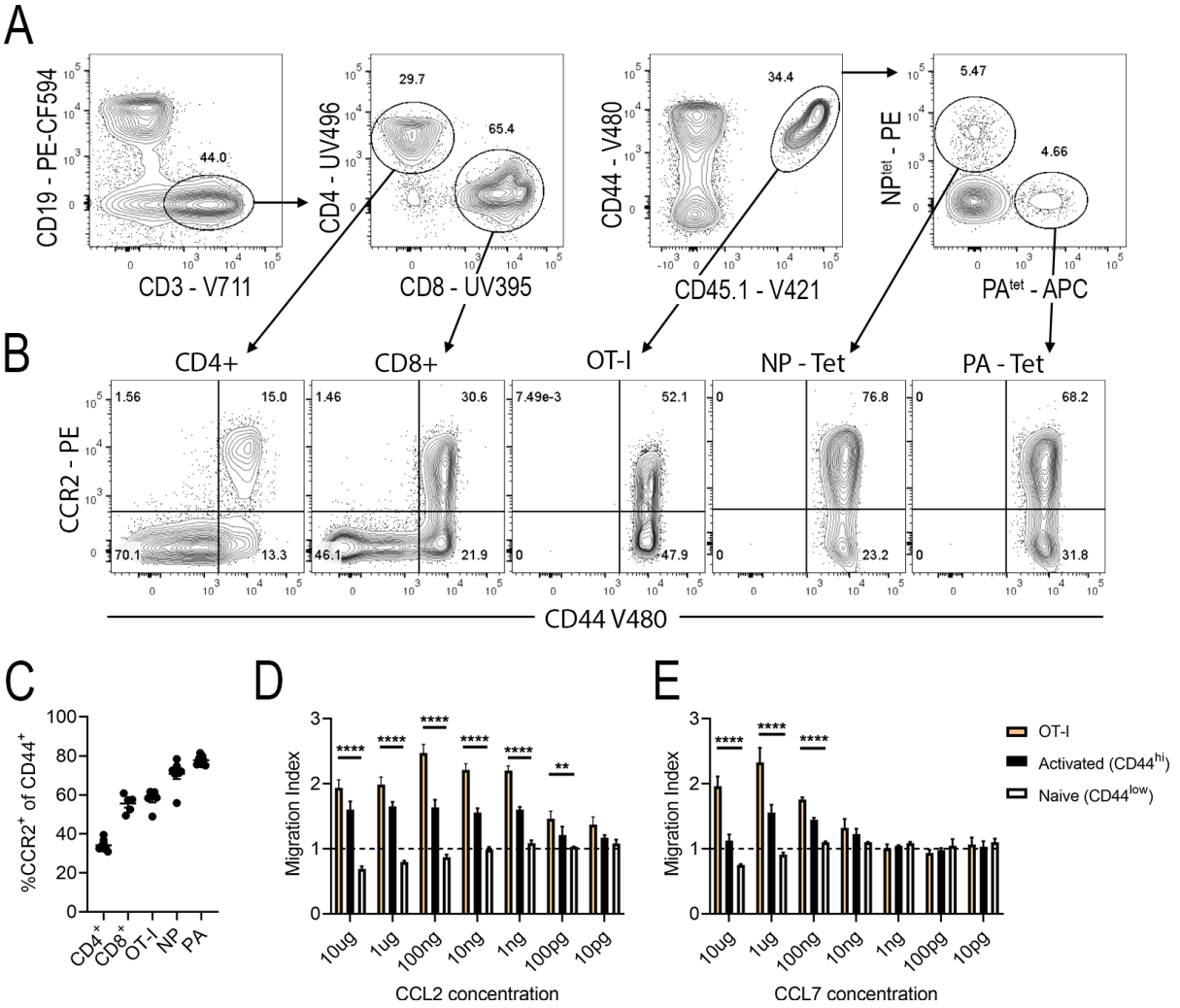

Figure 3.5: CCR2 is expressed on T cells in the circulation around peak T cell expansion
Naïve OT-I cells (10^4) were transferred into C57BL/6 mice that were infected with x31-Ova 24 hours later. T cells in the blood were analysed for CCR2 expression on day 8 post-infection. **A-B)** Representative flow cytometry for the identification of T cells in the blood and their expression of CCR2. **C)** Quantification of CCR2 expression on host endogenous $CD4^+$ and $CD8^+$ T cells, OT-I cells, and NP-tetramer- and PA-tetramer-specific T cells present in the blood. **D-E)** Ex-vivo chemotaxis of OT-I cells and endogenous $CD44^+$ (activated) and $CD44^-$ (naïve) $CD8^+$ T cells from the spleen of day 10 x31-Ova infected mice to CCL2 **D)** and CCL7 **E)**. Data are presented as mean ± SEM (**(C)** n=6 mice), representative of three independent experiments. (**(D-E)** n=3 mice) **p≤0.01, ****p≤0.0001 (Two-way ANOVA).

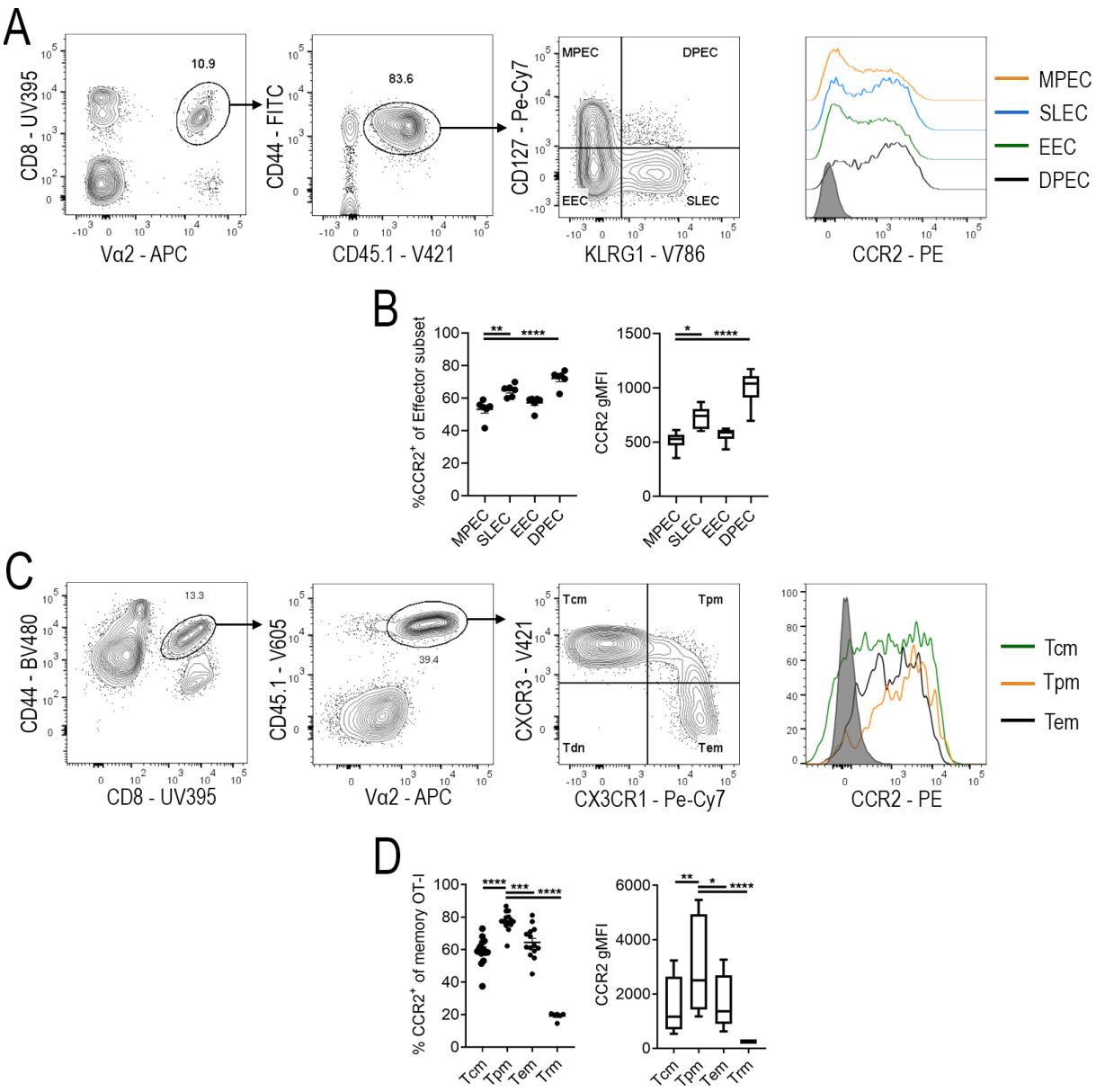

Figure 3.6: Expression of CCR2 on effector and memory T cells in circulation

OT-I cells (10^4) were transferred into naïve C57BL/6 hosts that were infected with x31-Ova 24 hours later. **A)** Representative flow cytometry of CCR2 expression on peripheral blood effector OT-I cell subsets on day 9 post-infection. **B)** Percentage CCR2 expression and gMFI on the indicated OT-I cell effector subsets. **C)** representative flow cytometry of CCR2 expression on circulating memory OT-I cells present in the blood on day 35 post-influenza infection. **D)** percentage CCR2 expression and gMFI on the indicated OT-I memory cell subsets. Data are presented as mean ± SEM (**(B)** n=6 mice), representative of 2 independent experiments. (**(D)** n=14 mice), pooled from 2 independent experiments. *p≤0.05, **p≤0.01, ***p≤0.001. ****p≤0.0001 (One-way ANOVA).

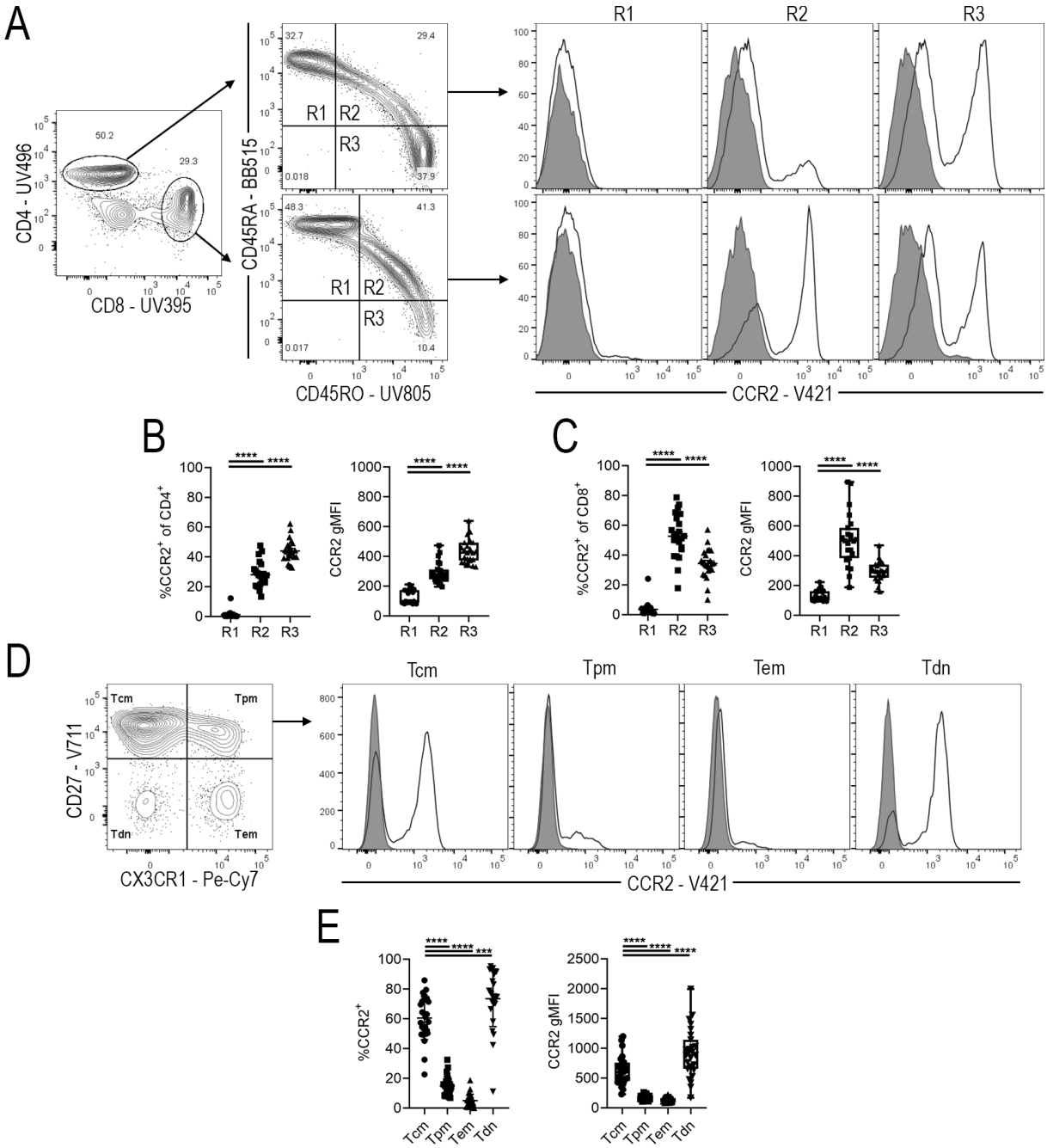

Figure 3.7: CCR2 is expressed on human central memory T cells

Human peripheral blood mononuclear cells isolated from healthy donors were stained for CCR2. **A)** Representative flow cytometry of CCR2 expression on human, live, $CD3^+$, $CD4^+$ and $CD8^+$, $CD45RA^+CD45RO^-$ (R1), $CD45RA^+$ $CD45RO^+$ (R2) and $CD45RA^-$ $CD45RO^+$ (R3) cells (black line) and isotype staining (shaded histogram). CCR2 expression and gMFI on the indicated $CD4^+$ **B)** and $CD8^+$ **C)** naïve and antigen-experienced T cells. **D)** Representative flow cytometry of CCR2 expression on human $CD3^+CD8^+CD45RA^-$ circulating memory T cell subsets (black line) and isotype staining (shaded histogram). **E)** CCR2 expression and gMFI on $CD8^+$ circulating memory T cell subsets. Data are presented as mean ± SEM (n=21 human donors), pooled from 3 independent experiments. ***p≤0.001, ****p≤0.0001 (One-way ANOVA).

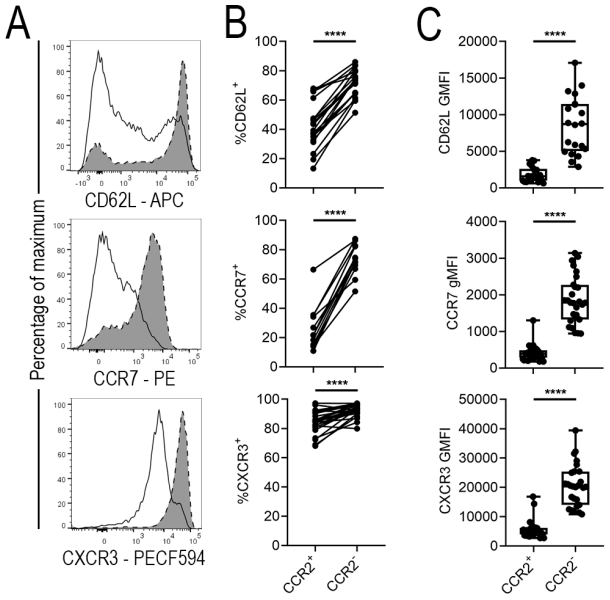

Figure 3.8: CCR2-expressing human Tcm cells have lower expression of lymph node homing molecules and CXCR3

Human CD45RO$^+$ CD27$^+$ CX$_3$CR1$^-$ central memory T cells were stained for lymph node homing markers. **A)** representative flow cytometry of surface markers on CD3$^+$CD8$^+$CCR2$^+$ (solid line) and CCR2$^-$ (dashed line) Tcm cells. **B)** and **C)** The percentage of CCR2$^+$ and CCR2$^-$ Tcm cells expressing and gMFI of the indicated markers. (n=27 human donors), pooled from 3 independent experiments. ****p≤0.0001 (unpaired Students *t*-test).

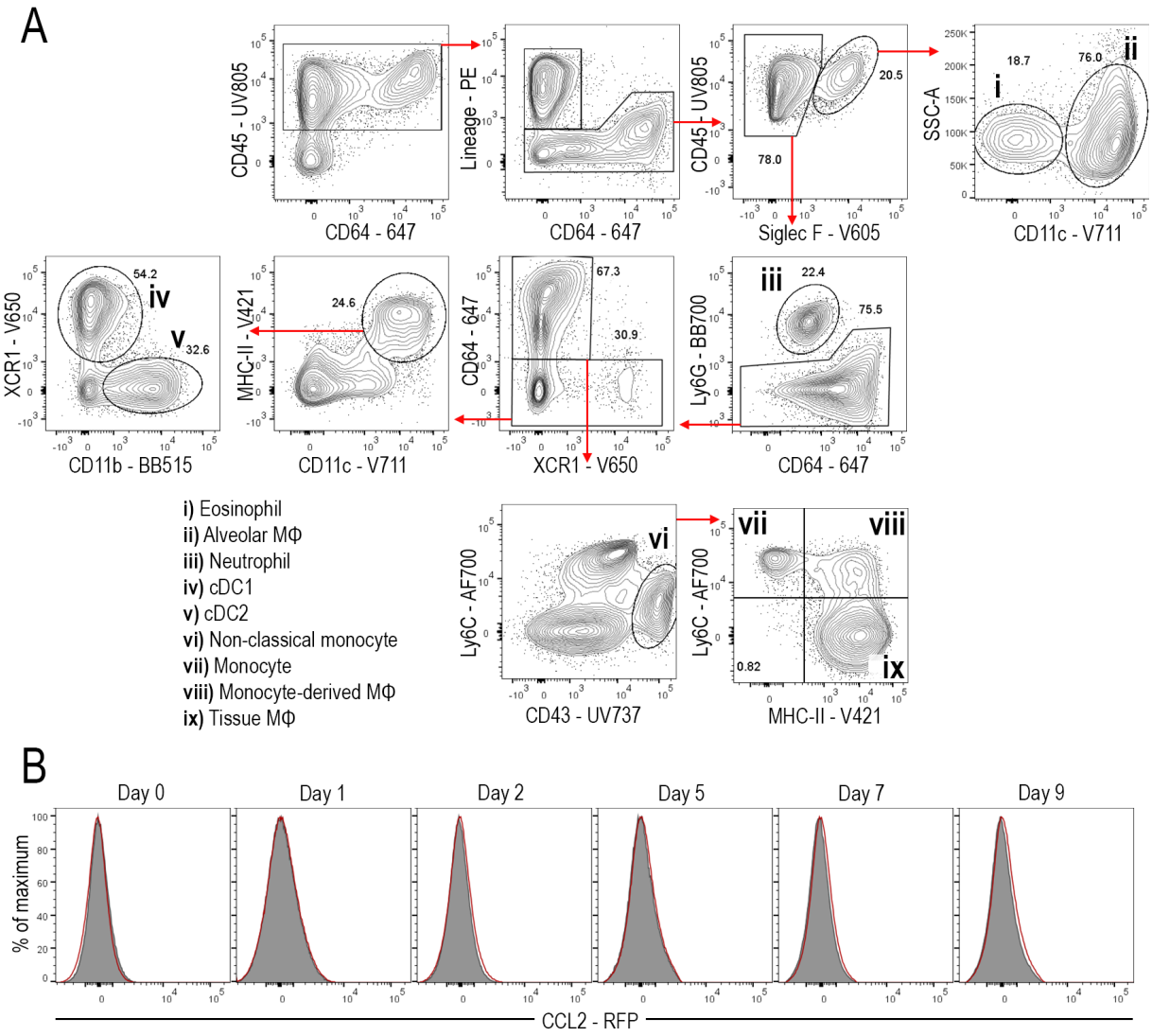

Figure 3.9: Gating strategy for the identification of reporter-positive myeloid cell subsets in the lungs.

Gating strategy used for the identification of reporter-positive cells in CCL2-RFP mice. **A)** Representative flow cytometry for the identification of myeloid cell subsets in the lungs of day 5 A/HK-x31 infected mice. Pre-gated on live, lineage negative cells. Siglec F^+ $CD11c^-$ Eosinophils **(i)**, Siglec F^+ $CD11c^-$ alveolar macrophages **(ii)**, $Ly6G^+$ Neutrophils **(iii)**, $CD64^-$ $CD11c^+$, $MHC\text{-}II^+$ $XCR1^+$ cDC1s **(iv)**, $CD64^-$ $CD11c^+$, $MHC\text{-}II^+$ $CD172\alpha^+$ cDC2s **(v)**, $CD64^+$ $CD11b^+$ $F4\text{-}80^+$ $MerTK^-$ $CD43^+$ non-classical monocytes **(vi)**, $CD64^+$ $CD11b^+$ $F4\text{-}80^+$ $MerTK^-$ $CD43^-$ $Ly6C^+$ $MHC\text{-}II^-$ monocytes **(vii)**, $CD64^+$ $CD11b^+$ $F4\text{-}80^+$ $MerTK^{+/-}$ $CD43^-$ $Ly6C^+$ $MHC\text{-}II^+$ monocyte-derived macrophage **(viii)** and $CD64^+$ $CD11b^+$ $F4\text{-}80^+$ $MerTK^{+/-}$ $CD43^-$ $Ly6C^-$ $MHC\text{-}II^+$ tissue macrophage **(ix)**. **B)** Absence of RFP expression in lineage-positive (CD3, CD19, CD90, NK1.1, TCRα) cells in the lungs on day 5 post A/HK-x31 infection.

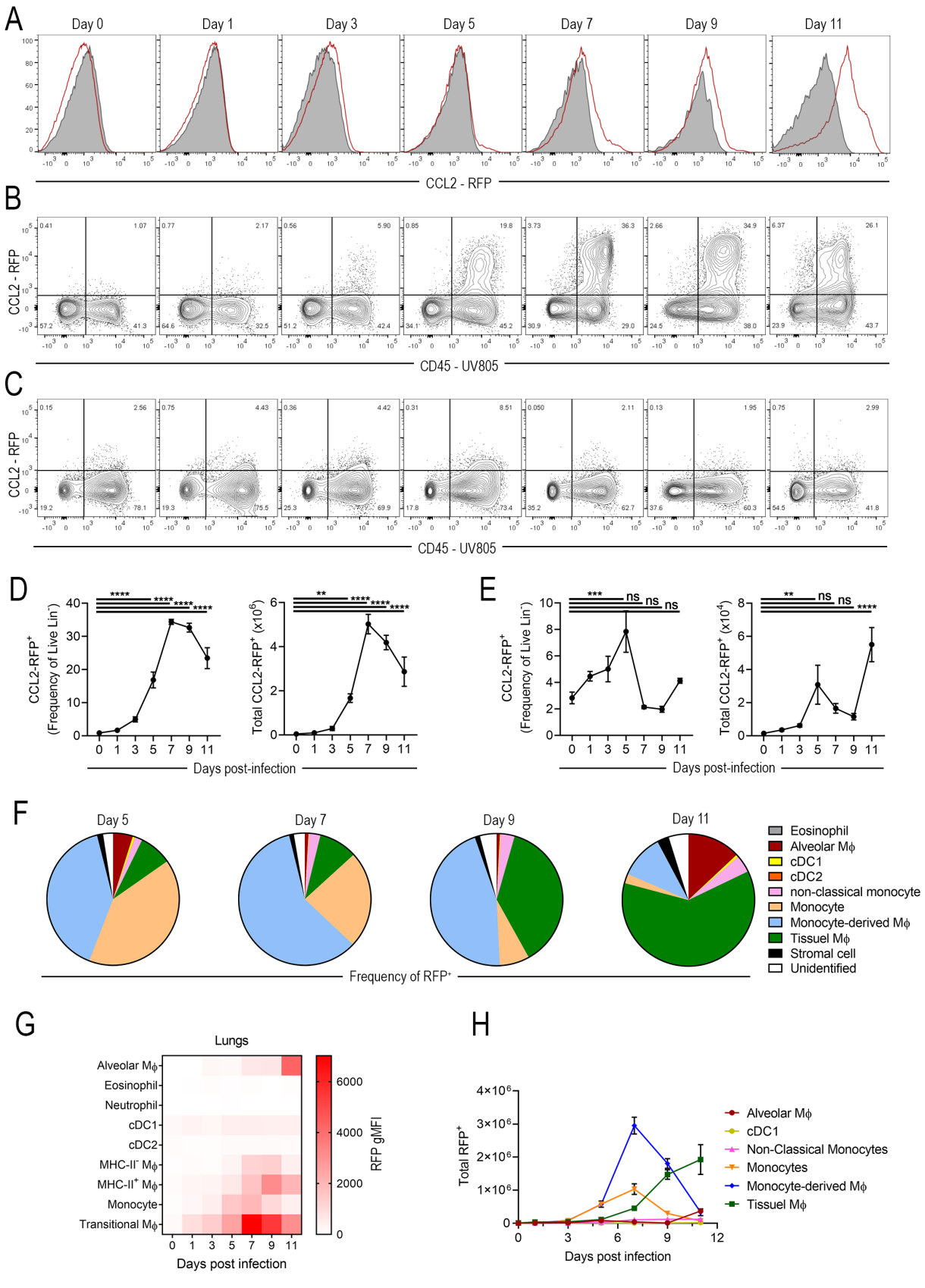
A
Day 0
Day 1
Day 3
Day 5
Day 7
Day 9
Day 11
CCL2 - RFP
B
CCL2 - RFP
CD45 - UV805
C
CCL2 - RFP
CD45 - UV805
D
CCL2-RFP+ (Frequency of Live Lin-)
Total CCL2-RFP+ (x10^6)
Days post-infection
E
CCL2-RFP+ (Frequency of Live Lin-)
Total CCL2-RFP+ (x10^4)
Days post-infection
F
Day 5
Day 7
Day 9
Day 11
Frequency of RFP+
Eosinophil
Alveolar Mϕ
cDC1
cDC2
non-classical monocyte
Monocyte
Monocyte-derived Mϕ
Tissuel Mϕ
Stromal cell
Unidentified
G
Lungs
Alveolar Mϕ
Eosinophil
Neutrophil
cDC1
cDC2
MHC-II- Mϕ
MHC-II+ Mϕ
Monocyte
Transitional Mϕ
Days post infection
RFP gMFI
H
Total RFP+
Days post infection
Alveolar Mϕ
cDC1
Non-Classical Monocytes
Monocytes
Monocyte-derived Mϕ
Tissuel Mϕ

Figure 3.10: Monocytes and monocyte-derived cells are the major CCL2-producing cells during primary influenza infection

CCL2-RFP mice were infected with A/HK-x31 and on the indicated days post-infection the lungs and mLN were analysed for reporter expression. **A)** CCL2-reporter expression in alveolar macrophages in the lungs (red line) relative to reporter-negative controls (shaded histograms). CCL2-reporter expression in live, alveolar Mϕ-negative, lineage negative cells in the lungs **B)** and mLN **C)** at the indicated time points post-infection. The frequency and total number of live, lineage-negative RFP^+ cells present in the lungs **D)**, and mLN **E)**. **F)** The frequency of the indicated cell subset among total RFP^+ cells in the lungs on the indicated days post-infection. **G)** The gMFI for RFP in the indicated myeloid cell subsets in the lungs over the course of A/HK-x31 infection. **H)** The total number of RFP^+ cells present in the lungs over the course of A/HK-x31 infection. Data are presented as mean ± SEM (n=5 mice per time point). $^{ns}p>0.05$ = not significant, $^{*}p\leq0.05$, $^{**}p\leq0.01$, $^{***}p\leq0.001$, $^{****}p\leq0.001$ (One-way ANOVA).

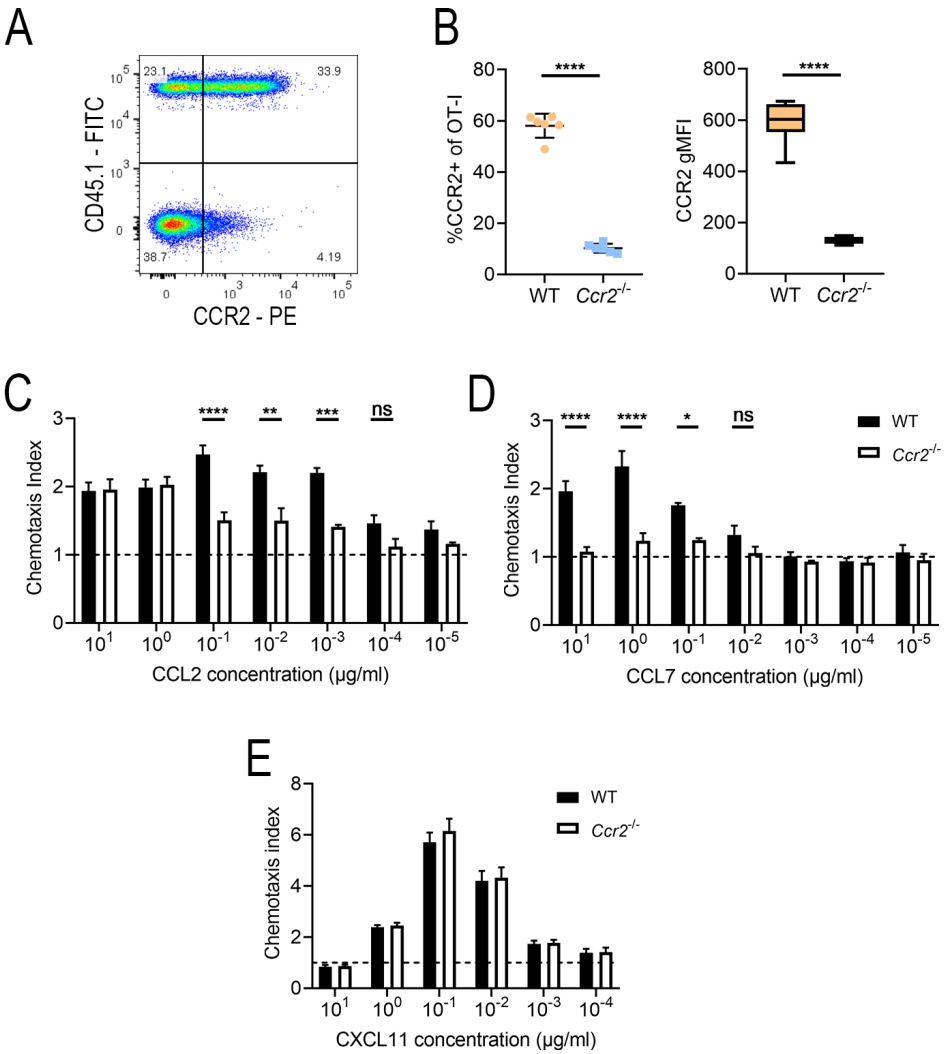

Figure 3.11: *Ccr2*-deficient OT-I cells do not express surface CCR2 and are non-responsive to CCR2 ligands

Naïve WT and *Ccr2*$^{-/-}$ OT-I cells (10^4) were co-transferred into C57BL/6 hosts that were infected with x31-Ova 24 hours later. **A)** Representative flow cytometry of αCCR2 staining on WT (CD45.1$^+$) and *Ccr2*$^{-/-}$ (CD45.1$^-$) OT-I cells in the blood of day 8 x31-Ova-infected mice. **B)** The frequency of, and gMFI, for CCR2 expression on OT-I cells in the blood of day 8 x31-Ova-infected mice. **C-E)** *Ex-vivo* chemotaxis of WT and *Ccr2*$^{-/-}$ OT-I cells taken from the spleens of day 14 x31-Ova-infected mice in response to the CCR2 ligands CCL2 **C)** and CCL7 **D)** and the CXCR3 ligand CXCL11 **E)**. Data are presented as mean ± SEM (**(B)** n=6 mice), representative of 2 independent experiments. (**(C-E)** n=3 mice), representative of 2 independent experiments. ^{ns}p>0.05 = not significant, *p≤0.05, **p≤0.01, ***p≤0.001, ****p≤0.001 (**(B)** paired Students *t*-test. **(D-E)** Two-way ANOVA).

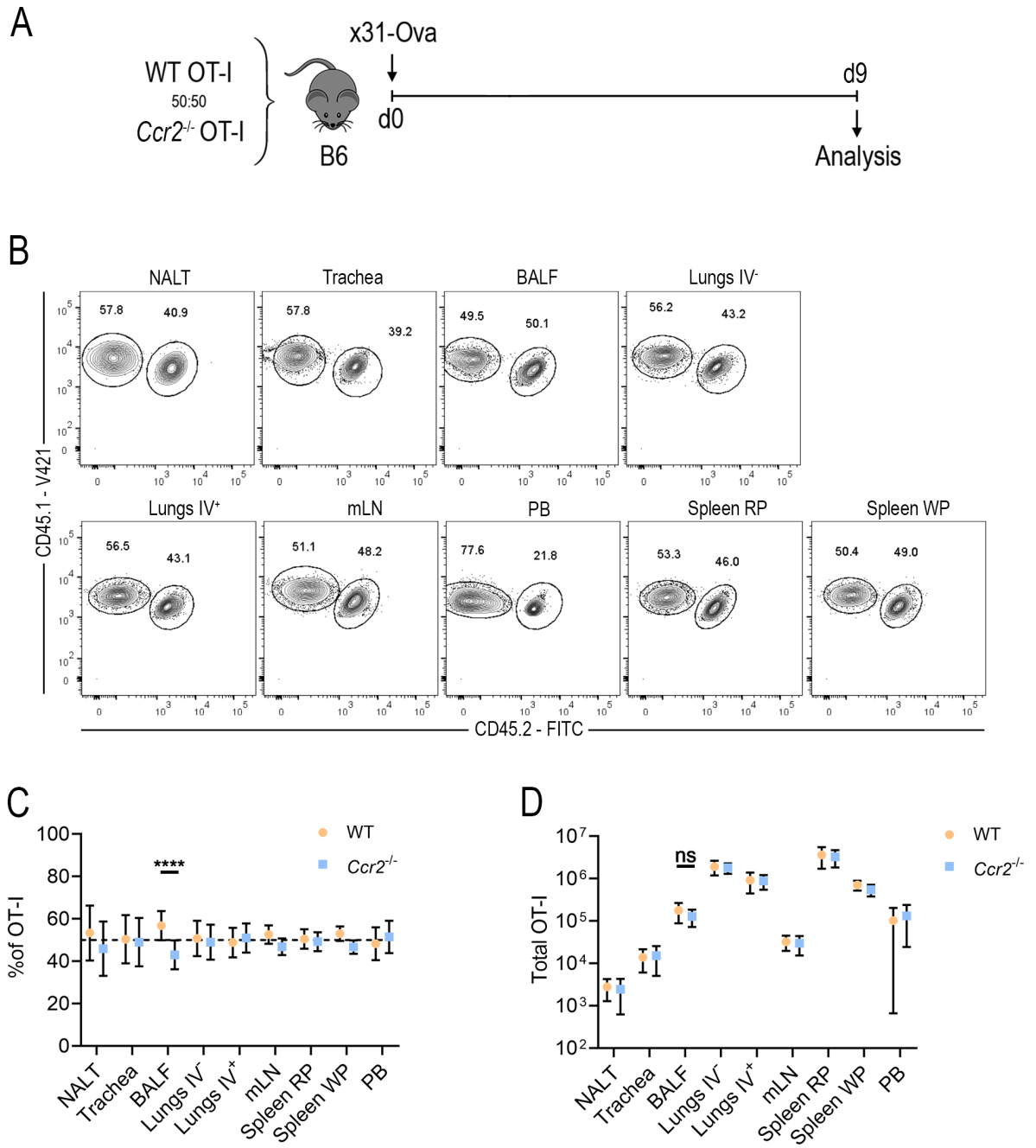

Figure 3.12: CCR2 deficiency does not impact the magnitude of the OT-I effector response to influenza

Naïve WT and *Ccr2*$^{-/-}$ OT-I cells (10^4) were transferred into C57BL/6 hosts that were infected with 10TCID$_{50}$ x31-Ova 24 hours later. Nine days after influenza infection the OT-I effector response was analysed. **A)** Experimental plan. **B)** Representative flow cytometry of recovered WT (CD45.1$^+$) and *Ccr2*$^{-/-}$ (CD45.1$^+$CD45.2$^+$) OT-I cells in the indicated tissues. The percentage **C)** and total number **D)** of OT-I cells recovered from the indicated tissues. PB numbers indicate cells per mL of blood. Data are presented as mean ± SD (n=14 mice), pooled from two independent experiments. $^{ns}p>0.05$ = not significant, ****$p\leq0.0001$ (Two-way ANOVA).

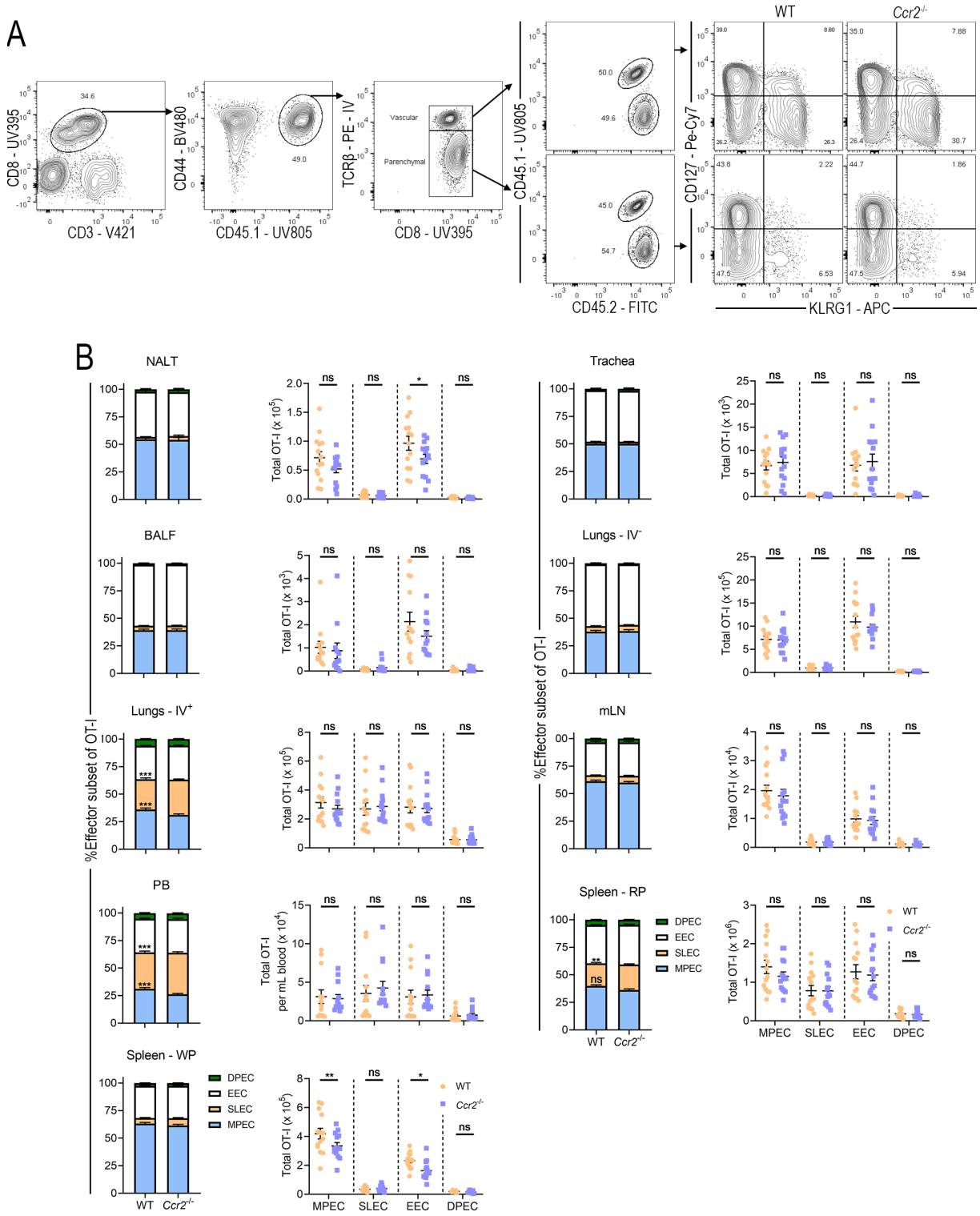

Figure 3.13: Ccr2 deficiency has minor impacts on the development of effector OT-I cells
A) Representative flow cytometry for the identification of $CD127^{+}KLRG1^{-}$ MPECs, $CD127^{+}KLRG1^{+}$ DPECs, $CD127^{+}KLRG1^{-}$ SLECs, and $CD127^{-}KLRG1^{-}$ EECs in the lungs of day 9 x31-Ova infected mice. **B)** The frequency and total number of effector-subset OT-I cells recovered from the indicated organs. Data are presented as mean ± SEM (n=14 mice), pooled from 2 independent experiments. $^{ns}p>0.05$ = not significant, $^{*}p\leq0.05$, $^{**}p\leq0.01$, $^{***}p\leq0.001$ (Two-way ANOVA).

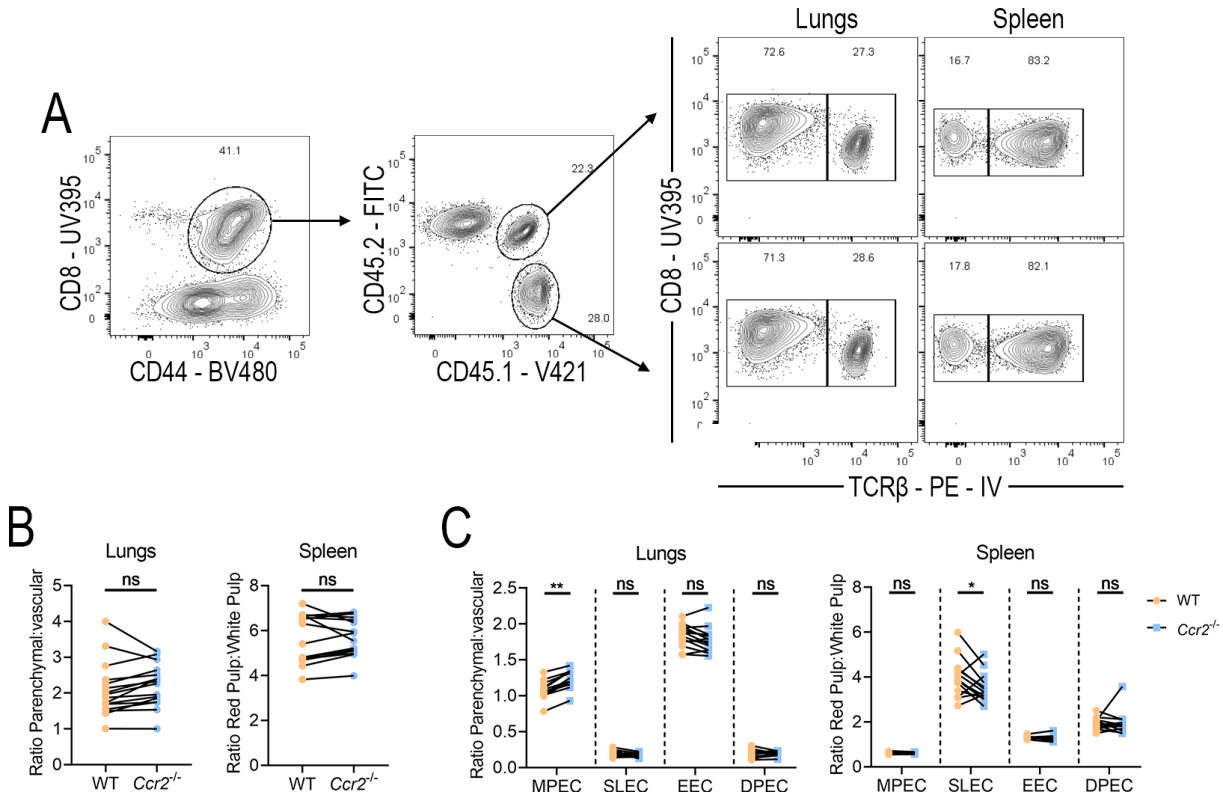

Figure 3.14: CCR2 does not influence T cell localisation in the lungs or spleen during influenza infection

Naïve WT and *Ccr2*$^{-/-}$ OT-I cells (10^4) were transferred into C57BL/6 hosts that were infected with 10TCID$_{50}$ x31-Ova 24 hours later. Nine days post-infection mice were administered 3µg of αTCR β IV 3 minutes prior to sacrifice and the ratio of IV-labelled to unlabelled cells in the lungs and spleen quantified. **A)** representative flow cytometry of vascular labelling of CD45.1$^+$ WT and CD45.1$^+$ CD45.2$^+$ *Ccr2*$^{-/-}$ OT-I cells in the lungs and spleen on day 9 post x31-Ova infection. **B)** the ratio of total IV$^+$ to IV$^-$ OT-I cells in the lungs and spleen. **C)** The ratio of IV$^+$ to IV$^-$ OT-I effector cell subsets in the lungs and spleen. (n=14 mice), pooled from 2 independent experiments. ^{ns}p>0.05 = not significant, *p≤0.05, **p≤0.01 (**(B)** paired Students *t*-test. **(C)** Two-way ANOVA).

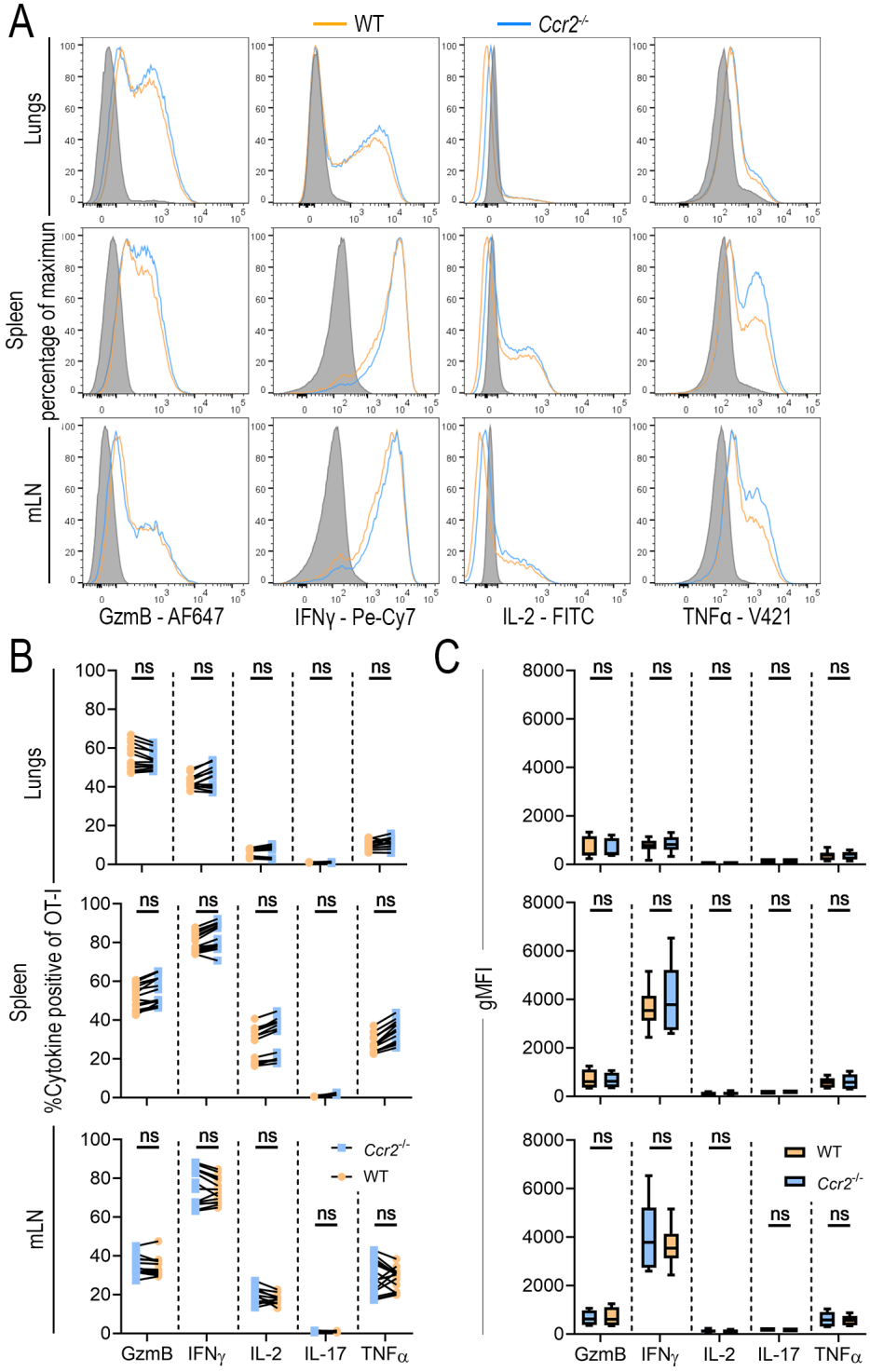

Figure 3.15: T cell effector potential is not altered in the absence of CCR2

OT-I cells recovered from the lungs, mLN and spleen of day 9 x31-Ova-infected mice were stimulated *ex-vivo* with SIINFEKL and OT-I cells analysed for production of effector cytokines and granzyme B. **A)** Representative flow cytometry of cytokine and granzyme production in WT (orange) and *Ccr2*$^{-/-}$ (blue) OT-I cells relative to naïve endogenous CD8^{+} T cells (shaded). The percentage **B)** and gMFI **C)** of cytokine and granzyme B expression in OT-I cells in the indicated organs. Data are presented as mean ± SEM (n=14 mice), pooled from 2 independent experiments. $^{ns}p>0.05$ = not significant, (Two-way ANOVA).

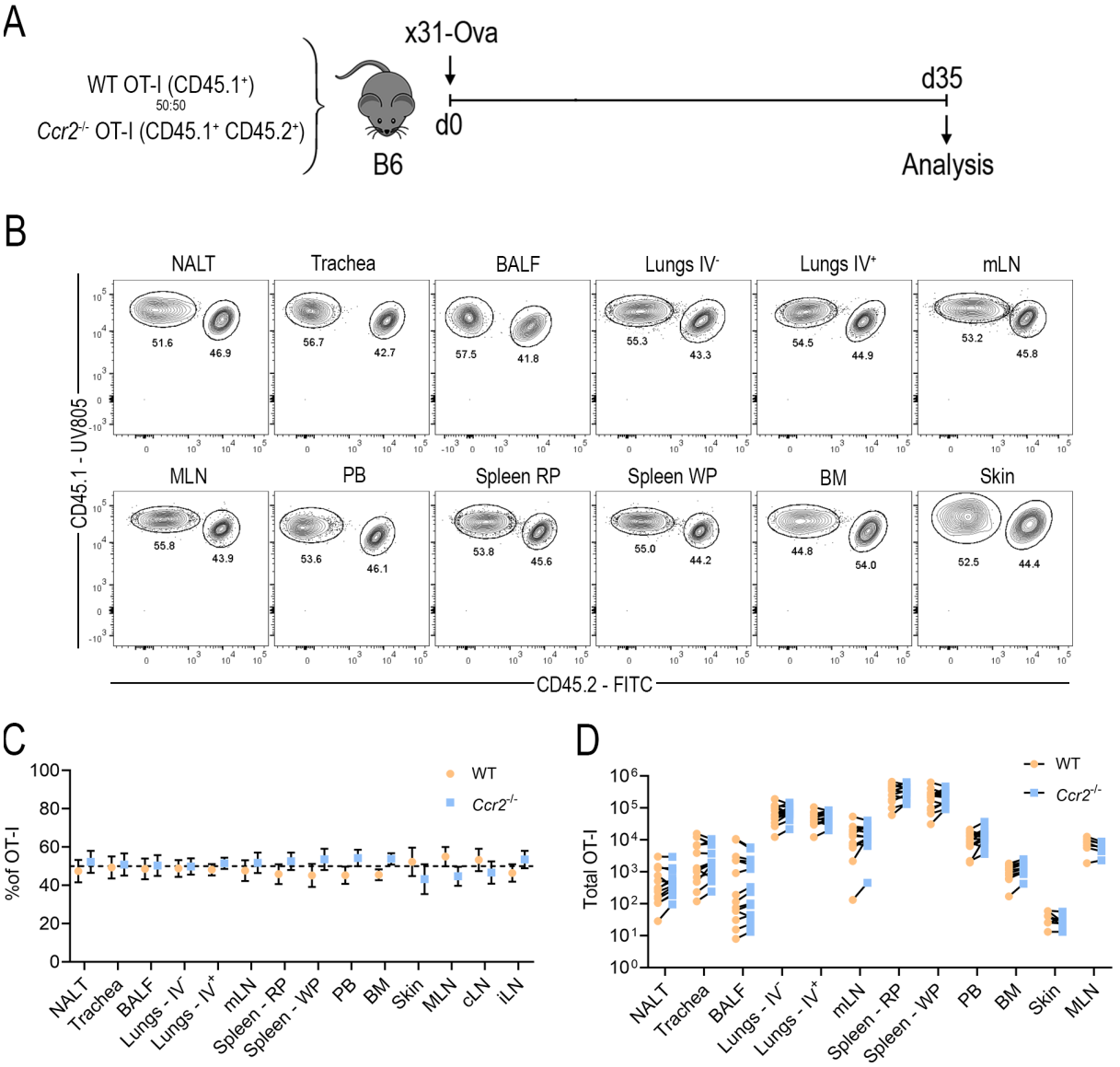

Figure 3.16: CCR2 is not required for the formation of memory CD8⁺ T cell populations
Naïve WT and *Ccr2*$^{-/-}$ OT-I cells (10^4) were co-transferred into naïve C57BL/6 hosts that were infected with x31-Ova 24 hours later. Thirty five days post-influenza infection the OT-I memory response was analysed. **A)** Experimental outline. **B)** Representative flow cytometry of recovered WT (CD45.1$^+$) and *Ccr2*$^{-/-}$ (CD45.1$^+$CD45.2$^+$) OT-I cells in the tissues indicated. The percentage **C)** and total number **D)** of OT-I cells recovered from the tissues indicated. Data are presented as mean ± SEM (n=14 mice), pooled from 2 independent experiments.

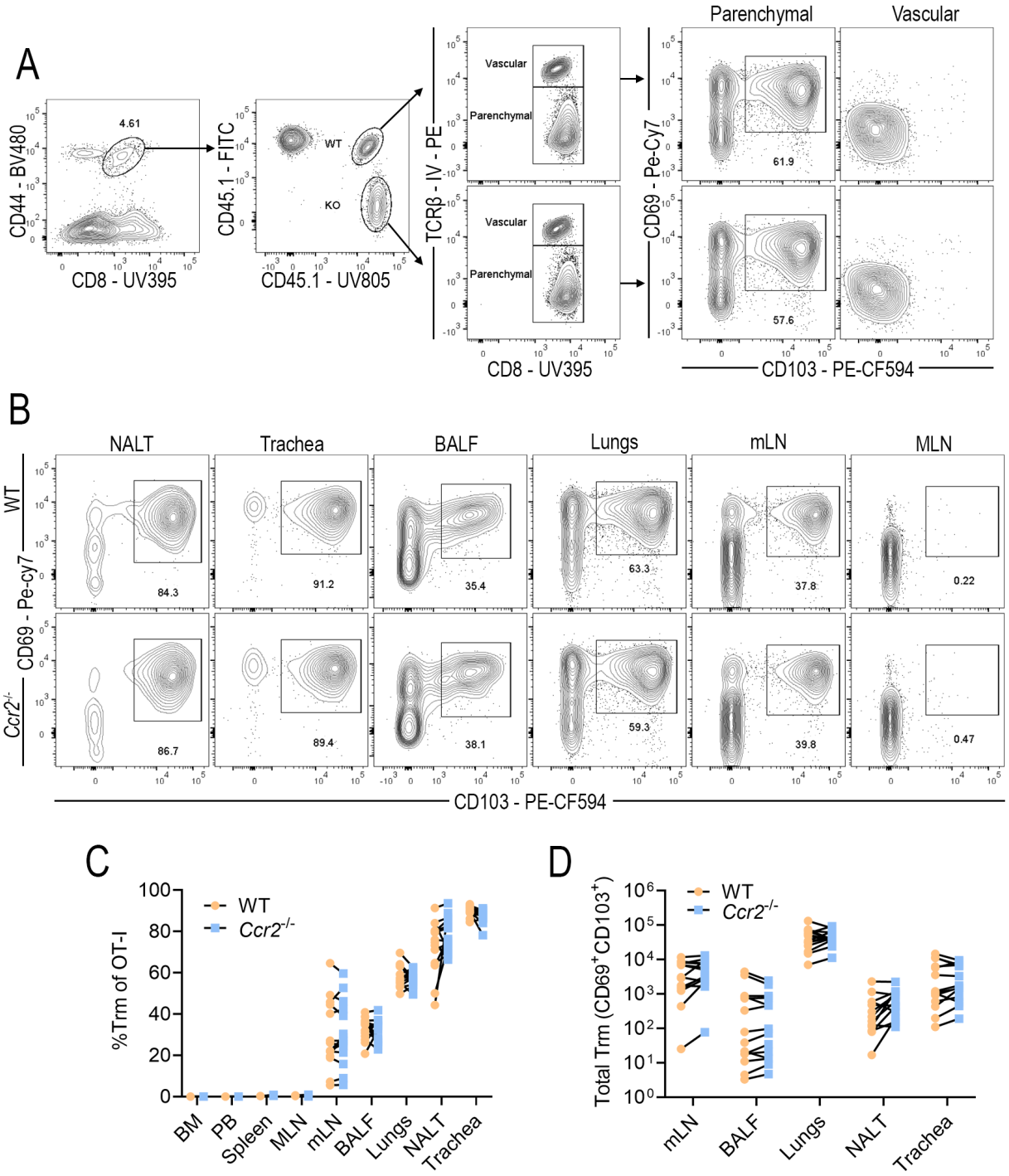

Figure 3.17: Cell intrinsic CCR2 is not required for the formation of tissue-resident memory cells.

Naïve WT and *Ccr2*$^{-/-}$ OT-I cells (10^4) were co-transferred into naïve C57BL/6 hosts that were infected with x31-Ova 24 hours later. Thirty five days post-influenza infection the upper and lower respiratory tract, lung-draining mLN, and non-draining MLN were analysed for the presence of resident memory OT-I cells. **A)** Representative flow cytometry for the identification of CD69$^+$CD103$^+$ Trm cells among total vascular-negative cells in C57BL/6 hosts. **B)** Representative flow cytometry of WT and *Ccr2*$^{-/-}$ OT-I Trm populations in barrier tissues and SLOs 35 days post-influenza infection. The frequency **C)** and total number **D)** of Trm cells recovered from day 35 influenza infected mice. Data pooled from 2 independent experiments.

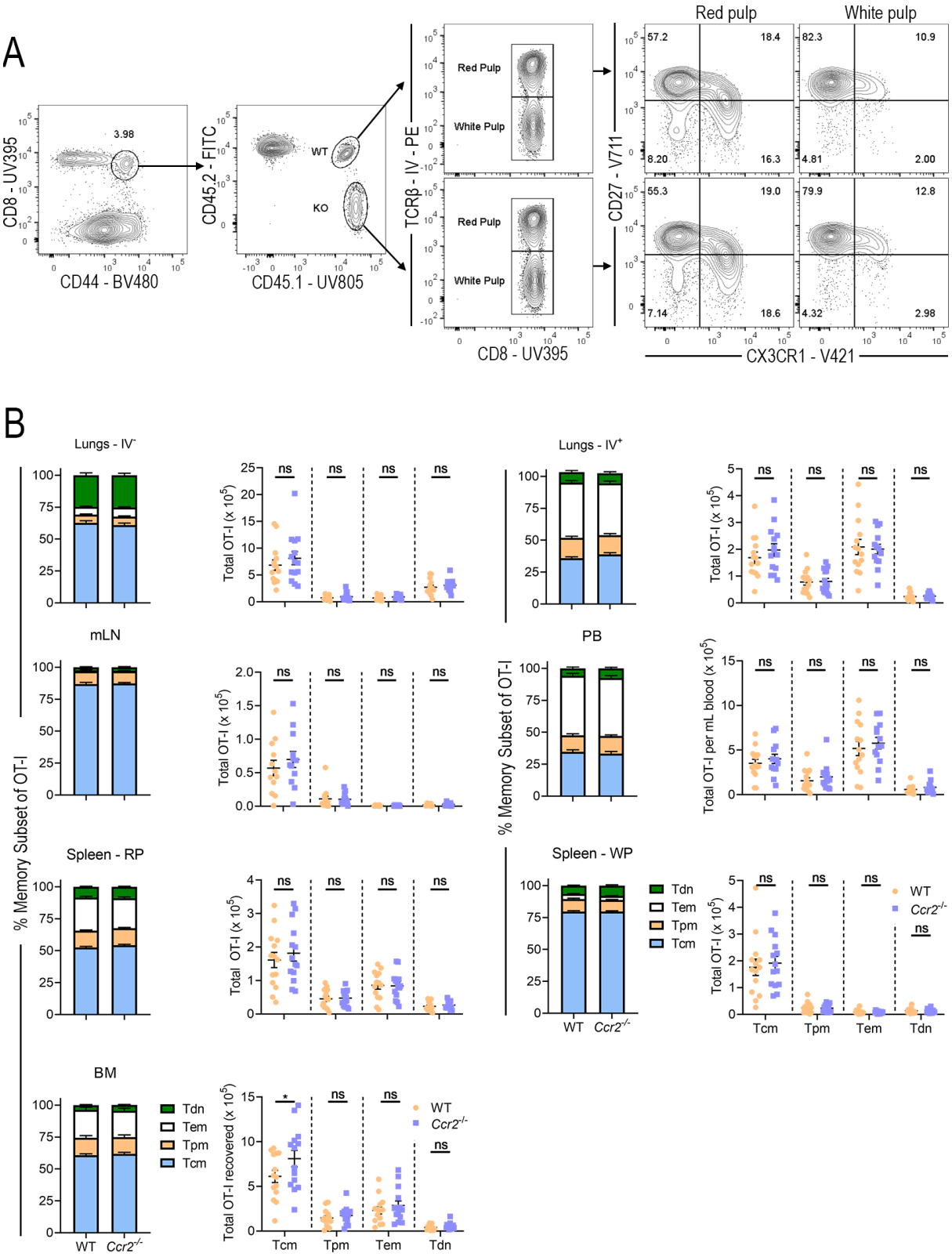
A
CD8 - UV395
CD44 - BV480
3.98
CD45.2 - FITC
CD45.1 - UV805
WT
KO
TCRβ - IV - PE
Red Pulp
White Pulp
CD8 - UV395
CD27 - V711
CX3CR1 - V421
Red pulp
White pulp
57.2
18.4
8.20
16.3
82.3
10.9
4.81
2.00
55.3
19.0
7.14
18.6
79.9
12.8
4.32
2.98
B
Lungs - IV-
Lungs - IV+
mLN
PB
Spleen - RP
Spleen - WP
BM
% Memory Subset of OT-I
Total OT-I (x 10^5)
Total OT-I per mL blood (x 10^5)
Total OT-I recovered (x 10^5)
ns
*
Tdn
Tem
Tpm
Tcm
WT
Ccr2-/-
Tcm
Tpm
Tem
Tdn

Figure 3.18: There is no cell-intrinsic requirement for CCR2 in the formation of circulating memory subsets

The spleen, BM, PB and lungs were analysed for the formation of $CD27^+$ $CX3CR1^-$ Tcm cells, $CD27^+$ $CX3CR1^+$ Tpm cells, $CD27^-$ $CX3CR1^+$ Tem cells, and $CD27^-$ $CX3CR1^-$ Tdn cells 35 days post x31-Ova infection. **A)** Representative flow cytometry for the identification of WT and *Ccr2*$^{-/-}$ OT-I circulating memory cell subsets in the spleen 35 days post influenza infection. **B)** The frequency and total number of circulating memory cells recovered from the indicated tissues. Data are presented as mean ± SEM (n=14 mice), pooled from 2 independent experiments. $^{ns}p>0.05$ = not significant, $^{*}p\leq0.05$ (Two-way ANOVA).

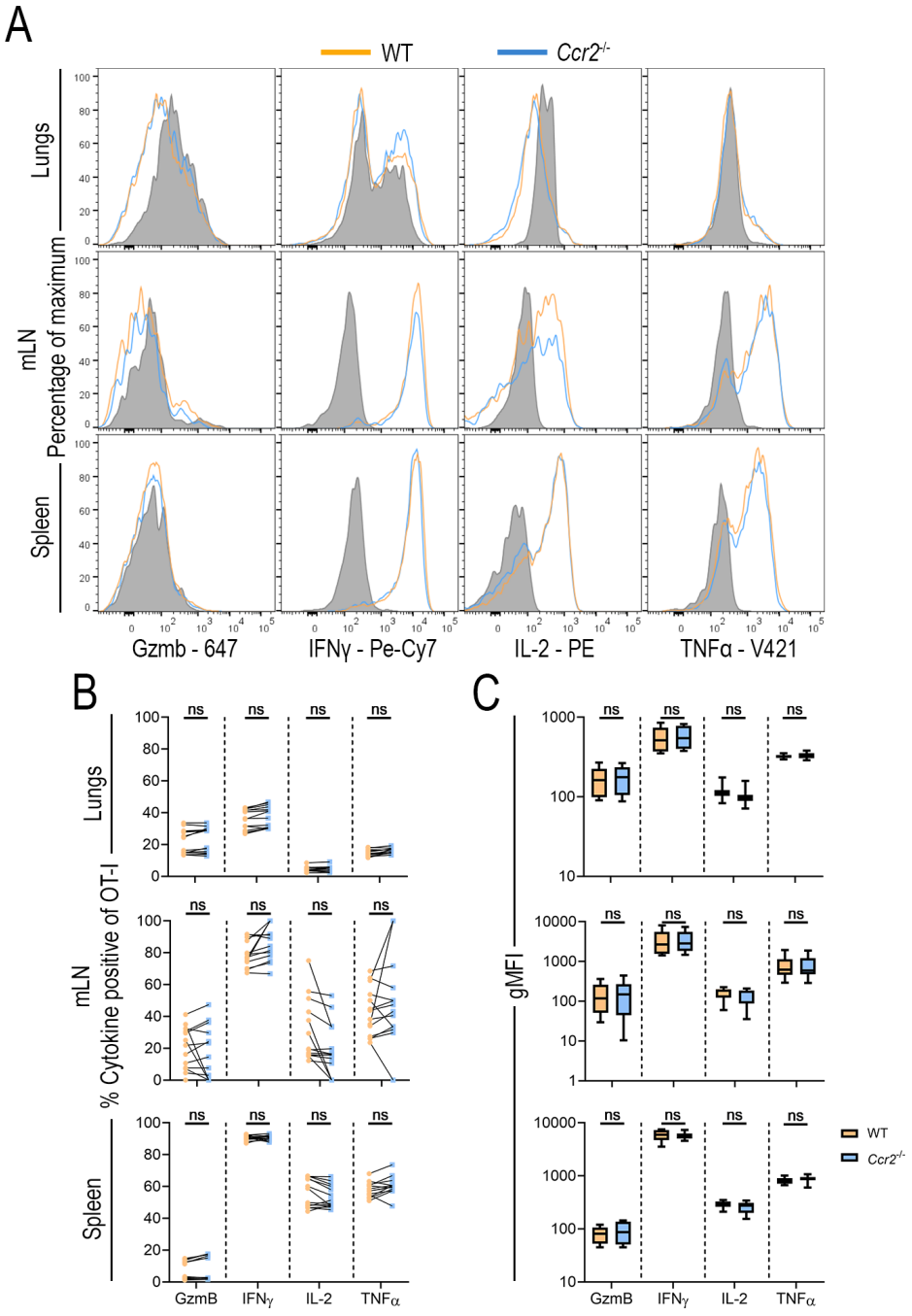

Figure 3.19: *Ccr2*-deficiency has no impact on memory CD8$^+$ T cell effector potential.
Memory OT-I cells were stimulated *ex-vivo* with SIINFEKL and production of effector cytokines and granzyme B was determined. **A)** Representative flow cytometry histograms of effector cytokine and granzyme B production in WT (orange) and *Ccr2*$^{-/-}$ (blue) OT-I cells present in the lungs, mLN and spleen, relative to naïve endogenous CD8$^+$ T cells (shaded histogram). The percentage of cytokine and granzyme B production by OT-I cells **B)** and gMFI for cytokines and granzyme B **C)**. Data are presented as mean ± SEM (n=14 mice), pooled from two independent experiments. $^{ns}p>0.05$ = not significant (Two-way ANOVA).

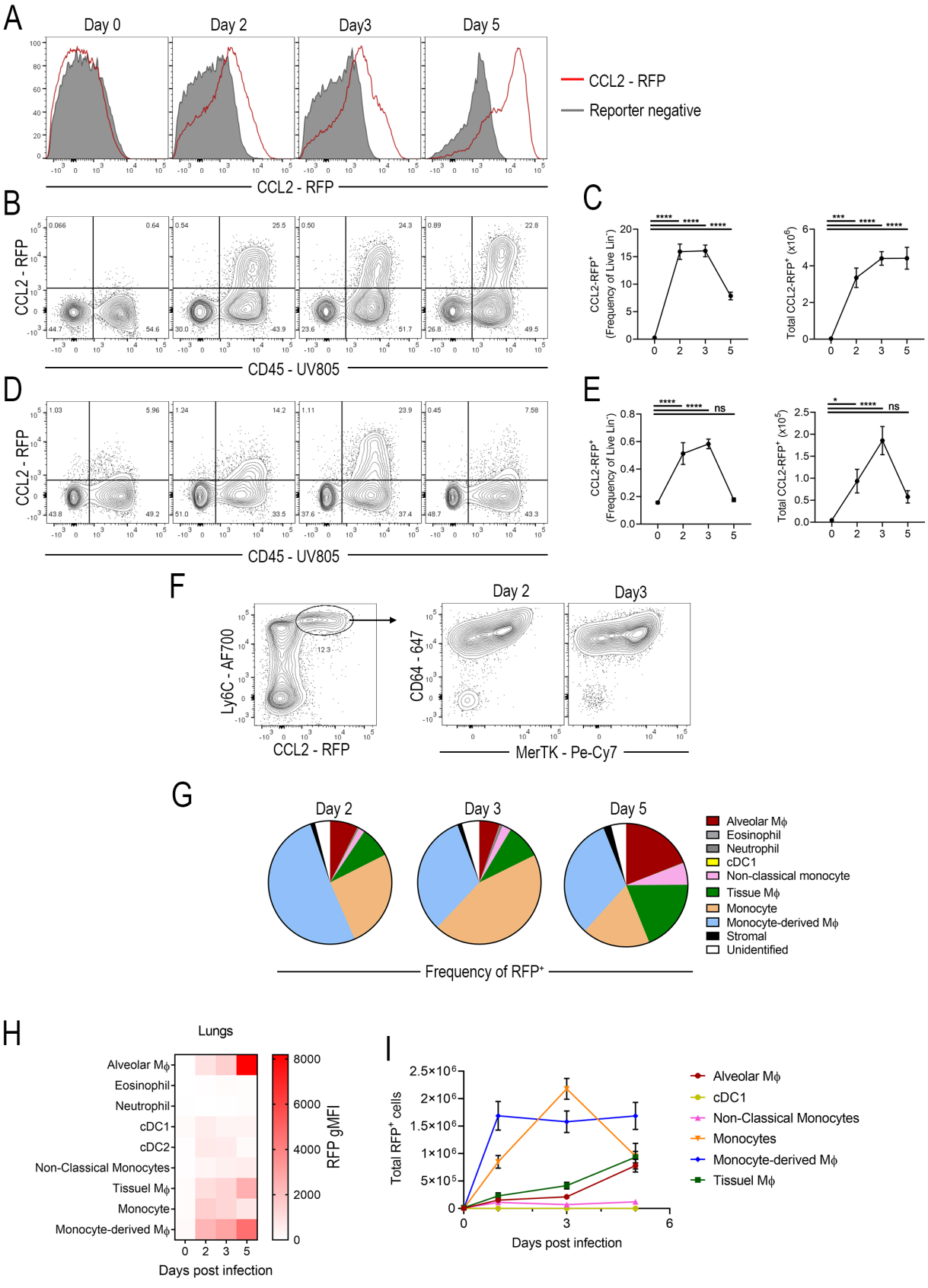
A
Day 0
Day 2
Day3
Day 5
CCL2 - RFP
Reporter negative
CCL2 - RFP
B
CCL2 - RFP
CD45 - UV805
C
CCL2-RFP+ (Frequency of Live Lin-)
Total CCL2-RFP+ (x10^6)
D
CCL2 - RFP
CD45 - UV805
E
CCL2-RFP+ (Frequency of Live Lin-)
Total CCL2-RFP+ (x10^5)
ns
F
Day 2
Day3
Ly6C - AF700
CCL2 - RFP
CD64 - 647
MerTK - Pe-Cy7
G
Day 2
Day 3
Day 5
Alveolar Mϕ
Eosinophil
Neutrophil
cDC1
Non-classical monocyte
Tissue Mϕ
Monocyte
Monocyte-derived Mϕ
Stromal
Unidentified
Frequency of RFP+
H
Lungs
Alveolar Mϕ
Eosinophil
Neutrophil
cDC1
cDC2
Non-Classical Monocytes
Tissuel Mϕ
Monocyte
Monocyte-derived Mϕ
RFP gMFI
Days post infection
I
Total RFP+ cells
Alveolar Mϕ
cDC1
Non-Classical Monocytes
Monocytes
Monocyte-derived Mϕ
Tissuel Mϕ
Days post infection

Figure 3.20: Monocytes and Macrophages rapidly produce CCL2 after A/PR8 challenge

CCL2-RFP mice were challenged with A/PR8 35 days post-A/HK-x31-infection and on the indicated days post-challenge the lungs and mLN were analysed for reporter expression. **A)** Representative histograms of CCL2-reporter expression in alveolar Mϕ in the lungs (red line) relative to reporter negative controls (shaded histograms). CCL2-reporter expression in live, alveolar Mϕ negative, lineage-negative cells in the lungs **B)** and mLN **C)** on the indicated time points post-challenge. The frequency and total number of live, lineage-negative RFP^+ cells present in the lungs **D)**, and mLN **E)**. **F)** Representative flow cytometry of CD6 and MerTK expression on $Ly6C^+$ RFP^+ cells in the mLN on days 2 and 3 post-challenge. **G)** The frequency of the indicated cell subset among total RFP^+ cells in the lungs on the indicated days post-challenge. **H)** The gMFI for RFP in the indicated myeloid cell subsets in the lungs over the course of A/PR8-challenge. **I)** The total number of RFP^+ cells present in the lungs over the course of A/PR8-challenge. Data are presented as mean ± SEM (n=7 mice). $^{ns}p>0.05$ = not significant, $^{*}p\leq0.05$, $^{***}p\leq0.001$, $^{****}p\leq0.001$ (One-way ANOVA).

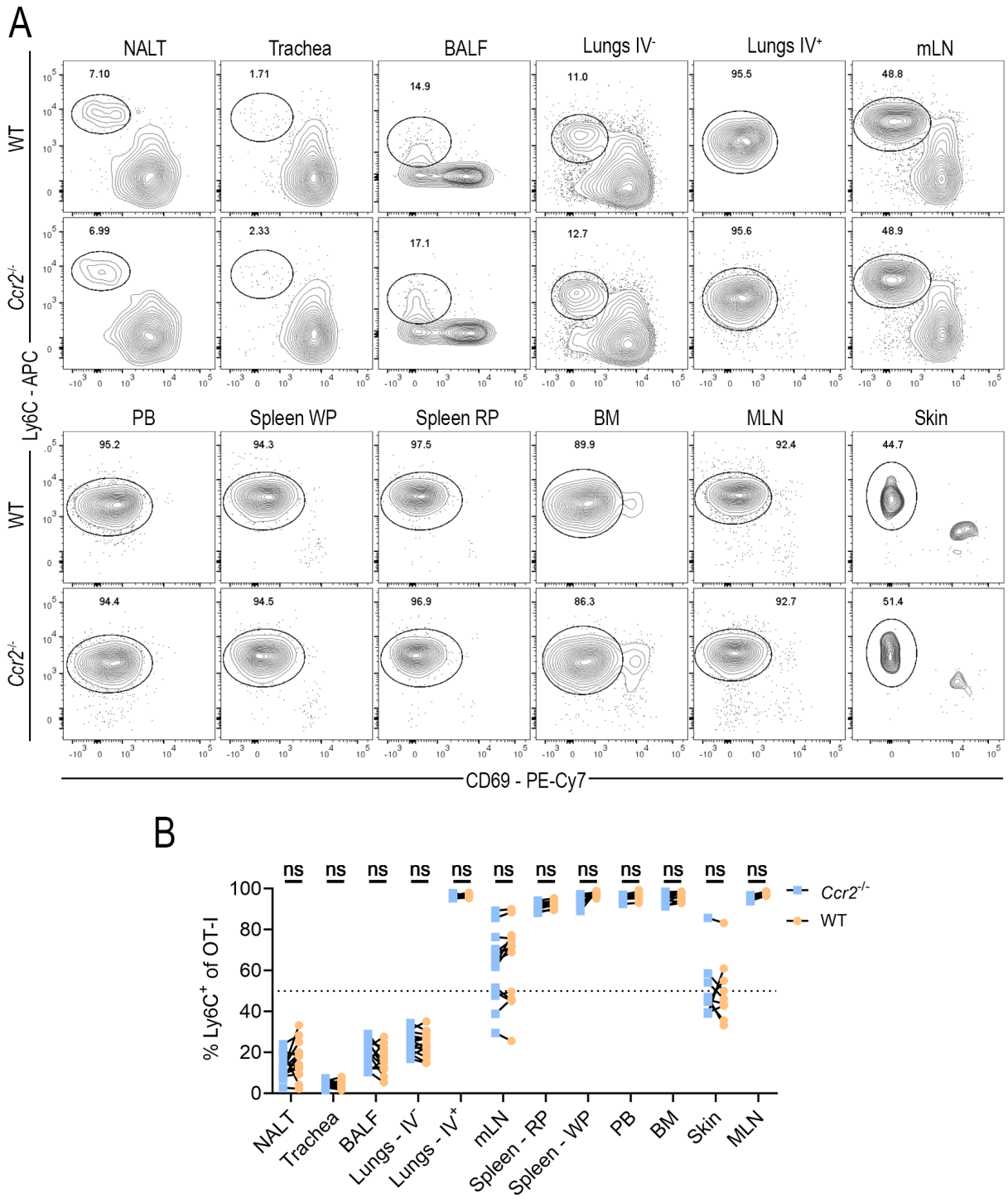

Figure 3.21: Homeostatic trafficking of circulating memory cells is normal in the absence of Ccr2

Peripheral tissues, SLOs, and BM were assessed for the presence of Ly6C$^+$ CD69$^-$ tissue-surveying circulating memory cells 35 days post x31-Ova infection. **A)** Representative flow cytometry of Ly6C$^+$ CD69$^-$ WT and *Ccr2*$^{-/-}$ OT-I putative circulating memory T cells in the indicated tissues. **B)** Quantification of **A)**. Data are presented as mean ± SEM (n=14 mice), pooled from 2 independent experiments. ^{ns}p>0.05 = not significant (Two-way ANOVA).

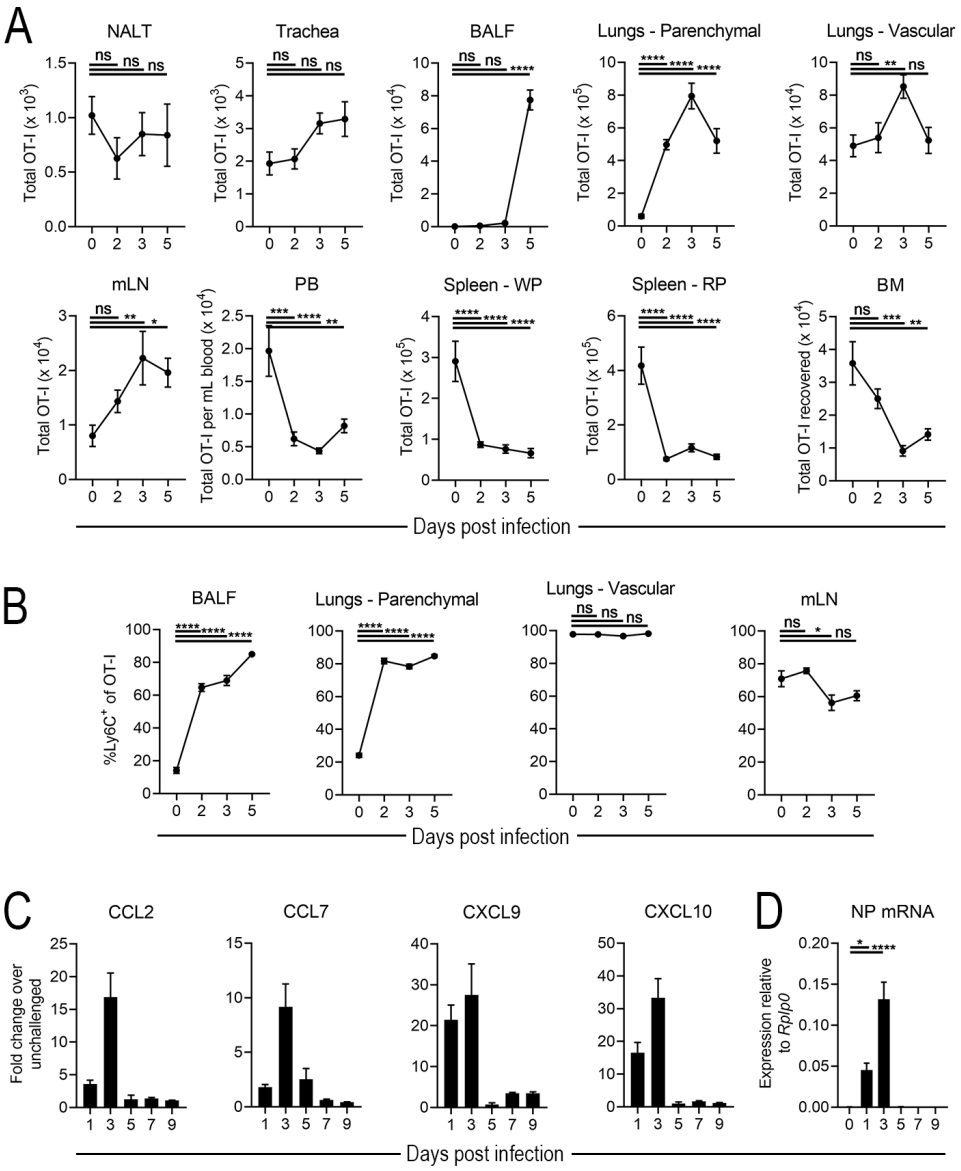

Figure 3.22: Memory OT-I cells infiltrate the infected lungs within 48-72 hours of PR8 challenge

OT-I immune mice were challenged with A/PR8 and the movement of memory OT-I cells tracked on day 0 (no challenge), 2, 3, and 5 post-challenge. **A)** Total number of OT-I cells recovered from the indicated organs over the course of A/PR8 challenge. **B)** Frequency of $Ly6C^+$ cells among OT-I cells in the indicated organs following A/PR8 challenge. **C)** Inflammatory chemokine mRNA expression in the lungs of A/PR8-challenged x31-Ova-immune mice, displayed as fold-change over resting memory. **D)** Influenza NP mRNA in the lungs of A/PR8 challenged x31-Ova-immune mice, expression relative to *Rplp0*. Data are presented as mean ± SEM. (**(a-B)** n=7 mice per time point), representative of 3 independent experiments. (**(C-D)** n=4 mice per time point). $^{ns}p>0.05$ = not significant, $^{*}p\leq0.05$, $^{**}p\leq0.01$, $^{***}p\leq0.001$, $^{****}p\leq0.0001$ (One-way ANOVA).

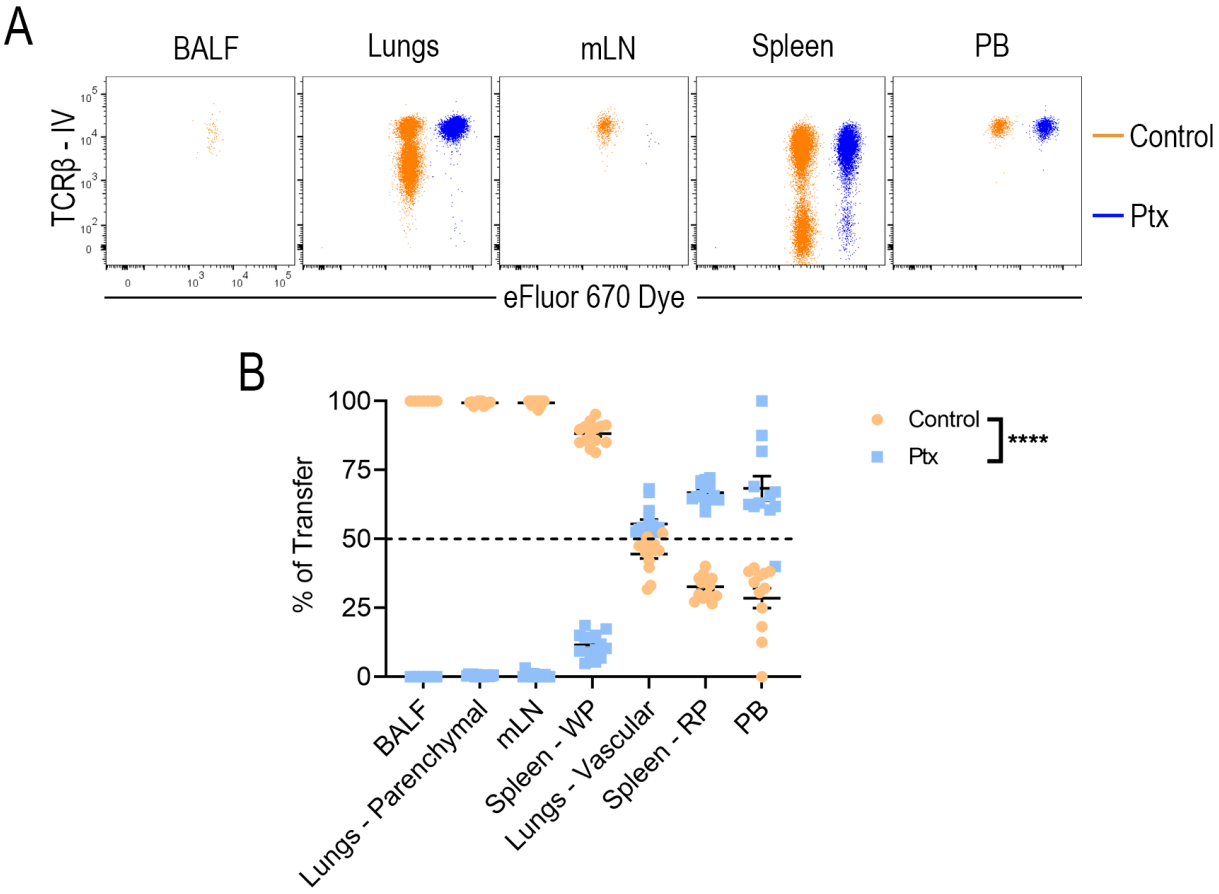

Figure 3.23: Pertussis toxin-treated OT-I cells fail to migrate into inflamed lungs and lymph nodes.

OT-I cells were enriched from the spleens of day 21 x31-Ova-immunised mice, labelled with a fluorescent proliferation dye, and treated *ex-vivo* with pertussis toxin or control media prior to co-transfer into day 6 A/PR8 infected hosts. **A)** Representative flow cytometry of pertussis toxin-treated (blue) and control (orange) OT-I cells in the indicated organs 12 hours after transfer. **B)** Recovery of pertussis toxin-treated and control treated cells in the indicated organs 12 hours after transfer. Data are presented as mean ± SEM (n=12 mice), pooled from 2 independent experiments. ****p≤0.0001 (Two-way ANOVA).

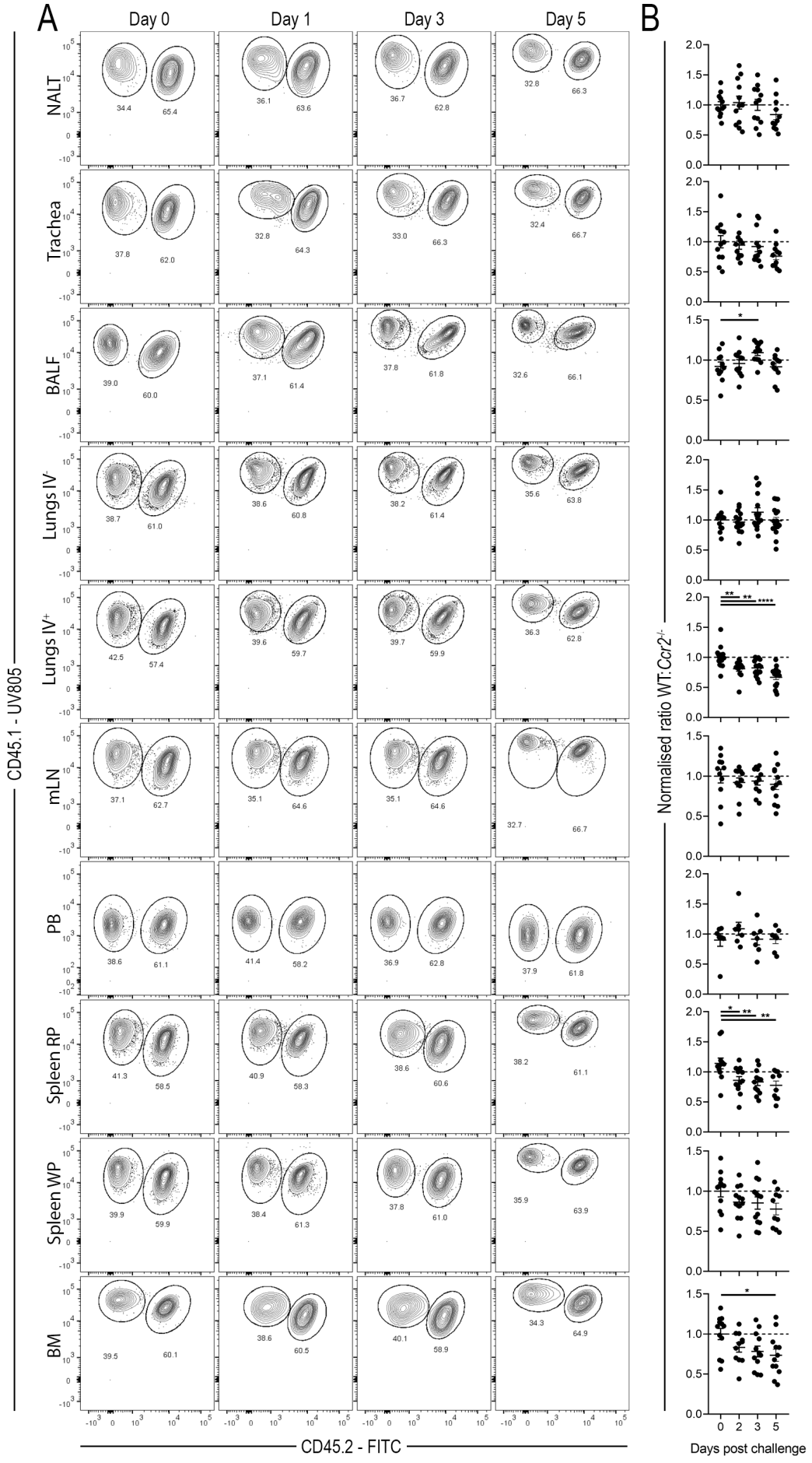
A
Day 0
Day 1
Day 3
Day 5
NALT
Trachea
BALF
Lungs IV-
Lungs IV+
mLN
PB
Spleen RP
Spleen WP
BM
34.4
65.4
36.1
63.6
36.7
62.8
32.8
66.3
37.8
62.0
32.8
64.3
33.0
66.3
32.4
66.7
39.0
60.0
37.1
61.4
37.8
61.8
32.6
66.1
38.7
61.0
38.6
60.8
38.2
61.4
35.6
63.8
42.5
57.4
39.6
59.7
39.7
59.9
36.3
62.8
37.1
62.7
35.1
64.6
35.1
64.6
32.7
66.7
38.6
61.1
41.4
58.2
36.9
62.8
37.9
61.8
41.3
58.5
40.9
58.3
38.6
60.6
38.2
61.1
39.9
59.9
38.4
61.3
37.8
61.0
35.9
63.9
39.5
60.1
38.6
60.5
40.1
58.9
34.3
64.9
CD45.1 - UV805
CD45.2 - FITC
B
Normalised ratio WT:Ccr2-/-
Days post challenge
0
2
3
5

Figure 3.24: Migration of memory T cells into inflamed tissue occurs independently of the chemokine receptor CCR2.

OT-I-immune mice were challenged with A/PR8 and the frequencies of WT and *Ccr2*$^{-/-}$ memory OT-I cells tracked on days 0 (no challenge), 2, 3, and 5 post-challenge. **A)** Representative flow cytometry of WT (CD45.1^{+}) and (*Ccr2*$^{-/-}$ CD45.1^{+}CD45.2^{+}) OT-I cells in the indicated organs at the indicated time points post A/PR8-challenge. **B)** The ratio of WT to *Ccr2*$^{-/-}$ OT-I cells on the indicated days post-infection, normalised to the ratio in unchallenged (day 0) mice. Data are presented as mean ± SEM (n=13 mice), pooled from 2 independent experiments. *p≤0.05, **p≤0.01, ***p≤0.001, ****p≤0.0001 (One-way ANOVA).

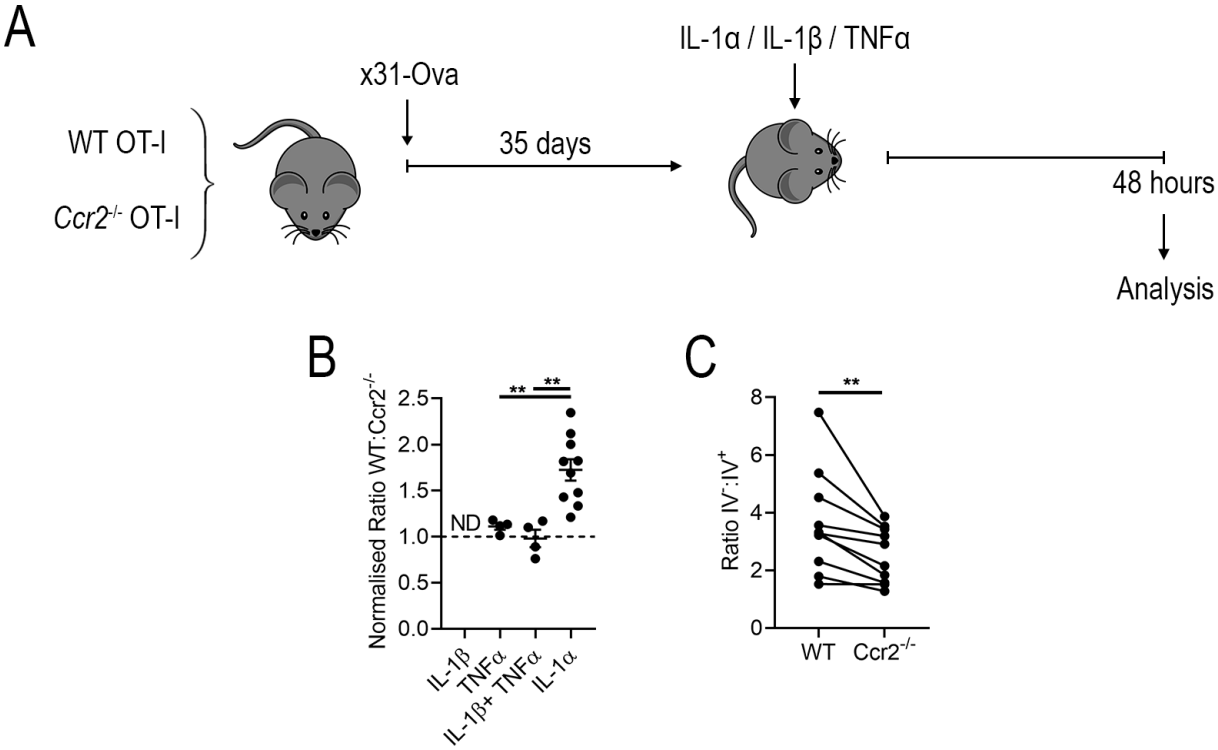

Figure 3.25: T cell recruitment into cytokine-treated ears is impaired in the absence of CCR2. OT-I immune mice were injected in the ear pinna with combinations of IL-1α, IL-1β, and TNFα and accumulation of WT and *Ccr2*$^{-/-}$ OT-I cells into cytokine-treated ears determined by flow cytometry. **A)** Experimental plan. **B)** The ratio of WT to *Ccr2*$^{-/-}$ OT-I cells present in the vascular-negative fraction of cytokine-treated ears normalised to the ratio of WT to *Ccr2*$^{-/-}$ cells in the circulation. **C)** The ratio of vascular-negative to vascular positive WT and *Ccr2*$^{-/-}$ OT-I cells present in cytokine treated ears. ND = not detected. n=4-5 mice per condition for IL-1β- , and TNFα-treated mice. Data are presented as mean ± SEM (n=10 mice for IL-1α treated mice), pooled from 2 independent experiments. **p≤0.01 (**(B)** One-way ANOVA. **(C)** paired Students *t*-test.)

4 | The role of host CCR2 in influenza challenge

4.1 Introduction

The results obtained from CCL2-reporter mice during primary A/HK-x31 infection and A/PR8 challenge presented in chapter 3 identified monocytes and monocyte-derived cells as cells likely to play a key role in interacting with CCR2-expressing $CD8^+$ T cells during influenza infection. Although removing the ability of $CD8^+$ T cells to respond to CCL2-producing monocytes did not have any impact on $CD8^+$ T cell effector or memory differentiation, it was still unclear if monocytes were capable of influencing these T cell fates. Monocytes and their derivatives have been shown to influence the polarisation of $CD4^+$ T helper subsets in bacterial, fungal, and viral infections, and in autoimmune disease [135–137, 326, 327]. In viral infection of the lungs, monocytes have also been implicated in regulating T cell expansion, however how they augment T cell expansion, and how this impacts the development of effector and memory populations is not clear [120]. Additionally, monocytes have been shown to regulate the function of memory $CD8^+$ T cells during recall responses, both by providing chemokines that influence the positioning of memory T cells, and through the provision of inflammatory cytokines that stimulate production of effector cytokines by memory cells [124, 328]. Thus, in this chapter, monocytes were investigated for a role in shaping influenza-specific $CD8^+$ T cell effector and memory cell differentiation following influenza infection, and in regulating influenza-specific memory $CD8^+$ T cell function during a heterosubtypic influenza-challenge.

4.2 Monocytes and monocyte-derived cells are reduced in number in the lungs and mLN of influenza-infected *Ccr2*$^{-/-}$ mice

Results from the previous chapter identified monocytes and monocyte-derived cells as a major source of CCL2, and these cells were hypothesised to interact with CCR2-expressing $CD8^+$ T cells. As monocytes are dependent on the chemokine receptor CCR2 to exit the bone marrow during acute inflammation [122], and results from the previous chapter indicated that cell-intrinsic CCR2 was dispensable for $CD8^+$ T cell fate decisions, *Ccr2*$^{-/-}$ mice were used to determine the contribution of monocytes to $CD8^+$ T cell responses during influenza infection. First, it was investigated how the distribution of monocyte populations identified in **Fig. 3.9** was altered in the respiratory tract and mLN of *Ccr2*$^{-/-}$ mice after influenza infection. *Ccr2*$^{-/-}$ and WT littermate controls were infected with $100TCID_{50}$ A/HK-x31 and MNP populations infiltrating the lungs, airways, and mLN were tracked on days 3, 5, 7 and 9 post-infection. Following A/HK-x31 infection there were significant reductions in all populations of monocyte and monocyte-derived cells in the lungs of *Ccr2*$^{-/-}$ mice by day 7 post-infection relative to WT mice, with the most abundant subset, monocyte-derived Mϕ, displaying a 60-fold reduction in the lungs of *Ccr2*$^{-/-}$ mice at days 7 and 9 **(Fig. 4.1A-B)**. These reductions were also seen in cells recovered from the BALF of infected mice, although the extent of the reduction was lower in the airways compared to the lungs **(Fig. 4.1C-D)**. Though the extent of monocyte infiltration into the mLN was smaller than that observed in the respiratory tract, there was a statistically significant reduction in the total number of F4-80^+ CD172α^+ Ly6C^+ monocytes in the mLNs of *Ccr2*$^{-/-}$

mice relative to WT mice on days 3, 5 and 9 post A/HK-x31 infection **(Fig. 4.1E)**. Together, these data demonstrate that in influenza infected mice monocytes and monocyte-derived cells are recruited to the respiratory tract and mLN in a CCR2-dependent manner.

4.3 Host deficiency of *Ccr2* compromises OT-I cell memory formation

To determine the impact of monocytes on the $CD8^+$ T cell effector response to influenza infection 10^4 naïve OT-I cells were transferred into *Ccr2*$^{-/-}$ or WT littermate controls prior to infection with x31-Ova **(Fig. 4.2A)**. On day 9 post x31-Ova infection mice were injected IV with 3µg of αCD45 to label vascular cells and the differentiation of $CD127^+$ MPECs and $KLRG1^+$ SLECs determined in the respiratory tract and SLOs using the gating strategy outlined in **Fig. 4.2B**. With the exception of the PB, where there was a reduction in OT-I cells in *Ccr2*$^{-/-}$ hosts, equivalent numbers of OT-I cells were recovered from the organs of *Ccr2*$^{-/-}$ and WT hosts **(Fig. 4.2C)**. Analysis of OT-I effector cell differentiation in the airways, lungs, mLN, spleen and PB revealed that effector differentiation was largely unaltered in *Ccr2*$^{-/-}$ host mice 9 days post-infection **(Fig. 4.2D)**. There was a small but statistically significant decrease in the percentage of MPECs in the white pulp of the spleen of *Ccr2*$^{-/-}$ hosts, although this was not reflected in the total number of MPECs present. The reduction of OT-I cells in the PB of *Ccr2*$^{-/-}$ host mice was not specific to any particular effector T cell subset as there were equivalent reductions in each of the effector subsets examined **(Fig. 4.2D)**. Together, these data demonstrate that monocytes and their derivatives do not overtly influence the differentiation of effector T cell subsets during influenza infection.

It has been demonstrated that monocytes can provide cytokines during T cell priming that influence the effector potential of $CD4^+$ T cells [128, 329]. Thus, it was next determined if the reduction in CCL2-producing monocyte populations in *Ccr2*$^{-/-}$ hosts had an impact on the acquisition of OT-I effector potential. Single-cell suspensions were prepared from the lungs and mLN of WT and *Ccr2*$^{-/-}$ mice were stimulated *ex vivo* with SIINFEKL in the presence of protein transport inhibitors to determine effector cytokine and granzyme B production in transferred OT-I cells. After *ex vivo* stimulation with SIINFEKL, OT-I cells present at the priming site (mLN) and effector site (lungs) of WT and *Ccr2*$^{-/-}$ hosts displayed similar expression of effector cytokines **(Fig. 4.3A)**. OT-I cells from the lungs of *Ccr2*$^{-/-}$ mice displayed a small, but statistically significant, increase in both the frequency and gMFI of IFNγ-expressing cells **(Fig. 4.3B-C)**. There were no differences in cytokine or granzyme B production by OT-I cells isolated from the mLN of WT and *Ccr2*$^{-/-}$ hosts **(Fig. 4.3B-C)**. Therefore, monocytes have minimal impact on the development of $CD8^+$ T cell effector potential.

Next, the persistence and memory phenotype of OT-I cells was determined in *Ccr2*$^{-/-}$ and WT hosts 35 days post-infection **(Fig. 4.4A)**. Analysis of memory populations showed that, in *Ccr2*$^{-/-}$ hosts compared to WT hosts at day 35 post-infection, there was a significant reduction in the number of OT-I cells present in every compartment analysed, except in the PB where there was no statistically significant difference in the number or frequency of OT-I cells recovered **(Fig. 4.4B)**. For the respiratory tract and the mLN there was a 3-fold reduction

in the total number of OT-I cells recovered from *Ccr2*$^{-/-}$ hosts, and a 2-fold reduction in OT-I cells recovered from the splenic white and red pulp **(Fig. 4.4C)**. These differences did not appear to be a result of altered migration of these memory cells, as the distribution of these cells between the lung vasculature and the parenchyma, and the red pulp and white pulp of the spleen was equivalent between WT and *Ccr2*$^{-/-}$ hosts **(Fig. 4.4D)**. It has been reported that lack of CD4^{+} T cell help during priming, or increased exhaustion, can lead to reduced numbers of CD8^{+} T cells at memory timepoints, and that this can present as an increase in the frequency of KLRG1^{+} SLECs in the memory population that develops [303]. To determine if this was potentially an underlying cause for the reduction in OT-I cell numbers in *Ccr2*$^{-/-}$ hosts, OT-I cells were stained for CD127 and KLRG1 to delineate these effector subsets in the spleen **(Fig. 4.4E)**. At this timepoint however, there were no differences in the frequency of these effector subsets in either WT or *Ccr2*$^{-/-}$ hosts. These results indicate that OT-I cells responding to x31-Ova infection in *Ccr2*$^{-/-}$ hosts have compromised memory formation that is not likely a result of impaired priming.

To determine if the reduced numbers of memory OT-I cells observed in *Ccr2*$^{-/-}$ host mice was confined to a particular memory subset, a more detailed analysis of memory OT-I cells present at day 35 was performed. Analysis of OT-I cells in the respiratory tract and mLN revealed that there was no difference in the formation of CD69^{+} CD103^{+} Trm cells in the airways, lung parenchyma and mLN of WT and *Ccr2*$^{-/-}$ hosts **(Fig. 4.5A-B)**. However, while the frequency of Trm cells among total OT-I cells in these compartments was equivalent between WT and *Ccr2*$^{-/-}$ hosts, there was a statistically significant reduction in the total number of Trm cells recovered in each of those organs **(Fig. 4.5C)**. In SLOs of WT and *Ccr2*$^{-/-}$ mice, the formation of circulating memory subsets was also equivalent, however, in the PB there was an increased frequency of Tem cells recovered from *Ccr2*$^{-/-}$ host mice and a reduction in Tcm cells **(Fig. 4.5D-E)**. This difference in frequency was also reflected in the total number of Tcm and Tem subsets recovered per mL of PB in *Ccr2*$^{-/-}$ host mice **(Fig. 4.5E)**. Like those results seen for Trm cells, while the frequencies of the different circulating memory cell subsets was mostly equivalent between WT and *Ccr2*$^{-/-}$ hosts, the total number of each circulating-memory cell subset was reduced in all organs in *Ccr2*$^{-/-}$ hosts, but these differences only reached statistical significance for the Tcm cells in the mLN and splenic WP, and for Tcm and Tem cells present in the red pulp of the spleen and the circulation **(Fig. 4.5E)**. These data suggest that there is no requirement for host CCR2 in the differentiation of memory T cell subsets. However, there is a cell-extrinsic requirement for CCR2 in the optimal formation or maintenance of long-lived CD8^{+} memory pools.

Data generated thus far revealed that, in regards to relative frequencies of specific memory subsets, the formation of circulating and resident memory cell subsets was intact in *Ccr2*$^{-/-}$ hosts, however, there was a reduction in the total number present. Next, it was determined if the effector potential of those memory cells recovered from WT and *Ccr2*$^{-/-}$ host mice was compromised. After *ex vivo* restimulation with SIINFEKL, OT-I cells from the spleen and lungs of dat 35 x31-Ova-infected WT and *Ccr2*$^{-/-}$ hosts displayed similar expression of effector cytokines and granzyme B. As expected, the frequency of granzyme B expression and the gMFI of granzyme B was higher in OT-I cells from the lungs compared to the spleen. In contrast, the production of effector cytokines IFNγ, IL-2 and TNFα was more pronounced in OT-I cells from the spleen **(Fig. 4.6A)**. Despite the reduction in number, and regardless of their anatomical location, memory OT-I cells recovered from WT or *Ccr2*$^{-/-}$ hosts displayed no difference in the ability to produce effector cytokines or granzyme B, or in the mean fluorescence intensity for

those cytokines and molecules after *ex-vivo* stimulation **(Fig. 4.6B-C)**. These data demonstrate that while there are reduced numbers of memory cells in *Ccr2*$^{-/-}$ hosts, the effector potential of those remaining cells is unaltered.

Next, it was determined if the defect in the quantity of memory OT-I cells recovered from *Ccr2*$^{-/-}$ mice also applied to host endogenous influenza-specific CD8^{+} T cells. WT and *Ccr2*$^{-/-}$ mice were therefore infected with A/HK-x31 and on day 35 post infection influenza nucleoprotein (NP)- and viral polymerase (PA)-specific memory CD8^{+} T cells were assessed in the respiratory tract, SLOs and PB using tetramers as outlined in the gating strategy in **Fig. 4.7A**. With the exception of the mLN of *Ccr2*$^{-/-}$ mice, where there was a 2-fold statistically significant reduction in NP-specific cells recovered, and the vasculature of the lungs, where there was a small but statistically significant reduction in NP-specific cells recovered, the total number of influenza-specific CD8^{+} T cells recovered was equivalent between WT and *Ccr2*$^{-/-}$ mice **(Fig. 4.7B)**. However, it must be noted that the reduced number of influenza-specific memory T cells in the mLN may be due to the reduced overall cellularity of that organ in *Ccr2*$^{-/-}$ mice at this time point, which displayed a 2-fold reduction in the total number of cells recovered relative to WT mice **(Fig. 4.7C)**. Next, the formation of influenza-specific resident memory cells was determined for the airways, mLN, and the IV^{-} fraction of the lungs **(Fig. 4.8A)**. Of those cells recovered from the respiratory tract and mLN of WT and *Ccr2*$^{-/-}$ mice, there were equivalent frequencies of Trm cells for both NP- and PA-specific T cells **(Fig. 4.7B)**. There was also no difference between WT and *Ccr2*$^{-/-}$ mice with respect to the total number of influenza-specific Trms recovered from the lungs. However, there was a statistically significant 2-fold reduction in the number of NP-specific Trms recovered from the lungs **(Fig 4.8C)**. There was equivalent formation of the different circulating memory CD8^{+} T cell subsets in the mLN, PB and spleen in WT and *Ccr2*$^{-/-}$ mice **(Fig. 4.9A-B)**. However, in *Ccr2*$^{-/-}$ mice there was a statistically significant 2-fold reduction in the number of NP- and PA-specific Tcm cells that were recovered from the mLN and a slight reduction in the number of PA-specific T cells recovered from the WP of the spleen **(Fig. 4.9C)**. Together, these data indicate that, in contrast to that observed with memory OT-I cells in *Ccr2*$^{-/-}$ mice, where memory T cells were reduced in number in all compartments analysed, influenza-specific memory CD8^{+} T cells recovered from *Ccr2*$^{-/-}$ mice had mostly normal memory formation, with the exception of the mLN, which had a 2-fold reduction in NP-specific memory cells.

Lastly the effector potential of influenza-specific CD8^{+} memory T cells from WT and *Ccr2*$^{-/-}$ hosts was assessed. Single-cell suspensions from the spleen and lungs of day 35 post A/HK-x31 infected mice were stimulated *ex-vivo* with PMA and secretion of IFNγ and presence of granzyme B in influenza-specific T cells was quantified **(Fig. 4.10A)**. The expression of IFNγ was relatively similar for both NP- and PA-specific T cells in the lungs and spleen. Granzyme B expression was higher in cells present in the lungs whereas cells isolated from the spleen expressed higher levels of IFNγ, similar to those results seen in memory OT-I cells isolated from WT and *Ccr2*$^{-/-}$ hosts **(Fig. 4.10A)**. Overall there was no difference between the frequency or gMFI of IFNγ and granzyme B expression in NP- and PA-specific T cells isolated from WT or *Ccr2*$^{-/-}$ mice **(Fig. 4.10B-E**. These results demonstrate that, similar to those results seen in OT-I cells recovered from WT and *Ccr2*$^{-/-}$ hosts, global deficiency in CCR2 does not impair the effector potential of influenza-specific CD8^{+} T cells.

4.4 Host Ccr2 is required for optimal protection during heterosubtypic influenza challenge

Data generated thus far indicated that there was minimal requirement for CCR2 in the generation of $CD8^+$ T cell effector responses, and in the formation of endogenous influenza-specific memory populations. Previous studies utilising lethal influenza challenge in *Ccr2*$^{-/-}$ mice had demonstrated increased morbidity in *Ccr2*$^{-/-}$ mice relative to WT [330], which was attributed to a reduction in memory $CD8^+$ T cell maintenance prior to influenza challenge [118, 330]. However, data in the present study indicated that, under the conditions tested, the total number of endogenous NP- and PA-specific memory T cells was largely unaltered in *Ccr2*$^{-/-}$ mice, and thus, would not be able to explain the increased morbidity following challenge in those studies mentioned above. Thus, to determine if *Ccr2* deletion had any impact on the host response to influenza challenge under the conditions tested in this study, WT and *Ccr2*$^{-/-}$ mice were immunised with $100TCID^{50}$ A/HK-x31 or $1TCID_{50}$ A/PR8, or immunised with $100TCID_{50}$ A/HK-x31 and challenged with $500TCID_{50}$ A/PR8 and weight loss monitored over the course of infection or challenge **(Fig. 4.11A)**. For both primary and secondary infections with A/HK-x31 and A/PR8 these infectious doses result in mild weight loss that can be used as a readout of viral control. During a primary infection with either A/HK-x31 or A/PR8 there was no significant difference in weight loss between WT and *Ccr2*$^{-/-}$ mice **(Fig. 4.11B-C)**. However, when A/HK-x31 immune mice were challenged with a lethal dose of A/PR8 both WT and *Ccr2*$^{-/-}$ displayed equivalent weight loss until day 3 post challenge, at which time WT mice began to stabilise and recover weight. In contrast, *Ccr2*$^{-/-}$ mice continued to lose weight for another 2 days at a rate similar rate to naïve mice **(Fig. 4.11D)**. Weight loss peaked in *Ccr2*$^{-/-}$ mice at day 5 post-challenge at which time they began to recover, though at a slower rate than their WT littermate controls. This weight loss was not specific to the A/PR8 virus as naïve WT and *Ccr2*$^{-/-}$ mice that were infected with a sub-lethal dose of A/PR8 had similar morbidity **(Fig. 4.11C)**. These results demonstrate that *Ccr2*$^{-/-}$ mice are impaired in their ability to control secondary, but not primary, influenza challenges despite the normal formation of influenza-specific memory populations after primary A/HK-x31 infection.

To determine if this difference in morbidity seen upon challenge was due to impaired control of the virus, viral titres in the lungs of A/HK-x31 immune WT and *Ccr2*$^{-/-}$ mice during A/PR8 challenge were determined by qPCR. On days 3 (peak weight loss for WT mice) and 5 (peak weight loss for *Ccr2*$^{-/-}$ mice) post-A/PR8 challenge, lungs from WT and *Ccr2*$^{-/-}$ mice were snap frozen and qPCR used to determine the presence of influenza NP mRNA **(Fig. 4.12A)**. NP mRNA was detectable on day 3 post A/PR8-challenge with statistically significantly higher levels of NP transcripts detected in *Ccr2*$^{-/-}$ mice at day 3 compared to WT mice. By day 5 post-challenge NP mRNA was no longer detectable in the lungs of WT mice, however, in the lungs of *Ccr2*$^{-/-}$ mice there was still a statistically significant increase in NP mRNA present **(Fig. 4.12A)**. Next, ELISAs were performed with BAL washes from WT and *Ccr2*$^{-/-}$ mice at days 0, 3 and 5 post-challenge to determine if there were differences in the secretion of the effector cytokine IFNγ. At both days 3 and 5 post-challenge there was a statistically significant reduction in IFNγ present in BAL washes recovered from *Ccr2*$^{-/-}$ mice compared to WT controls, however, this was

not seen during the primary response to A/HK-x31 **(Fig. 4.12B)**. To determine if the increased viral titres present in the lungs of *Ccr2*$^{-/-}$ mice was due to reduced *in vivo* cytotoxicity, differentially-labelled, NP peptide-pulsed and scrambled peptide-pulsed splenocytes were injected IV into A/HK-x31 immunised WT and *Ccr2*$^{-/-}$ mice **(Fig. 4.12C)**. Twenty four hours after injection of peptide-pulsed splenocytes, spleens were removed from recipient mice and the frequency of target and non-target cells determined by flow cytometry **(Fig. 4.12D-E)**. Both WT and *Ccr2*$^{-/-}$ mice displayed robust *in vivo* cytotoxic capability, with each lysing on average 45-50% of NP peptide-pulsed target cells relative to non-target controls. Although *Ccr2*$^{-/-}$ mice appeared to have slightly higher *in vivo* cytotoxic capability, this did not reach statistical significance. Together, these results demonstrate that, compared to WT mice, *Ccr2*$^{-/-}$ mice have an impaired ability to control secondary influenza infection. During secondary infections, *Ccr2*$^{-/-}$ mice have increased viral titres in the lungs, which is associated with increased morbidity and reduced production of the effector cytokine IFNγ.

Despite the reduction in the level of IFNγ recovered from the BALF of *Ccr2*$^{-/-}$ mice, results from **Fig. 4.10** had already indicated that resting memory influenza-specific cells isolated from the lungs of *Ccr2*$^{-/-}$ mice displayed no defect in IFNγ production after *ex vivo* stimulation with PMA. To determine if the ability of influenza-specific T cells to produce IFNγ changes over the course of A/PR8 challenge, or if other IFNγ-producing cells were impaired in their ability to secrete this cytokine during challenge, single cell suspensions from the lungs were taken from WT and *Ccr2*$^{-/-}$ mice on days 3 and 5 after A/PR8-challenge and stimulated *ex-vivo* with PMA to assess IFNγ production. Despite the reduction in IFNγ protein in the BALF of *Ccr2*$^{-/-}$ mice, CD45^{+} cells in the lungs of *Ccr2*$^{-/-}$ mice had a near 4-fold increase in the frequency of IFNγ^{+} cells on day 3 post-challenge, although this changed by day 5 where WT mice had a higher frequency of IFNγ^{+} cells **(Fig. 4.13A)**. The increased IFNγ staining in *Ccr2*$^{-/-}$ mice was mainly due to CD4^{+} and CD8^{+} T cells which had 3-fold higher frequency of IFNγ^{+} cells after stimulation relative to WT controls **(Fig. 4.13B-C)**, NK and NKT cells also had significantly higher frequency of IFNγ producing cells. By day 5 post-challenge the frequency of IFNγ producing cells was higher in CD44^{+} CD4^{+} T cells from WT mice compared to *Ccr2*$^{-/-}$ mice, but was equivalent between all other cell types analysed. However, there was a statistically siginficant 2-fold reduction in the total number of CD8^{+} CD44^{+} cells present in the lungs of *Ccr2*$^{-/-}$ mice compared to WT mice by day 5 post infection, suggesting that while the frequency of IFNγ-producing cells was equivalent, overall IFNγ production by this population would still be compromised **(Fig. 4.13D)**. Thus, *ex vivo* stimulation of IFNγ-producing cells following A/PR8 challenge revealed that T cells from day 3 A/PR8 challenged *Ccr2*$^{-/-}$ mice had a greater potential to produce IFNγ, however, the reverse was true at day 5 post-challenge. Despite this, there was a reduction in the presence of IFNγ in BALF washed recovered from these mice at both days 3 and 5 post-challenge.

The results from **Fig. 4.13** did not show a defect in the frequency of IFNγ producing CD8^{+} T cells cells isolated from the lungs of *Ccr2*$^{-/-}$ mice, but did reveal a decrease in the total number of CD8^{+} T cells present in the lungs of *Ccr2*$^{-/-}$ mice on day 5 post challenge which may have contributed to impaired viral control. This decrease at this time point could be due to increased death, decreased proliferation, or decreased recruitment of memory CD8^{+} T cells into the challenged lungs. First, a potential role for host CCR2 in the recruitment of circulating memory cells to the inflamed lungs was investigated. Experiments performed in the previous chapter

had eliminated a cell-intrinsic role for CCR2 in the recruitment of memory OT-I cells into A/PR8 challenged lungs **(Fig. 3.24)**. While there was no cell-intrinsic role for CCR2 in memory T cell recruitment to the inflamed lung, circulating memory cells could rely on the recruitment of monocytes to the inflamed lung, where these cells would secrete chemokines and cytokines that promote inflammation that could further recruit circulating memory cells, as has been described in inflamed skin [331]. If this was occurring, influenza-specific T cell numbers would be reduced in the lungs of *Ccr2*$^{-/-}$ mice and potentially increased in other peripheral tissues over the course of A/PR8-challenge. To determine if there was a reduction in the recruitment of CD8^{+} T cells into the lungs of A/PR8-challenged *Ccr2*$^{-/-}$ mice, A/HK-x31-immune WT and *Ccr2*$^{-/-}$ hosts were challenged with A/PR8 and organs taken on days 3, 5 and 7 post-challenge to track the presence of influenza-specific CD8^{+} T cells using the gating strategy outlined in **Fig. 4.14A**. By day 3 post-challenge the number of influenza-specific CD8^{+} T cells present in all organs analysed was equivalent between WT and *Ccr2*$^{-/-}$ mice, despite the differences seen in resting memory CD8^{+} T cells in the mLN and lung vasculature of *Ccr2*$^{-/-}$ mice **(Fig. 4.7B)**. By day 5 post-challenge there were significant differences in the total number of PA-specific T cells recovered from the lung parenchyma and vasculature of *Ccr2*$^{-/-}$ mice, but not in any other organ. By day 7, with the exception of the airways, there were significant reductions in the total number of both PA- and NP-specific T cells recovered from all tissues of *Ccr2*$^{-/-}$ mice compared to WT mice **(Fig. 4.14B)**. As the recruitment of memory CD8^{+} T cells to inflamed lungs occurs within 48-72 hours of challenge **(Fig. 3.20)**, and as the reduction in influenza-specific cells was present in all tissues analysed only at day 7 post-challenge, it is unlikely that the reduction in the number of influenza-specific T cells observed in *Ccr2*$^{-/-}$ mice was due to a defect in recruitment. A more likely explanation for the reduced numbers is increased death upon activation, or a reduction in the secondary expansion of influenza-specific cells.

The possibility of decreased proliferation of influenza-specific memory T cells in *Ccr2*$^{-/-}$ mice was determined using BrdU, a thymidine analog that is incorporated into the DNA of dividing cells and can be detected using fluorescently-conjugated antibodies, revealing cells that have undergone proliferation, or are actively proliferating. A/HK-x31-immune WT and *Ccr2*$^{-/-}$ mice were challenged with A/PR8 and given 2 injections of BrdU 24 and 12 hours prior to sacrifice, and influenza-specific CD8^{+} cells from the lungs and mLN were stained on days 3, 5 and 7 post A/PR8-challenge for intra-nuclear BrdU and Ki67, the latter marker a nuclear protein that is present during all active phases of the cell cycle (G1, S, G2, and mitosis), but is absent in quiescent cells (G0), using the gating strategy outlined in **Fig. 4.15A**. There was a statistically significant reduction observed in the frequency of both NP- and PA-specific CD8^{+} T cells that had incorporated BrdU and were expressing the cell-cycle marker Ki67 in the lungs of *Ccr2*$^{-/-}$ mice on day 3 post challenge. On day 5 post challenge however, there was no significant difference in staining for these markers and, by day 7 post infection, influenza-specific cells in the lungs of *Ccr2*$^{-/-}$ mice displayed higher frequencies of BrdU incorporation and Ki67 expression **(Fig. 4.15B)**. At no time-point post-infection was there a difference in BrdU incorporation in influenza-specific cells in the mLN between WT and *Ccr2*$^{-/-}$ mice **(Fig. 4.15C)**. In the lungs of *Ccr2*$^{-/-}$ mice the total number of influenza-specific cells that were BrdU^{+} Ki67^{+} was statistically significantly reduced on days 3 and 5 post infection relative to influenza-specific cells in WT mice, however by day 7 post infection the number of proliferating cells was not statistically significantly different **(Fig. 4.15D)**. The remaining tetramer-negative CD44^{+} CD8^{+} T cells present in the lung parenchyma of *Ccr2*$^{-/-}$ mice did not show a significant reduction in BrdU incorporation compared

to WT mice, although host endogenous $CD4^+$ $CD44^+$ T cells in *Ccr2*$^{-/-}$ mice did take up less of the DNA analog **(Fig. 4.15E)**. Together, these results indicate that influenza-specific memory $CD8^+$ T cells and $CD4^+$ T cells in the lungs, but not mLN, of *Ccr2*$^{-/-}$ mice proliferate less during the early stages of A/PR8 challenge, suggesting the increased morbidity in *Ccr2*$^{-/-}$ mice during A/PR8 challenge could be due to reduced memory T cell re-activation and expansion in the lungs, at these early time points.

4.5 Cell-intrinsic CCR2 is not required for $CD8^+$ T cell memory expansion

To investigate the CCR2-dependent mechanism that promotes the re-expansion of memory T cells in the lungs of influenza challenged mice, a cell-intrinsic requirement for CCR2 in memory T cell re-expansion was investigated. Naïve WT and *Ccr2*$^{-/-}$ OT-I cells were co-transferred into naïve B6 hosts that were infected with x31-Ova 24 hours later, and left for 35 days to develop resting memory populations. Mice containing WT and *Ccr2*$^{-/-}$ resting memory OT-I cells were either mock-challenged, or challenged with PR8-Ova, and left to recover for a further 35 days to generate primary and secondary memory populations respectively **(Fig. 4.16A)**. The respiratory tract, PB, and SLOs were analysed for the presence of primary and secondary memory OT-I cells, and the fold-expansion of these cells was calculated by dividing the total number of WT or *Ccr2*$^{-/-}$ OT-I cells in challenged mice, by the equivalent population in mock-challenged mice **(Fig. 4.16B)**. In this experimental setting, if cell-intrinsic CCR2 expression was required for the optimal re-expansion of memory OT-I cells, the fold-expansion of WT OT-I cells after challenge, relative to mock-challenged mice, would be higher than that of *Ccr2*$^{-/-}$ OT-I cells 35 days post PR8-Ova-challenge. After PR8-Ova-challenge OT-I cells increased in numbers in all organs analysed with the largest difference seen in the airways, where a relatively stable population of resident-memory cells were present that had, on average, 50-fold more cells recovered from challenged mice compared to mock-challenged mice. However, In all the organs analysed there were no statistically significant differences in the expansion of WT and *Ccr2*$^{-/-}$ OT-I cells relative to mock-challenged mice **(Fig. 4.16B)**. These results demonstrate that cell-intrinsic CCR2 is not required for the re-expansion of memory OT-I cells.

4.6 Fc-receptor-expressing cells are reduced in numbers in the lungs of *Ccr2*$^{-/-}$ mice following A/PR8 challenge

The reduction in BrdU incorporation and Ki67 expression in T cells in the lungs of *Ccr2*$^{-/-}$ mice during A/PR8 challenge potentially reflects a defect in antigen-presentation at those timepoints. Recently, a population of cDCs that acquires expression of Fc-receptors during infection and inflammation has been described [90]. This cDC subset, termed 'inflammatory-cDC2s', could be identified through intermediate expression of CD64 and binding

of the MAR-1 antibody. These inf-cDC2s shared a high degree of phenotypic similarity to both monocytes and Mϕ, were shown to drive robust T cell proliferation *ex vivo*, and had a partial reliance on CCR2 for tissue access [90]. Despite using the same gating strategy as Bosteels *et al.*, this cDC subset could not be reliably detected in the lungs of A/PR8 infected mice by flow cytometry (data not shown). However, it was also reported that in addition to expression of Fc-receptors, inf-cDC2s were negative for the pan-monocyte/Mϕ marker F4-80 and presumably, as they are a cDC subset, the Mϕ marker MerTK [90]. Thus, utilising a modified version of the gating strategy for MNP subsets outlined in **Fig. 3.9**, inf-cDCs were identified in the lungs as $CD64^+$ $F4\text{-}80^-$ $MerTK^-$ $CD11c^+$ $MHC\text{-}II^+$ cells, after pre-gating on live, lineage-negative, $CD45^+$, Siglec F^-, $Ly6G^-$, $CD43^-$ cells **(Fig. 4.17A)**. To confirm that these inf-cDCs were the same as those identified by Bosteels *et al.* expression of CD64 was quantified on $F4\text{-}80^-$ $MerTK^-$ inf-cDCs, relative to $F4\text{-}80^+$ $MerTK^-$ monocytes and $F4\text{-}80^+$ $MerTK^+$ Mϕ, which should display much higher expression of this marker [90]. Over the course of A/PR8 challenge $F4\text{-}80^-$ $MerTK^-$ inf-cDCs displayed much lower expression of this Fc-receptor relative to $F4\text{-}80^+$ $MerTK^-$ monocytes and $F4\text{-}80^+$ $MerTK^+$ Mϕ **(Fig. 4.17B-C)**, as was reported for inf-cDCs [90]. Thus, this alternative gating strategy was used for the identification of inf-cDCs in A/PR8-challenged lungs.

To determine which antigen-presenting cells were disrupted during A/PR8-challenge in *Ccr2*$^{-/-}$ mice, the lungs of A/HK-x31-immune WT and *Ccr2*$^{-/-}$ mice were screened for MNP subsets, as identified in **Fig. 3.8** and **Fig. 4.17A**, by flow cytometry on days 0 (no challenge), 3, 5, and 7 post A/PR8-challenge. Prior to challenge there were no statistically significant differences in the total number of the different MNP subsets present in the lungs of WT and *Ccr2*$^{-/-}$ mice **(Fig. 4.18A)**. Over the course of A/PR8 challenge the number of cDC1 and cDC2 subsets recovered from the lungs rapidly declined, but was not statistically significantly different between WT and *Ccr2*$^{-/-}$ mice. At day 3 post-challenge there was a 2-fold reduction in the total number of alveolar Mϕ recovered from the lungs of *Ccr2*$^{-/-}$ mice, though this difference was not seen at days 5 or 7. Consistent with results from Bosteel *et al.* [90] inf-cDCs were absent from the lungs of WT and *Ccr2*$^{-/-}$ mice prior to challenge, but were rapidly recruited to the tissue after A/PR8-challenge. The number of inf-cDCs recruited to the lungs of *Ccr2*$^{-/-}$ mice, however, was statistically significantly reduced over the course of A/PR8-challenge relative to WT controls. The other major MNP subsets that were disrupted over the course of A/PR8-challenge were monocytes and monocyte-derived cells **(Fig. 4.18A)**, summarised in **(Fig. 4.18B)**. While in unchallenged A/HK-x31-immune mice there were no differences in the total number of monocytes, monocyte-derived macrophages and tissue macrophages, all these cell subsets were statistically significantly reduced in number by day 3 post A/PR8-challenge and numbers were statistically significantly reduced over the course of challenge. Thus, in the lungs of *Ccr2*$^{-/-}$ mice over the course of A/PR8-challenge, monocytes, monocyte-derived cells and inf-cDCs are all statistically significantly reduced in numbers, suggesting that these reductions in APC numbers may be responsible for the reduction in influenza-specific T cell proliferation, and effector cytokine production.

As the antigen-presenting cells that were statistically significantly reduced in number in the lungs of *Ccr2*$^{-/-}$ mice over the course of A/PR8 challenge were inf-cDCs, and monocytes and their derivatives, potential models were investigated to target these MNP subsets during A/PR8 challenge and assess their role in secondary expansion of T cells during influenza challenge. To assess the contributions of monocytes and monocyte-derived

cells to the secondary expansion of memory $CD8^+$ T cells *Ccr2*-DTR mice were used, as these mice are commonly used as a model for monocyte depletion during infection [108, 124, 162, 301, 332–336]. In these mice all cells expressing *Ccr2* also express the diptheria toxin (Dtx) receptor, and administration of Dtx to these mice results in the depletion of CCR2-expressing cells. As these mice would also potentially deplete CCR2-expressing T cells, an OT-I T cell transfer system was used. Naïve OT-I cells were transferred into CCR2-DTR mice or WT littermate controls that were infected with x31-Ova 24 hours later. One day prior to A/PR8-challenge, and every two days thereafter, mice were injected with 10ng/g Dtx to deplete CCR2-expressing cells. Twenty four and 12 hours prior to endpoint, mice were given an IP injection of BrdU to label proliferating cells, and taken on day 3 post challenge to assess memory OT-I cell responses **(Fig. 4.19A)**. Despite its common use as monocyte-targeted depleter, administration of Dtx in the CCR2-DTR mice resulted in broad, and extensive, depletion of monocytes, non-classical monocytes, alveolar Mϕ, cDCs and granulocytes **(Fig. 4.19B-C)**. Despite this widespread depletion of myeloid cells, the recruitment of memory OT-I cells into the lungs and airways was equivalent between WT and CCR2-DTR mice. However, there were statistically significant reductions in the number of memory OT-I cells present in SLOs and the PB **(Fig. 4.19D)**.

As memory OT-I cells displayed equivalent infiltration of A/PR8 infected WT and *Ccr2*-DTR mice, it was next determined if the widespread depletion of myeloid cells in the lungs had any impact on memory OT-I cell proliferation *in situ*. Memory OT-I cells were identified in the lung parenchyma and the incorporation of BrdU and expression of Ki67 was assessed by flow cytometry **(Fig. 4.20A)**. In contrast to those results observed in *Ccr2*$^{-/-}$ mice, the frequency of OT-I cells positive for, and gMFI, of both BrdU and Ki67 was higher in CCR2-depleted hosts than in WT host mice, demonstrating that depletion of CCR2-expressing cells leads to higher rates of proliferation in the lungs **(Fig. 4.20B-C)**. Apoptosis in memory OT-I cells was also determined by annexin V and propridium iodide (PI) staining **(Fig. 4.20D)**. Annexin V is a protein that binds to phosphatidylserine, a phospholipid that is normally present on the intracellular leaflet of the plasma membrane in viable cells, but during early apoptosis, membrane integrity is lost and phosphatidylserine translocates to the cell surface where it can be bound by annexin V. In cells undergoing late-stage apoptosis, or necrotic cell death, nuclear membrane integrity is lost and PI can bind to nuclear DNA, revealing necrotic, or late-stage apoptotic cells. On day 3 post A/PR8-challenge the frequency of annexin V^- PI^- live OT-I cells, and annexin V^+ PI^- early apoptotic OT-I cells was equivalent between WT and CCR2-DTR hosts treated with Dtx. However, the frequency of annexin V^+ PI^+ late apoptotic cells was statistically significantly higher in CCR2-DTR hosts relative to WT hosts **(Fig. 4.20E)**. Single-cell suspensions from the lungs of WT and CCR2-DTR mice were also stimulated *ex-vivo* with SIINFEKL to determine cytokine production by memory OT-I cells **(Fig. 4.20F)**. While there was no difference in the ability of OT-I cells to produce IFNγ, OT-I cells present in the lungs of CCR2-DTR mice had a statistically significant reduction in the frequency of IL-2-expressing cells after stimulation **(Fig. 4.20G)**. Together, these results indicate that in A/PR8-challenged mice depleted of CCR2-expressing cells, there is increased turnover of memory OT-I cells present in the lungs and a concurrent defect in the ability of those memory cells to produce the cytokine IL-2.

4.7 Conclusion

Analysis of OT-I responses in *Ccr2*$^{-/-}$ mice, where monocyte numbers in peripheral tissues are greatly reduced, revealed no major impact on the generation of effector responses, but a significant reduction in the pool of memory OT-I cells 35 days post-influenza infection. This defect in memory generation did not affect any particular memory subset, but reflected a general reduction in memory OT-I cell numbers. Although there were defects seen in the overall number of OT-I memory cells present, the number of host influenza-specific memory CD8^{+} T cell populations was not significantly altered in *Ccr2*$^{-/-}$ mice. Despite this normal endogenous memory formation, *Ccr2*$^{-/-}$ mice had significantly increased morbidity, and viral RNA in the lungs during secondary, but not primary, influenza challenge. This increased morbidity upon challenge was also associated with a reduction in IFNγ recovered from BAL washes of A/PR8-challenged *Ccr2*$^{-/-}$ mice, however CD8^{+} T cells recovered from the lungs of *Ccr2*$^{-/-}$ mice after challenge had normal, or elevated, IFNγ production after *ex vivo* stimulation and equivalent *in vivo* cytotoxicity. Since the formation and function of both resident and circulating memory cell populations was equivalent between WT and *Ccr2*$^{-/-}$ mice prior to challenge, this demonstrated a CCR2-dependent role for optimal host protection during influenza challenge. Analysis of memory T cell responses over the course of A/PR8-challenge revealed a defect in the re-activation of memory T cells in the lungs, but not lung-draining mLN, of *Ccr2*$^{-/-}$ mice. This was reflected as a reduction in the frequency and number of BrdU^{+} Ki67^{+} influenza-specific CD8^{+} T cells early after infection which ultimately resulted in the suboptimal expansion of memory cells, and potentially delayed viral clearance. The antigen-presenting cell subsets in the lungs that were most affected by the loss of CCR2 during A/PR8 challenge were monocytes and their derivatives, and inf-cDCs. Thus, CCR2 is likely required for trafficking of APC subsets to the influenza-infected lungs during challenge to drive the optimal re-activation and secondary expansion of memory T cells *in situ* to ensure host protection. This may indicate a unique functional role for the newly-described inf-cDC subset in the optimal reactivation of memory CD8^{+} T cells *in situ* for host protection during influenza challenge.

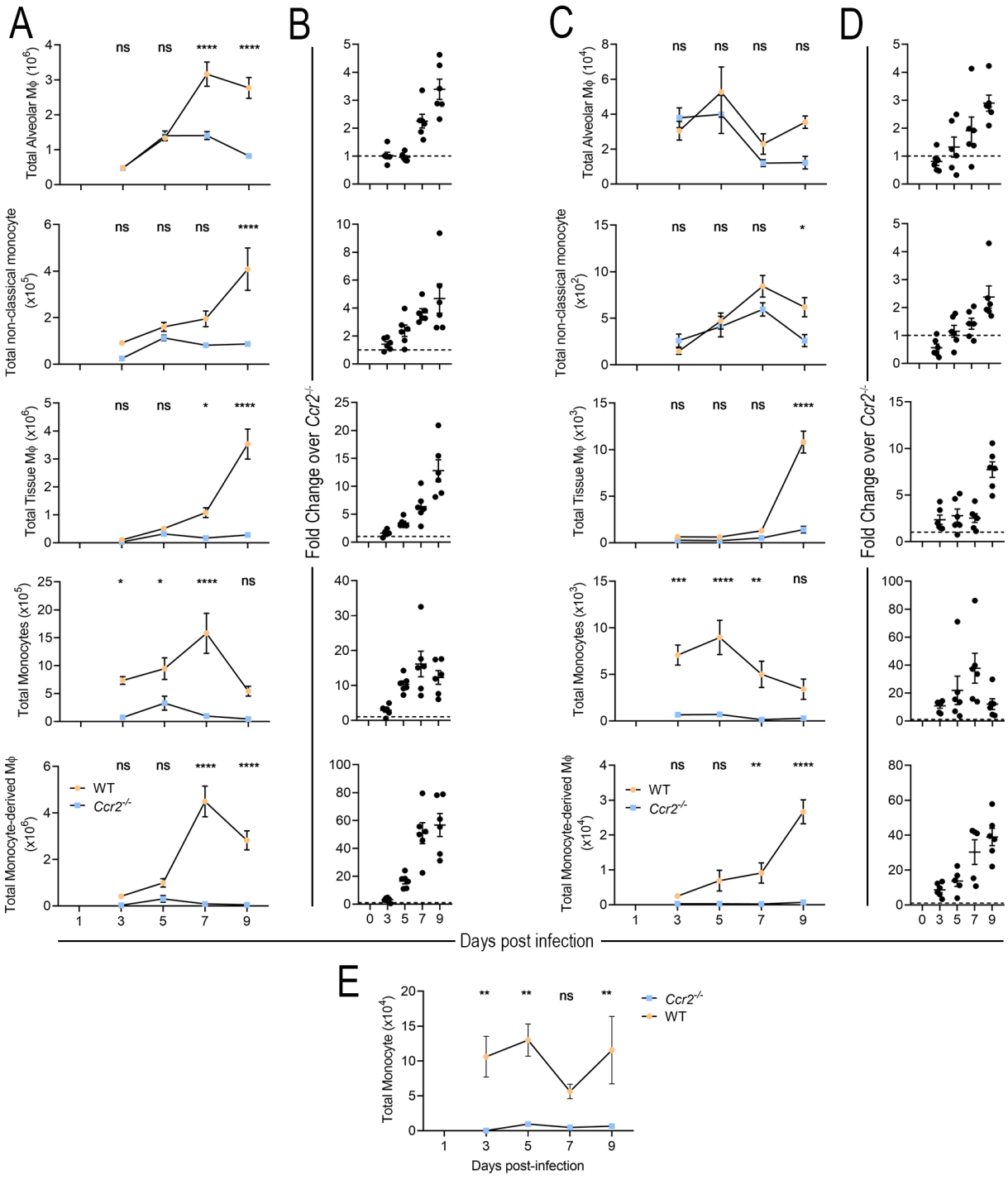

Figure 4.1: Reduced numbers of MNPs in the lungs, airways and draining mLN of *Ccr2*$^{-/-}$ mice following influenza infection.

WT and *Ccr2*$^{-/-}$ mice were infected with A/HK-x31 and the number of MNPs in the lungs **A)** and BALF **C)**, as identified in **Fig 3.8**, were determined by flow cytometry. **B)** and **D)** fold-change in MNP numbers in the lungs and BALF of WT mice relative to *Ccr2*$^{-/-}$ mice. **E)** The total number of lineage-negative, Ly6C^{+}, CD172α^{+}, F4-80^{+} monocytes in the lung-draining mLN of WT and *Ccr2*$^{-/-}$ mice over the course of infection. Data are presented as mean ± SEM (n=6 mice per group, per time point). ^{ns}p>0.05 = not significant, *p≤0.05, ***p≤0.001, ****p≤0.0001 (Two-way ANOVA).

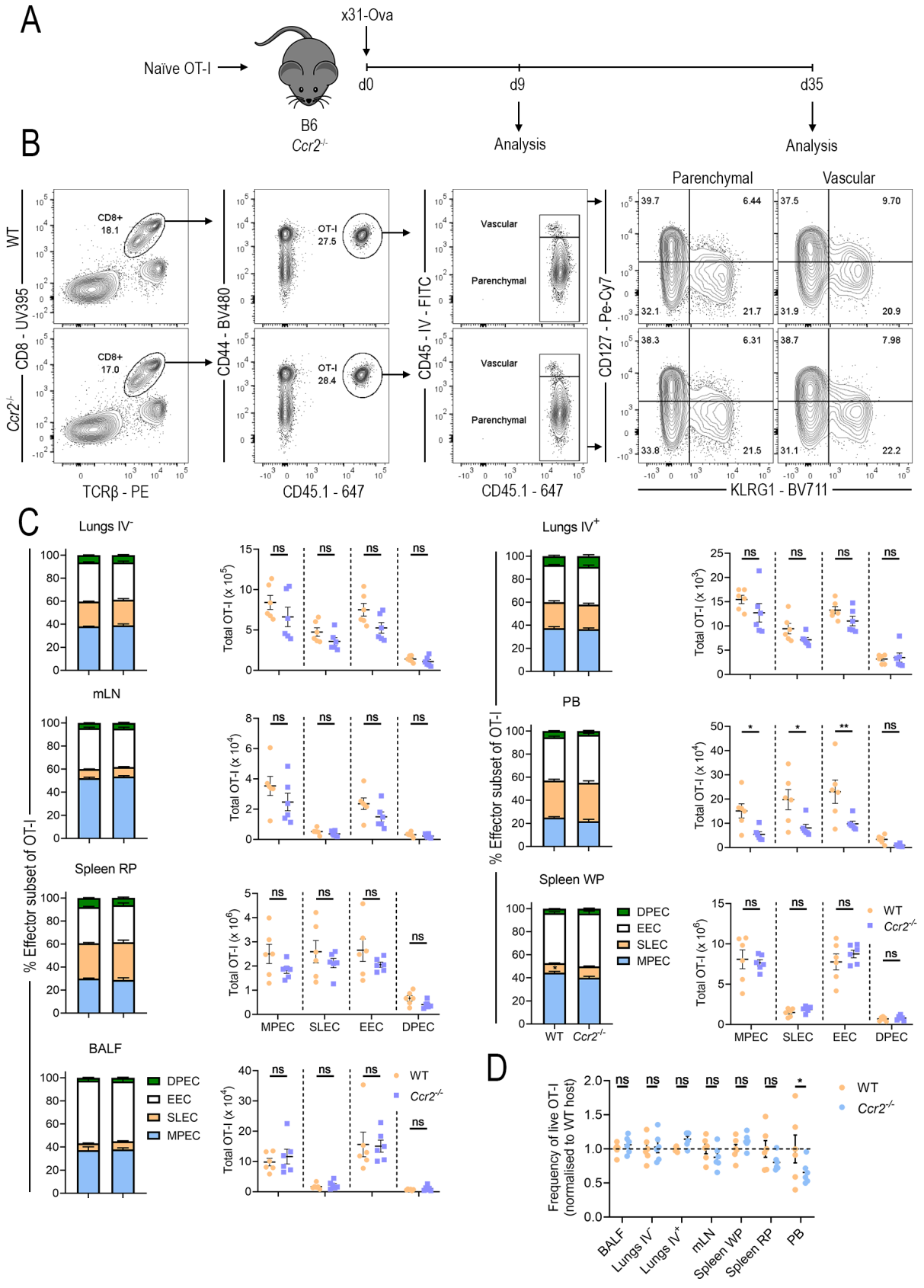
A
Naïve OT-I
x31-Ova
B6
Ccr2-/-
d0
d9
d35
Analysis
Analysis
B
WT
Ccr2-/-
CD8 - UV395
CD8+
18.1
CD8+
17.0
TCRβ - PE
CD44 - BV480
OT-I
27.5
OT-I
28.4
CD45.1 - 647
CD45 - IV - FITC
Vascular
Parenchymal
Vascular
Parenchymal
CD45.1 - 647
CD127 - Pe-Cy7
Parenchymal
Vascular
39.7
6.44
32.1
21.7
37.5
9.70
31.9
20.9
38.3
6.31
33.8
21.5
38.7
7.98
31.1
22.2
KLRG1 - BV711
C
Lungs IV-
Lungs IV+
mLN
PB
Spleen RP
Spleen WP
BALF
% Effector subset of OT-I
Total OT-I (x 10^5)
Total OT-I (x 10^3)
Total OT-I (x 10^4)
Total OT-I (x 10^6)
ns
*
**
DPEC
EEC
SLEC
MPEC
WT
Ccr2-/-
MPEC
SLEC
EEC
DPEC
D
Frequency of live OT-I (normalised to WT host)
BALF
Lungs IV-
Lungs IV+
mLN
Spleen WP
Spleen RP
PB
WT
Ccr2-/-

Figure 4.2: Host deficiency of *Ccr2* does not impact the generation of OT-I effector responses subsets following influenza infection.

Naïve OT-I cells (10^4) were transferred into WT and *Ccr2*$^{-/-}$ hosts that were infected with x31-Ova 24 hours later. Nine days post x31-Ova-infection, OT-I effector responses were analysed. **A)** Experimental plan to determine the requirement of host CCR2 in the generation of WT OT-I responses to influenza infection. **B)** Representative flow cytometry for the identification of OT-I effector subsets present in the lungs at day 9 post-influenza infection. **C)** The frequency of live OT-I cells recovered from the indicated tissues of WT and *Ccr2*$^{-/-}$ hosts, normalised to the frequency of OT-I cells recovered from WT hosts. **D)** Frequency and total number of OT-I effector subsets in the indicated organs at day 9 post infection. Data are presented as mean ± SEM (n=6 mice per group), representative of two independent experiments. $^{ns}p>0.05$ = not significant, $^{*}p\leq0.05$ (Two-way ANOVA).

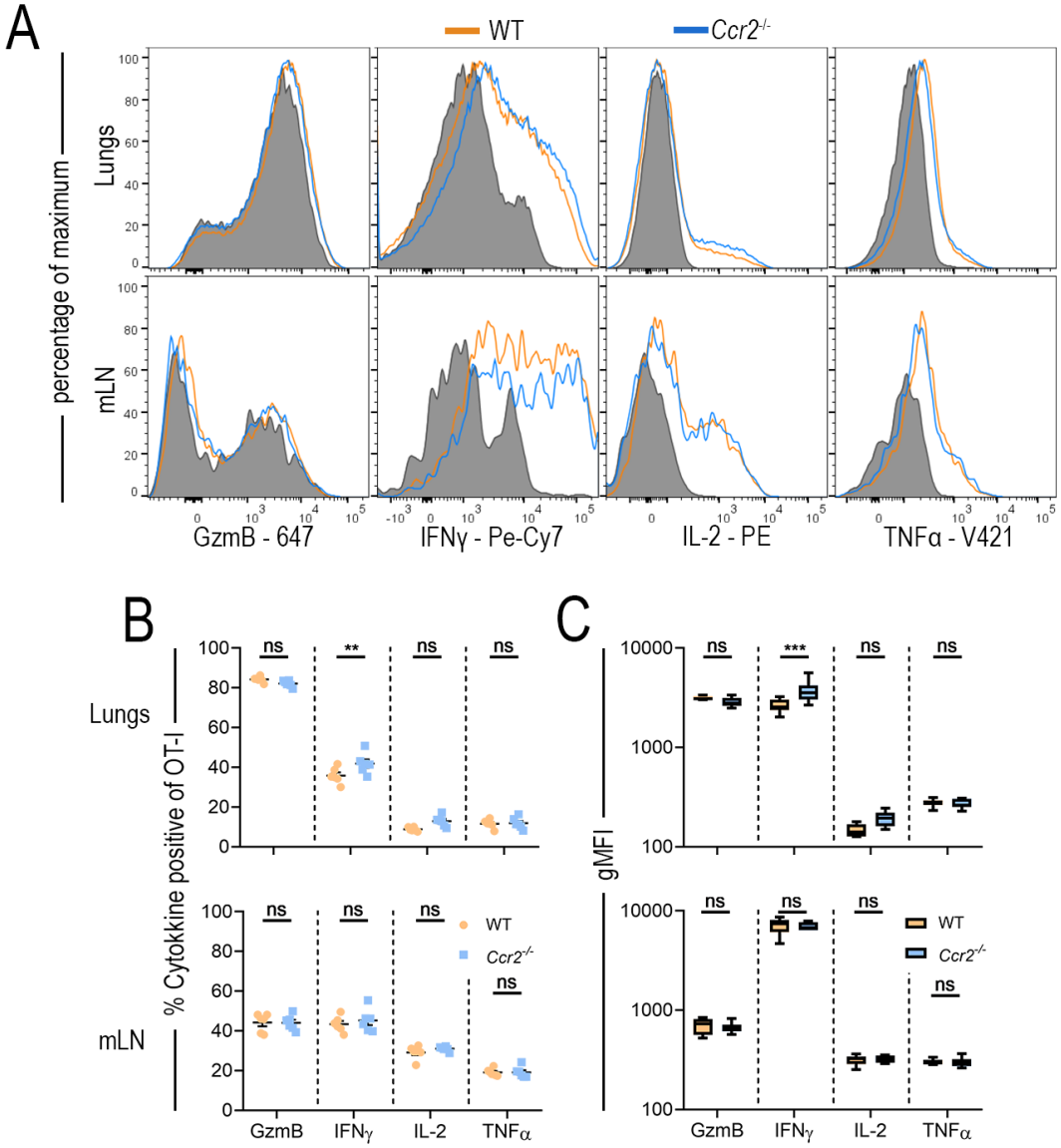

Figure 4.3: Host expression of *Ccr2* is not required for the acquisition of OT-I effector potential

A) Representative histograms of effector cytokine and granzyme B production after 4 hours of *ex-vivo* SIINFEKL stimulation of OT-I cells from the lungs and mLN of day 9 influenza-infected WT (orange) or *Ccr2*$^{-/-}$ (blue) host mice relative to unstimulated WT OT-I cells (shaded histogram). The percentage of cytokine- or granzyme B-positive **B)** and gMFI **C)** of OT-I cells present in the lungs and mLN of WT and *Ccr2*$^{-/-}$ hosts. Data are presented as mean ± SEM (n=6 mice per group), representative of 2 independent experiments. $^{ns}p>0.05$ = not significant, $^{**}p\leq0.01$, $^{***}p\leq0.001$ (Two-way ANOVA).

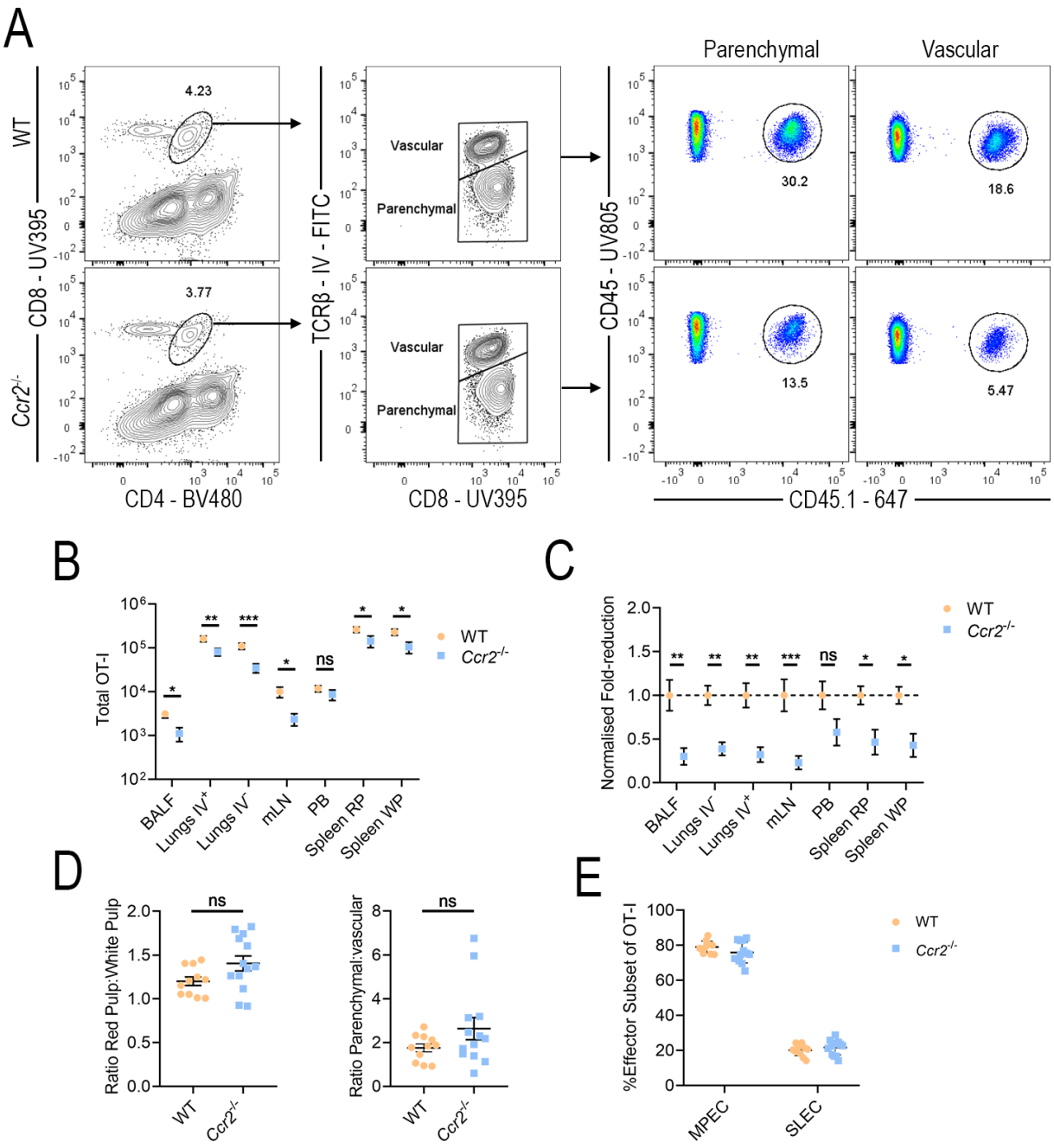

Figure 4.4: Reduced number of memory OT-I cells in *Ccr2*$^{-/-}$ hosts 35 days after influenza infection

Naïve OT-I cells (10^4) were transferred into WT and *Ccr2*$^{-/-}$ hosts that were infected with x31-Ova 24 hours later Thirty five days post x31-Ova-infection memory OT-I development was analysed. **A)** Representative flow cytometry for the identification of transferred OT-I cells in the lungs of WT and *Ccr2*$^{-/-}$ host mice. **B)** Total number of OT-I cells recovered from the indicated tissue of WT and *Ccr2*$^{-/-}$ hosts. **C)** The normalised fold-reduction of OT-I cells recovered from *Ccr2*$^{-/-}$ host mice relative to WT hosts. **D)** The distribution of OT-I cells between the parenchyma and vasculature of the lungs, and the red pulp and white pulp of the spleen, determined by intravascular labelling. **E)** The frequency of CD127$^+$KLRG1$^-$ MPECs and CD127$^-$KLRG1$^+$ SLECs in the red pulp of the spleen of WT and *Ccr2*$^{-/-}$ host mice. Data are presented as mean ± SEM (n=13 *Ccr2*$^{-/-}$ host mice, n=11 WT littermate host mice), pooled from two independent experiments. $^{ns}p>0.05$ = not significant, $^{*}p\leq0.05$, $^{**}p\leq0.01$, $^{***}p\leq0.001$ (**(B-C)** Two-way ANOVA. **(D)** unpaired Students *t*-test).

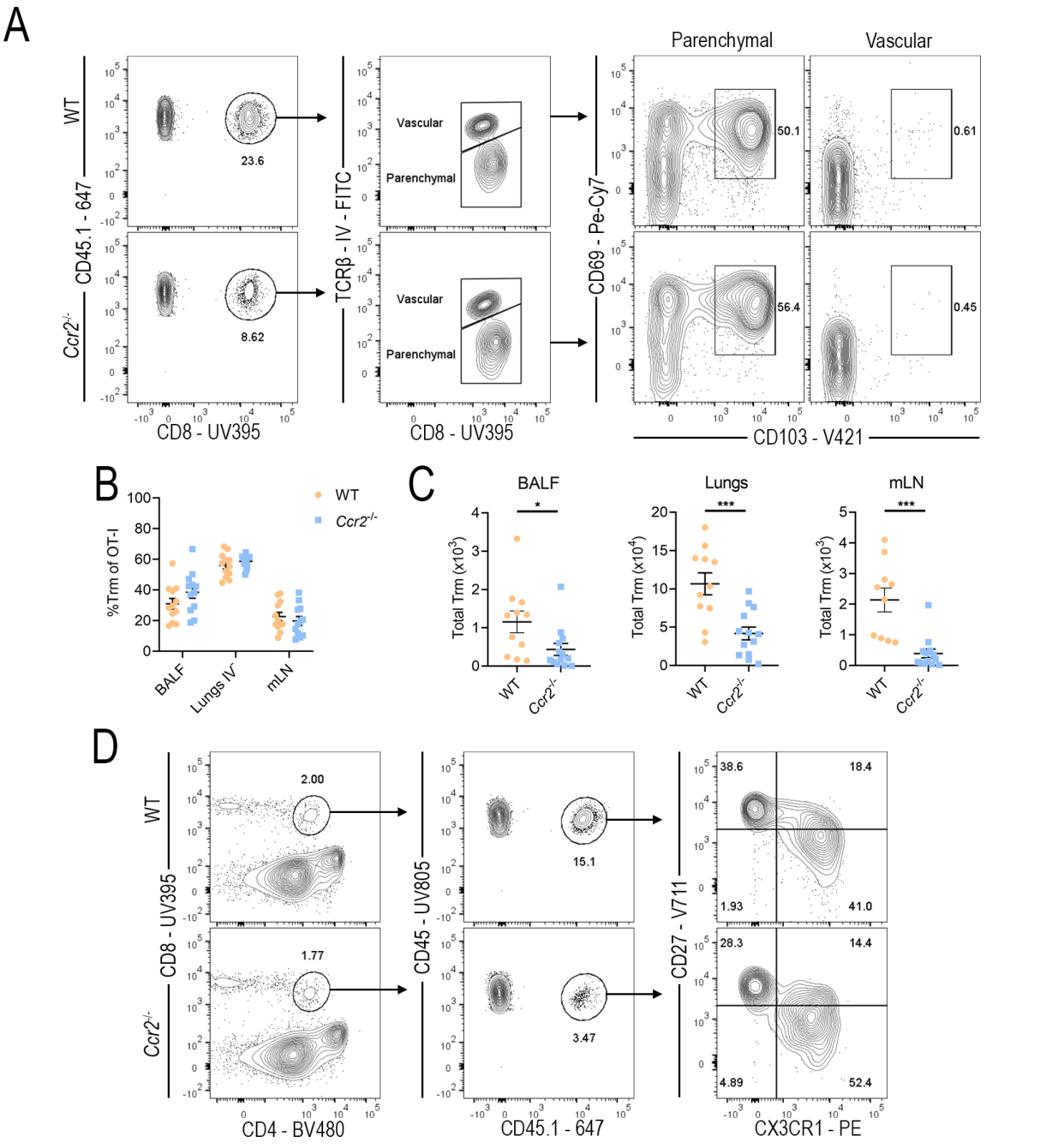
A
Parenchymal
Vascular
WT
CD45.1 - 647
Ccr2-/-
23.6
8.62
CD8 - UV395
TCRβ - IV - FITC
Vascular
Parenchymal
CD69 - Pe-Cy7
50.1
0.61
56.4
0.45
CD103 - V421
B
%Trm of OT-I
WT
Ccr2-/-
BALF
Lungs IV-
mLN
C
BALF
Lungs
mLN
Total Trm (x10³)
Total Trm (x10⁴)
D
2.00
1.77
CD8 - UV395
CD4 - BV480
CD45 - UV805
15.1
3.47
CD45.1 - 647
CD27 - V711
38.6
18.4
1.93
41.0
28.3
14.4
4.89
52.4
CX3CR1 - PE
E
mLN
PB
Spleen - WP
Spleen - RP
%memory subset of OT-I
Absolute number (x 10³)
Absolute number (x 10⁴)
Tcm
Tpm
Tem
Tdn
ns

Figure 4.5: Memory OT-I cells have develop normally, but are reduced in number in *Ccr2*$^{-/-}$ hosts

A) Representative flow cytometry for the identification of Trm OT-I cells in the lungs of WT and *Ccr2*$^{-/-}$ hosts 35 days post x31-Ova infection. The frequency **B)** and total number **C)** of CD69^{+}CD103^{+} Trm cells among total parenchymal cells, in the indicated organs. **D)** Representative flow cytometry for the identifcation of circulating memory OT-I cells in the spleen of WT and *Ccr2*$^{-/-}$ host mice 35 days after x31-Ova infection. **E)** The frequency and total number of circulating memory OT-I cell subsets in the indicated organs 35 days after x31-Ova infection. Data are presented as mean ± SEM (n=11 WT hosts, n=13 *Ccr2*$^{-/-}$ hosts), pooled from 2 independent experiments. ^{ns}p>0.05 = not significant, *p≤0.05, ***p≤0.001, ****p≤0.0001 (**(C)** unpaired Students *t*-test, **(D)** Two-way ANOVA).

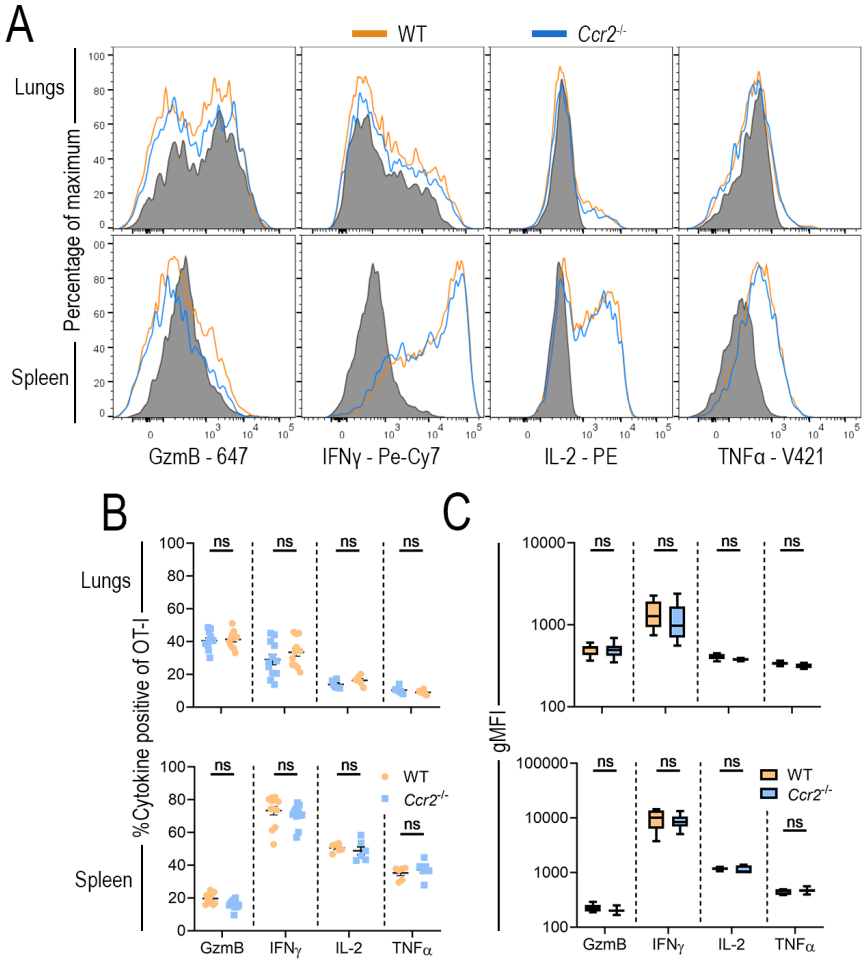

Figure 4.6: Memory OT-I cells in *Ccr2*$^{-/-}$ hosts display normal cytokine and granzyme B expression

Cells recovered from the spleen and lungs of WT and *Ccr2*$^{-/-}$ host mice were stimulated *ex-vivo* with SIINFEKL. **A)** Representative histograms of cytokine and granzyme B expression in OT-I cells present in the lungs and spleen of WT (orange) and *Ccr2*$^{-/-}$ (blue) host mice. The percentage of cytokine- and granzyme B-expressing **B)** and gMFI **C)** of OT-I cells in the lungs or spleen of WT and *Ccr2*$^{-/-}$ hosts. Data are presented as mean ± SEM (n=13 *Ccr2*$^{-/-}$ mice, n=11 WT littermate host mice), pooled from two independent experiments. $^{ns}p>0.05$ = not significant (Two-way ANOVA).

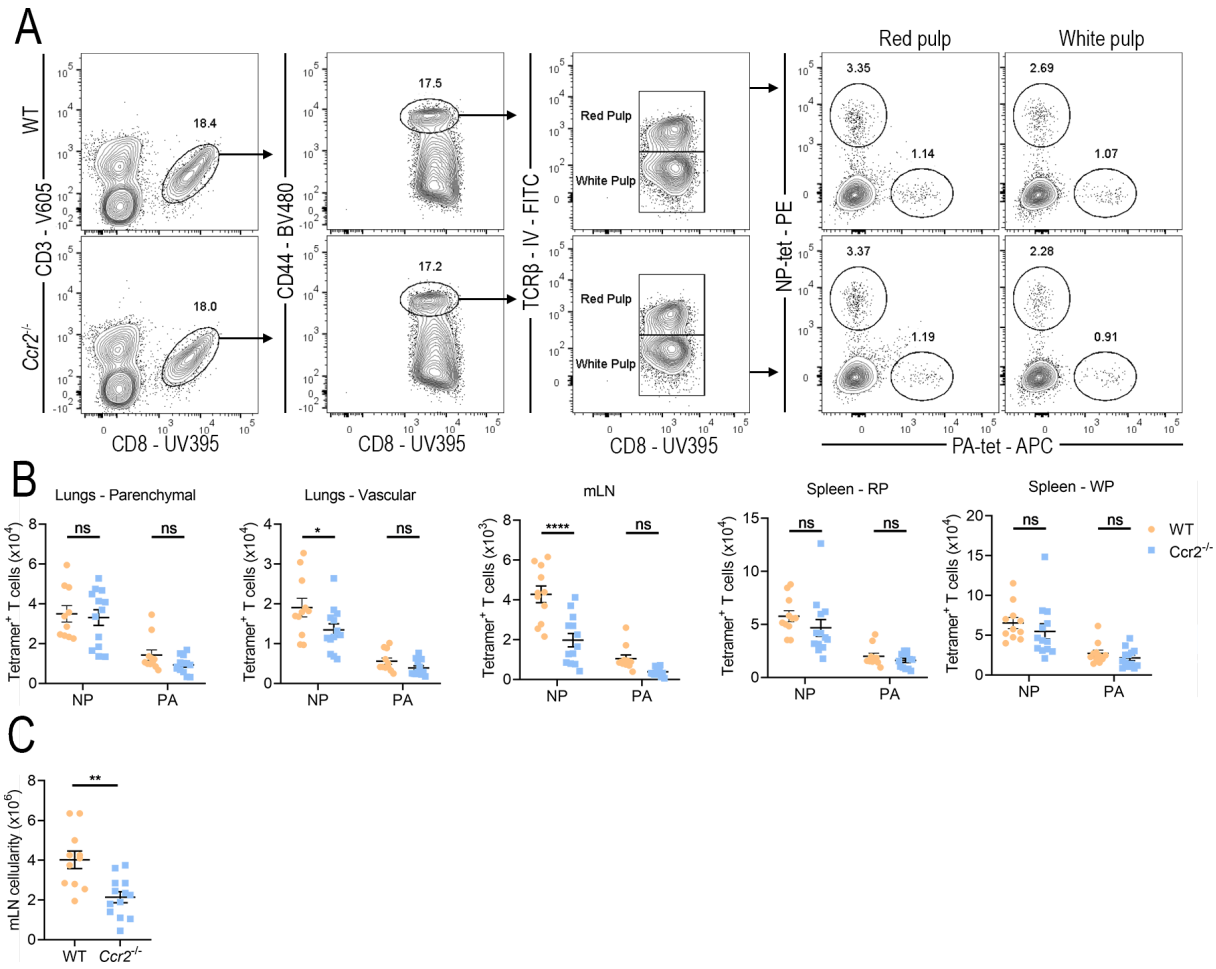

Figure 4.7: Tetramer-specific CD8$^+$ T cells in *Ccr2*$^{-/-}$ mice display normal memory development

WT and *Ccr2*$^{-/-}$ mice were immunised with A/HK-x31. Thirty five days after infection the formation of NP and PA influenza-specific memory C8$^+$ T cells was assessed. **A)** Representative flow cytometry for the identification of influenza NP- and PA-specific T cells in the spleen of WT and *Ccr2*$^{-/-}$ host mice 35 days post-A/HK-x31-infection. **B)** The total number of NP and PA influenza-specific memory T cells recovered from the indicated organs. **C)** The total cellularity of mLNs recovered from 35dpi WT and *Ccr2*$^{-/-}$ mice. Data are presented as mean ± SEM (n=12 mice per group), pooled from 2 independent experiments. $^{ns}p>0.05$ = not significant, $^{*}p\leq0.05$, $^{**}p\leq0.01$, $^{****}p\leq0.0001$ (**(B)** Two-way ANOVA, **(C)** unpaired Students *t*-test).

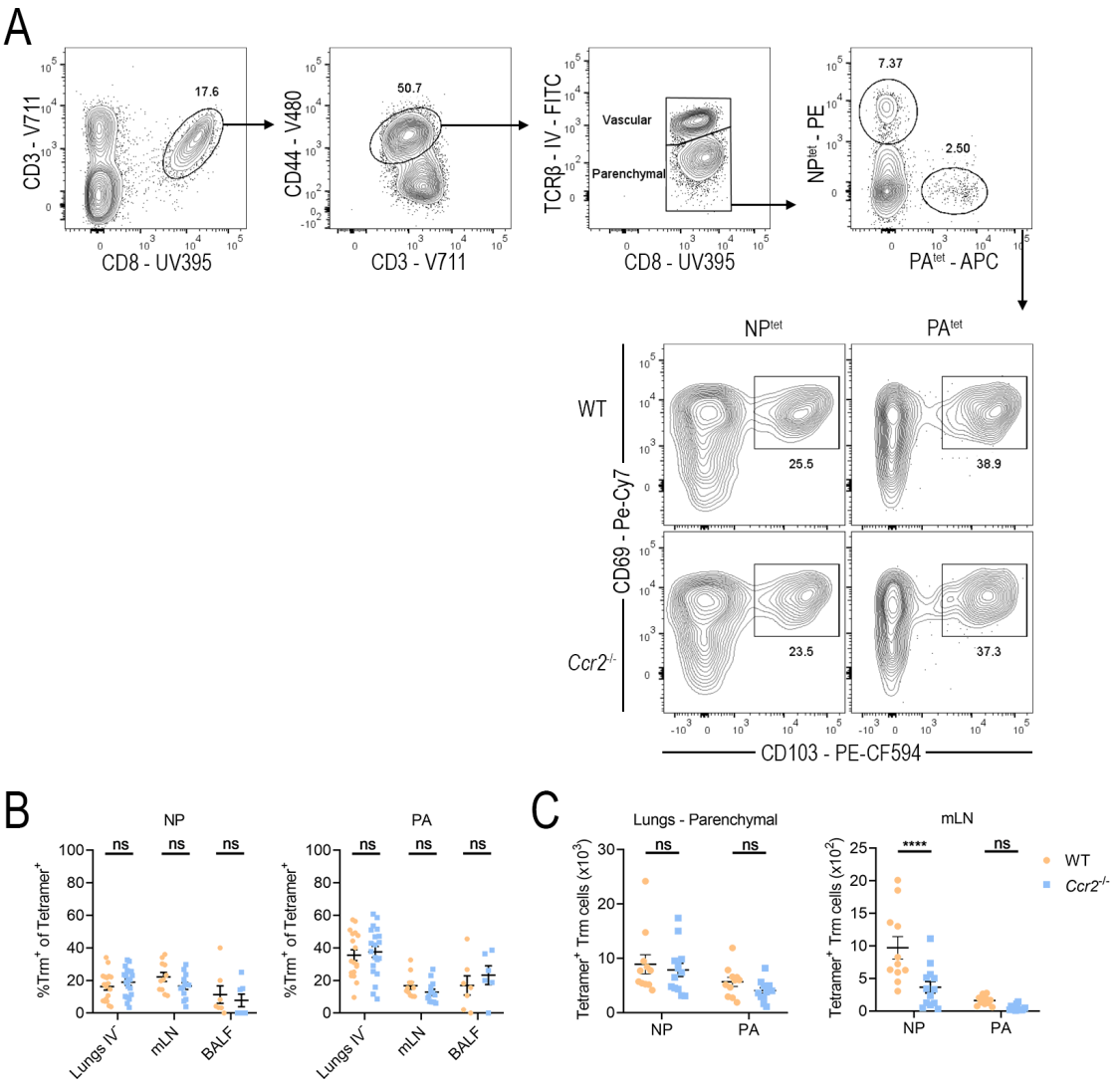

Figure 4.8: Normal development of influenza-specific host CD8$^+$ resident-memory cells in *Ccr2*$^{-/-}$ mice.

A) Representative flow cytometry for the identification of influenza NP- and PA-specific CD8$^+$ Trm cells in the lungs of WT and *Ccr2*$^{-/-}$ mice 35 days post A/HK-x31-infection. The frequency **B)** and total number **C)** of NP and PA influenza-specific CD69$^+$CD103$^+$ Trm cells among total IV$^-$ cells in the respiratory tract and mLN of WT and *Ccr2*$^{-/-}$ mice. Data are presented as mean ± SEM (n=7-21 mice), pooled from 2-3 independent experiments. ^{ns}p>0.05 = not significant, ****p≤0.0001 (Two-way ANOVA).

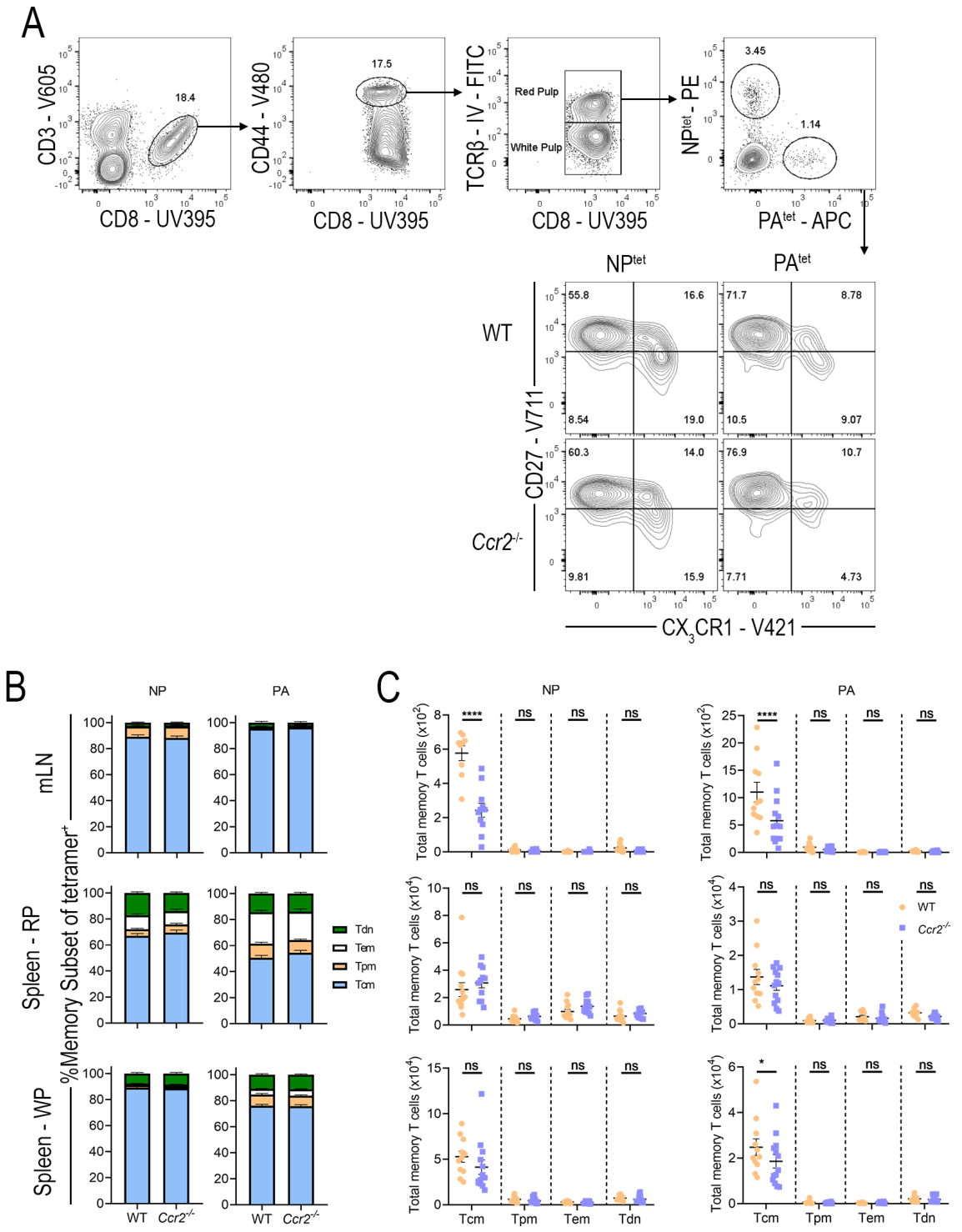

Figure 4.9: Normal development of influenza-specific host CD8$^+$ circulating memory cells in *Ccr2*$^{-/-}$ mice.

A) Representative flow cytometry for the identification of influenza NP- and PA-specific CD8$^+$ circulating memory T cells in the red pulp of the spleen 35 days post-A/HK-x31 infection. The frequency **B)** and total number **C)** of circulating memory cells recovered from the indicated organs 35 days post A/HK-x31-infection. Data are presented as mean ± SEM (n=12 mice per group), pooled from 2 independent experiments. $^{ns}p>0.05$ = not significant, $^{*}p\leq0.05$, $^{****}p\leq0.0001$ (Two-way ANOVA).

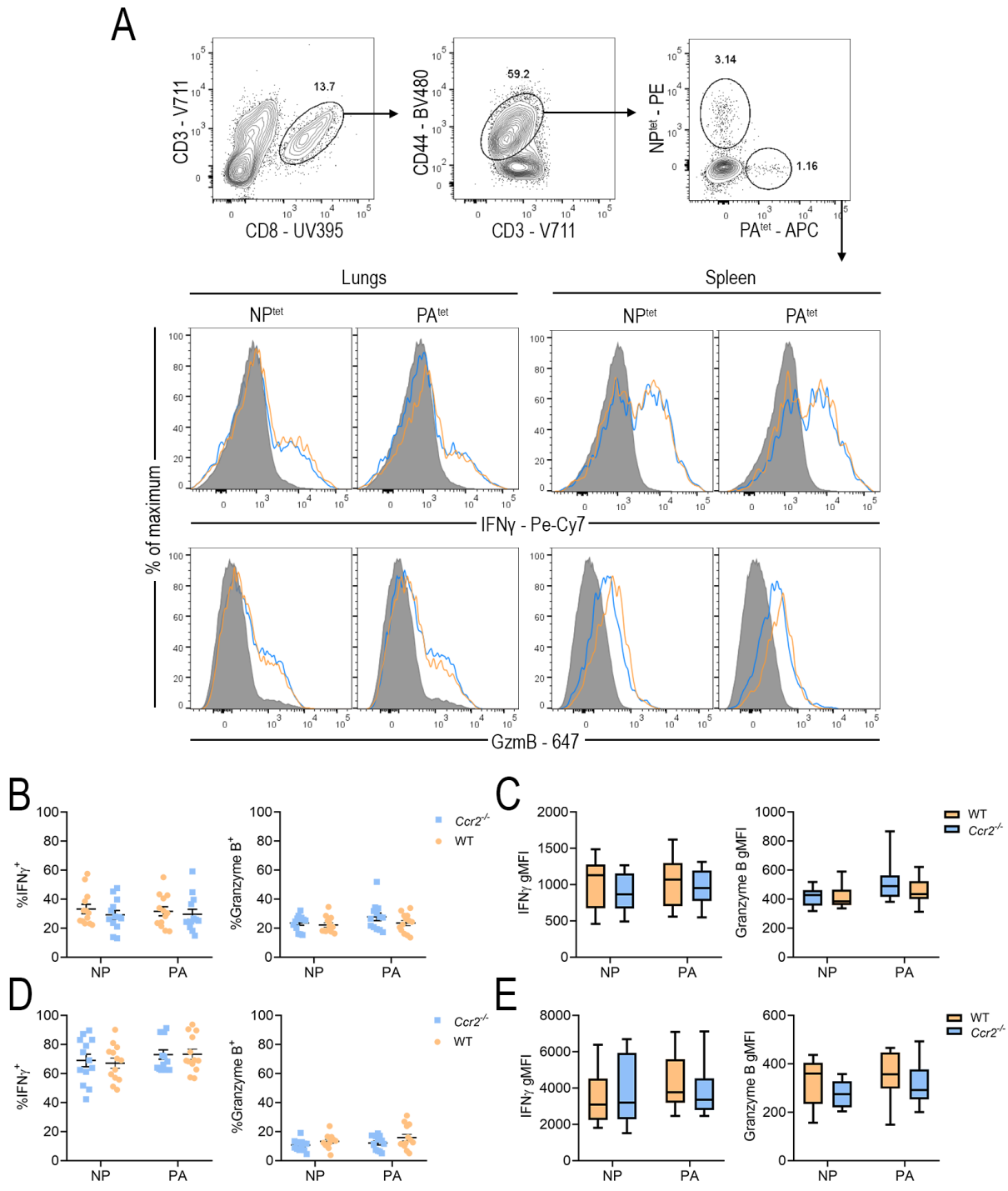

Figure 4.10: Influenza-specific memory CD8⁺ T cells from *Ccr2*$^{-/-}$ mice display normal effector potential

Cells isolated from the spleen and lungs of WT and *Ccr2*$^{-/-}$ mice 35 days post-A/HK-x31-infection and were stimulated *ex-vivo* with PMA. **A)** Representative histograms of the expression of INFγ and granzyme B in NP- and PA-specific T cells present in the lungs and spleen of WT (orange) and *Ccr2*$^{-/-}$ (blue) mice relative to naïve CD8⁺ T cells (shaded histogram). The frequency and gMFI of cytokine expression was determined in tetramer-specific cells present in the lungs **B)** and **C)** and the spleen **D)** and **E)**. Data are presented as mean ± SEM (n=12 mince per group), pooled from 2 independent experiments.

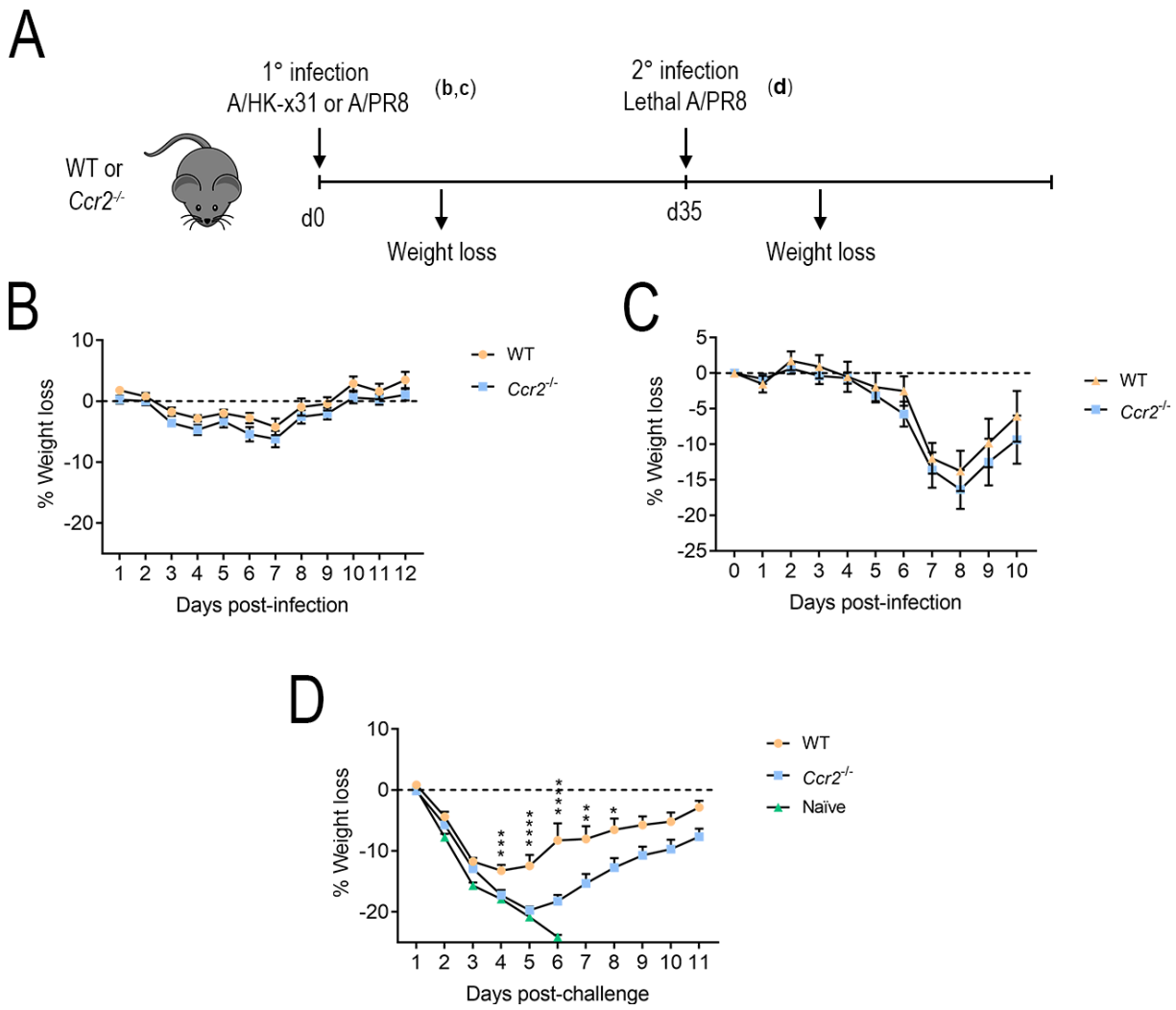

Figure 4.11: A/HK-x31-immune *Ccr2*$^{-/-}$ mice have increased morbidity upon a lethal A/PR8 challenge

A) Experimental plan for the assessment of the response of WT and *Ccr2*$^{-/-}$ mice to primary or secondary influenza challenge. **B)** Weight loss of WT and *Ccr2*$^{-/-}$ mice after primary infection with 100TCID$_{50}$ A/HK-x31. **C)** Weight loss of WT and *Ccr2*$^{-/-}$ mice after primary infection with 1TCID50$_{50}$ A/PR8. **D)** weight loss of A/HK-x31-immune WT and *Ccr2*$^{-/-}$ mice and naïve controls after a lethal challenge with 500TCID$_{50}$ PR8. Data are presented as mean ± SEM (**(B)** and **(D)** n=11-16 mice per group), pooled from 2 independent experiments. (**(C)** n=6 mice per group). ***p≤0.001, ****p≤0.0001 (Two-way ANOVA).

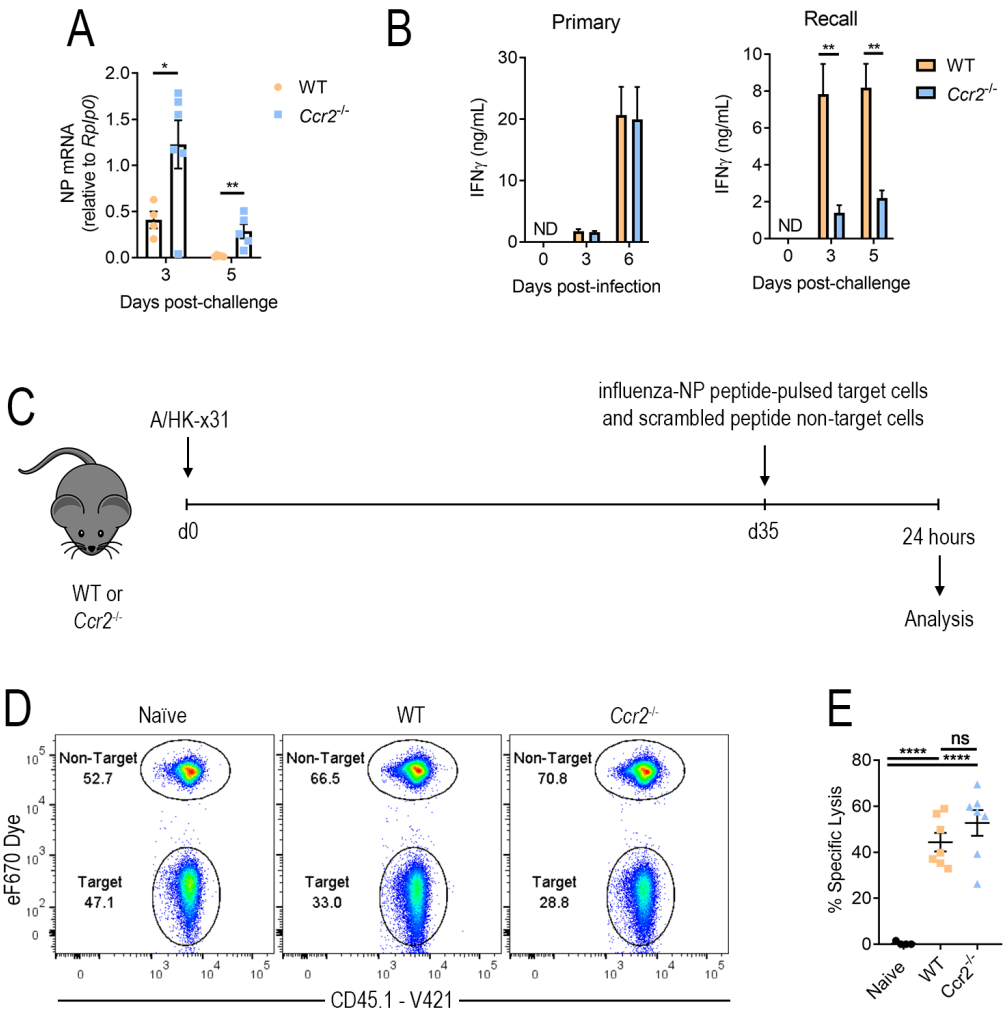

Figure 4.12: A/HK-x31-immune *Ccr2*$^{-/-}$ mice have increased viral loads in the lungs and decreased IFNγ in the BALF during a lethal PR8 challenge

A/HK-x31 immune WT and *Ccr2*$^{-/-}$ mice were challenged with 500TCID$_{50}$ A/PR8 to test the memory response to influenza. **A)** Influenza NP mRNA in the lungs of WT and *Ccr2*$^{-/-}$ mice on days 3 and 5 post-A/PR8-challenge. **B)** IFNγ ELISAs on BALF washes of primary A/HK-x31-infected and A/HK-x31-immune A/PR8-challenged WT and *Ccr2*$^{-/-}$ mice on the indicated days post-challenge. **C)** Experimental plan for the assessment of the *in-vivo* cytotoxicity of resting memory WT and *Ccr2*$^{-/-}$ mice. **D)** Representative flow cytometry of NP-peptide-pulsed and scrambled peptide-pulsed splenocytes in the spleens of A/HK-x31-immune WT and *Ccr2*$^{-/-}$, or naïve control mice 24 hours after cell transfer. **E)** Quantification of *in-vivo* cytotoxicity assay. Data are presented as mean ± SEM (**(A-B)** n=5-6 mice per group, **(E)** n=7 mice per group). ^{ns}p>0.05 = not significant, *p≤0.05, **p≤0.01, ****p≤0.0001 (**(A-C)** Two-way AVONA. **(E)** One-Way ANOVA).

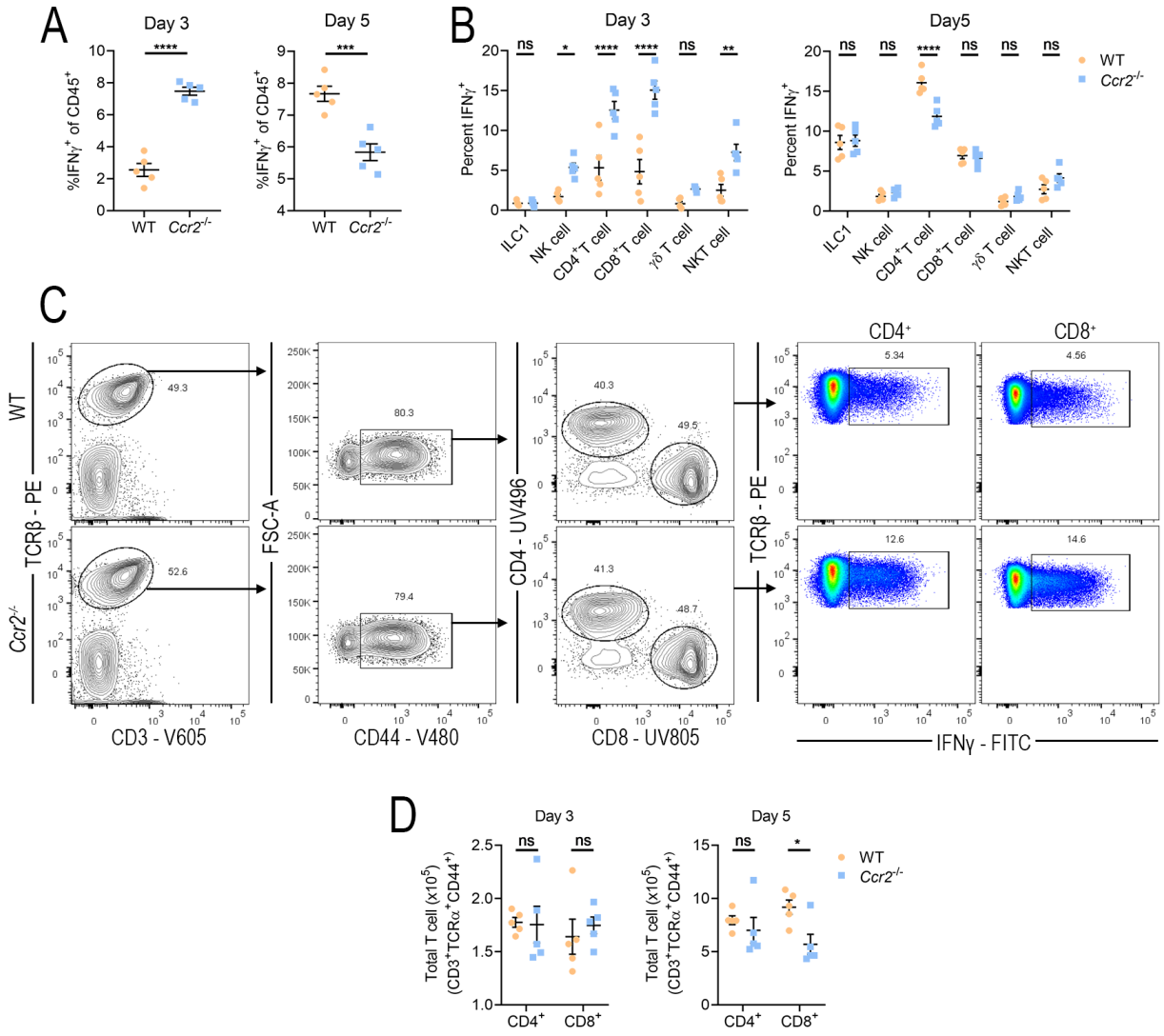

Figure 4.13: Aberrant expression of IFNγ in the lungs of A/PR8-challenged *Ccr2*$^{-/-}$ mice after *ex vivo* stimulation

Cells isolated from the lungs of day 3 and 5 A/PR8-challenged A/HK-x31-immune WT and *Ccr2*$^{-/-}$ mice were stimulated *ex vivo* with PMA to asses cytokine production. **A)** The percent IFNγ-positive cells among live CD45^{+} cells on day 3 and 5 post A/PR8-challenge. **B)** The percent IFNγ-positive cells among the indicated adaptive and innate-like cells present in the lungs on the indicated days post-challenge. **C)** Representative flow cytometry of intracellular IFNγ staining in CD4^{+} and CD8^{+} T cells from the lungs of WT and *Ccr2*$^{-/-}$ mice 3 days post A/PR8-challenge. **D)** The total number of CD4^{+} and CD8^{+} T cells recovered from the lungs of WT and *Ccr2*$^{-/-}$ mice on the indicated days post challenge. Data are presented as mean ± SEM (n=5 mice per group, per timepoint), representative of 2 independent experiments. $^{ns}p>0.05$ = not significant, *p≤0.05, ***p≤0.001, ****p≤0.0001 (**(A)** unpaired Students **t**-test. **(B)** and **(D)** Two-way ANOVA).

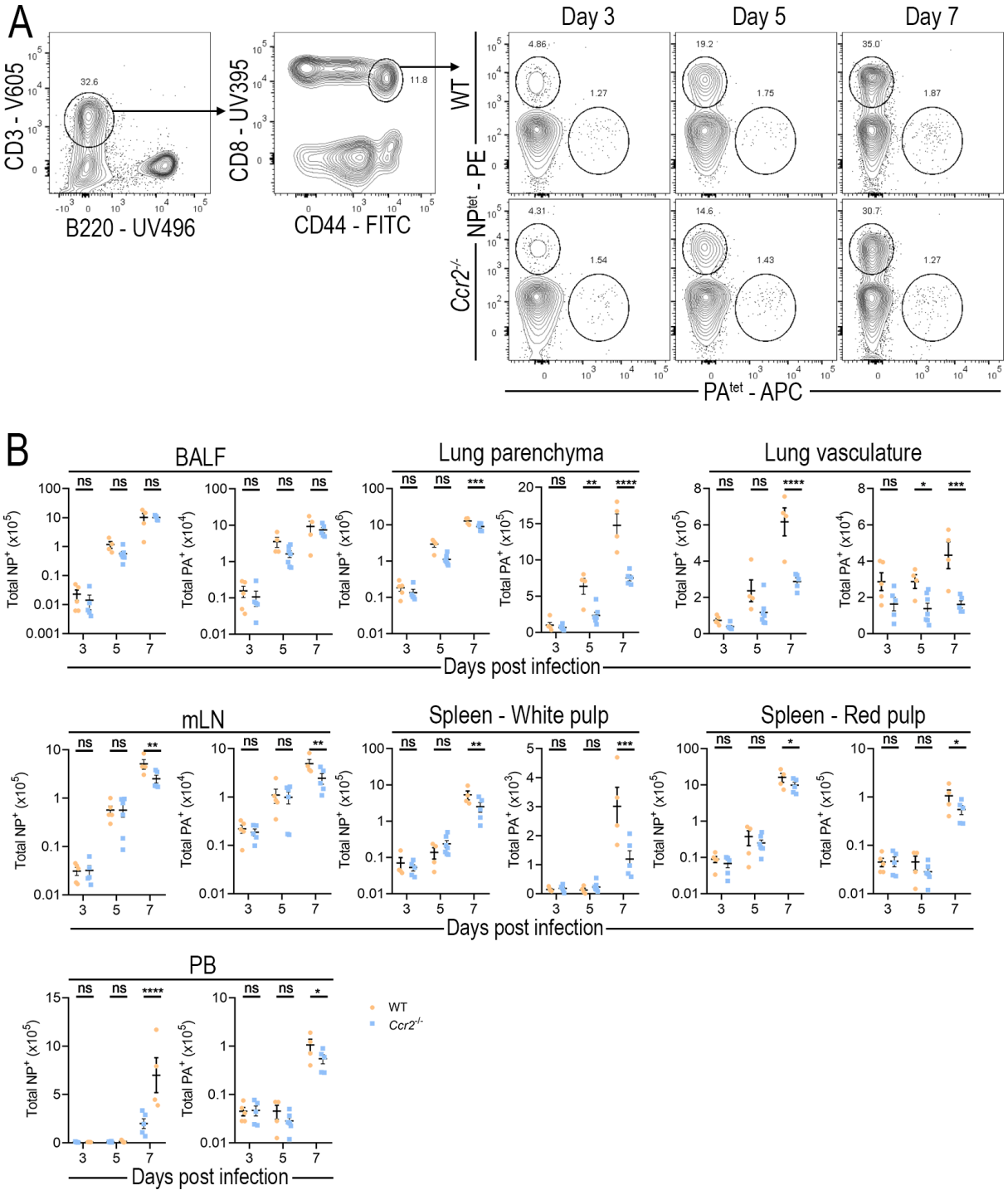

Figure 4.14: Influenza-specific memory T cell numbers are reduced in *Ccr2*$^{-/-}$ mice following A/PR8-challenge

A/HK-x31 immune WT and *Ccr2*$^{-/-}$ mice were challenged with 500TCID$_{50}$ A/PR8 and the distribution of influenza-specific memory T cells determined over the course of infection. **A)** Representative flow cytometry of influenza-specific CD8^{+} T cells in the blood of WT and *Ccr2*$^{-/-}$ mice on days 3, 5 and 7 post A/PR8-challenge. **B)** The total number of influenza-specific CD8^{+} T cells recovered from the indicated organs of WT and *Ccr2*$^{-/-}$ mice following A/PR8 challenge. Data are presented as mean ± SEM (n=4-7 mice per group, per timepoint). ^{ns}p>0.05 = not significant, *p≤0.05, **p≤0.01, ***p≤0.001, ****p≤0.0001 (Two-way ANOVA).

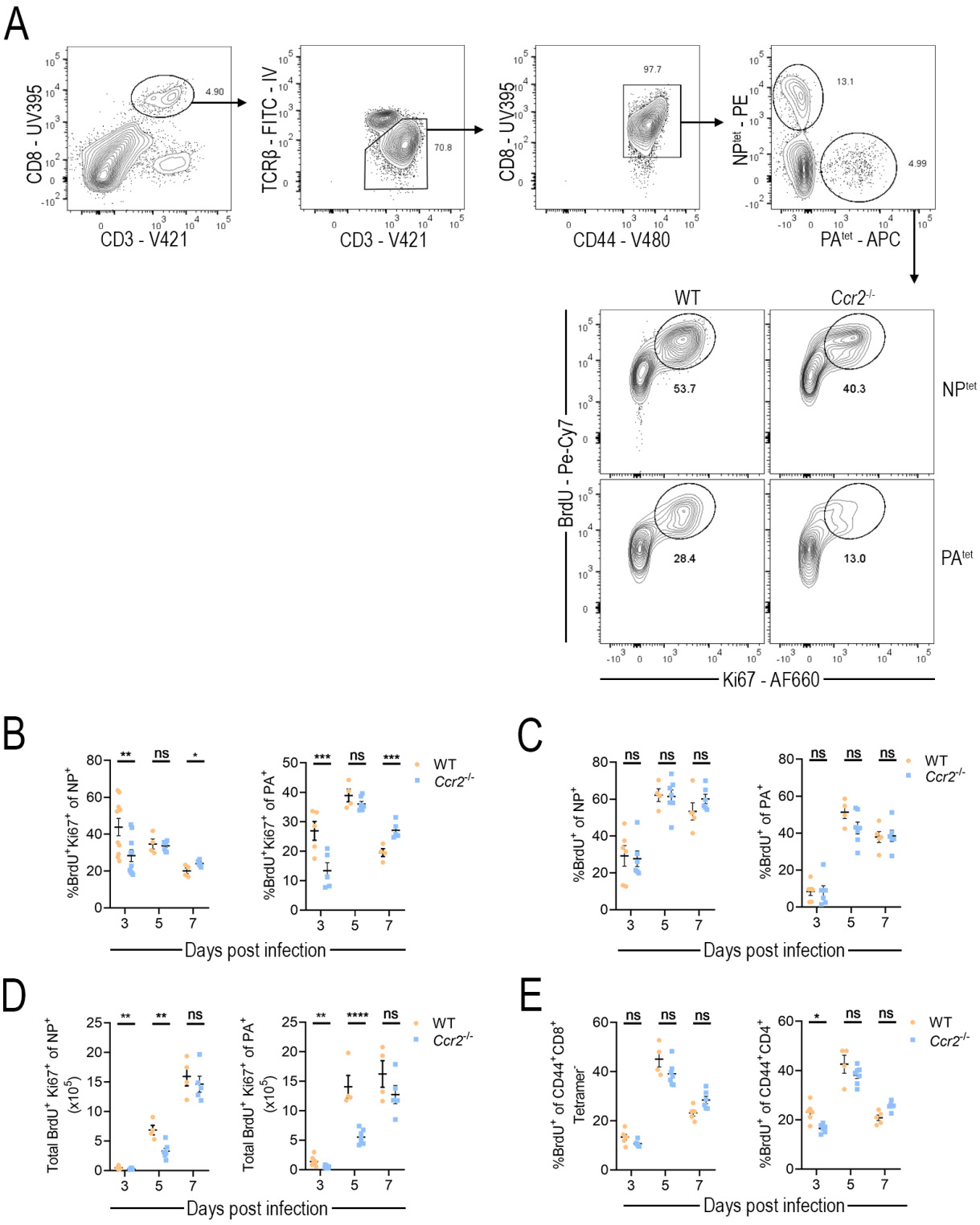

Figure 4.15: Influenza-specific and host endogenous T cells in the lungs of *Ccr2*$^{-/-}$ have reduced BrdU incorporation following A/PR8 challenge

A/HK-x31-immune WT and *Ccr2*$^{-/-}$ mice were challenged with 500TCID$_{50}$ A/PR8 and T cell proliferation was assessed during the recall response. To determine cell division mice were injected with 1mg BrdU 20 and 12 hours prior to sacrifice. **A)** Representative flow cytometry of BrdU staining in influenza-specific CD8$^+$ T cells in the lungs of WT and *Ccr2*$^{-/-}$ mice following A/PR8-challenge. The frequency of BrdU$^+$ Ki67$^+$ influenza-specific CD8$^+$ T cells in the lungs **B)** and BrdU $^+$ influenza-specific CD8$^+$ T cells in the mLN **C)** of WT and *Ccr2*$^{-/-}$ mice. **D)** The total number of BrdU$^+$ Ki67$^+$ influenza-specific CD8$^+$ T cells in the lungs. **E)** The frequency of BrdU$^+$ endogenous CD4$^+$ and CD8$^+$ tetramer$^-$ cells in the lungs of WT and *Ccr2*$^{-/-}$ mice. Data are presented as mean ± SEM (n=4-7 mice per group, per timepoint). ^{ns}p>0.05 = not significant, *p≤0.05, **p≤0.01, ***p≤0.001, ****p≤0.0001 (Two-way ANOVA).

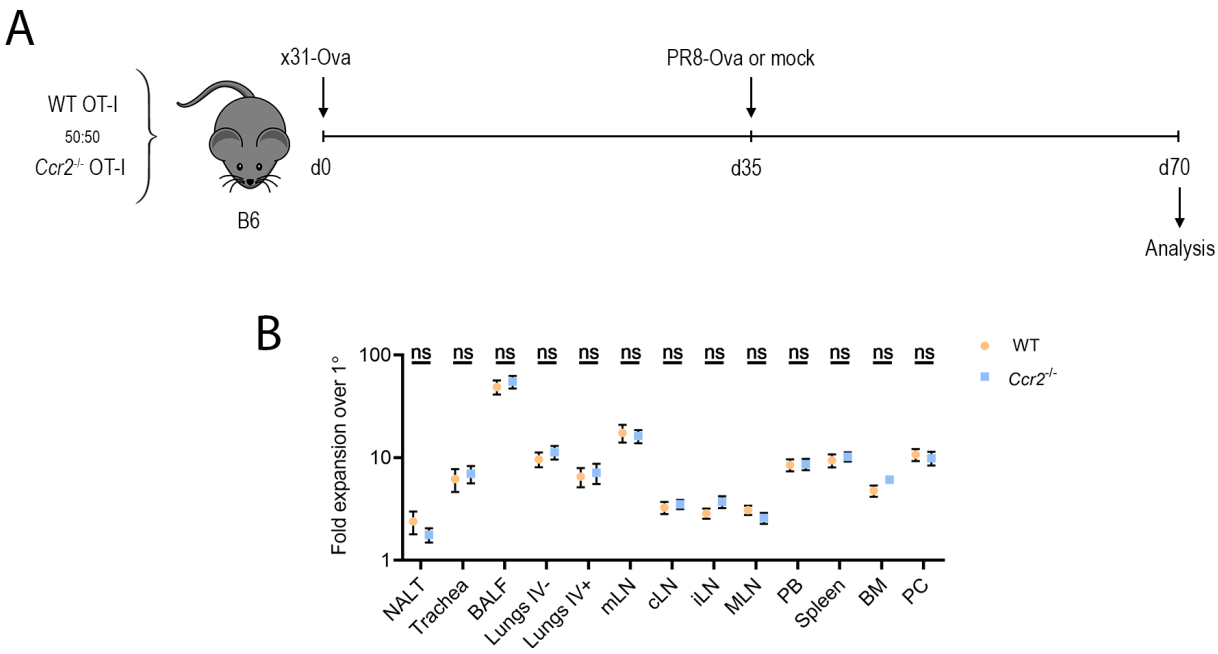

Figure 4.16: T cell-intrinsic CCR2 expression is not required for secondary expansion of CD8$^+$ memory T cells

C57BL/6 mice were mock-challenged or challenged with with PR8-Ova 35 days after x31-Ova immunisation to generate primary and secondary OT-I memory populations respectively. **A)** Experimental plan for the generation of primary and secondary WT and *Ccr2*$^{-/-}$ memory OT-I cells. **B)** Expansion of WT and *Ccr2*$^{-/-}$ OT-I secondary memory cells relative to primary OT-I memory populations was determined for the indicated tissues. Data are presented as mean ± SEM (n=12 mice per condition), pooled from 2 independent experiments. $^{ns}p>0.05$ = not significant (Two-way ANOVA).

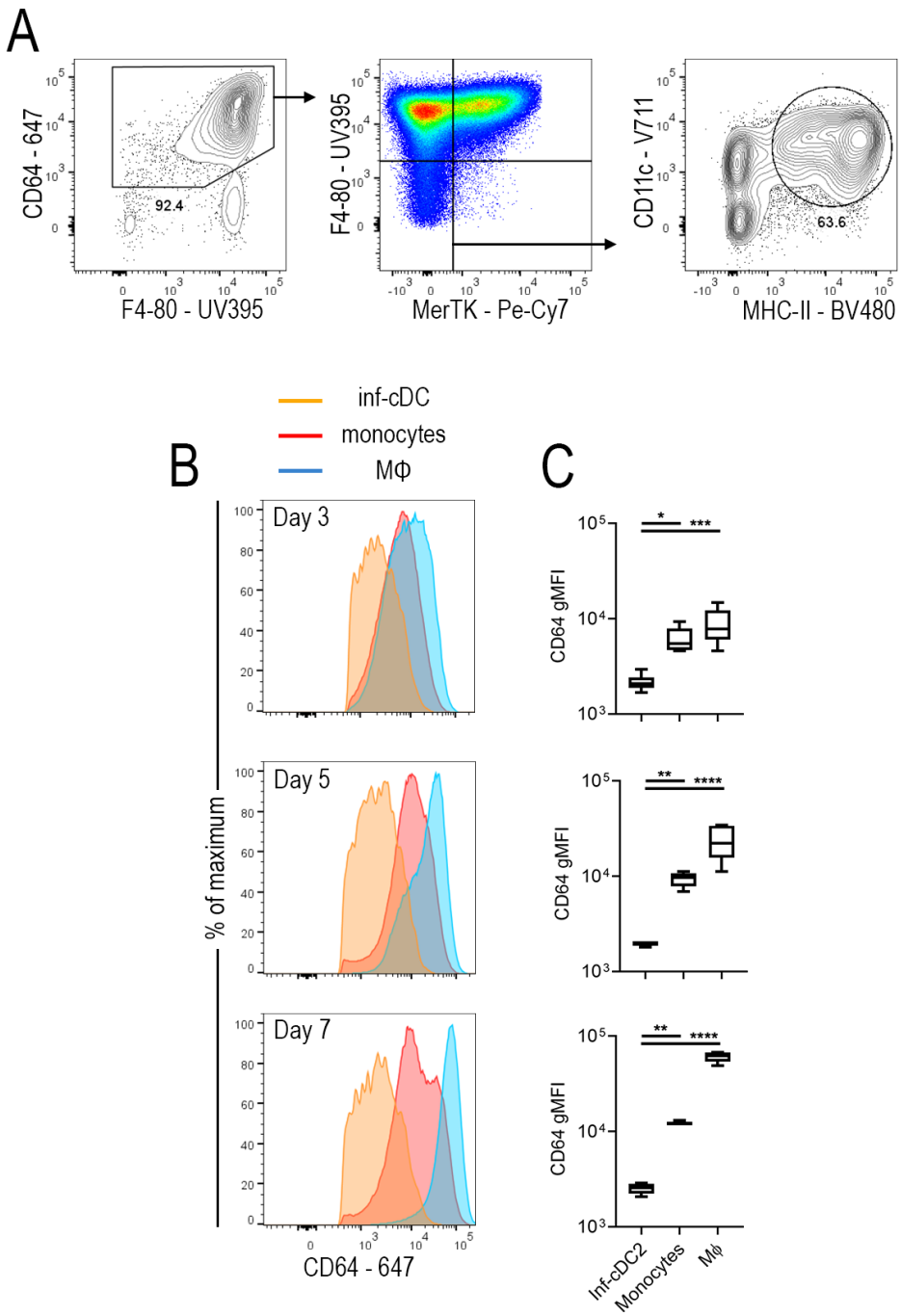

Figure 4.17: An alternative gating strategy for the identification of inflammatory-cDCs
A/HK-x31 immune mice were challenged with A/PR8 and MNP subsets in the lungs identified by flow cytometry as in **Fig. 3.8**. **A)** Representative flow cytometry for the identification CD64^{+} F4-80^{-} MerTK^{-} CD11c^{+} MHC-II^{+} putative inflammatory-cDCs on day 5 post A/PR8 infection (pre-gated on live, lineage negative, CD45^{+}, Siglec F^{-}, Ly6G^{-}, CD43^{-} cells). **B)** Surface expression of CD64 on inflammatory-cDC2s, F4-80^{+} MerTK^{-} monocytes, and F4-80^{+} MerTK^{+} Mϕ subsets in the lungs 5 days post A/PR8 challenge. **C)** CD64 gMFI in the indicated MNP subsets over the course of A/PR8 challenge. *p≤0.05, **p≤0.01, ***p≤0.001, ****p≤0.0001 (One-way ANOVA).

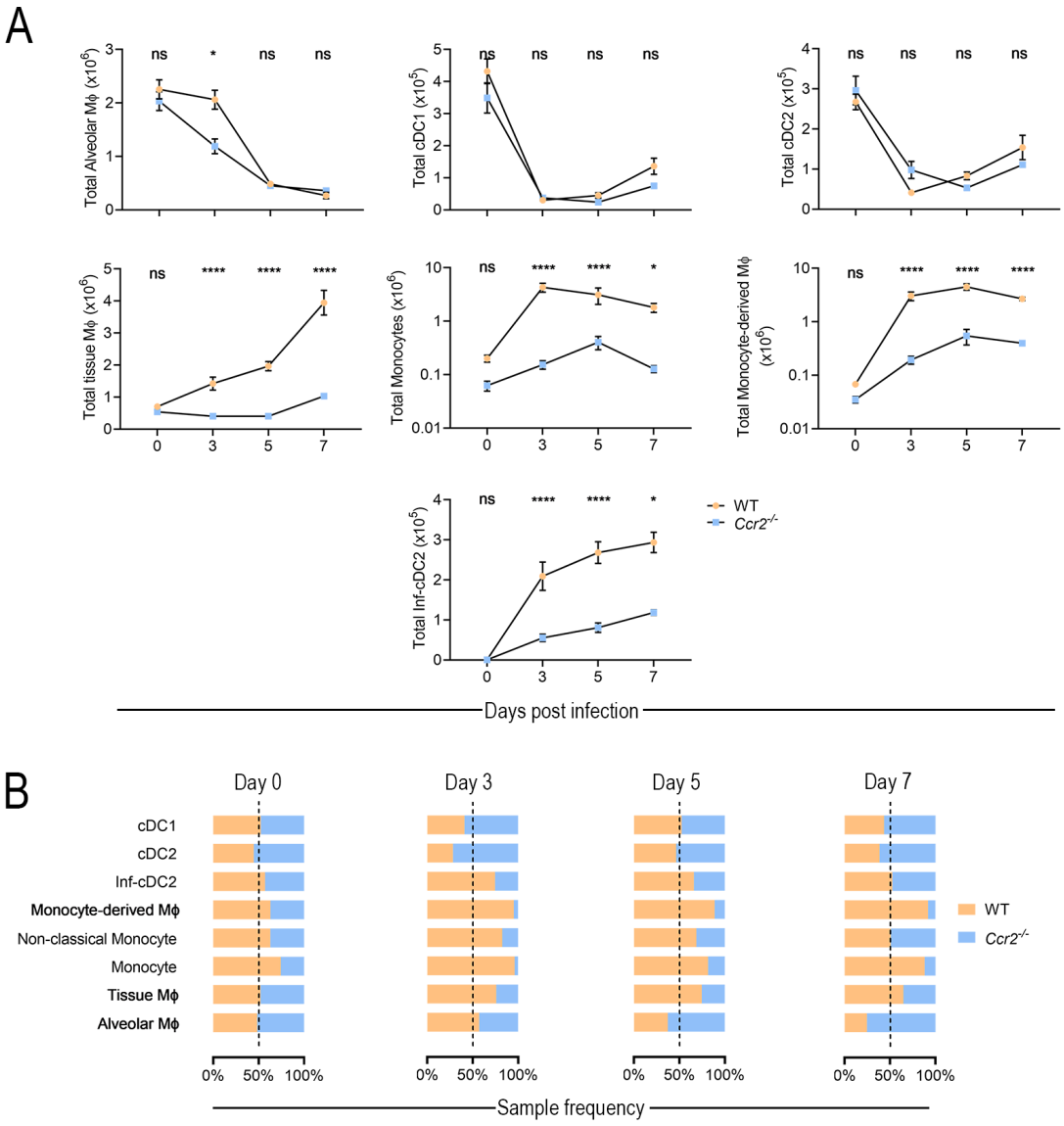

Figure 4.18: Major disruptions in monocytes, monocyte-derived cells and inflammatory cDC2s in the lungs of *Ccr2*$^{-/-}$ mice during A/PR8 challenge

A/HK-x31-immune WT and *Ccr2*$^{-/-}$ mice were challenged with A/PR8 and the number of MNPs present in the lung tracked over the course of infection. **A)** The total number of the indicated MNP subset recovered from the lungs of A/PR8 challenged WT and *Ccr2*$^{-/-}$ mice on the indicated day post-challenge. **B)** The frequency of each indicated indicated cell subset among a pooled sample of equal numbers of live, CD45^{+} lineage^{-} cells from the lungs of WT and *Ccr2*$^{-/-}$ mice on the indicated days post PR8 challenge. Data are presented as mean ± SEM (n=4-12 mice per group, per timepoint). $^{ns}p>0.05$ = not significant, $^{*}p\leq0.05$, $^{****}p\leq0.0001$ (Two-way ANOVA.)

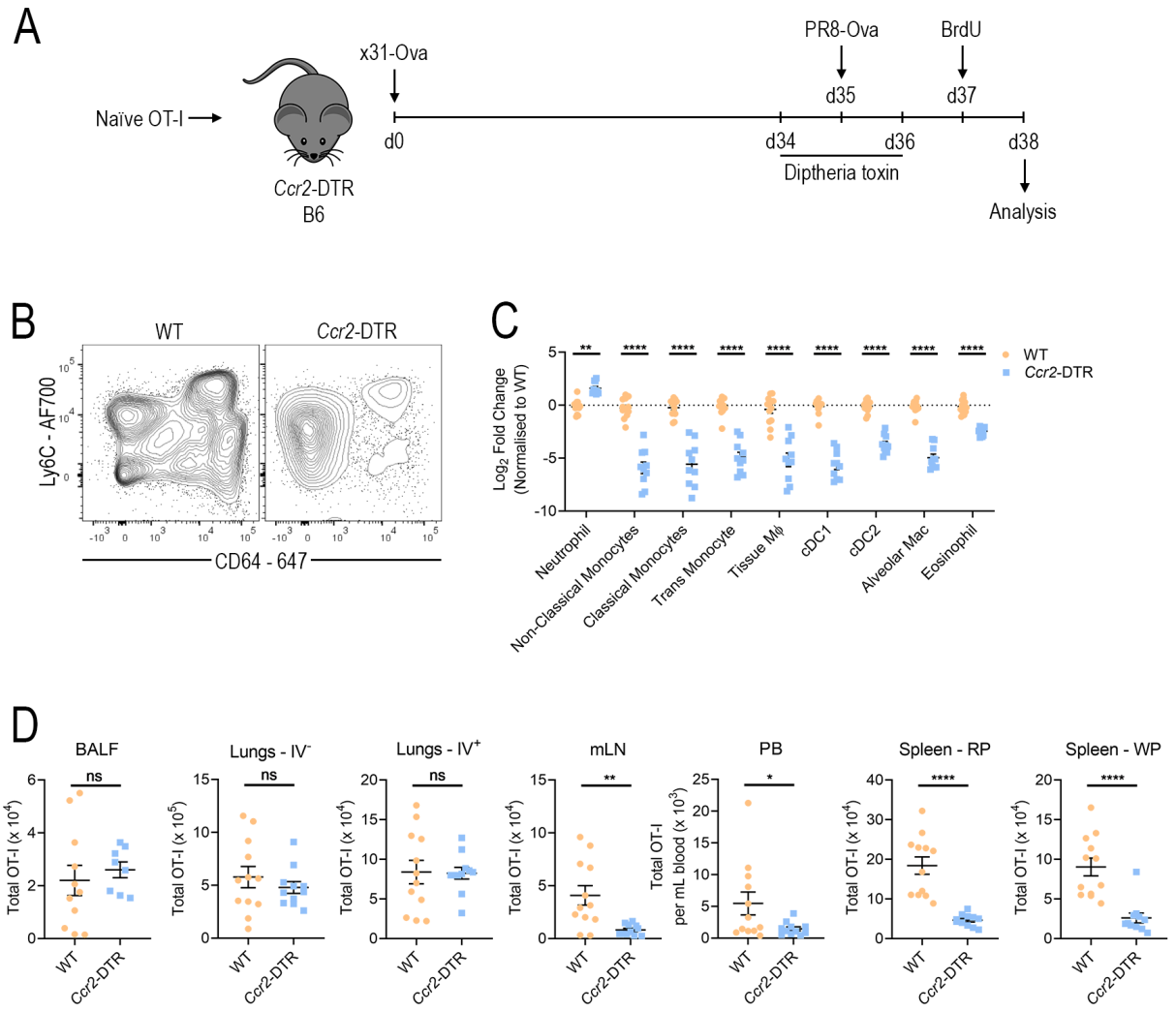

Figure 4.19: Depletion of CCR2-expressing cells during influenza challenge does not alter T cell recruitment into the lungs

Naïve OT-I cells (10^4) were transferred into WT and *Ccr2*-DTR host mice that were infected with x31-Ova 24 hours later. Thirty five days post x31-Ova-infection WT and *Ccr2*-DTR hosts were challenged with PR8-Ova and the memory OT-I response to infection, after depletion of CCR2-expressing cells, was measured on day 3 post-challenge. **A)** Experimental plan to assess OT-I responses to anamnestic challenge in CCR2-depleted mice. **B)** Representative flow cytometry of lineage-negative $Ly6C^+$ $CD64^+$ myeloid cells in the lungs of WT and CCR2-DTR mice on day 3 post PR8-Ova challenge, after Dtx administration. **C)** The Log_2 fold-change in the indicated myeloid cell subsets in the lungs of WT and *Ccr2*-DTR mice on day 3 post PR8-Ova challenge, after Dtx administration, normalised to WT mice. **D)** The total number of OT-I cells recovered from the indicated organs of WT and *Ccr2*-DTR host mice. Data are presented as mean ± SEM (n=12 WT n=11 *Ccr2*-DTR hosts), pooled from 2 independent experiments. $^{ns}p>0.05$ = not significant, $^{*}p\leq0.05$, $^{**}p\leq0.01$, $^{***}p\leq0.001$, $^{****}p\leq0.0001$ (**(C)** Two-way ANOVA. **(D)** unpaired Students *t*-test).

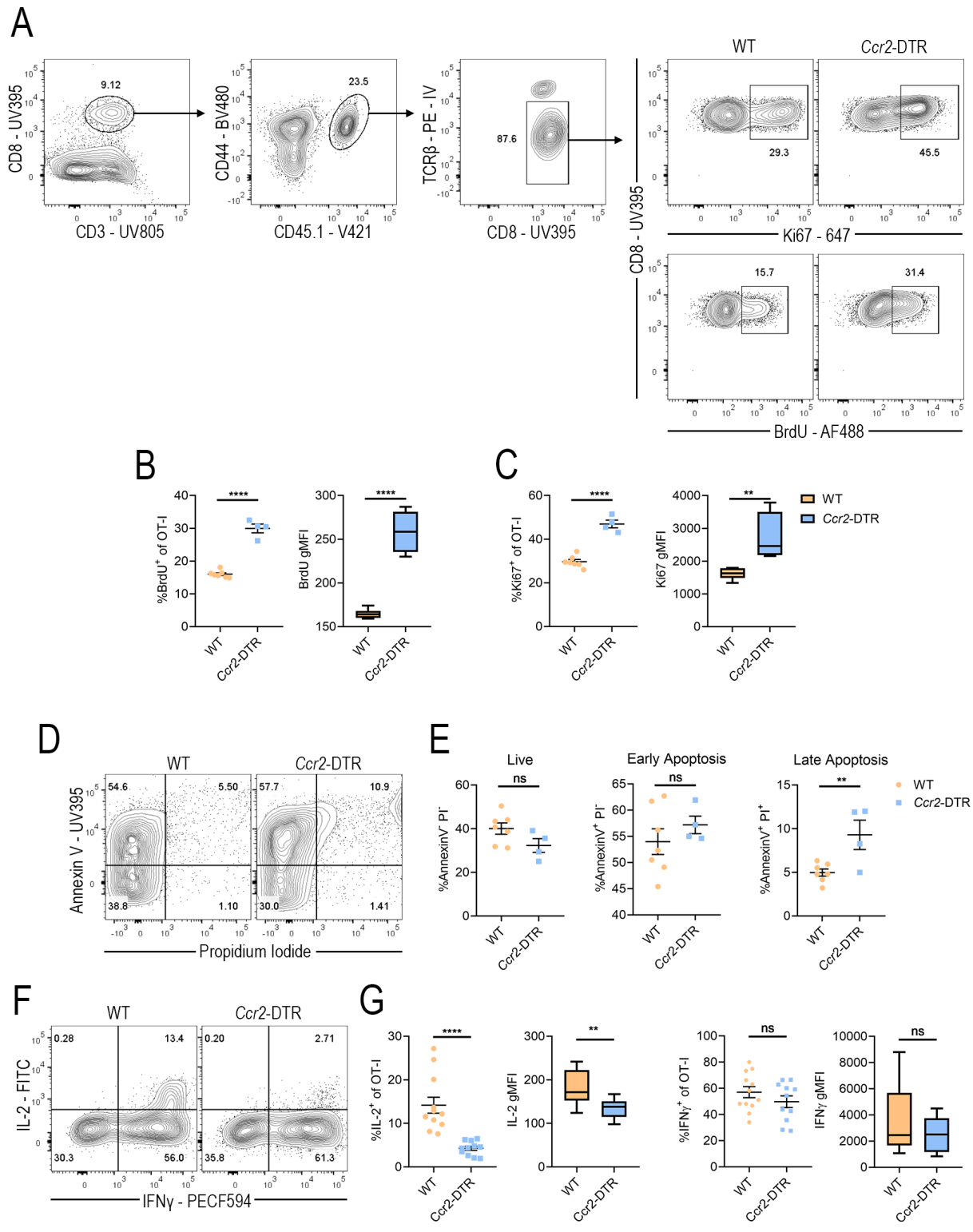
A
CD8 - UV395
CD3 - UV805
9.12
CD44 - BV480
CD45.1 - V421
23.5
TCRβ - PE - IV
CD8 - UV395
87.6
WT
Ccr2-DTR
CD8 - UV395
Ki67 - 647
29.3
45.5
15.7
31.4
BrdU - AF488
B
%BrdU+ of OT-I
BrdU gMFI
****
WT
Ccr2-DTR
C
%Ki67+ of OT-I
Ki67 gMFI
**
WT
Ccr2-DTR
D
WT
Ccr2-DTR
Annexin V - UV395
Propidium Iodide
54.6
5.50
38.8
1.10
57.7
10.9
30.0
1.41
E
Live
Early Apoptosis
Late Apoptosis
ns
**
%AnnexinV- PI-
%AnnexinV+ PI-
%AnnexinV+ PI+
WT
Ccr2-DTR
F
WT
Ccr2-DTR
IL-2 - FITC
IFNγ - PECF594
0.28
13.4
30.3
56.0
0.20
2.71
35.8
61.3
G
%IL-2+ of OT-I
IL-2 gMFI
%IFNγ+ of OT-I
IFNγ gMFI
****
**
ns
ns
WT
Ccr2-DTR

Figure 4.20: Depletion of CCR2-expressing cells during influenza challenge leads to increased turnover of OT-I cells in the lungs

Naïve OT-I cells (10^4) were transferred into WT and *Ccr2*-DTR host mice that were infected with x31-Ova 24 hours later. Thirty five days post x31-Ova-infection WT and *Ccr2*-DTR hosts were challenged with PR8-Ova and the memory OT-I response to infection, after depletion of CCR2-expressing cells, was measured on day 3 post-challenge. **A)** Representative flow cytometry of BrdU and Ki67 staining in OT-I cells in the lungs of WT or *Ccr2*-DTR mice on day 3 post PR8-Ova challenge. **B)** The percentage of OT-I cells that had incorporated BrdU and gMFI for BrdU staining. **C)** The percentage of OT-I cells expressing Ki67 and gMFI for Ki67 staining. **D)** Representative flow cytometry for the identification of apoptotic OT-I cells in WT and *Ccr2*-DTR hosts. **E)** The frequency of Annexin V^- PI^- live, Annexin V^+ PI^- early-apoptotic, and Annexin V^+ PI^+ late-apoptotic OT-I cells in the lungs of WT and *Ccr2*-DTR host mice. **F)** Representative flow cytometry of IL-2 and IFNγ production in OT-I cells from the lungs of WT and *Ccr2*-DTR host mice 4 hours after *ex vivo* SIINFEKL stimulation. **G)** The percent cytokine-producing and gMFI for IL-2 and IFNγ in OT-I cells from the lungs of WT and *Ccr2*-DTR hosts. Data are presented as mean ± SEM (**(B-E)** n=7 WT n=4 *Ccr2*-DTR hosts. **(G)** n=12 WT n=11 *Ccr2*-DTR hosts), pooled from 2 independent experiments. $^{ns}p>0.05$ = not significant, $^{**}p\leq0.01$, $^{***}p\leq0.001$, $^{****}p\leq0.0001$ (unpaired Students *t*-test).

5 | Discussion

5.1 Introduction

The initial aim of this project was to identify the migratory cues that ultimately shape $CD8^+$ T cell responses to viral infection. A comprehensive chemokine receptor screen identified CCR2 as a potential candidate for this role. Although expression of this receptor had previously been identified in $CD8^+$ T cells in a number of different infectious and non-infectious settings, no studies investigating the functional role of CCR2 in $CD8^+$ T cell biology had been reported. Using a combination of genetic knockout and transgenic T cell transfer approaches it was shown that, under the conditions tested, there is no cell-intrinsic role for CCR2 in the development of effector responses to influenza infection, the establishment of long-lived memory populations, or in the acquisition of effector potential. The expression pattern of CCR2 on circulating memory T cells also led to the investigation of its role in regulating tissue recruitment in a non-anamnestic influenza challenge model. However, these experiments demonstrated that CCR2 was also dispensable for $CD8^+$ T cell trafficking into virally-inflamed peripheral tissue and lymph nodes. There was, however, a role shown for CCR2 in the infiltration of circulating memory OT-I cells into skin inflamed by IL-1α treatment. Therefore, under the conditions tested, this study does not support a cell-intrinsic role for CCR2 in the recruitment of memory $CD8^+$ cells during viral recall, but does support a cell-intrinsic role for CCR2 in T cell immunosurveillance of inflamed skin under certain contexts. Investigations into the cellular source of the CCR2 ligand, CCL2, demonstrated that monocytes and monocyte-derived cells were the major CCL2-producing cell following influenza infection. These results informed experiments aimed at assessing the role these CCL2-producing cells had in shaping the anti-influenza immune response through the use of broad *Ccr2*$^{-/-}$ mice, which have defective monocyte recruitment during infection. These experiments showed that host CCR2 was required for the optimal formation of long-lived memory OT-I cell populations, but had no impact on the development of endogenous influenza-specific memory $CD8^+$ T cells. Despite the relatively normal distribution and function of endogenous memory $CD8^+$ T cells, x31-immune *Ccr2*$^{-/-}$ mice had increased morbidity during lethal A/PR8 challenge which was associated with higher viral burden, and decreased IFNγ in the BALF. The defect in viral control upon challenge was associated with a decrease in T cell re-activation in the lungs, which led to sub-optimal expansion of memory T cells during challenge. Therefore, the data in this study do not support a cell-intrinsic role for CCR2 in $CD8^+$ T cell fate but demonstrate a requirement for host CCR2 for the optimal function of memory T cells during memory T cell responses to influenza challenge. This discussion will expand on the key aspects of this study.

5.2 The expression of CCR2 by $CD8^+$ T cells.

CCR2 transcripts or protein have been reported to be expressed by $CD8^+$ T cells activated by diverse intracellular pathogens in the respiratory and gastrointestinal tracts [299, 300, 337], from viral infection via intravenous or intraperitoneal infection routes [209, 254, 301, 309, 338], as well as in $CD8^+$ T cells present in cancer and autoimmune disease [339, 340], after stimulation by *ex vivo* peptide-pulsed DCs [302], DNA-based vaccination

[303], and in virtual memory cells [197, 341]. The data presented here extend the reports of CCR2 expression by more comprehensively analysing the phenotype of the cells that were expressing this receptor, and the timing of expression during influenza infection. Some chemokine receptors and adhesion molecules are associated with activation in specific contexts, and may regulate tissue-specific homing of those cells, including α4β7 and CCR9 induction in gut-associated lymphoid tissue for T cell homing to the gastrointestinal tract [68, 69], and CLA and CCR10 and CCR4 induction in skin-draining lymph nodes for T cell homing to the skin [70, 71]. Other chemokine receptors, such as CCR5, have been reported to have consistent expression of transcripts across infectious models, but context-dependent presentation of the receptor on the cell surface to regulate cell function [76, 189]. While other receptors yet have been reported to perform a function restricted to a specific activation state, such as S1PR1 for lymph node and peripheral tissue egress of mature, differentiated T cells [342], CX3CR1 for the patrolling of the vasculature by terminal effector cells [246, 253], or CXCR6 to position memory precursor cells in the airways for Trm differentiation [77]. The broad expression of CCR2 seen across those reports mentioned above, and here, early after activation and in diverse effector and memory subsets, indicates that it is unlikely that CCR2 is induced in specific infectious contexts, or for tissue-specific homing, but instead is potentially expressed as a default part of $CD8^+$ T cell activation, similar to CXCR3. Thus, similar to CXCR3, in this project CCR2 was hypothesised to be involved in a broad $CD8^+$ T cell function with the potential to influence the majority of activated $CD8^+$ T cells [162, 190, 294].

Expression of CCR2 was not limited to any individual effector or memory subset and was relatively evenly expressed across these subsets, unlike some other chemokine receptors, such as CXCR3 and CX_3CR1, that decrease, or increase in expression as cells become more effector-like [162, 246]. As effector cells transitioned into long-lived memory cells, expression of CCR2 remained on circulating memory populations but was down-regulated on Trm cells in the lung. As Trm cells undergo transcriptional changes to establish a program of residency, it is possible that the transcription factors that regulate this residency program, such as RUNX2, HOBIT, and KLF2, also cause downregulation of CCR2 [78, 343]. The suppression of *Ccr2* in resident memory cells and its continued expression on all circulating memory subsets suggest that this receptor potentially performs a function that is specific to circulating memory cells. Given the ability of these cells to rapidly deploy themselves to lymphoid and non-lymphoid tissues during inflammation, it was further hypothesised that CCR2 regulates tissue egress in a manner similar to that of bone marrow monocytes [122], or tissue access, which will be discussed later in this chapter.

The restricted expression of CCR2 observed on human Tcm cells contrasted with those results seen in mice, where CCR2 expression is present on all circulating memory cell subsets and was generally associated with cells that have a greater effector potential [310]. However, whether this is a true interspecies difference, or is a reflection of the different conditions under which CCR2 expression was examined, is unclear. However, in support of the former, human CCR2, in contrast to murine, is more promiscuous in its ligand binding and CCL2, CCL7, CCL8, CCL13, and CCL16 are all reported ligands of human CCR2 [344]. In this context, the multiple ligands for human CCR2 could enable complex regulatory functions and a degree of redundancy within the chemokine system to ensure effective immune defense. While CCL2, CCL8, and CCL13 all have broad expression in humans,

active in the majority of peripheral tissues, CCL7 and CCL8 have much more restricted expression, with CCL7 transcripts reported in the bone marrow and adipose tissue, and CCL8 transcripts only detected in the liver [345]. The CCL7 axis could be used by human Tcm cells for homing to the bone marrow where there is homeostatic maintenance and turnover of these cells, as has been reported for mice [346–348]. In support of this, human bone marrow contains a large reservoir of memory cells [349, 350], although the precise phenotype of those memory cells is unclear. The white adipose tissue of mice has also been reported as a reservoir for circulating memory T cells [351], and localisation of memory cells within adipose tissue prompts metabolic changes that support T cell longevity and recall function. Additionally, in the present study, Tcm cells from human donors that express CCR2 displayed a lower lymph node homing capacity than CCR2-negative Tcm cells, as indicated by reduced expression of the lymph node homing markers CCR7 and CD62L. It has been demonstrated in mice that Tcm cells are able to rapidly infiltrate NLT during viral infection [235, 290], and at homeostasis small populations of $CD8^+$ and $CD4^+$ Tcm cells can be detected in human NLT [265, 352]. Taken together, with the reduced lymph node homing capacity, CCR2-expressing Tcm cells could represent a transient surface phenotype acquired during recirculation, or a stable subset that preferentially localises to NLT during inflammation. Given more time, it would be interesting to extend the experiments in this study by performing a more thorough characterisation of these $CCR2^+$ human Tcm cells to determine how they relate to the human T stem cell memory subset [353], or to determine if they represent a functionally distinct subset of Tcm cells.

5.3 Regulation of effector and memory cell differentiation

Several reports have demonstrated the importance of inflammatory chemokine receptors, such as CXCR3 and CCR5 for the optimal differentiation of effector $CD8^+$ T cell populations [162, 291–294, 354]. During $CD8^+$ T cell activation in SLOs these inflammatory chemokine receptors are expressed early after TCR stimulation and direct activated cells to inflammatory niches, or to antigen-bearing cDCs, to drive effector differentiation. Immunofluorescent analysis of $CD8^+$ T cell responses in several different infectious models have demonstrated that the lymph node interfollicular and capsular environments serve as important microanatomical niches for these T cell-cDC interactions [39, 105, 155, 165, 250, 294, 354]. In these settings the initial activation of T cells often occurs within the paracortex and, as the response progresses, activated $CD8^+$ T cells migrate to capsular and interfollicular regions of the lymph node to complete their differentiation. In the present study it was observed that, like CXCR3, CCR2 was expressed by OT-I cells after the first cell division in the lung-draining mLN, and the CCR2 ligand CCL2 was also detectable in mLN supernatants by ELISA by day 4 post influenza-infection. Although the number of CCL2-reporter-positive cells present in the mLN of CCL2-RFP mice was low following primary infection, there were some cells present at day 5 post infection, a time point at which influenza-specific T cells are actively dividing and differentiating [305]. Additionally, it is possible that the majority of the CCL2 present in the mLN drained from the inflamed lungs, as has been reported for CCL2 in other models of inflammation [16, 355]. Therefore, CCL2 would likely be present around interfollicular areas that are enriched for T cell activation clusters [105]. As it was observed in the present study that nearly all activated OT-I cells in the mLN on day

4 post x31-Ova infection were expressing CCR2, it was hypothesised that CCR2 could be involved in the fate determination of these cells, potentially by recruiting them to those inflammatory niches around interfollicular and capsular regions of the mLN. However, a series of in-depth experiments indicated that the initial expansion, effector differentiation, and the acquisition of effector potential of these cells was unaffected in the absence of CCR2, which did not support a cell-intrinsic role for CCR2 in any of these aspects of the effector response.

One striking observation that resulted from the present study was the identification of sustained expression of CCR2 in circulating memory T cells, but little expression in resident memory cells. In contrast to resident memory T cells, which are programmed to their fate within barrier tissues, the eventual development circulating memory cell subsets is tightly linked with the signals that a cell receives during its initial priming and expansion. The transcriptional networks established during cell priming can dictate the size of a memory population through clonal expansion, the relative abundance of central and effector memory subsets, and the ability of cells to survive the contraction phase [183, 184, 246, 356]. This is likely the reason why there was no difference in the distribution or number of circulating memory cells seen in *Ccr2*$^{-/-}$ OT-I cells, as their memory fate was likely sealed during initial activation, which was unaltered in the absence of CCR2. In addition to influencing the differentiation of CD8^{+} T cells, chemokine receptors have the potential to influence the maintenance of circulating memory cells, which is regulated primarily through common ɣ-chain cytokines, particularly IL-7 and IL-15 [357–360]. At homeostasis these cytokines are expressed by stromal cells, primarily fibroblasts [361, 362]. As fibroblasts also constitutively produce low levels of CCL2 [42, 133] it was hypothesised that these cells create a microenvironment within tissues that support the continual maintenance of circulating memory cells in a CCL2-CCR2 dependent manner. However, this hypothesis was not supported, as no difference was observed in the number of *Ccr2*$^{-/-}$ memory CD8^{+} T cells present at memory timepoints in either lymphoid or non-lymphoid tissues.

Like the development of effector CD8^{+} T cell populations during the acute phase of an an infection, Trm cells also require chemokine-dependent localisation at barrier sites for their development [78], yet the tissue-specific requirements for this localisation are not fully understood. Analysis of CCL2-reporter mice following influenza infection showed that reporter-positive cells were present at 11 days post A/HK-x31 infection, a timepoint at which influenza-specific T cells are transitioning from expansion, to contraction, and memory formation. Concomitant with the resolution of influenza infection is the appearance of discrete patches of active tissue repair marked by the presence of keratin 5 [363–365]. In the post-influenza-infected lungs the generation of Trm cells is restricted to these micro-environments that have experienced tissue damage [281], although it is not clear which signals localise and retain cells at these areas. It is well established that monocytes and monocyte-derived Mϕ are critical for tissue-repair processes, and the CCL2-producing monocytes that are present late after infection are likely localised to areas of tissue damage where they can mediate tissue repair [366]. Additionally, some of the signals that promote tissue repair in these microenvironments also promote the maturation of Trm cells, as has been shown for the tissue healing factor NOTCH [367]. However, as the frequency and total number of WT and *Ccr2*$^{-/-}$ OT-I Trm cells present in the lung parenchyma was not altered in the absence of CCR2, it is unlikely that this receptor is involved in T cell localisation to these area of tissue damage to promote Trm development. Populations of Trm cells also transiently persist in the airways after infection, and it is known that these T cells are partially

reliant on CXCR6 to migrate from the lung parenchyma into the airways to form airway-resident Trm [77]. This process is also potentially regulated by CXCR3, although those studies utilised global CXCR3 knockout mice and it is not clear if the reduced numbers in the lungs and airways was due to a defect in recruitment, or priming of the cells, or both [65, 75]. Data obtained from the CCL2-reporter mice in the present study showed that alveolar Mϕ located in the airways began to produce CCL2 after the clearance of the virus, and *Ccr2*$^{-/-}$ OT-I cells also had a defect in their recruitment into the airways at day 9 post infection, suggesting that alveolar Mϕ may promote T cell recruitment into the airways in a partially CCR2-dependent manner. However, the reduction in alveolar Mϕ numbers did not have a lasting impact on the development of Trm populations in the airways. Together, the data presented here demonstrate that while the receptor and ligand are both present across the spectrum of T cell differentiation, CCR2 has no cell-intrinsic effect on CD8$^+$ T cell effector or memory cell differentiation.

Although no cell-intrinsic role for CCR2 was identified in the present study, it is possible that CCR2 expression by CD8$^+$ T cells is required in other infectious or disease settings. As mentioned, CCR2 transcripts or protein have been reported in CD8$^+$ T cells in a number of infectious, and non-infectious, settings [197, 209, 254, 299–303, 309, 337–341]. The present study focused on a single respiratory viral infection model, however, the migratory requirements for CD8$^+$ T cells may differ in other barrier tissues and infection, or disease, models. In future experiments it would be worthwhile looking in other infectious settings such as flank skin, or intravaginal HSV infection to assess CCR2 requirement in the skin and female reproductive tract respectively, or *Yersinia spp.* or *Salmonella typhimurium* infection by oral gavage to assess responses in the gastrointestinal tract. Additionally, the analyses performed on *Ccr2*$^{-/-}$ OT-I cells in the present study focused on the most obvious outcomes of CD8$^+$ T cell activation; differentiation of effector subsets, the formation of long-lived memory cells, and acquisition of effector potential. Although no differences were seen in any of these analyses, performing a detailed RNAseq analysis on populations of WT and *Ccr2*$^{-/-}$ OT-I cells isolated from the mLN or lungs of mice at the peak of the OT-I response to infection, or at memory timepoints, may reveal any impact of this receptor on CD8$^+$ T cell activation, differentiation, and function, including more subtle effects than could not be detected in the present study.

5.4 Memory CD8$^+$ T cell trafficking during influenza challenge

Circulating memory cells are able to establish a body-wide state of immunosurveillance regardless of the initial site of infection [318]. In the present study it was hypothesised that CCR2 may have an important role in a recall setting, where populations of circulating memory CD8$^+$ T cells expressing CCR2 are poised to rapidly infiltrate early-inflamed peripheral tissue or lymph nodes in a CCR2-dependent manner. Evidence for this exists *in vitro* where the transendothelial migration of human effector CD8$^+$ T cells across TNFα-stimulated endothelial layers was shown to be CCR2-dependent [34]. Although CCL2-reporter expression was not observed in CD45$^-$ cells in the lungs, blood endothelial cells within postcapillary venules have high expression of ACKR1, which can bind and translocate CCL2 from the tissue parenchyma to the blood lumen [13, 14, 57]. Atypical chemokine

receptors expressed on HEVs in lymph nodes have also been shown to perform the same function, transporting lymph drained chemokines from the lymph node to the lumen of blood vessels to facilitate monocyte recruitment and, therefore, this same chemokine axis may be used by CCR2-expressing Tcm and Tpm cells to enable their rapid recruitment into LNs draining inflamed tissue [16]. In the present study, inhibition of GPCRs through Ptx treatment of memory OT-I cells demonstrated that the migration of circulating memory cells into the inflamed lungs and mLN was entirely dependent on GPCR signalling which, while indirect, supports the involvement of one or more chemokine receptors in this process. However, when directly tested, the data clearly showed that the migration of *Ccr2*$^{-/-}$ OT-I cells into inflamed tissue during *in vivo* challenge was similar to that of WT. Interestingly, the frequency of cells in the circulation was significantly altered, where there was a greater ratio of *Ccr2*$^{-/-}$ to WT OT-I cells in the vasculature of the lungs, the red pulp of the spleen, and in the bone marrow. These results are consistent in some regards with the *in vitro* data from Shulman *et al.* [34], where, when translating the findings of Shulman *et al.* into an *in vivo* context, a higher frequency of *Ccr2*$^{-/-}$ OT-I cells in vascular fractions would be expected if these cells are not infiltrating inflamed tissues and SLOs. However, there was not a corresponding decrease in the number of *Ccr2*$^{-/-}$ OT-I cells in peripheral tissue, as would be expected if CCR2 was required for early tissue infiltration, indicating that CCR2 is dispensable for recruitment of CD8^{+} T cells into inflamed lungs and mLN. It is possible that while *Ccr2*$^{-/-}$ OT-I cell migration to inflamed lungs, mLN and upper airways is normal, these cells have reduced trafficking to non-target, uninfected tissue, such as the gastrointestinal tract (GIT). As it has previously been reported that CD8^{+} T cell migration into the GIT is partly CCR2-dependent [337], some WT OT-I cells that have been mobilised to the blood may migrate into that tissue in a CCR2-dependent manner, leaving a higher frequency of *Ccr2*$^{-/-}$ OT-I cells in the circulation. The work from Shulman *et al.* [34] also showed that the dependence on CCR2 for transendothelial migration was lost if the endothelial layers were co-stimulated with IFNγ and TNFα, presumably by increasing CXCL9 and or CXCL10 expression by the endothelial cells in an IFNγ-dependent manner, and providing T cells an alternative trigger for transendothelial migration via CXCR3 [34]. This could explain why no role was observed for CCR2 in the recruitment of memory OT-I cells into the inflamed lung parenchyma and the mLN, as CXCL9 and CXCL10 are rapidly produced during re-infection in an IFNγ-dependent manner [79, 287, 368]. The presence of host endogenous Trm cells in the lungs prior to challenge likely results in rapid IFNγ production that results in secretion of CXCL9 and CXCL10 to promote T cell recruitment [288], and although these are non-anamnestic challenges, bystander memory T cells can be activated to produce IFNγ in a cytokine dependent, antigen independent, manner by local monocytes to provide IFNγ [124, 129].

Due to the presence of multiple chemokine axes that are available to memory CD8^{+} T cells infiltrating influenza-infected lungs during A/PR8 challenge, it was hypothesised that the reason there was no role identified for CCR2 in tissue infiltration was due to chemokine receptor redundancy. Thus, while there was no cell-intrinsic role for CCR2, it is possible that CCR2 works synergistically with other chemokine receptors to regulate CD8^{+} T cell fate and function. This hypothesis was explored in several ways in the present study, but, due to technical difficulties with these experiments, the hypothesis could not be adequately addressed **(Appendix Fig. 6.1,6.2)**. Those experiments were based on the observation that although the influenza-infected lungs expressed a diverse range of chemokines, expression of the CXCR3 ligands CXCL9 and 10, and the CCR5 ligands CCL3, 4 and 5 were

particularly prominent. These chemokine axes both have important roles in $CD8^+$ T cell biology, and were two likely candidates for chemokine receptor redundancy. In the present study, some preliminary experiments were performed to assess any degree of redundancy within these receptors in regards to T cell recruitment to inflamed tissue in a non-anamnestic influenza challenge model. However, co-transfer of WT and *Ccr2*$^{-/-}$ memory OT-I cells into day 4 A/PR8-infected *Ifnγ*$^{-/-}$ hosts, which fail to express CXCL9 and CXCL10, 4 hours prior to analysis did not reveal any defect in migration of *Ccr2*$^{-/-}$ OT-I cells into inflamed tissue **(Appendix Fig. 6.1)**. Additionally, attempts at neutralising CXCR3 with a commercially-available antibody, or CXCR3 and CCR5 with peptide antagonists, were also unsuccessful at inhibiting *Ccr2*$^{-/-}$ OT-I cell migration into inflamed tissue **(Appendix Fig. 6.2)**. However, the *in vivo* efficacy of the small molecule antagonists was questionable, and the CXCR3 neutralising antibody may have been causing organism-wide depletion of OT-I cells, rather than neutralisation of the receptor. To better assess potential synergy between these chemokine receptors *Ccr2*$^{-/-}$ mice could be crossed with *Cxcr3*$^{-/-}$ mice, to generate dual knockout mice that would allow determination of redundancy with these two receptors, similar to that previously observed with CCR5 and CXCR3 during influenza infection [292]. Potential synergy between CCR2 and CCR5 would be harder to assess as these two genes are within close proximity of each other on the same chromosome, effectively eliminating the possibility of breeding double knockout mice [369]. The recently generated iCCR-deficient mice, in which the entire region of the genome that contains the genes for CCR1, CCR2, CCR3 and CCR5 has been removed [74], could potentially be used to assess the combined contribution of these receptors to $CD8^+$ T cell fate and function. Though these mice also lack CCR1 and CCR3, these receptors are not expressed on responding $CD8^+$ T cells [370], and though *Ccr1* mRNA was detected in influenza specific OT-I cells, the protein was not detectable on $CD8^+$ T cells in this study using a commercially-available antibody (data not shown). The iCCR mice could also be crossed with *Cxcr3*$^{-/-}$ mice and TCR transgenic strains, such as the OT-I mouse, to generate inflammatory chemokine receptor deficient $CD8^+$ T cells to allow the most thorough investigation of inflammatory chemokine receptor redundancy in $CD8^+$ T cell biology to date.

5.5 Memory $CD8^+$ T cell trafficking into cytokine-stimulated ears

In contrast to those results seen during influenza challenge, the trafficking of *Ccr2*$^{-/-}$ memory OT-I cells into ear pinna treated with IL-1α, but not IL-1β or TNFα, was significantly impaired compared to WT. Despite signalling through the same receptor, IL-1RI, IL-1α and IL-1β had dramatically different effects on memory cell migration, with IL-1β-treated ears displaying no measurable OT-I cell recruitment by flow cytometry. These results are consistent with the *in vivo* biological activities of these cytokines as IL-1α and IL-1β have been shown to have non-redundant functions in peripheral tissues in regards to innate and adaptive cell recruitment [82, 371, 372]. For example, in a study by Natsuaki *et al.* [82] it was demonstrated that cutaneous administration of IL-1α, but not IL-1β, promoted clustering of DCs around perivascular regions of the mouse dermis. The IL-1α-dependent clustering of dermal DCs was critical for recruitment of effector T cells and their ongoing proliferation and IFNɣ secretion *in situ.* Although the specific chemotactic signals that promoted the recruitment of T cells were not fully investigated in that study, reports have shown that IL-1α signalling through IL-1RI can induce CCL2 and

CCL5 expression, although the full extent of chemokine expression has not been reported. Regardless, the data presented here begin to form the basis of a model that potentially represents the first described mechanism for chemokine-dependent T cell immunosurevillance of peripheral tissues **(Fig. 6.1)**. In this model, stressed, damaged, or dying cells release IL-1α which stimulates production of CCR2 ligands by local immune and stromal cells. These chemokine signals are sensed by circulating memory T cells in the bloodstream that are then prompted to migrate into the inflamed tissue. Once in the inflamed tissue the T cells can scan for cognate antigen, or the presence of overt inflammation in the form of inflammasome-derived IL-18 and IL-1β, with sensing of either resulting in IFNγ production, amplification of local CXCL9 and CXCL10 secretion, and further infiltration of T cells to combat the potential infection. Although a feed-forward loop such as this had been described for the amplification of innate responses to infection, whether this mechanism is co-opted by memory T cells of the adaptive immune system is not known. Additional work would be needed to confirm that the migration of WT T cells into IL-1α treated ears is lost in *Il1r1*$^{-/-}$ hosts, that migration of *Ccr2*$^{-/-}$ T cells is restored when IL-1α is co-injected with IFNγ, and investigate the full extent of how IL-1α, IL-1β, and TNFα treatment regulate chemokine expression in peripheral tissue.

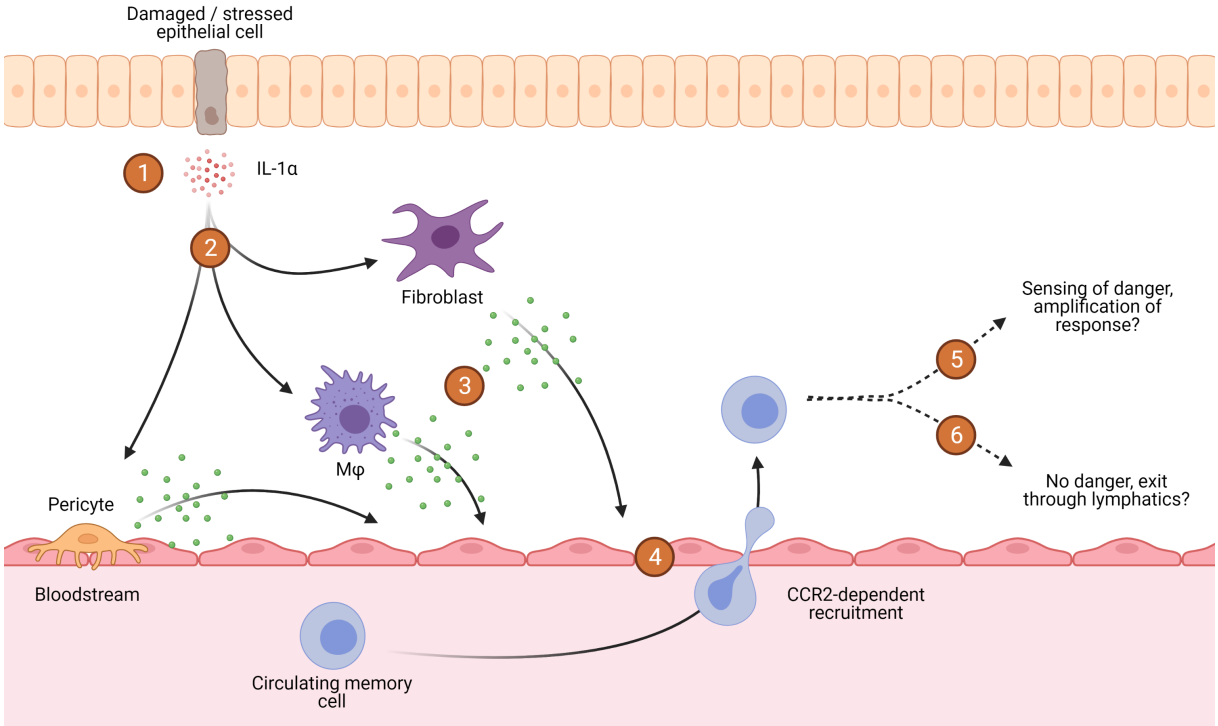

Figure 5.1: Working model for the CCR2-dependent immunosurveillance of damaged peripheral tissue

1) Damaged or stressed epithelial cells secrete IL-1α into the local tissue. **2)** Nearby IL-1RI expressing stromal cells, tissue Mϕ and vascular-associated cells such as pericytes sense IL-1α and **3)** produce CCR2 ligands, as well as secondary effector cytokines that increase the expression of chemokines and adhesion molecules by endothelial cells. **4)** Circulating memory T cells bind to, and cross, inflamed endothelial cells in a partially CCR2-dependent manner. Once in the inflamed tissue T cells either **5)** Sense damage signals in the tissue, in the form of cognate antigen or inflammatory cytokines and amplify the response through IFNγ secretion, or **6)** Do not encounter any signals that result in amplification of the response and return to the circulation via the afferent lymphatics.

5.6 Monocyte influence on the generation of effector and memory T cell responses

During the course of this study a report was published that suggested that monocytes and their derivatives are important for the long-term maintenance of memory OT-I cell populations [118]. Using *Ccr2*$^{-/-}$ mice, where monocyte egress from the bone marrow is inhibited during inflammation, Desai *et al.* [118] observed normal OT-I cell expansion and contraction, but decreased numbers of resident and circulating memory OT-I cells following an intranasal vaccinia virus infection in *Ccr2*$^{-/-}$ hosts relative to WT hosts 50 days post-infection. Although the authors did not provide a mechanism for the decreased memory pool in *Ccr2*$^{-/-}$ hosts, they hypothesised that interactions with monocytes long after the resolution of infection could be required for the maintenance of memory CD8^{+} T cells. A more recent report, using the same transfer approach but in influenza infection, suggested that influenza antigen was presented by pulmonary monocytes to drive the monocyte-dependent development of OT-I Trm cells within the lung [330]. Using *in vitro* co-culture systems those authors showed that OT-I cells that were co-cultured with FACS-sorted monocytes from day 8 x31-Ova infected lungs upregulated the canonical Trm marker CD103, indicating that monocytes may have the potential to drive Trm differentiation. In addition to the reduction in the formation of resident memory OT-I cells Dunbar *et al.* [330] also reported a reduction in the total number of endogenous NP-specific Trm cells present in *Ccr2*$^{-/-}$ hosts relative to WT hosts 45 days after influenza infection. While the data presented here regarding the development of resident memory OT-I cells in *Ccr2*$^{-/-}$ hosts is consistent with that of Desai *et al.* [118] and Dunbar *et al.* [330], a major difference between these previous publications and the present study is that the total number of host influenza-specific memory CD8^{+} T cells was largely unaffected by the absence of CCR2. It is unclear as to why the results in the present study differ from the work of mentioned above, but the work presented here is performed with littermate-derived control mice, while the work of those studies [118, 330] relied on knockout mice bred in-house and control mice sourced from a commercial facility. Although the use of littermate controls still has some limitations [373, 374], these mice are less prone to genetic variation and the potential effects of the microbiome on immune development during embryogenesis and the pre-weaning period [375–377], and thus represents a model that may be less prone to artefacts. Why this difference in memory formation affects OT-I cells and not endogenous influenza-specific memory cells is also unclear, although one explanation may be in the size of a memory T cell population a host can reliably maintain. The size of the memory OT-I population that is present 35 days post-influenza infection is far greater than the size of the endogenous influenza-specific memory CD8^{+} T cell population. As all memory T cell subsets require IL-15 signalling for their long-term maintenance [78, 272], and as monocytes have been reported as a source of IL-15 *in vivo* [127, 359, 378], the overall reduction in OT-I memory cell numbers could be due to a reduction in IL-15-dependent maintenance by monocytes in *Ccr2*$^{-/-}$ mice. For memory OT-I cells there could be higher competition for limited IL-15 which leads to enhanced contraction, whereas, under normal circumstances, the small number of influenza-specific memory CD8^{+} T cells do not have to compete for these signals. If this was an underlying cause for the difference in OT-I numbers then future experiments aimed at transferring a more physiologically relevant number of naive OT-I cells, 10^2 instead of 10^4, may reverse the loss

of OT-I memory cells seen in *Ccr2*$^{-/-}$ hosts.

5.7 The impact of *Ccr2* deficiency on the memory response to heterosubtypic challenge

Another of the major findings of this study was a demonstrated requirement for CCR2 for optimal host protection in the context of lethal heterosubtypic challenge with influenza. Analysis of x31-immune *Ccr2*$^{-/-}$ mice during A/PR8 challenge revealed increased weight loss that was associated with an increased viral load and decreased IFNγ in the airways, relative to WT mice, indicating that the establishment of an early IFNγ-dependent antiviral state is compromised in *Ccr2*$^{-/-}$ mice. Despite the reduction in IFNγ in the airways, T cells from the lungs of day 3 A/PR8 challenged *Ccr2*$^{-/-}$ mice had a higher frequency of IFNγ expression after *ex-vivo* stimulation with PMA, although their cytokine production potential was equivalent in resting memory mice. As T cell infiltration into the lungs of day 3 A/PR8 challenged WT and *Ccr2*$^{-/-}$ mice was equivalent, the decrease in IFNγ in the BALF was potentially due to reduced re-activation of memory cells *in situ*. It has previously been reported that with repetitive TCR stimulation, T cells lose the ability to produce IFNγ [379]. This previous observation, paired with the observed reduction in BrdU incorporation seen in the present study in T cells from the lungs of *Ccr2*$^{-/-}$ mice on day 3 post-challenge, suggests that T cells in the lungs of *Ccr2*$^{-/-}$ mice had received reduced TCR stimulation, which may have preserved a greater effector potential in these cells just prior to *ex vivo* stimulation. In support of this, the percentage of IFNγ-expressing CD8^{+} T cells from *Ccr2*$^{-/-}$ mice at day 3 post-challenge more closely resembled the IFNγ production seen in resting memory cells. Over the course of A/PR8 challenge, numbers of cDC1s, cDC2s and alveolar Mϕ were similar in WT and *Ccr2*$^{-/-}$ mice, however, monocytes, monocyte-derived cells, and inf-cDCs were significantly reduced in numbers in *Ccr2*$^{-/-}$ mice, which would likely reduce the number of antigen-presenting cells memory T cell are able to interact with for their reactivation *in situ*, and result in lower IFNγ present in the airways. Although the ability of monocytes to present viral antigen on MHC-I *in vivo* is contentious, recent *in vivo* imaging studies have shown that CD8^{+} T cells form stable interactions with monocytes in the trachea of influenza infected mice [380], and blockade of MHC-I *in vivo* reduces T cell interactions with monocytes in the trachea. It is debatable whether or not such interactions with monocytes drive T cell proliferation, possibly due to the lack of costimulatory molecules expressed by these cells, but it is generally well accepted that these interactions can promote the secretion of effector cytokines by antigen-specific T cells [314], possibly through the provision of cytokines such as IL-1β and IL-18 [124, 127, 129, 381, 382]. These reports, along with data presented here, implicate monocytes, monocyte-derived cells, and inf-cDCs in the lungs as important mediators of effector cytokine production in memory CD8^{+} T cells *in situ* during influenza challenge.

5.8 Memory cell proliferation in the lungs after A/PR8 challenge

In addition to the increased morbidity and reduced effector cytokines in the airways of A/PR8-challenged *Ccr2*$^{-/-}$ mice, there was a significant reduction in the number of proliferating influenza-specific memory T cells in the lungs during the early stages of A/PR8 challenge. Although the precise mechanism that resulted in this proliferation defect remained unclear in the present study, one hypothesis that was partially investigated, but remains unresolved, was whether a reduction in antigen presentation to memory T cells, due to the paucity of monocyte-derived cells and inf-cDCs in the lungs of influenza-challenged *Ccr2*$^{-/-}$ mice, was an underlying cause. Previous reports investigating lethal influenza challenge have suggested a correlation between monocyte infiltrates and optimal host protection [361], although exactly how monocytes provide this enhanced protection was unclear. Other studies have suggested that monocytes were required for optimal CD8^{+} memory T cell maintenance prior to challenge, and this reduction in the pool of influenza-specific memory T cells in the absence of monocytes ultimately compromised the response of *Ccr2*$^{-/-}$ mice to A/PR8 challenge [118, 330]. Additionally it was suggested that this maintenance of memory T cell numbers by monocytes is dependent on presentation of cognate antigen by these cells [120]. The data presented in the present study indicate no major differences in endogenous memory CD8^{+} cell populations between WT and *Ccr2*$^{-/-}$ mice prior to, or shortly following, A/PR8 challenge, and the contribution of monocyte antigen presentation to CD8^{+} T cell biology is controversial [89, 90, 136, 383]. Historically, monocytes have been difficult to separate from cDC2s, particularly in inflammatory settings, because they share very similar surface markers [89, 136, 141, 143, 173, 177]. As a result, many papers that have attempted to determine functional outcomes of monocyte-T cell or cDC2-T cell interactions are difficult to interpret because of potential contamination of one cell subset with the other. However, the most recent data published suggest that most of the cells that were previously considered to be monocyte-derived DCs are actually an inflammatory subset of cDC2s that are derived from a committed pre-cDC precursor, and are not functionally related to monocytes [90]. In that report inf-cDC2s sorted from the lungs and mLN of infected mice, rather than monocytes and monocyte-derived cells as identified by Bosteels *et al.* [90], were shown to efficiently drive naïve CD8^{+} T cell proliferation and, importantly, are partially dependent on CCR2 for their migration into inflamed lungs. In the present study, a thorough examination of the MNP subsets in the lungs of WT and *Ccr2*$^{-/-}$ mice during recall did not show any differences in the number of cDC1s and cDC2s, but found a large reduction in the number of monocytes and monocyte-derived cells in *Ccr2*$^{-/-}$ mice relative to WT. Although the gating strategy employed was not identical to that outlined by Bosteels *et al.* [90], there was also a significant reduction in the total number of inf-cDC2s present in the lungs of *Ccr2*$^{-/-}$ mice throughout A/PR8 challenge. Of note, cDC1 and cDC2 numbers in the lung rapidly declined after A/PR8 challenge, as these cells presumably matured and migrated to the draining mLN, and this exodus of lung cDCs was quickly replaced by inf-cDCs by day 3 post-challenge. Results from the recall kinetics during non-anamnestic challenge showed that large numbers of circulating memory OT-I cells infiltrate the inflamed lung within 48-72 hours of A/PR8 challenge, coinciding with the appearance of inf-cDCs in the lung. Thus, it is possible that T cells infiltrating the lungs during A/PR8 challenge require interactions with this inf-cDC subset for their optimal expansion *in situ* and that CCR2 expression by both subsets plays an important role in their colocalization within the tissue. Although these observations, alongside the antigen-presenting

capacity of monocytes and inf-cDCs reported by Bosteels *et al.* [90], implicate inf-cDCs as important regulators of memory T cell expansion, the specific antigen-presenting capabilities of lung-derived monocytes and inf-cDCs during influenza challenge would have to be compared through experimentation. This will be discussed shortly.

One intriguing observation from this work is that while the proliferation of memory T cells appears compromised during secondary challenge, the proliferation of T cells during primary infection is unaltered, despite the same reduction in MNP numbers in primary A/HK-x31 infected lungs while activated T cells are present (from day 7 post infection). This difference in proliferation between a primary infection and a secondary challenge could be driven by differences intrinsic to the $CD8^+$ memory T cells present in *Ccr2*$^{-/-}$ mice, or memory cell extrinsic factors that arise as a result of the viral challenge. Some potential mechanisms relating to the latter possibility will be discussed here. A possible mechanism by which antigen presentation specifically to memory T cells is reduced in the lungs of *Ccr2*$^{-/-}$ mice is compromised Fc-receptor-mediated uptake and antigen presentation of immune complex-derived antigens by MNPs. A number of different MNP subsets were significantly reduced in number in the lungs of *Ccr2*$^{-/-}$ mice, but one common theme among the affected cells is the expression of Fc receptors. The expression of Fcγ receptors by monocytes, Mϕ, and inf-cDCs enables these cells to efficiently internalise IgG immune comxplexes (ICs) and either degrade the internalised material, or process it for presentation to T cells *in situ* [90, 150]. In a primary response to influenza infection class-switched IgG antibodies begin to appear at low titres by day 7 post-infection, around the time the virus is cleared from the host, and steadily increase for about one month after which relatively high antibody titers are maintained for life [384, 385]. Due to these kinetics in antibody responses it is probable the contribution of Fc-receptor-dependent antigen-capture and presentation is low in a primary response, but high titres of high-affinity, class-switched, antibodies prior to challenge leads to enhanced Fc-receptor-dependent antigen-capture and presentation to memory T cells. Although the primary target of the B cell response to influenza are surface proteins such as hemagglutinin and neuraminidase, B cells also generate high titers of non-neutralising antibodies against internal viral proteins such as NP and PA [386–388]. Thus, in a heterosubtypic challenge, where the antibodies generated in the primary response no longer efficiently bind surface HA and NA proteins, the contribution of neutralisation by the humoral response is minimal, but not completely absent, as non-neutralising antibodies can still form immune complexes that alter the antigen presenting capacity of MNPs [387, 389]. Internalisation of ICs through Fc-receptors and signalling through the intracellular FcR tripartite motif-containing protein 21 (TRIM21) promotes degradation of internalised antigen and presentation on MHC-I [390]. Additionally, expression of TRIM21 is increased in MNP subsets under inflammatory conditions [391], which likely increases the amount of internalised Ab-complexed antigen that is presented on MHC-I by these cells [390]. T cell proliferation is also much greater when APCs are presenting antibody-bound, rather than soluble, antigen [150, 181, 182]. Thus, it is possible that ICs are captured by inf-cDCs, or monocytes and their derivatives, in the lungs, where these cells then present captured influenza antigen to recently-recruited memory $CD8^+$ T cells to drive their secondary expansion. This concept has been demonstrated in B cell-deficient mice, where transfer of serum from A/HK-x31-immune mice into B cell-deficient A/HK-x31 immune μMT mice prior to A/HK-x31 challenge resulted in greater levels of influenza-specific $CD8^+$ T cell proliferation, indicating that the presence of α-influenza antibodies, and the formation of influenza ICs, can augment expansion of memory T cells. As cDC1s and cDC2s do not express Fc receptors [150], or only express

them at very low levels, these cells likely acquire antigen through phagocytosis, rather than receptor mediated uptake of opsonised antigen, and thus may preferentially migrate to the mLN to present antigen to naïve and memory T cells. In contrast, the newly-recruited inf-cDCs and monocyte-derived cells may be poised to capture ICs at the site of infection and present this antigen to recently-recruited circulating memory cells, and resident memory cells **(Fig. 5.2)**. This potentially represents a previously unappreciated division of labour among APC subsets in the activation of naïve and memory T cells.

It has also been shown that the formation of ICs at late stages of influenza infection is required to program the proliferative potential of some influenza-specific $CD8^+$ memory T cell clones. Léon *et al.* [387] showed that the formation of memory NP-specific $CD8^+$ T cells is normal in mice that are depleted of B cells during primary influenza infection, upon recall, however, memory $CD8^+$ cells from B cell-depleted mice displayed a cell-intrinsic defect in their secondary expansion [387]. This is unlikely to be the underlying cause of reduced T cell proliferation in the present study as the defect in proliferation observed in the present study affected both NP- and PA-specific memory T cells, whereas the mechanism proposed by Léon *et al.* [387] only affected NP-specific T cells. However, this same model of B cell-depletion could be used to assess the contribution of IC-formation and capture to the re-expansion of memory T cells in WT and *Ccr2*$^{-/-}$ mice. Although administration of αCD20 antibodies to WT and *Ccr2*$^{-/-}$ mice to deplete B cells prior to primary A/HK-x31 infection may introduce a pre-programmed defect in NP-specific memory T cell expansion, this would affect both WT and *Ccr2*$^{-/-}$ mice equally. If the defect in memory T cell expansion was due to differences in Fc-receptor-dependent antigen capture, *Ccr2*$^{-/-}$ mice depleted of B cells, and thus ICs, should exhibit memory T cell expansion similar to that of WT mice. This model could be further confirmed by performing transfer of serum from A/HK-x31 immmune mice into B cell-depleted WT and *Ccr2*$^{-/-}$ mice prior to challenge, which would potentially rescue memory T cell expansion in WT, but not *Ccr2*$^{-/-}$ mice. Additionally, Fc common γ chain floxed mice could be generated and used to specifically assess the function of Fc receptors *in vivo*. By crossing these mice to lineage-specific Cre-inducible mice (covered in detail later) and inducing Cre-recombinase expression prior to A/PR8 challenge the effect of Fc receptors on $CD8^+$ T cell priming would be preserved, while still enabling the assessment of Fc-receptors on memory T cell reactivation.

While the experiments outlined above would begin to address the potential mechanism by which antigen-presentation to memory T cells is compromised, they would not provide any information as to which particular MNP subset, or subsets, are responsible for that process. Attempting to separate out the individual contributions of monocytes, monocyte-derived cells, and inf-cDCs to memory $CD8^+$ T cell re-activation in the lungs is difficult, as no reliable *in vivo* methods currently exist to specifically target these subsets [90]. Initial attempts at removing monocytes from mice during challenge utilised the CCR2-DTR mouse, as this is a common model used for monocyte depletion in various infections [108, 124, 131, 162, 301, 332–336]. However, in the present study, the *Ccr2*-DTR mouse was found to not be a viable option for assessing the specific contributions of monocytes to memory T cell responses, as the administration of Dtx caused broad myeloid cell depletion. Thus, in the setting of influenza infection at least, the *Ccr2*-DTR mouse is not a monocyte-specific depletion strategy. Another depletion strategy could be the use of the RB6-8C5 depleting antibody, which targets the Ly6C/Ly6G complex Gr-1 expressed by neutrophils and monocytes, although what overlap this depleting antibody also has with Ly6C-expressing

circulating memory T cells, and inf-cDCs, would first have to be assessed, as this antibody has been reported to partially deplete those cells [392]. Another approach could be the use of clodronate-loaded liposomes which, when delivered IV, deplete the majority of circulating monocytes, but not cDC populations. Additionally, mouse strains could potentially be generated to target specific MNP subsets. By crossing the recently generated *Ms4a3*-Cre mouse, which marks mature peripheral monocytes and granulocytes, but not tissue cDCs [132], with *Rosa*-26-DTR mice [393], the depletion of monocytes, but not inf-cDCs, could be achieved. Currently, there are no reliable depletion strategies or lineage tracing methods that are available that specifically target cDC2s or inf-cDCs to determine their individual contributions during an immune response. However, as inf-cDCs rely on cell-intrinsic IFNα signalling for their development, a potential model to assess their contributions to T cell reactivation would be generation and comparison of cDC-specific *Zbtb46*-Cre *Ifnar1*$^{fl/fl}$ mice to WT mice during influenza challenge. As cDC1 and cDC2 migration is not altered in the absence of CCR2, but migration of inf-cDC2s is, the loss of CCR2 could also potentially be restricted to inf-cDC2s by crossing *Zbtb46*-Cre mice to *Ccr2*$^{fl/fl}$ mice. Similar deletion of *Ccr2* specifically in monocytes could be achieved by crossing the Ms4a3-Cre mouse to *Ccr2*$^{fl/fl}$ mice. An alternative technique to assess interaction of these cells in the infected lungs would be histo-cytometry [394, 395], a method that combines the spatial information provided by immunofluorescence with the phenotypical information provided by flow cytometry. Staining for MNP subsets using the markers CD11c, MHC-II, CD64, F4-80, CD11b, and XCR1 along with T cell markers, and markers of cell proliferation such as Ki67 or BrdU, could be used to determine if proliferating T cells present in the lungs during recall preferentially co-localise with different cDC subsets, or with monocytes and their derivatives. Lastly, transfer approaches could potentially be utilised to reconstitute *Ccr2*$^{-/-}$ mice with WT monocytes or inf-cDC2s during A/PR8 challenge in attempt to rescue the CD8^{+} T cell recall response, though these experiments present technical hurdles, as sorting sufficient cells for transfer is a major challenge. Given further time, several of these approaches would have been explored.

While the mechanisms proposed above outline a defect in influenza-specific T cell proliferation that is a result of extrinsic factors that are altered during challenge, they do not account for a qualitative defect in CD8^{+} memory T cells prior to challenge that could result in decreased proliferation. As previously mentioned, the proliferative potential of memory T cells can be pre-programmed during their initial priming [387]. In a recent study, Low *et al.* [396] demonstrated that the reactivation of memory T cells in the lungs after influenza-challenge can be mediated by a diverse range of professional and non-professional APCs [396]. In that report the authors showed that, in an adoptive transfer model, memory Nur77-GFP OT-I cells, which report TCR signalling, displayed no differences in reporter expression in the lungs after A/PR8 challenge in CD11c-DTR-, XCR1-DTR-, or CD169-DTR-depleted hosts, μMT$^{-/-}$ hosts, or αGr-1-depleted hosts, relative to WT host hosts. In contrast, reporter expression in the mLN during challenge was entirely dependent on the presence of cDCs [396]. Those results results presented by Low *et al.* [396] suggest that in the present study, in the lungs of *Ccr2*$^{-/-}$ mice, the absence of the antigen-presenting capability of monocytes and their derivatives, and inf-cDCs, should be compensated for by other antigen-presenting cells, potentially driving their proliferation. Therefore, another potential cause for the reduction in T cell proliferation in *Ccr2*$^{-/-}$ mice may be a pre-programmed defect in proliferation upon reactivation. This concept of a pre-programmed defect has previously been demonstrated to occour through a number of different mechanisms, but is primarily regulated by T cell interactions with co-stimulatory molecules expressed

by APCs during priming [170, 387]. Co-stimulation of $CD8^+$ T cells by APCs during priming is not required for the initial expansion and formation of memory $CD8^+$ T cells, but does program their proliferative potential upon re-infection [397]. As the number of NP- and PA-specific memory $CD8^+$ T cells in the lungs and spleen of resting memory WT and *Ccr2*$^{-/-}$ mice was equivalent, the proliferative potential of these cells could potentially be assessed through *ex vivo* co-culture of proliferation dye-labeled T cells with NP and PA peptide-pulsed bone marrow dendritic cells (BMDCs). However, given that influenza-specific T cell division in the mLN was equivalent in WT and *Ccr2*$^{-/-}$ mice following challenge, and given that the defect in proliferation in the lungs also affected $CD4^+$ T cells, it is unlikely that this defect is pre-programmed. Another possibility is increased death of memory cells upon reactivation, as $CD8^+$ T cells that are primed by un-licensed cDCs upregulate TNF-related apoptosis-inducing ligand (TRAIL) which regulates activation-induced cell death upon secondary stimulation [398]. An analysis of cell death in influenza-specific memory T cells over the course of A/PR8 challenge would need to be performed to verify this.

It should also be noted that WT and *Ccr2*$^{-/-}$ mice were administered BrdU 20 hours prior to analysis, and the presence of proliferating cells in the lungs may not be entirely due to proliferation *in situ*. It is possible that circulating memory cells were activated, and expanded, in the mLN and the $Brdu^+$ $Ki67^+$ cells present in the lung parenchyma were secondary-effector cells that had exited the mLN and migrated to the lung parenchyma. However, a feature unique to the lungs after infection is the formation of induced bronchus-associated lymphoid tissues (iBALT). These are tertiary lymphoid organs (TLOs) that form in response to pulmonary antigenic stimulation, and have important roles in re-activation of immune cells in both anamnestic and non-anamnestic infections [321, 399, 400]. Using splenectomized, Lt$\alpha^{-/-}$ mice, which lack all SLOs, Moyron-Quiroz *et al.* [321] demonstrated that memory $CD8^+$ T cells can be activated, and proliferate, in iBALT structures during influenza-challenge. It has also been demonstrated that the formation of iBALT relies on the presence of cDCs and, of relevance to the present study, iBALT formation is normal in the lungs of *Ccr2*$^{-/-}$ mice following influenza infection [401]. Additionally, though by day 7 post-A/PR8 challenge there were significant differences in influenza-specific $CD8^+$ T cell numbers in all organs except the BALF, there were already significant reductions in influenza-specific $CD8^+$ T cell numbers in the lungs on day 5 post-challenge, potentially due to the reduced proliferation *in situ*. Together, these observation support the conclusion that T cell proliferation in the lung is compromised in *Ccr2*$^{-/-}$ mice.

5.9 Conclusion

This project has investigated the role of the inflammatory chemokine receptor CCR2 in shaping $CD8^+$ T cell responses to viral infection. The conclusions based on the initial aims are as follows:

- There is no cell-intrinsic role for CCR2 in the generation of $CD8^+$ T cell effector or memory populations, or in the acquisition of effector potential.
- There is no cell-intrinsic requirement for CCR2 in the recruitment of $CD8^+$ T cells into inflamed tissue

during influenza challenge.

- There is a cell-intrinsic requirement for CCR2 in the optimal recruitment of memory OT-I cells during sterile inflammation when peripheral tissue is treated with IL-1α.
- Monocytes and monocyte-derived cells are the main source of the chemokine CCL2 during influenza infection. The absence of these cells, however, has no impact on the generation of endogenous influenza-specific effector or memory populations.
- The optimal expansion of influenza-specific memory $CD8^+$ T cells *in situ* during A/PR8 challenge is compromised in *Ccr2*$^{-/-}$ mice, resulting in increased morbidity and higher viral titres.
- Reduced numbers of inflammatory cDC2s, monocytes, and monocyte derived cells in the lungs of influenza infected *Ccr2*$^{-/-}$ mice may compromise the memory T cell response to PR8 challenge.

The appropriate and efficient reactivation of memory cells is required for optimal protection in the case of re-infection. A model for T cell reactivation following heterosubtypic influenza challenge stemming from this project **(Fig. 5.2)** represents a novel division of labour among APC subsets that may serve to maximise memory T cell expansion, while preserving antigen presentation to naïve T cells. In this model, during A/PR8-challenge, the majority of tissue cDCs acquire antigen, mature, and migrate to the draining mLN to present antigen to lymph node homing naïve and memory T cells. In the lungs, large numbers of MNPs and inf-cDCs are recruited, and these cells phagocytose soluble antigen or acquire it through Fc-receptor-mediated phacocytosis of immune complexes formed by non-neutralising α-influenza antibodies. These cells interact with influenza-specific memory T cells that are resident in the lungs, or have been recently-recruited from the circulation, to drive their proliferation and the secretion of effector cytokines. When the recruitment of MNPs to A/PR8 infected lungs is compromised, as observed in *Ccr2*$^{-/-}$ mice, antigen capture and presentation to memory T cells is reduced in the early stages of challenge. This results in reduced T cell proliferation which leads to sub-optimal expansion of the secondary effector population and a reduction in the overall secretion of effector cytokines. Together, this compromises the anti-viral state established in the lungs, and results in a higher viral burden that takes longer to be cleared. Understanding the processes that regulate the function of memory T cells *in vivo* is critical for a better understanding how immune cells collaborate to curtail infection, and inform the design of vaccines to target the generation of specific memory subsets.

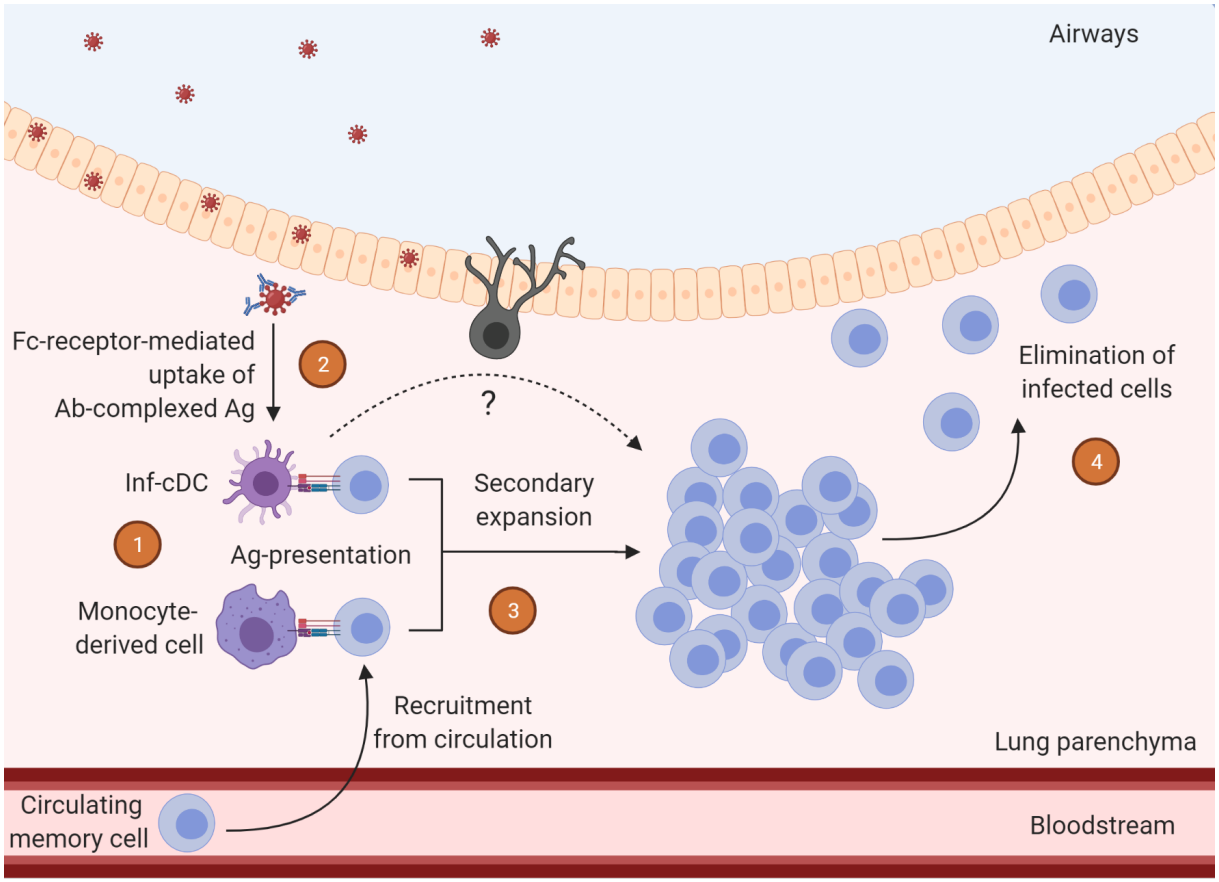

Figure 5.2: Proposed mechanism for memory T cell reactivation *in situ* during influenza challenge

1) During heterosubtypic influenza challenge Fc-receptor-expressing inf-cDCs and monocytes are recruited to the infected tissue. **2)** IgG complexed virus, and lytic cellular contents, are taken up by tissue resident M, monocyte-derived cells, and infcDC2 via Fcγ receptors, and processed for presentation on MHC-I. **3)** Circulating memory T cells arriving in the lungs on day 2-3 post challenge, and potentially resident memory T cells, interact with APCs and initiate their secondary expansion *in situ*. **4)** Secondary effectors clear influenza-infected cells from the lungs which is required for the optimal control of secondary infections. When monocyte-derived cells and inflammatory cDC2s are reduced in numbers in the lungs, as in *Ccr2*$^{-/-}$ mice, antigen-presentation to memory T cells is compromised, reducing the secondary expansion of these cells and impairing viral control.

6 | Appendix

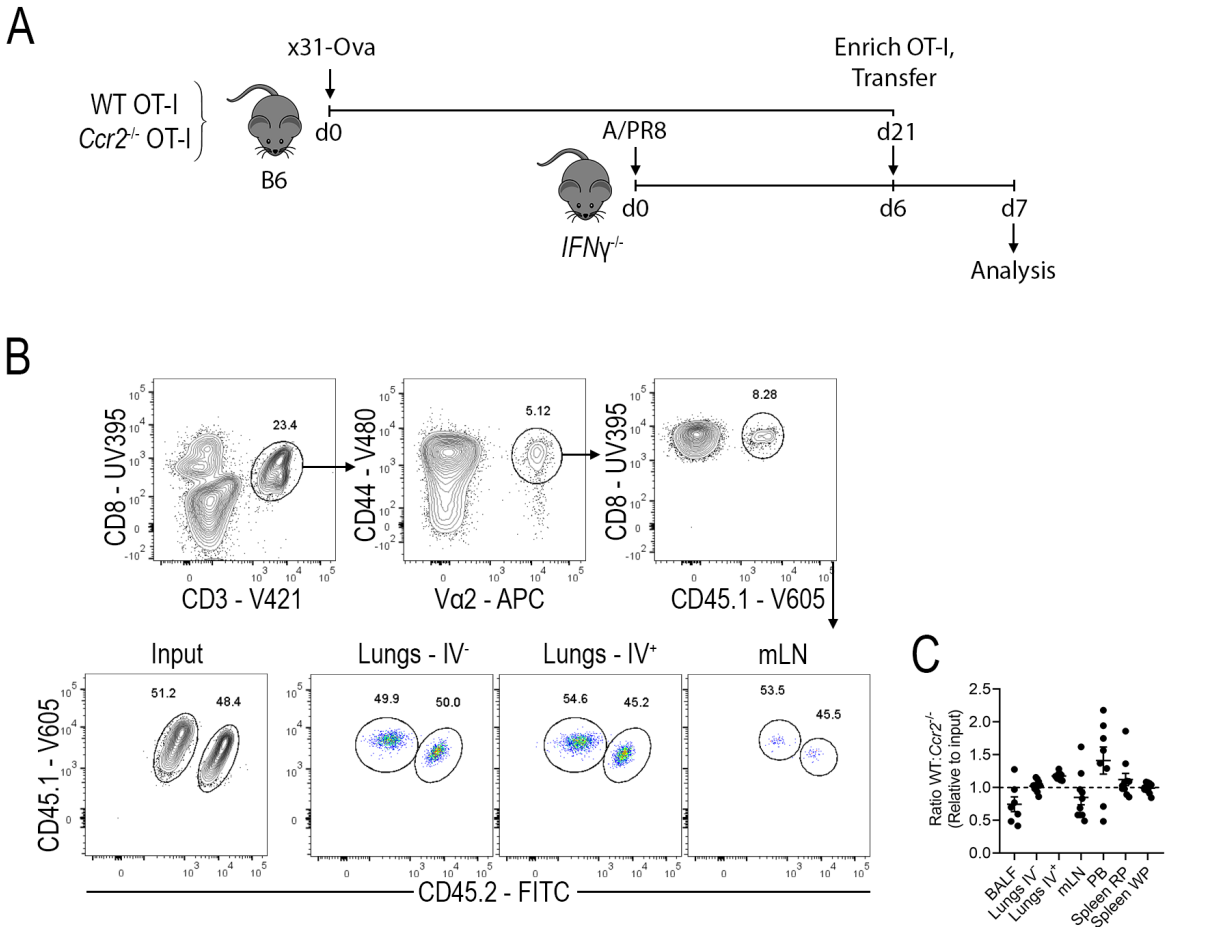

Figure 6.1: Recruitment of Ccr2$^{-/-}$ memory cells into inflamed tissue is unaltered in the absence of CXCR3 ligands

Circulating memory OT-I cells were enriched from spleens of day 21 x31-OVA infected mice and transferred into day 6 A/PR8 infected IFNγ$^{-/-}$ host mice, four hours after transfer the localisation of memory T cells was determined by flow cytometry. **a)** Experimental setup. **b)** Representative flow cytometry for the identification of transferred WT (CD45.1^{+}) and *Ccr2*$^{-/-}$ (CD45.1^{+}, CD45.2^{+}) OT-I cells in IFNγ$^{-/-}$ host mice. **c)** the ratio of recovered WT to *Ccr2*$^{-/-}$ OT-I cells in the indicated tissues, normalised to input. n=10 mice, data pooled from 2 independent experiments. Mean ± SEM.

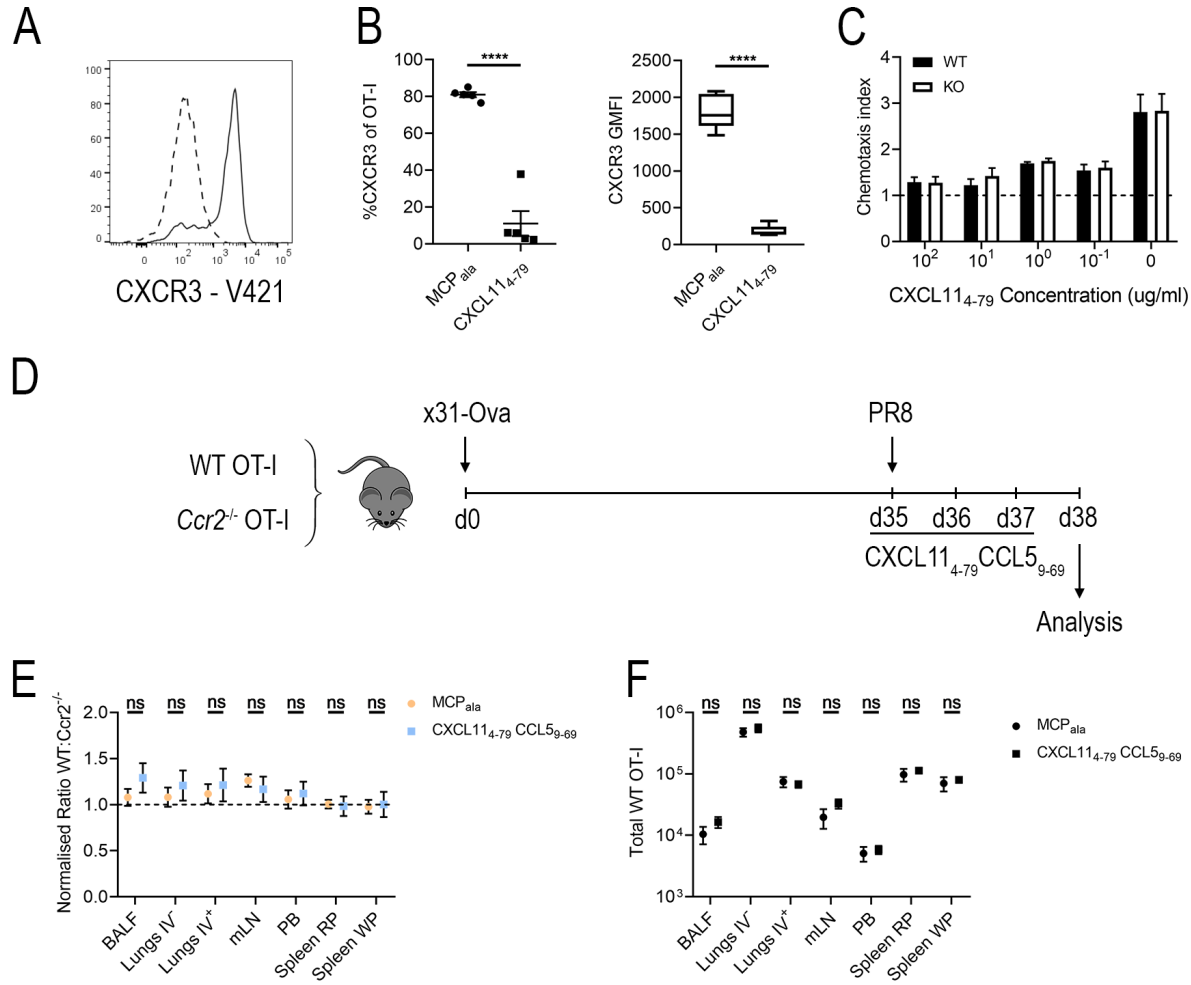

Figure 6.2: Antagonism of CXCR3 and CCR5 does not alter the recall kinetics of WT and *Ccr2*$^{-/-}$ memory OT-I cells

a) Representative flow cytometry of CXCR3 expression on resting memory OT-I cells after 3 hours incubation with the CXCR3 antagonist CXCL11$_{4\text{-}79}$ (dotted histogram) or control peptide (solid histogram). **b)** Percent CXCR3 expressing OT-I cells and CXCR3 gMFI of OT-I cells after 3 hours incubation with CXCL11$_{4\text{-}79}$ or control peptide - MCP$_{ala}$ - at 37degrees. **c)** *in vitro* chemotaxis of WT and *Ccr2*$^{-/-}$ OT-I cells to 1ug/mL functional CXCL11 in the presence of CXCL11$_{4\text{-}79}$. **d)** Experimental plan to assess the *in vivo* migration of WT and *Ccr2*$^{-/-}$ OT-I cells into inflamed tissue in the presence of chemokine receptor antagonists. **e)** Ratio of WT:*Ccr2*$^{-/-}$ OT-I cells recovered from the indicated organs of CXCL11$_{4\text{-}79}$, and CCL5$^{9\text{-}69}$ or MCP$_{ala}$ treated KO OT-I immune mice on day 3 post PR8 challenge, data normalised to MCP^{ala} control group. **f)** Total number of WT OT-I cells recovered from the indicated organs of CXCL11$_{4\text{-}79}$, CCL5$^{9\text{-}69}$ or MCP^{ala} treated mice on day 3 post PR8 challenge. n=10 mice CXCL11$_{4\text{-}79}$, CCL5$^{9\text{-}69}$ n=9 mice MCP$_{ala}$, data pooled from two independent experiments. **b)** students paired *t*-test. **e-f)** One-way ANOVA. Mean ± SEM. **** p≤0.0001.

References

1. Duneau, D. *et al.* Stochastic variation in the initial phase of bacterial infection predicts the probability of survival in D. melanogaster. *Elife* **6** (Oct. 2017).
2. Bromley, S. K., Mempel, T. R. & Luster, A. D. Orchestrating the orchestrators: chemokines in control of T cell traffic. *Nat Immunol* **9,** 970–980 (Sept. 2008).
3. Farsakoglu, Y., McDonald, B. & Kaech, S. M. Motility Matters: How $CD8^+$ T-Cell Trafficking Influences Effector and Memory Cell Differentiation. *Cold Spring Harb Perspect Biol* (May 2021).
4. Rahimi, R. A. & Luster, A. D. Chemokines: Critical Regulators of Memory T Cell Development, Maintenance, and Function. *Adv Immunol* **138,** 71–98 (2018).
5. Griffith, J. W., Sokol, C. L. & Luster, A. D. Chemokines and chemokine receptors: positioning cells for host defense and immunity. *Annu. Rev. Immunol.* **32,** 659–702 (2014).
6. Steen, A., Larsen, O., Thiele, S. & Rosenkilde, M. M. Biased and g protein-independent signaling of chemokine receptors. *Front Immunol* **5,** 277 (2014).
7. Hirsch, E. *et al.* Central role for G protein-coupled phosphoinositide 3-kinase gamma in inflammation. *Science* **287,** 1049–1053 (Feb. 2000).
8. Nelson, C. D. *et al.* Targeting of diacylglycerol degradation to M1 muscarinic receptors by beta-arrestins. *Science* **315,** 663–666 (Feb. 2007).
9. Krupnick, J. G. & Benovic, J. L. The role of receptor kinases and arrestins in G protein-coupled receptor regulation. *Annu. Rev. Pharmacol. Toxicol.* **38,** 289–319 (1998).
10. Goodman, O. B. *et al.* Beta-arrestin acts as a clathrin adaptor in endocytosis of the beta2-adrenergic receptor. *Nature* **383,** 447–450 (Oct. 1996).
11. Beautrait, A. *et al.* A new inhibitor of the β-arrestin/AP2 endocytic complex reveals interplay between GPCR internalization and signalling. *Nat Commun* **8,** 15054 (Apr. 2017).
12. Comerford, I., Litchfield, W., Harata-Lee, Y., Nibbs, R. J. & McColl, S. R. Regulation of chemotactic networks by 'atypical' receptors. *Bioessays* **29,** 237–247 (Mar. 2007).
13. Thiriot, A. *et al.* Differential DARC/ACKR1 expression distinguishes venular from non-venular endothelial cells in murine tissues. *BMC Biol.* **15,** 45 (May 2017).
14. Pruenster, M. *et al.* The Duffy antigen receptor for chemokines transports chemokines and supports their promigratory activity. *Nat Immunol* **10,** 101–108 (Jan. 2009).
15. Baekkevold, E. S. *et al.* The CCR7 ligand elc (CCL19) is transcytosed in high endothelial venules and mediates T cell recruitment. *J. Exp. Med.* **193,** 1105–1112 (May 2001).
16. Palframan, R. T. *et al.* Inflammatory chemokine transport and presentation in HEV: a remote control mechanism for monocyte recruitment to lymph nodes in inflamed tissues. *J. Exp. Med.* **194,** 1361–1373 (Nov. 2001).

17. Park, P. W., Reizes, O. & Bernfield, M. Cell surface heparan sulfate proteoglycans: selective regulators of ligand-receptor encounters. *J. Biol. Chem.* **275,** 29923–29926 (Sept. 2000).

18. Proudfoot, A. E. *et al.* Glycosaminoglycan binding and oligomerization are essential for the in vivo activity of certain chemokines. *Proc Natl Acad Sci* **100,** 1885–1890 (Feb. 2003).

19. Patel, D. D. *et al.* Chemokines have diverse abilities to form solid phase gradients. *Clin. Immunol.* **99,** 43–52 (Apr. 2001).

20. Russo, E. *et al.* Intralymphatic CCL21 Promotes Tissue Egress of Dendritic Cells through Afferent Lymphatic Vessels. *Cell Rep* **14,** 1723–1734 (Feb. 2016).

21. Ulvmar, M. H. *et al.* The atypical chemokine receptor CCRL1 shapes functional CCL21 gradients in lymph nodes. *Nat Immunol* **15,** 623–630 (July 2014).

22. Mionnet, C. *et al.* CX3CR1 is required for airway inflammation by promoting T helper cell survival and maintenance in inflamed lung. *Nat. Med.* **16,** 1305–1312 (Nov. 2010).

23. Borst, O. *et al.* The inflammatory chemokine CXC motif ligand 16 triggers platelet activation and adhesion via CXC motif receptor 6-dependent phosphatidylinositide 3-kinase/Akt signaling. *Circ. Res.* **111,** 1297–1307 (Oct. 2012).

24. Hundhausen, C. *et al.* Regulated shedding of transmembrane chemokines by the disintegrin and metalloproteinase 10 facilitates detachment of adherent leukocytes. *J. Immunol.* **178,** 8064–8072 (June 2007).

25. Tanaka, Y., Adams, D. H. & Shaw, S. Proteoglycans on endothelial cells present adhesion-inducing cytokines to leukocytes. *Immunol. Today* **14,** 111–115 (Mar. 1993).

26. Weninger, W. *et al.* Specialized contributions by alpha(1,3)-fucosyltransferase-IV and FucT-VII during leukocyte rolling in dermal microvessels. *Immunity* **12,** 665–676 (June 2000).

27. Stark, K. *et al.* Capillary and arteriolar pericytes attract innate leukocytes exiting through venules and 'instruct' them with pattern-recognition and motility programs. *Nat Immunol* **14,** 41–51 (Jan. 2013).

28. Nourshargh, S. & Alon, R. Leukocyte migration into inflamed tissues. *Immunity* **41,** 694–707 (Nov. 2014).

29. McEver, R. P. Selectins: lectins that initiate cell adhesion under flow. *Curr. Opin. Cell Biol.* **14,** 581–586 (Oct. 2002).

30. Nolz, J. C. & Harty, J. T. IL-15 regulates memory $CD8^+$ T cell O-glycan synthesis and affects trafficking. *J. Clin. Invest.* **124,** 1013–1026 (Mar. 2014).

31. Pober, J. S. & Sessa, W. C. Evolving functions of endothelial cells in inflammation. *Nat. Rev. Immunol.* **7,** 803–815 (Oct. 2007).

32. Cinamon, G., Shinder, V., Shamri, R. & Alon, R. Chemoattractant signals and beta 2 integrin occupancy at apical endothelial contacts combine with shear stress signals to promote transendothelial neutrophil migration. *J. Immunol.* **173,** 7282–7291 (Dec. 2004).

33. Shulman, Z. *et al.* Lymphocyte crawling and transendothelial migration require chemokine triggering of high-affinity LFA-1 integrin. *Immunity* **30,** 384–396 (Mar. 2009).

34. Shulman, Z. *et al.* Transendothelial migration of lymphocytes mediated by intraendothelial vesicle stores rather than by extracellular chemokine depots. *Nat Immunol* **13,** 67–76 (Dec. 2011).

35. Abtin, A. *et al.* Perivascular macrophages mediate neutrophil recruitment during bacterial skin infection. *Nat Immunol* **15,** 45–53 (2014).

36. Badovinac, V. P., Haring, J. S. & Harty, J. T. Initial T cell receptor transgenic cell precursor frequency dictates critical aspects of the $CD8^+$ T cell response to infection. *Immunity* **26,** 827–841 (June 2007).

37. Jenkins, M. K. & Moon, J. J. The role of naive T cell precursor frequency and recruitment in dictating immune response magnitude. *J. Immunol.* **188,** 4135–4140 (May 2012).

38. Warnock, R. A., Askari, S., Butcher, E. C. & von Andrian, U. H. Molecular mechanisms of lymphocyte homing to peripheral lymph nodes. *J. Exp. Med.* **187,** 205–216 (Jan. 1998).

39. Eickhoff, S. *et al.* Robust Anti-viral Immunity Requires Multiple Distinct T Cell-Dendritic Cell Interactions. *Cell* **162,** 1322–37 (2015).

40. Girard, J. P., Moussion, C. & Förster, R. HEVs, lymphatics and homeostatic immune cell trafficking in lymph nodes. *Nat Rev Immunol* **12,** 762–773 (Nov. 2012).

41. Bajenoff, M. *et al.* Stromal cell networks regulate lymphocyte entry, migration, and territoriality in lymph nodes. *Immunity* **25,** 989–1001 (Dec. 2006).

42. Malhotra, D. *et al.* Transcriptional profiling of stroma from inflamed and resting lymph nodes defines immunological hallmarks. *Nat Immunol* **13,** 499–510 (2012).

43. Chauveau, A. *et al.* Visualization of T Cell Migration in the Spleen Reveals a Network of Perivascular Pathways that Guide Entry into T Zones. *Immunity* **52,** 794–807 (May 2020).

44. Beltman, J. B., Marée, A. F., Lynch, J. N., Miller, M. J. & de Boer, R. J. Lymph node topology dictates T cell migration behavior. *J. Exp. Med.* **204,** 771–780 (Apr. 2007).

45. Lo, C. G., Xu, Y., Proia, R. L. & Cyster, J. G. Cyclical modulation of sphingosine-1-phosphate receptor 1 surface expression during lymphocyte recirculation and relationship to lymphoid organ transit. *J Exp Med* **201,** 291–301 (2005).

46. Matloubian, M. *et al.* Lymphocyte egress from thymus and peripheral lymphoid organs is dependent on S1P receptor 1. *Nature* **427,** 355–360 (Jan. 2004).

47. Tomura, M. *et al.* Monitoring cellular movement in vivo with photoconvertible fluorescence protein "Kaede" transgenic mice. *Proc Natl Acad Sci* **105,** 10871–10876 (Aug. 2008).

48. Mandl, J. N. *et al.* Quantification of lymph node transit times reveals differences in antigen surveillance strategies of naive $CD4^+$ and $CD8^+$ T cells. *Proc Natl Acad Sci* **109,** 18036–18041 (Oct. 2012).

49. Shiow, L. R. *et al.* CD69 acts downstream of interferon-alpha/beta to inhibit S1P1 and lymphocyte egress from lymphoid organs. *Nature* **440,** 540–544 (Mar. 2006).

50. De Filippo, K. *et al.* Mast cell and macrophage chemokines CXCL1/CXCL2 control the early stage of neutrophil recruitment during tissue inflammation. *Blood* **121,** 4930–4937 (June 2013).

51. Evavold, C. L. & Kagan, J. C. Inflammasomes: Threat-Assessment Organelles of the Innate Immune System. *Immunity* **51,** 609–624 (Oct. 2019).

52. Kagnoff, M. F. & Eckmann, L. Epithelial cells as sensors for microbial infection. *J. Clin. Invest.* **100,** 6–10 (July 1997).

53. Chou, R. C. *et al.* Lipid-cytokine-chemokine cascade drives neutrophil recruitment in a murine model of inflammatory arthritis. *Immunity* **33,** 266–278 (Aug. 2010).

54. Murphy, J. E., Robert, C. & Kupper, T. S. Interleukin-1 and cutaneous inflammation: a crucial link between innate and acquired immunity. *J. Invest. Dermatol.* **114,** 602–608 (Mar. 2000).

55. Collins, N. *et al.* Skin $CD4^+$ memory T cells exhibit combined cluster-mediated retention and equilibration with the circulation. *Nat Commun* **7,** 11514 (May 2016).

56. Hickman, H. D. *et al.* CXCR3 chemokine receptor enables local $CD8^+$ T cell migration for the destruction of virus-infected cells. *Immunity* **42,** 524–37 (2015).

57. Girbl, T. *et al.* Distinct Compartmentalization of the Chemokines CXCL1 and CXCL2 and the Atypical Receptor ACKR1 Determine Discrete Stages of Neutrophil Diapedesis. *Immunity* **49,** 1062–1076 (Dec. 2018).

58. Mikhak, Z., Strassner, J. P. & Luster, A. D. Lung dendritic cells imprint T cell lung homing and promote lung immunity through the chemokine receptor CCR4. *J Exp Med* **210,** 1855–1869 (Aug. 2013).

59. Srivastava, R. *et al.* CXCL10/CXCR3-Dependent Mobilization of Herpes Simplex Virus-Specific $CD8^+$ TEM and $CD8^+$ TRM Cells within Infected Tissues Allows Efficient Protection against Recurrent Herpesvirus Infection and Disease. *J Virol* **91** (July 2017).

60. Shin, H. & Iwasaki, A. A vaccine strategy that protects against genital herpes by establishing local memory T cells. *Nature* **491,** 463–467 (2012).

61. Xu, J. *et al.* Chemokine receptor CXCR3 is required for lethal brain pathology but not pathogen clearance during cryptococcal meningoencephalitis. *Science Advances* **6** (2020).

62. Klein, R. S. *et al.* Neuronal CXCL10 Directs CD8 T-Cell Recruitment and Control of West Nile Virus Encephalitis. *Journal of Virology* **79,** 11457–11466 (2005).

63. Campanella, G. S. V. *et al.* Chemokine receptor CXCR3 and its ligands CXCL9 and CXCL10 are required for the development of murine cerebral malaria. *Proc Natl Acad Sci* **105,** 4814–4819 (2008).

64. Lindell, D. M., Lane, T. E. & Lukacs, N. W. CXCL10/CXCR3-mediated responses promote immunity to respiratory syncytial virus infection by augmenting dendritic cell and CD8 T cell efficacy. *European Journal of Immunology* **38,** 2168–2179 (2008).

65. Kohlmeier, J. E. *et al.* CXCR3 directs antigen-specific effector $CD4^+$ T cell migration to the lung during parainfluenza virus infection. *J Immunol* **183,** 4378–84 (2009).

66. Ariotti, S. *et al.* Subtle CXCR3-Dependent Chemotaxis of CTLs within Infected Tissue Allows Efficient Target Localization. *The Journal of Immunology* **195,** 5285–5295 (2015).

67. Chow, M. T. *et al.* Intratumoral Activity of the CXCR3 Chemokine System Is Required for the Efficacy of Anti-PD-1 Therapy. *Immunity* **50,** 1498–1512 (June 2019).

68. Johansson-Lindbom, B. *et al.* Selective generation of gut tropic T cells in gut-associated lymphoid tissue (GALT): requirement for GALT dendritic cells and adjuvant. *J. Exp. Med.* **198,** 963–969 (Sept. 2003).

69. Stenstad, H. *et al.* Gut-associated lymphoid tissue-primed $CD4^+$ T cells display CCR9-dependent and -independent homing to the small intestine. *Blood* **107,** 3447–3454 (May 2006).

70. Morales, J. *et al.* CTACK, a skin-associated chemokine that preferentially attracts skin-homing memory T cells. *Proc Natl Acad Sci* **96,** 14470–14475 (Dec. 1999).

71. Homey, B. *et al.* CCL27-CCR10 interactions regulate T cell-mediated skin inflammation. *Nat. Med.* **8,** 157–165 (Feb. 2002).

72. Matsuzaki, G., Yamasaki, M., Tamura, T. & Umemura, M. Dispensable role of chemokine receptors in migration of mycobacterial antigen-specific CD4 T cells into Mycobacterium-infected lung. *Immunobiology* **224,** 440–448 (2019).

73. Hoft, S. G. *et al.* The Rate of CD4 T Cell Entry into the Lungs during Mycobacterium tuberculosis Infection Is Determined by Partial and Opposing Effects of Multiple Chemokine Receptors. *Infection and Immunity* **87** (2019).

74. Dyer, D. P. *et al.* Chemokine Receptor Redundancy and Specificity Are Context Dependent. *Immunity* **50,** 378–389 (Feb. 2019).

75. Slutter, B., Pewe, L. L., Kaech, S. M. & Harty, J. T. Lung airway-surveilling CXCR3(hi) memory $CD8^+$ T cells are critical for protection against influenza A virus. *Immunity* **39,** 939–48 (2013).

76. Kohlmeier, J. E. *et al.* The chemokine receptor CCR5 plays a key role in the early memory $CD8^+$ T cell response to respiratory virus infections. *Immunity* **29,** 101–13 (2008).

77. Wein, A. N. *et al.* CXCR6 regulates localization of tissue-resident memory CD8 T cells to the airways. *J. Exp. Med.* **216,** 2748–2762 (Dec. 2019).

78. Mackay, L. K. *et al.* The developmental pathway for $CD103^+CD8^+$ tissue-resident memory T cells of skin. *Nat Immunol* **14,** 1294–301 (2013).

79. Iijima, N. & Iwasaki, A. A local macrophage chemokine network sustains protective tissue-resident memory CD4 T cells. *Science* **346,** 93–98 (2014).

80. Wakim, L. M., Woodward-Davis, A. & Bevan, M. J. Memory T cells persisting within the brain after local infection show functional adaptations to their tissue of residence. *Proc Natl Acad Sci* **107,** 17872–17879 (Oct. 2010).

81. Bergsbaken, T. & Bevan, M. J. Proinflammatory microenvironments within the intestine regulate the differentiation of tissue-resident $CD8^+$ T cells responding to infection. *Nat Immunol* **16,** 406–414 (Apr. 2015).

82. Natsuaki, Y. *et al.* Perivascular leukocyte clusters are essential for efficient activation of effector T cells in the skin. *Nat Immunol* **15,** 1064–1069 (Nov. 2014).

83. Harris, T. H. *et al.* Generalized Lévy walks and the role of chemokines in migration of effector $CD8^+$ T cells. *Nature* **486,** 545–548 (June 2012).

84. Guilliams, M. *et al.* Dendritic cells, monocytes and macrophages: a unified nomenclature based on ontogeny. *Nat Rev Immunol* **14,** 571–8 (2014).

85. Van Furth, R. *et al.* The mononuclear phagocyte system: a new classification of macrophages, monocytes, and their precursor cells. *Bull World Health Organ* **46,** 845–852 (1972).

86. Van Furth, R. & Cohn, Z. A. The origin and kinetics of mononuclear phagocytes. *J Exp Med* **128,** 415–435 (Sept. 1968).

87. Yona, S. *et al.* Fate mapping reveals origins and dynamics of monocytes and tissue macrophages under homeostasis. *Immunity* **38,** 79–91 (2013).

88. Jakubzick, C. *et al.* Minimal differentiation of classical monocytes as they survey steady-state tissues and transport antigen to lymph nodes. *Immunity* **39,** 599–610 (2013).

89. Guilliams, M. *et al.* Unsupervised High-Dimensional Analysis Aligns Dendritic Cells across Tissues and Species. *Immunity* **45,** 669–684 (2016).

90. Bosteels, C. *et al.* Inflammatory Type 2 cDCs Acquire Features of cDC1s and Macrophages to Orchestrate Immunity to Respiratory Virus Infection. *Immunity* **52** (2020).

91. Gomez Perdiguero, E. *et al.* Tissue-resident macrophages originate from yolk-sac-derived erythro-myeloid progenitors. *Nature* **518,** 547–51 (2015).

92. Groom, J. R. & Luster, A. D. $C\text{-}Myb^+$ Erythro-Myeloid Progenitor-Derived Fetal Monocytes Give Rise to Adult Tissue-Resident Macrophages. *Immunol. Cell Biol.* **89,** 207–215 (Feb. 2011).

93. Sheng, J., Ruedl, C. & Karjalainen, K. Most Tissue-Resident Macrophages Except Microglia Are Derived from Fetal Hematopoietic Stem Cells. *Immunity* **43,** 382–393 (Aug. 2015).

94. T'Jonck, W., Guilliams, M. & Bonnardel, J. Niche signals and transcription factors involved in tissue-resident macrophage development. *Cell. Immunol.* **330,** 43–53 (Aug. 2018).

95. Bain, C. C. & Mowat, A. M. The monocyte-macrophage axis in the intestine. *Cell Immunol* **291,** 41–48 (2014).

96. Aegerter, H. *et al.* Influenza-induced monocyte-derived alveolar macrophages confer prolonged antibacterial protection. *Nat Immunol* **21,** 145–157 (Feb. 2020).

97. Mondor, I. *et al.* Lymphatic Endothelial Cells Are Essential Components of the Subcapsular Sinus Macrophage Niche. *Immunity* **50,** 1453–1466 (June 2019).

98. Ajami, B., Bennett, J. L., Krieger, C., McNagny, K. M. & Rossi, F. M. Infiltrating monocytes trigger EAE progression, but do not contribute to the resident microglia pool. *Nat. Neurosci.* **14,** 1142–1149 (July 2011).

99. Holt, P. G., Strickland, D. H., Wikstrom, M. E. & Jahnsen, F. L. Regulation of immunological homeostasis in the respiratory tract. *Nat Rev Immunol* **8,** 142–52 (2008).

100. Okabe, Y. & Medzhitov, R. Tissue biology perspective on macrophages. *Nat Immunol* **17,** 9–17 (Jan. 2016).

101. Hetzel, M. *et al.* Effective hematopoietic stem cell-based gene therapy in a murine model of hereditary pulmonary alveolar proteinosis. *Haematologica* **105,** 1147–1157 (Apr. 2020).

102. Neupane, A. S. *et al.* Patrolling Alveolar Macrophages Conceal Bacteria from the Immune System to Maintain Homeostasis. *Cell* (Aug. 2020).

103. Hickman, H. D. *et al.* Chemokines control naive $CD8^+$ T cell selection of optimal lymph node antigen presenting cells. *J. Exp. Med.* **208,** 2511–2524 (Nov. 2011).

104. Bernhard, C. A., Ried, C., Kochanek, S. & Brocker, T. $CD169^+$ macrophages are sufficient for priming of CTLs with specificities left out by cross-priming dendritic cells. *Proc Natl Acad Sci* **112,** 5461–5466 (Apr. 2015).

105. Reynoso, G. V. *et al.* Lymph node conduits transport virions for rapid T cell activation. *Nat Immunol* **20,** 602–612 (May 2019).

106. Calverley, M., Erickson, S., Read, A. J. & Harmsen, A. G. Resident alveolar macrophages are susceptible to and permissive of Coxiella burnetii infection. *PLoS One* **7,** e51941 (2012).

107. Nikitina, E., Larionova, I., Choinzonov, E. & Kzhyshkowska, J. Monocytes and Macrophages as Viral Targets and Reservoirs. *Int J Mol Sci* **19** (Sept. 2018).

108. Bergsbaken, T., Bevan, M. J. & Fink, P. J. Local Inflammatory Cues Regulate Differentiation and Persistence of $CD8^+$ Tissue-Resident Memory T Cells. *Cell Rep* **19,** 114–124 (Apr. 2017).

109. Hettinger, J. *et al.* Origin of monocytes and macrophages in a committed progenitor. *Nat Immunol* **14,** 821–830 (Aug. 2013).

110. Cabeza-Cabrerizo, M., Cardoso, A., Minutti, C. M., Pereira da Costa, M. & Reis E Sousa, C. Dendritic Cells Revisited. *Annu Rev Immunol* (Jan. 2021).

111. Hashimoto, D., Miller, J. & Merad, M. Dendritic cell and macrophage heterogeneity in vivo. *Immunity* **35,** 323–335 (Sept. 2011).

112. Guilliams, M. *et al.* Alveolar macrophages develop from fetal monocytes that differentiate into long-lived cells in the first week of life via GM-CSF. *J Exp Med* **210,** 1977–92 (2013).

113. Ginhoux, F. *et al.* Fate mapping analysis reveals that adult microglia derive from primitive macrophages. *Science* **330,** 841–845 (Nov. 2010).

114. Geissmann, F., Jung, S. & Littman, D. R. Blood monocytes consist of two principal subsets with distinct migratory properties. *Immunity* **19,** 71–82 (2003).

115. Auffray, C. *et al.* Monitoring of blood vessels and tissues by a population of monocytes with patrolling behavior. *Science* **317,** 666–670 (Aug. 2007).

116. Menezes, S. *et al.* The Heterogeneity of Ly6C(hi) Monocytes Controls Their Differentiation into $iNOS^+$ Macrophages or Monocyte-Derived Dendritic Cells. *Immunity* **45,** 1205–1218 (2016).

117. Patel, D. F. *et al.* Neutrophils restrain allergic airway inflammation by limiting ILC2 function and monocyte-dendritic cell antigen presentation. *Sci Immunol* **4** (2019).

118. Desai, P., Tahiliani, V., Stanfield, J., Abboud, G. & Salek-Ardakani, S. Inflammatory monocytes contribute to the persistence of CXCR3hi CX3CR1lo circulating and lung-resident memory $CD8^+$ T cells following respiratory virus infection. *Immunol. Cell Biol.* **96,** 370–378 (Apr. 2018).

119. Lin, K. L., Suzuki, Y., Nakano, H., Ramsburg, E. & Gunn, M. D. CCR2$^+$ Monocyte-Derived Dendritic Cells and Exudate Macrophages Produce Influenza-Induced Pulmonary Immune Pathology and Mortality. *The Journal of Immunology* **180,** 2562–2572 (2008).

120. Aldridge J. R., J. *et al.* TNF/iNOS-producing dendritic cells are the necessary evil of lethal influenza virus infection. *Proc Natl Acad Sci* **106,** 5306–11 (2009).

121. Swirski, F. K. *et al.* Identification of splenic reservoir monocytes and their deployment to inflammatory sites. *Science* **325,** 612–6 (2009).

122. Serbina, N. V. & Pamer, E. G. Monocyte emigration from bone marrow during bacterial infection requires signals mediated by chemokine receptor CCR2. *Nat Immunol* **7,** 311–317 (Mar. 2006).

123. Xiong, H. *et al.* Innate Lymphocyte/Ly6C(hi) Monocyte Crosstalk Promotes Klebsiella Pneumoniae Clearance. *Cell* **165,** 679–689 (Apr. 2016).

124. Soudja, S. M., Ruiz, A. L., Marie, J. C. & Lauvau, G. Inflammatory monocytes activate memory CD8$^+$ T and innate NK lymphocytes independent of cognate antigen during microbial pathogen invasion. *Immunity* **37,** 549–62 (2012).

125. Kim, Y. G. *et al.* The Nod2 sensor promotes intestinal pathogen eradication via the chemokine CCL2-dependent recruitment of inflammatory monocytes. *Immunity* **34,** 769–780 (May 2011).

126. Ngo, L. Y. *et al.* Inflammatory monocytes mediate early and organ-specific innate defense during systemic candidiasis. *J. Infect. Dis.* **209,** 109–119 (Jan. 2014).

127. Domínguez-Andrés, J. *et al.* Inflammatory Ly6Chigh Monocytes Protect against Candidiasis through IL-15-Driven NK Cell/Neutrophil Activation. *Immunity* **46,** 1059–1072 (June 2017).

128. Iijima, N., Mattei, L. M. & Iwasaki, A. Recruited inflammatory monocytes stimulate antiviral Th1 immunity in infected tissue. *Proc Natl Acad Sci* **108,** 284–289 (Jan. 2011).

129. Maurice, N. J., McElrath, M. J., Andersen-Nissen, E., Frahm, N. & Prlic, M. CXCR3 enables recruitment and site-specific bystander activation of memory CD8$^+$ T cells. *Nat Commun* **10,** 4987 (Nov. 2019).

130. Kang, S. J., Liang, H. E., Reizis, B. & Locksley, R. M. Regulation of hierarchical clustering and activation of innate immune cells by dendritic cells. *Immunity* **29,** 819–33 (2008).

131. Leal, J. M. *et al.* Innate cell microenvironments in lymph nodes shape the generation of T cell responses during type I inflammation. *Sci Immunol* **6** (Feb. 2021).

132. Liu, X. *et al.* Cell-Type-Specific Interleukin 1 Receptor 1 Signaling in the Brain Regulates Distinct Neuroimmune Activities. *Immunity* **50,** 317–333 (Feb. 2019).

133. Dasoveanu, D. C. *et al.* Lymph node stromal CCL2 limits antibody responses. *Sci Immunol* **5** (Mar. 2020).

134. Sammicheli, S. *et al.* Inflammatory monocytes hinder antiviral B cell responses. *Sci Immunol* **1** (Oct. 2016).

135. Hohl, T. M. *et al.* Inflammatory monocytes facilitate adaptive CD4 T cell responses during respiratory fungal infection. *Cell Host Microbe* **6,** 470–481 (Nov. 2009).

136. Plantinga, M. *et al.* Conventional and monocyte-derived CD11b$^+$ dendritic cells initiate and maintain T helper 2 cell-mediated immunity to house dust mite allergen. *Immunity* **38,** 322–335 (Feb. 2013).

137. León, B., Lopez-Bravo, M. & Ardavin, C. Monocyte-derived dendritic cells formed at the infection site control the induction of protective T helper 1 responses against Leishmania. *Immunity* **26,** 519–531 (Apr. 2007).

138. Wu, X. *et al.* Mafb lineage tracing to distinguish macrophages from other immune lineages reveals dual identity of Langerhans cells. *J Exp Med* **213,** 2553–2565 (Nov. 2016).

139. Nakano, H. *et al.* Migratory properties of pulmonary dendritic cells are determined by their developmental lineage. *Mucosal Immunol* **6,** 678–691 (July 2013).

140. Mesnil, C. *et al.* Resident CD11b$^+$Ly6C(-) lung dendritic cells are responsible for allergic airway sensitization to house dust mite in mice. *PLoS One* **7,** e53242 (2012).

141. Langlet, C. *et al.* CD64 expression distinguishes monocyte-derived and conventional dendritic cells and reveals their distinct role during intramuscular immunization. *J Immunol* **188,** 1751–1760 (Feb. 2012).

142. Wakim, L. M. & Bevan, M. J. Cross-dressed dendritic cells drive memory CD8$^+$ T-cell activation after viral infection. *Nature* **471,** 629–632 (Mar. 2011).

143. Tamoutounour, S. *et al.* Origins and functional specialization of macrophages and of conventional and monocyte-derived dendritic cells in mouse skin. *Immunity* **39,** 925–938 (Nov. 2013).

144. Kamphorst, A. O., Guermonprez, P., Dudziak, D. & Nussenzweig, M. C. Route of antigen uptake differentially impacts presentation by dendritic cells and activated monocytes. *J. Immunol.* **185,** 3426–3435 (Sept. 2010).

145. Larson, S. R. *et al.* Ly6C$^+$ monocyte efferocytosis and cross-presentation of cell-associated antigens. *Cell Death Differ.* **23,** 997–1003 (June 2016).

146. Samstein, M. *et al.* Essential yet limited role for CCR2$^+$ inflammatory monocytes during Mycobacterium tuberculosis-specific T cell priming. *Elife* **2,** e01086 (Nov. 2013).

147. Tacke, F. *et al.* Immature monocytes acquire antigens from other cells in the bone marrow and present them to T cells after maturing in the periphery. *J Exp Med* **203,** 583–97 (2006).

148. Cheong, C. *et al.* Microbial stimulation fully differentiates monocytes to DC-SIGN/CD209$^+$ dendritic cells for immune T cell areas. *Cell* **143,** 416–429 (Oct. 2010).

149. Flores-Langarica, A. *et al.* T-zone localized monocyte-derived dendritic cells promote Th1 priming to Salmonella. *Eur. J. Immunol.* **41,** 2654–2665 (Sept. 2011).

150. Guilliams, M., Bruhns, P., Saeys, Y., Hammad, H. & Lambrecht, B. N. The function of Fc receptors in dendritic cells and macrophages. *Nat Rev Immunol* **14,** 94–108 (Feb. 2014).

151. Wang, K. C., Chu, K. L., Batista, N. V. & Watts, T. H. Conserved and Differential Features of TNF Superfamily Ligand Expression on APC Subsets over the Course of a Chronic Viral Infection in Mice. *Immunohorizons* **2,** 407–417 (Dec. 2018).

152. Heijnen, I. A. *et al.* Antigen targeting to myeloid-specific human Fc gamma RI/CD64 triggers enhanced antibody responses in transgenic mice. *J Clin Invest* **97,** 331–338 (Jan. 1996).

153. Den Haan, J. M. & Bevan, M. J. Constitutive versus activation-dependent cross-presentation of immune complexes by CD8$^+$ and CD8(-) dendritic cells in vivo. *J Exp Med* **196,** 817–827 (Sept. 2002).

154. Akiyama, K. *et al.* Targeting apoptotic tumor cells to Fc gamma R provides efficient and versatile vaccination against tumors by dendritic cells. *J Immunol* **170,** 1641–1648 (Feb. 2003).

155. Brewitz, A. *et al.* CD8 T Cells Orchestrate pDC-XCR1 Dendritic Cell Spatial and Functional Cooperativity to Optimize Priming. *Immunity* **46,** 205–219 (2017).

156. Swiecki, M., Gilfillan, S., Vermi, W., Wang, Y. & Colonna, M. Plasmacytoid dendritic cell ablation impacts early interferon responses and antiviral NK and CD8$^+$ T cell accrual. *Immunity* **33,** 955–966 (Dec. 2010).

157. Hildner, K. *et al.* Batf3 Deficiency Reveals a Critical Role for CD8 Dendritic Cells in Cytotoxic T Cell Immunity. *Science* **322,** 1097–1100 (2008).

158. Yamazaki, C. *et al.* Critical Roles of a Dendritic Cell Subset Expressing a Chemokine Receptor, XCR1. *The Journal of Immunology* **190,** 6071–6082 (2013).

159. Zhang, J. G. *et al.* The dendritic cell receptor Clec9A binds damaged cells via exposed actin filaments. *Immunity* **36,** 646–57 (2012).

160. Desch, A. N. *et al.* CD103$^+$ pulmonary dendritic cells preferentially acquire and present apoptotic cell-associated antigen. *J. Exp. Med.* **208,** 1789–1797 (Aug. 2011).

161. Canton, J. *et al.* The receptor DNGR-1 signals for phagosomal rupture to promote cross-presentation of dead-cell-associated antigens. *Nat Immunol* **22,** 140–153 (Feb. 2021).

162. Shah, S., Grotenbreg, G. M., Rivera, A. & Yap, G. S. An extrafollicular pathway for the generation of effector CD8 T cells driven by the proinflammatory cytokine, IL-12. *eLife* **4** (2015).

163. Gatto, D. *et al.* The chemotactic receptor EBI2 regulates the homeostasis, localization and immunological function of splenic dendritic cells. *Nat Immunol* **14,** 446–453 (May 2013).

164. Smith, C. M. *et al.* Cognate CD4$^+$ T cell licensing of dendritic cells in CD8$^+$ T cell immunity. *Nat Immunol* **5,** 1143–1148 (Nov. 2004).

165. Hor, J. L. *et al.* Spatiotemporally Distinct Interactions with Dendritic Cell Subsets Facilitates CD4$^+$ and CD8$^+$ T Cell Activation to Localized Viral Infection. *Immunity* **43,** 554–65 (2015).

166. Hernandez, M. G., Shen, L. & Rock, K. L. CD40-CD40 ligand interaction between dendritic cells and CD8$^+$ T cells is needed to stimulate maximal T cell responses in the absence of CD4$^+$ T cell help. *J. Immunol.* **178,** 2844–2852 (Mar. 2007).

167. Bennett, S. R. *et al.* Help for cytotoxic-T-cell responses is mediated by CD40 signalling. *Nature* **393,** 478–480 (June 1998).

168. Heipertz, E. L., Davies, M. L., Lin, E. & Norbury, C. C. Prolonged antigen presentation following an acute virus infection requires direct and then cross-presentation. *J Immunol* **193,** 4169–77 (2014).

169. Belz, G. T., Bedoui, S., Kupresanin, F., Carbone, F. R. & Heath, W. R. Minimal activation of memory CD8$^+$ T cell by tissue-derived dendritic cells favors the stimulation of naive CD8$^+$ T cells. *Nat Immunol* **8,** 1060–6 (2007).

170. Ballesteros-Tato, A., Leon, B., Lee, B. O., Lund, F. E. & Randall, T. D. Epitope-specific regulation of memory programming by differential duration of antigen presentation to influenza-specific CD8$^+$ T cells. *Immunity* **41,** 127–40 (2014).

171. Giovanni, M. D. *et al.* Spatiotemporal regulation of type I interferon expression determines the antiviral polarization of CD4 T cells. *Nat Immunol* **21,** 321–330 (2020).

172. Kitano, M. *et al.* Imaging of the cross-presenting dendritic cell subsets in the skin-draining lymph node. *Proc Natl Acad Sci* **113,** 1044–1049 (2016).

173. Tamoutounour, S. *et al.* CD64 distinguishes macrophages from dendritic cells in the gut and reveals the Th1-inducing role of mesenteric lymph node macrophages during colitis. *European Journal of Immunology* (2012).

174. Bourdely, P. *et al.* Transcriptional and Functional Analysis of CD1c$^+$ Human Dendritic Cells Identifies a CD163$^+$ Subset Priming CD8$^+$CD103$^+$ T Cells. *Immunity* **53,** 335–352 (Aug. 2020).

175. Villani, A. C. *et al.* Single-cell RNA-seq reveals new types of human blood dendritic cells, monocytes, and progenitors. *Science* **356** (Apr. 2017).

176. Alcántara-Hernández, M. *et al.* High-Dimensional Phenotypic Mapping of Human Dendritic Cells Reveals Interindividual Variation and Tissue Specialization. *Immunity* **47,** 1037–1050 (Dec. 2017).

177. Dutertre, C. A. *et al.* Single-Cell Analysis of Human Mononuclear Phagocytes Reveals Subset-Defining Markers and Identifies Circulating Inflammatory Dendritic Cells. *Immunity* **51,** 573–589 (Sept. 2019).

178. Girard, M., Law, J. C., Edilova, M. I. & Watts, T. H. Type I interferons drive the maturation of human DC3s with a distinct costimulatory profile characterized by high GITRL. *Sci Immunol* **5** (Nov. 2020).

179. Bedford, J. G. *et al.* Unresponsiveness to inhaled antigen is governed by conventional dendritic cells and overridden during infection by monocytes. *Sci Immunol* **5** (Oct. 2020).

180. Regnault, A. *et al.* Fcgamma receptor-mediated induction of dendritic cell maturation and major histocompatibility complex class I-restricted antigen presentation after immune complex internalization. *J Exp Med* **189,** 371–380 (Jan. 1999).

181. Schuurhuis, D. H. *et al.* Immune complex-loaded dendritic cells are superior to soluble immune complexes as antitumor vaccine. *J Immunol* **176,** 4573–4580 (Apr. 2006).

182. Schuurhuis, D. H. *et al.* Antigen-antibody immune complexes empower dendritic cells to efficiently prime specific $CD8^+$ CTL responses in vivo. *J Immunol* **168,** 2240–2246 (Mar. 2002).

183. Joshi, N. S. *et al.* Inflammation directs memory precursor and short-lived effector $CD8^+$ T cell fates via the graded expression of T-bet transcription factor. *Immunity* **27,** 281–95 (2007).

184. Sarkar, S. *et al.* Functional and genomic profiling of effector CD8 T cell subsets with distinct memory fates. *J Exp Med* **205,** 625–640 (Mar. 2008).

185. Katakai, T., Habiro, K. & Kinashi, T. Dendritic cells regulate high-speed interstitial T cell migration in the lymph node via LFA-1/ICAM-1. *J. Immunol.* **191,** 1188–1199 (Aug. 2013).

186. Kaech, S. M. & Cui, W. Transcriptional control of effector and memory $CD8^+$ T cell differentiation. *Nat Rev Immunol* **12,** 749–61 (2012).

187. Chang, J. T., Wherry, E. J. & Goldrath, A. W. Molecular regulation of effector and memory T cell differentiation. *Nat Immunol* **15,** 1104–1115 (Dec. 2014).

188. Gerner, M. Y., Torabi-Parizi, P. & Germain, R. N. Strategically localized dendritic cells promote rapid T cell responses to lymph-borne particulate antigens. *Immunity* **42,** 172–185 (Jan. 2015).

189. Castellino, F. *et al.* Chemokines enhance immunity by guiding naive $CD8^+$ T cells to sites of $CD4^+$ T cell-dendritic cell interaction. *Nature* **440,** 890–895 (Apr. 2006).

190. Groom, J. R. *et al.* CXCR3 Chemokine Receptor-Ligand Interactions in the Lymph Node Optimize CD4 T Helper 1 Cell Differentiation. *Immunity* **37,** 1091–1103 (2012).

191. Mueller, S. N. *et al.* Regulation of homeostatic chemokine expression and cell trafficking during immune responses. *Science* **317,** 670–674 (Aug. 2007).

192. Groom, J. R. Regulators of T-cell fate: Integration of cell migration, differentiation and function. *Immunol Rev* **289,** 101–114 (May 2019).

193. Stemberger, C. *et al.* A single naive $CD8^+$ T cell precursor can develop into diverse effector and memory subsets. *Immunity* **27,** 985–97 (2007).

194. Gerlach, C. *et al.* Heterogeneous differentiation patterns of individual $CD8^+$ T cells. *Science* **340,** 635–639 (May 2013).

195. Buchholz, V. R. *et al.* Disparate individual fates compose robust $CD8^+$ T cell immunity. *Science* **340,** 630–635 (May 2013).

196. Mani, V. *et al.* Migratory DCs activate TGF-β to precondition naïve CD8 T cells for tissue-resident memory fate. *Science* **366** (2019).

197. Smith, N. L. *et al.* Developmental Origin Governs CD8 T Cell Fate Decisions during Infection. *Cell* **174** (2018).

198. D'Souza, W. N. & Hedrick, S. M. Cutting Edge: Latecomer CD8 T Cells Are Imprinted with a Unique Differentiation Program. *The Journal of Immunology* **177,** 777–781 (2006).

199. Badovinac, V. P., Porter, B. B. & Harty, J. T. $CD8^+$ T cell contraction is controlled by early inflammation. *Nat Immunol* **5,** 809–817 (Aug. 2004).

200. Tian, Y., Mollo, S. B., Harrington, L. E. & Zajac, A. J. IL-10 Regulates Memory T Cell Development and the Balance between Th1 and Follicular Th Cell Responses during an Acute Viral Infection. *J. Immunol.* **197,** 1308–1321 (Aug. 2016).

201. Kaech, S. M. & Ahmed, R. Memory CD8$^+$ T cell differentiation: initial antigen encounter triggers a developmental program in naïve cells. *Nat Immunol* **2,** 415–422 (May 2001).

202. Van Stipdonk, M. J., Lemmens, E. E. & Schoenberger, S. P. Naïve CTLs require a single brief period of antigenic stimulation for clonal expansion and differentiation. *Nat Immunol* **2,** 423–429 (May 2001).

203. Knudson, K. M., Goplen, N. P., Cunningham, C. A., Daniels, M. A. & Teixeiro, E. Low-affinity T cells are programmed to maintain normal primary responses but are impaired in their recall to low-affinity ligands. *Cell Rep* **4,** 554–565 (Aug. 2013).

204. Van Panhuys, N., Klauschen, F. & Germain, R. N. T-cell-receptor-dependent signal intensity dominantly controls CD4$^+$ T cell polarization In Vivo. *Immunity* **41,** 63–74 (July 2014).

205. Zehn, D., Lee, S. Y. & Bevan, M. J. Complete but curtailed T-cell response to very low-affinity antigen. *Nature* **458,** 211–4 (2009).

206. Prlic, M., Hernandez-Hoyos, G. & Bevan, M. J. Duration of the initial TCR stimulus controls the magnitude but not functionality of the CD8$^+$ T cell response. *J. Exp. Med.* **203,** 2135–2143 (Sept. 2006).

207. Chang, J. T. *et al.* Asymmetric T Lymphocyte Division in the Initiation of Adaptive Immune Responses. *Science* **315,** 1687–1691 (2007).

208. Chang, J. T. *et al.* Asymmetric proteasome segregation as a mechanism for unequal partitioning of the transcription factor T-bet during T lymphocyte division. *Immunity* **34,** 492–504 (Apr. 2011).

209. Borsa, M. *et al.* Modulation of asymmetric cell division as a mechanism to boost CD8$^+$ T cell memory. *Sci Immunol* **4** (Apr. 2019).

210. Arsenio, J. *et al.* Early specification of CD8$^+$ T lymphocyte fates during adaptive immunity revealed by single-cell gene-expression analyses. *Nat Immunol* **15,** 365–372 (Apr. 2014).

211. Contento, R. L. *et al.* CXCR4-CCR5: a couple modulating T cell functions. *Proc Natl Acad Sci* **105,** 10101–10106 (July 2008).

212. Chung, H. K., McDonald, B. & Kaech, S. M. The architectural design of CD8$^+$ T cell responses in acute and chronic infection: Parallel structures with divergent fates. *J Exp Med* **218** (Apr. 2021).

213. Topham, D. J., Tripp, R. A. & Doherty, P. C. CD8$^+$ T cells clear influenza virus by perforin or Fas-dependent processes. *J. Immunol.* **159,** 5197–5200 (Dec. 1997).

214. Allan, W., Carding, S. R., Eichelberger, M. & Doherty, P. C. hsp65 mRNA$^+$ macrophages and gamma delta T cells in influenza virus-infected mice depleted of the CD4$^+$ and CD8$^+$ lymphocyte subsets. *Microb. Pathog.* **14,** 75–84 (Jan. 1993).

215. Eichelberger, M., Allan, W., Zijlstra, M., Jaenisch, R. & Doherty, P. C. Clearance of influenza virus respiratory infection in mice lacking class I major histocompatibility complex-restricted CD8$^+$ T cells. *J. Exp. Med.* **174,** 875–880 (Oct. 1991).

216. Dustin, M. L. & Long, E. O. Cytotoxic immunological synapses. *Immunol. Rev.* **235,** 24–34 (May 2010).

217. Lopez, J. A. *et al.* Perforin forms transient pores on the target cell plasma membrane to facilitate rapid access of granzymes during killer cell attack. *Blood* **121,** 2659–2668 (Apr. 2013).

218. Chakrabarti, S. *et al.* Impaired membrane resealing and autoimmune myositis in synaptotagmin VII-deficient mice. *J. Cell Biol.* **162,** 543–549 (Aug. 2003).

219. Monlein, I. *et al.* Differential secretion of Fas ligand- or APO2 ligand/TNF-related apoptosis-inducing ligand-carrying microvesicles during activation-induced death of human T cells. *J. Immunol.* **167,** 6736–6744 (Dec. 2001).

220. Galluzzi, L. *et al.* Molecular mechanisms of cell death: recommendations of the Nomenclature Committee on Cell Death 2018. *Cell Death Differ.* **25,** 486–541 (Mar. 2018).

221. Sun, J., Madan, R., Karp, C. L. & Braciale, T. J. Effector T cells control lung inflammation during acute influenza virus infection by producing IL-10. *Nat Med* **15,** 277–84 (2009).

222. Trandem, K., Zhao, J., Fleming, E. & Perlman, S. Highly activated cytotoxic CD8 T cells express protective IL-10 at the peak of coronavirus-induced encephalitis. *J. Immunol.* **186,** 3642–3652 (Mar. 2011).

223. Palmer, E. M., Holbrook, B. C., Arimilli, S., Parks, G. D. & Alexander-Miller, M. A. IFNgamma-producing, virus-specific $CD8^+$ effector cells acquire the ability to produce IL-10 as a result of entry into the infected lung environment. *Virology* **404,** 225–230 (Sept. 2010).

224. Mackay, C. R., Marston, W. L. & Dudler, L. Naive and memory T cells show distinct pathways of lymphocyte recirculation. *J. Exp. Med.* **171,** 801–817 (Mar. 1990).

225. Sallusto, F., Lenig, D., Forster, R., Lipp, M. & Lanzavecchia, A. Two subsets of memory T lymphocytes with distinct homing potentials and effector functions. *Nature* **401,** 708–12 (1999).

226. Sallusto, F., Geginat, J. & Lanzavecchia, A. Central memory and effector memory T cell subsets: function, generation, and maintenance. *Annu Rev Immunol* **22,** 745–763 (2004).

227. Sallusto, F. & Lanzavecchia, A. Understanding dendritic cell and T-lymphocyte traffic through the analysis of chemokine receptor expression. *Immunol Rev* **177,** 134–140 (Oct. 2000).

228. Van der Most, R. G., Murali-Krishna, K. & Ahmed, R. Prolonged presence of effector-memory CD8 T cells in the central nervous system after dengue virus encephalitis. *Int Immunol* **15,** 119–125 (Jan. 2003).

229. Masopust, D., Vezys, V., Marzo, A. L. & Lefrançois, L. Preferential localization of effector memory cells in nonlymphoid tissue. *Science* **291,** 2413–2417 (Mar. 2001).

230. Wherry, E. J. *et al.* Lineage relationship and protective immunity of memory CD8 T cell subsets. *Nat Immunol* **4,** 225–234 (Mar. 2003).

231. Bromley, S. K., Thomas, S. Y. & Luster, A. D. Chemokine receptor CCR7 guides T cell exit from peripheral tissues and entry into afferent lymphatics. *Nat Immunol* **6,** 895–901 (Sept. 2005).

232. Debes, G. F. *et al.* Chemokine receptor CCR7 required for T lymphocyte exit from peripheral tissues. *Nat Immunol* **6,** 889–894 (Sept. 2005).

233. Schenkel, J. M., Fraser, K. A., Vezys, V. & Masopust, D. Sensing and alarm function of resident memory $CD8^+$ T cells. *Nat Immunol* **14,** 509–13 (2013).

234. Jiang, X. *et al.* Skin infection generates non-migratory memory $CD8^+$ T(RM) cells providing global skin immunity. *Nature* **483,** 227–231 (Feb. 2012).

235. Steinert, E. M. *et al.* Quantifying Memory CD8 T Cells Reveals Regionalization of Immunosurveillance. *Cell* **161,** 737–49 (2015).

236. Woodland, D. L. & Kohlmeier, J. E. Migration, maintenance and recall of memory T cells in peripheral tissues. *Nat Rev Immunol* **9,** 153–61 (2009).

237. Pennock, N. D. *et al.* T cell responses: naive to memory and everything in between. *Adv Physiol Educ* **37,** 273–283 (Dec. 2013).

238. Schulz, O., Hammerschmidt, S. I., Moschovakis, G. L. & Forster, R. Chemokines and Chemokine Receptors in Lymphoid Tissue Dynamics. *Annu Rev Immunol* **34,** 203–42 (2016).

239. Mueller, S. N., Gebhardt, T., Carbone, F. R. & Heath, W. R. Memory T cell subsets, migration patterns, and tissue residence. *Annu Rev Immunol* **31,** 137–61 (2013).

240. Farber, D. L., Yudanin, N. A. & Restifo, N. P. Human memory T cells: generation, compartmentalization and homeostasis. *Nat Rev Immunol* **14,** 24–35 (Jan. 2014).

241. Jameson, S. C. & Masopust, D. Understanding Subset Diversity in T Cell Memory. *Immunity* **48,** 214–226 (Feb. 2018).

242. Schenkel, J. M. & Masopust, D. Tissue-resident memory T cells. *Immunity* **41,** 886–897 (Dec. 2014).

243. White, J. T., Cross, E. W. & Kedl, R. M. Antigen-inexperienced memory CD8$^+$ T cells: where they come from and why we need them. *Nat Rev Immunol* **17,** 391–400 (June 2017).

244. Olson, J. A., McDonald-Hyman, C., Jameson, S. C. & Hamilton, S. E. Effector-like CD8$^+$ T cells in the memory population mediate potent protective immunity. *Immunity* **38,** 1250–60 (2013).

245. Bottcher, J. P. *et al.* Functional classification of memory CD8$^+$ T cells by CX3CR1 expression. *Nat Commun* **6,** 8306 (Sept. 2015).

246. Gerlach, C. *et al.* The Chemokine Receptor CX3CR1 Defines Three Antigen-Experienced CD8 T Cell Subsets with Distinct Roles in Immune Surveillance and Homeostasis. *Immunity* **45,** 1270–1284 (2016).

247. McCully, M. L., Kouzeli, A. & Moser, B. Peripheral Tissue Chemokines: Homeostatic Control of Immune Surveillance T Cells. *Trends Immunol* **39,** 734–747 (Sept. 2018).

248. Schaerli, P. & Moser, B. Chemokines: control of primary and memory T-cell traffic. *Immunol Res* **31,** 57–74 (2005).

249. Jung, Y. W., Rutishauser, R. L., Joshi, N. S., Haberman, A. M. & Kaech, S. M. Differential localization of effector and memory CD8 T cell subsets in lymphoid organs during acute viral infection. *J Immunol* **185,** 5315–5325 (Nov. 2010).

250. Kastenmuller, W. *et al.* Peripheral prepositioning and local CXCL9 chemokine-mediated guidance orchestrate rapid memory CD8$^+$ T cell responses in the lymph node. *Immunity* **38,** 502–13 (2013).

251. Sung, J. H. *et al.* Chemokine guidance of central memory T cells is critical for antiviral recall responses in lymph nodes. *Cell* **150,** 1249–63 (2012).

252. Von Andrian, U. H. & Mempel, T. R. Homing and cellular traffic in lymph nodes. *Nat Rev Immunol* **3,** 867–878 (Nov. 2003).

253. Buggert, M. *et al.* The Identity of Human Tissue-Emigrant CD8$^+$ T Cells. *Cell* **183,** 1946–1961 (Dec. 2020).

254. Loughhead, S. Immune Surveillance by Effector and Memory CD8$^+$ T Cells. *Harvard University* **Graduate School of Arts Sciences** (Oct. 2012).

255. Hirai, T. *et al.* Keratinocyte-Mediated Activation of the Cytokine TGF-β Maintains Skin Recirculating Memory CD8$^+$ T Cells. *Immunity* **50,** 1249–1261.e5 (2019).

256. Mackay, L. K. *et al.* T-box Transcription Factors Combine with the Cytokines TGF-beta and IL-15 to Control Tissue-Resident Memory T Cell Fate. *Immunity* **43,** 1101–11 (2015).

257. Wakim, L. M., Gupta, N., Mintern, J. D. & Villadangos, J. A. Enhanced survival of lung tissue-resident memory CD8$^+$ T cells during infection with influenza virus due to selective expression of IFITM3. *Nat Immunol* **14,** 238–245 (2013).

258. Pizzolla, A. *et al.* Resident memory CD8$^+$ T cells in the upper respiratory tract prevent pulmonary influenza virus infection. *Sci Immunol* **2** (June 2017).

259. Slutter, B. *et al.* Dynamics of influenza-induced lung-resident memory T cells underlie waning heterosubtypic immunity. *Sci Immunol* **2** (Jan. 2017).

260. Kurd, N. S. *et al.* Early precursors and molecular determinants of tissue-resident memory CD8$^+$ T lymphocytes revealed by single-cell RNA sequencing. *Science Immunology* (2020).

261. Bain, C. C. *et al.* TGFβR signalling controls CD103$^+$CD11b$^+$ dendritic cell development in the intestine. *Nat Commun* **8,** 620 (2017).

262. Stark, R. *et al.* T RM maintenance is regulated by tissue damage via P2RX7. *Sci Immunol* **3** (Dec. 2018).

263. Skon, C. N. *et al.* Transcriptional downregulation of S1pr1 is required for the establishment of resident memory CD8 T cells. *Nat Immunol* **14,** 1285–1293 (2013).

264. Urban, S. L. *et al.* Peripherally induced brain tissue-resident memory $CD8^+$ T cells mediate protection against CNS infection. *Nat Immunol* **21,** 938–949 (Aug. 2020).

265. Sathaliyawala, T. *et al.* Distribution and compartmentalization of human circulating and tissue-resident memory T cell subsets. *Immunity* **38,** 187–197 (Jan. 2013).

266. Kumar, B. V. *et al.* Human Tissue-Resident Memory T Cells Are Defined by Core Transcriptional and Functional Signatures in Lymphoid and Mucosal Sites. *SSRN Electronic Journal* (2018).

267. Mackay, L. K. *et al.* Cutting edge: CD69 interference with sphingosine-1-phosphate receptor function regulates peripheral T cell retention. *J Immunol* **194,** 2059–2063 (Mar. 2015).

268. Fernandez-Ruiz, D. *et al.* Liver-Resident Memory $CD8^+$ T Cells Form a Front-Line Defense against Malaria Liver-Stage Infection. *Immunity* **45,** 889–902 (Oct. 2016).

269. Mackay, L. K. *et al.* Long-lived epithelial immunity by tissue-resident memory T (TRM) cells in the absence of persisting local antigen presentation. *Proc Natl Acad Sci* **109,** 7037–7042 (May 2012).

270. Wu, T. *et al.* Lung-resident memory CD8 T cells (TRM) are indispensable for optimal cross-protection against pulmonary virus infection. *J Leukoc Biol* **95,** 215–24 (2014).

271. Park, S. L. *et al.* Local proliferation maintains a stable pool of tissue-resident memory T cells after antiviral recall responses. *Nat Immunol* **19,** 183–191 (2018).

272. Schenkel, J. M. *et al.* IL-15-Independent Maintenance of Tissue-Resident and Boosted Effector Memory CD8 T Cells. *J. Immunol.* **196,** 3920–3926 (May 2016).

273. Milner, J. J. *et al.* Heterogenous Populations of Tissue-Resident $CD8^+$ T Cells Are Generated in Response to Infection and Malignancy. *Immunity* **52,** 808–824 (May 2020).

274. Milner, J. J. *et al.* Runx3 programs CD8 T cell residency in non-lymphoid tissues and tumours. *Nature* **552,** 253–257 (2017).

275. Beura, L. K. *et al.* Intravital mucosal imaging of CD8 resident memory T cells shows tissue-autonomous recall responses that amplify secondary memory. *Nat Immunol* **19,** 173–182 (2018).

276. Behr, F. M. *et al.* Tissue-resident memory $CD8^+$ T cells shape local and systemic secondary T cell responses. *Nat Immunol* **21,** 1070–1081 (Sept. 2020).

277. Fonseca, R. *et al.* Developmental plasticity allows outside-in immune responses by resident memory T cells. *Nat Immunol* **21,** 412–421 (2020).

278. Beura, L. K. *et al.* T Cells in Nonlymphoid Tissues Give Rise to Lymph-Node-Resident Memory T Cells. *Immunity* **48** (2018).

279. Zammit, D. J., Turner, D. L., Klonowski, K. D., Lefrançois, L. & Cauley, L. S. Residual antigen presentation after influenza virus infection affects CD8 T cell activation and migration. *Immunity* **24,** 439–449 (Apr. 2006).

280. Takamura, S. *et al.* The route of priming influences the ability of respiratory virus–specific memory CD8 T cells to be activated by residual antigen. *The Journal of Experimental Medicine* **207,** 1153–1160 (2010).

281. Takamura, S. *et al.* Specific niches for lung-resident memory $CD8^+$ T cells at the site of tissue regeneration enable CD69-independent maintenance. *J Exp Med* **213,** 3057–3073 (2016).

282. Stolley, J. M. *et al.* Retrograde migration supplies resident memory T cells to lung-draining LN after influenza infection. *Journal of Experimental Medicine* **217** (2020).

283. Wijeyesinghe, S. *et al.* Expansible residence decentralizes immune homeostasis. *Nature* (Mar. 2021).

284. Schenkel, J. M., Fraser, K. A. & Masopust, D. Cutting edge: resident memory CD8 T cells occupy frontline niches in secondary lymphoid organs. *J Immunol* **192,** 2961–4 (2014).

285. Zens, K. D., Chen, J. K. & Farber, D. L. Vaccine-generated lung tissue-resident memory T cells provide heterosubtypic protection to influenza infection. *JCI Insight* **1** (2016).

286. Overstreet, M. G. *et al.* Inflammation-induced interstitial migration of effector $CD4^+$ T cells is dependent on integrin αV. *Nat Immunol* **14,** 949–958 (Sept. 2013).

287. Schenkel, J. M. *et al.* T cell memory. Resident memory CD8 T cells trigger protective innate and adaptive immune responses. *Science* **346,** 98–101 (Oct. 2014).

288. McMaster, S. R., Wilson, J. J., Wang, H. & Kohlmeier, J. E. Airway-Resident Memory CD8 T Cells Provide Antigen-Specific Protection against Respiratory Virus Challenge through Rapid IFN-gamma Production. *J Immunol* **195,** 203–9 (2015).

289. Mintern, J. D., Guillonneau, C., Carbone, F. R., Doherty, P. C. & Turner, S. J. Cutting edge: Tissue-resident memory CTL down-regulate cytolytic molecule expression following virus clearance. *J. Immunol.* **179,** 7220–7224 (Dec. 2007).

290. Osborn, J. F. *et al.* Enzymatic synthesis of core 2 O-glycans governs the tissue-trafficking potential of memory $CD8^+$ T cells. *Sci Immunol* **2** (Oct. 2017).

291. Hu, J. K., Kagari, T., Clingan, J. M. & Matloubian, M. Expression of chemokine receptor CXCR3 on T cells affects the balance between effector and memory CD8 T-cell generation. *Proc Natl Acad Sci* **108,** E118–E127 (2011).

292. Kohlmeier, J. E. *et al.* Inflammatory chemokine receptors regulate $CD8^+$ T cell contraction and memory generation following infection. *J Exp Med* **208,** 1621–34 (2011).

293. Kurachi, M. *et al.* Chemokine receptor CXCR3 facilitates $CD8^+$ T cell differentiation into short-lived effector cells leading to memory degeneration. *J Exp Med* **208,** 1605–20 (2011).

294. Duckworth, B. C. *et al.* Effector and stem-like memory cell fates are imprinted in distinct lymph node niches directed by CXCR3 ligands. *Nat Immunol* (Mar. 2021).

295. Kadoki, M. *et al.* Organism-Level Analysis of Vaccination Reveals Networks of Protection across Tissues. *Cell* **171,** 398–413 e21 (2017).

296. Helft, J. *et al.* Cross-presenting $CD103^+$ dendritic cells are protected from influenza virus infection. *J Clin Invest* **122,** 4037–47 (2012).

297. Hogquist, K. A. *et al.* T cell receptor antagonist peptides induce positive selection. *Cell* **76,** 17–27 (Jan. 1994).

298. Jenkins, M. R., Webby, R., Doherty, P. C. & Turner, S. J. Addition of a prominent epitope affects influenza A virus-specific $CD8^+$ T cell immunodominance hierarchies when antigen is limiting. *J. Immunol.* **177,** 2917–2925 (Sept. 2006).

299. Galkina, E. *et al.* Preferential migration of effector $CD8^+$ T cells into the interstitium of the normal lung. *J Clin Invest* **115,** 3473–3483 (Dec. 2005).

300. Lehmann, M. H. *et al.* CCL2 expression is mediated by type I IFN receptor and recruits NK and T cells to the lung during MVA infection. *J Leukoc Biol* **99,** 1057–64 (2016).

301. Xin, A. *et al.* A molecular threshold for effector $CD8^+$ T cell differentiation controlled by transcription factors Blimp-1 and T-bet. *Nat Immunol* **17,** 422–432 (Apr. 2016).

302. Mora, J. R. *et al.* Selective imprinting of gut-homing T cells by Peyer's patch dendritic cells. *Nature* **424,** 88–93 (July 2003).

303. Ahrends, T. *et al.* $CD4^+$ T cell help creates memory $CD8^+$ T cells with innate and help-independent recall capacities. *Nat Commun* **10,** 5531 (Dec. 2019).

304. Fujimura, N. *et al.* CCR2 inhibition sequesters multiple subsets of leukocytes in the bone marrow. *Sci Rep* **5,** 11664 (July 2015).

305. Lawrence, C. W. & Braciale, T. J. Activation, differentiation, and migration of naive virus-specific CD8$^+$ T cells during pulmonary influenza virus infection. *J. Immunol.* **173,** 1209–1218 (July 2004).

306. Pais Ferreira, D. *et al.* Central memory CD8$^+$ T cells derive from stem-like Tcf7hi effector cells in the absence of cytotoxic differentiation. *Immunity* **53,** 985–1000 (Nov. 2020).

307. Herndler-Brandstetter, D. *et al.* KLRG1 Effector CD8 T Cells Lose KLRG1, Differentiate into All Memory T Cell Lineages, and Convey Enhanced Protective Immunity. *Immunity* **48** (2018).

308. Milner, J. J. *et al.* Delineation of a molecularly distinct terminally differentiated memory CD8 T cell population. *Proc Natl Acad Sci* **117,** 25667–25678 (Oct. 2020).

309. Hudson, W. H. *et al.* Proliferating Transitory T Cells with an Effector-like Transcriptional Signature Emerge from PD-1$^+$ Stem-like CD8$^+$ T Cells during Chronic Infection. *Immunity* **51,** 1043–1058 (Dec. 2019).

310. Wirth, T. C. *et al.* Repetitive Antigen Stimulation Induces Stepwise Transcriptome Diversification but Preserves a Core Signature of Memory CD8 T Cell Differentiation. *Immunity* **33,** 128–140 (2010).

311. Desalegn, G. & Pabst, O. Inflammation triggers immediate rather than progressive changes in monocyte differentiation in the small intestine. *Nat Commun* **10,** 3229 (July 2019).

312. Zigmond, E. *et al.* Ly6C hi monocytes in the inflamed colon give rise to proinflammatory effector cells and migratory antigen-presenting cells. *Immunity* **37,** 1076–1090 (Dec. 2012).

313. Anderson, K. G. *et al.* Cutting edge: intravascular staining redefines lung CD8 T cell responses. *J Immunol* **189,** 2702–6 (2012).

314. Hufford, M. M., Kim, T. S., Sun, J. & Braciale, T. J. Antiviral CD8$^+$ T cell effector activities in situ are regulated by target cell type. *J Exp Med* **208,** 167–80 (2011).

315. Sun, J., Dodd, H., Moser, E. K., Sharma, R. & Braciale, T. J. CD4$^+$ T cell help and innate-derived IL-27 induce Blimp-1-dependent IL-10 production by antiviral CTLs. *Nat Immunol* **12,** 327–334 (Apr. 2011).

316. Hua, L. *et al.* Cytokine-dependent induction of CD4$^+$ T cells with cytotoxic potential during influenza virus infection. *J. Virol.* **87,** 11884–11893 (Nov. 2013).

317. Damjanovic, D. *et al.* Negative regulation of lung inflammation and immunopathology by TNFα during acute influenza infection. *Am. J. Pathol.* **179,** 2963–2976 (Dec. 2011).

318. Masopust, D. *et al.* Activated primary and memory CD8 T cells migrate to nonlymphoid tissues regardless of site of activation or tissue of origin. *J. Immunol.* **172,** 4875–4882 (Apr. 2004).

319. Vasanthakumar, A. *et al.* Sex-specific adipose tissue imprinting of regulatory T cells. *Nature* **579,** 581–585 (Mar. 2020).

320. Tan, H. X. *et al.* Inducible Bronchus-Associated Lymphoid Tissues (iBALT) Serve as Sites of B Cell Selection and Maturation Following Influenza Infection in Mice. *Front Immunol* **10,** 611 (2019).

321. Moyron-Quiroz, J. E. *et al.* Role of inducible bronchus associated lymphoid tissue (iBALT) in respiratory immunity. *Nat. Med.* **10,** 927–934 (Sept. 2004).

322. Gaya, M. *et al.* Host response. Inflammation-induced disruption of SCS macrophages impairs B cell responses to secondary infection. *Science* **347,** 667–72 (2015).

323. Beura, L. K. *et al.* CD4$^+$ resident memory T cells dominate immunosurveillance and orchestrate local recall responses. *J Exp Med* **216,** 1214–1229 (2019).

324. Cyster, J. & Goodnow, C. Pertussis toxin inhibits migration of B and T Lymphocytes into splenic white pulp cords. *J. Exp. Med.* **182,** 581–586 (Aug. 1995).

325. Netea, M. G., van de Veerdonk, F. L., van der Meer, J. W., Dinarello, C. A. & Joosten, L. A. Inflammasome-independent regulation of IL-1-family cytokines. *Annu Rev Immunol* **33,** 49–77 (2015).

326. Nakano, H. *et al.* Blood-derived inflammatory dendritic cells in lymph nodes stimulate acute T helper type 1 immune responses. *Nat Immunol* **10,** 394–402 (2009).

327. Ko, H. J. *et al.* GM-CSF-responsive monocyte-derived dendritic cells are pivotal in Th17 pathogenesis. *J Immunol* **192,** 2202–2209 (Mar. 2014).

328. Shin, K. S. *et al.* Monocyte-Derived Dendritic Cells Dictate the Memory Differentiation of $CD8^+$ T Cells During Acute Infection. *Front Immunol* **10,** 1887 (2019).

329. De Koker, S. *et al.* Inflammatory monocytes regulate Th1 oriented immunity to CpG adjuvanted protein vaccines through production of IL-12. *Sci Rep* **7,** 5986 (July 2017).

330. Dunbar, P. R. *et al.* Pulmonary monocytes interact with effector T cells in the lung tissue to drive TRM differentiation following viral infection. *Mucosal Immunol* **13,** 161–171 (Jan. 2020).

331. Prizant, H. *et al.* CXCL10 peripheral activation niches couple preferred sites of Th1 entry with optimal APC encounter. *bioRxiv* **166,** 4697–4704 (Oct. 2020).

332. Romano, A. *et al.* Divergent roles for $Ly6C^+CCR2^+CX3CR1^+$ inflammatory monocytes during primary or secondary infection of the skin with the intra-phagosomal pathogen Leishmania major. *PLoS Pathog* **13,** e1006479 (June 2017).

333. Seo, S. U. *et al.* Intestinal macrophages arising from $CCR2^+$ monocytes control pathogen infection by activating innate lymphoid cells. *Nat Commun* **6,** 8010 (Aug. 2015).

334. Caffrey, A. K. *et al.* IL-1α signaling is critical for leukocyte recruitment after pulmonary Aspergillus fumigatus challenge. *PLoS Pathog* **11,** e1004625 (Jan. 2015).

335. Espinosa, V. *et al.* Inflammatory monocytes orchestrate innate antifungal immunity in the lung. *PLoS Pathog* **10,** e1003940 (Feb. 2014).

336. Shi, C. *et al.* $Ly6G^+$ neutrophils are dispensable for defense against systemic Listeria monocytogenes infection. *J Immunol* **187,** 5293–5298 (Nov. 2011).

337. Terwey, T. H. *et al.* CCR2 is required for CD8-induced graft-versus-host disease. *Blood* **106,** 3322–3330 (Nov. 2005).

338. Yao, C. *et al.* Single-cell RNA-seq reveals TOX as a key regulator of $CD8^+$ T cell persistence in chronic infection. *Nat Immunol* **20,** 890–901 (July 2019).

339. Mack, M. *et al.* Expression and characterization of the chemokine receptors CCR2 and CCR5 in mice. *J Immunol* **166,** 4697–4704 (Apr. 2001).

340. Mikucki, M. E. *et al.* Non-redundant requirement for CXCR3 signalling during tumoricidal T-cell trafficking across tumour vascular checkpoints. *Nat Commun* **6** (2015).

341. White, J. T. *et al.* Virtual memory T cells develop and mediate bystander protective immunity in an IL-15-dependent manner. *Nat Commun* **7,** 11291 (Apr. 2016).

342. Benechet, A. P. *et al.* T cell-intrinsic S1PR1 regulates endogenous effector T-cell egress dynamics from lymph nodes during infection. *Proc Natl Acad Sci* **113,** 2182–2187 (Feb. 2016).

343. Kumar, B. V. *et al.* Human Tissue-Resident Memory T Cells Are Defined by Core Transcriptional and Functional Signatures in Lymphoid and Mucosal Sites. *Cell Rep* **20,** 2921–2934 (Sept. 2017).

344. Chu, H. X. *et al.* Role of CCR2 in inflammatory conditions of the central nervous system. *J Cereb Blood Flow Metab* **34,** 1425–1429 (Sept. 2014).

345. Uhlén, M. *et al.* Proteomics. Tissue-based map of the human proteome. *Science* **347,** 1260419 (Jan. 2015).

346. Parretta, E. *et al.* CD8 cell division maintaining cytotoxic memory occurs predominantly in the bone marrow. *J. Immunol.* **174,** 7654–7664 (June 2005).

347. Banerjee, A. *et al.* Cutting edge: The transcription factor eomesodermin enables $CD8^+$ T cells to compete for the memory cell niche. *J. Immunol.* **185,** 4988–4992 (Nov. 2010).

348. Mazo, I. B. *et al.* Bone marrow is a major reservoir and site of recruitment for central memory CD8$^+$ T cells. *Immunity* **22,** 259–70 (2005).

349. Okhrimenko, A. *et al.* Human memory T cells from the bone marrow are resting and maintain long-lasting systemic memory. *Proc Natl Acad Sci* **111,** 9229–9234 (June 2014).

350. Pangrazzi, L. *et al.* The impact of body mass index on adaptive immune cells in the human bone marrow. *Immun Ageing* **17,** 15 (2020).

351. Han, S. J. *et al.* White Adipose Tissue Is a Reservoir for Memory T Cells and Promotes Protective Memory Responses to Infection. *Immunity* **47,** 1154–1168 e6 (2017).

352. Thome, J. J. *et al.* Spatial map of human T cell compartmentalization and maintenance over decades of life. *Cell* **159,** 814–828 (Nov. 2014).

353. Gattinoni, L. *et al.* A human memory T cell subset with stem cell-like properties. *Nat Med* **17,** 1290–1297 (Sept. 2011).

354. Ozga, A. J. *et al.* pMHC affinity controls duration of CD8$^+$ T cell-DC interactions and imprints timing of effector differentiation versus expansion. *J. Exp. Med.* **213,** 2811–2829 (Nov. 2016).

355. Gretz, J. E., Norbury, C. C., Anderson, A. O., Proudfoot, A. E. & Shaw, S. Lymph-borne chemokines and other low molecular weight molecules reach high endothelial venules via specialized conduits while a functional barrier limits access to the lymphocyte microenvironments in lymph node cortex. *J. Exp. Med.* **192,** 1425–1440 (Nov. 2000).

356. Ataide, M. A. *et al.* BATF3 programs CD8$^+$ T cell memory. *Nat Immunol* **21,** 1397–1407 (Nov. 2020).

357. Schluns, K. S., Kieper, W. C., Jameson, S. C. & Lefrançois, L. Interleukin-7 mediates the homeostasis of naïve and memory CD8 T cells in vivo. *Nat Immunol* **1,** 426–432 (Nov. 2000).

358. Ku, C. C., Murakami, M., Sakamoto, A., Kappler, J. & Marrack, P. Control of homeostasis of CD8$^+$ memory T cells by opposing cytokines. *Science* **288,** 675–678 (Apr. 2000).

359. McGill, J., Van Rooijen, N. & Legge, K. L. IL-15 trans-presentation by pulmonary dendritic cells promotes effector CD8 T cell survival during influenza virus infection. *J Exp Med* **207,** 521–34 (2010).

360. Pulle, G., Vidric, M. & Watts, T. H. IL-15-Dependent Induction of 4-1BB Promotes Antigen-Independent CD8 Memory T Cell Survival. *The Journal of Immunology* **176,** 2739–2748 (2006).

361. Cruz, J. L. *et al.* Monocyte-derived dendritic cells enhance protection against secondary influenza challenge by controlling the switch in CD8$^+$ T-cell immunodominance. *Eur. J. Immunol.* **47,** 345–352 (Feb. 2017).

362. Link, A. *et al.* Fibroblastic reticular cells in lymph nodes regulate the homeostasis of naive T cells. *Nat Immunol* **8,** 1255–1265 (Nov. 2007).

363. Kumar, P. A. *et al.* Distal airway stem cells yield alveoli in vitro and during lung regeneration following H1N1 influenza infection. *Cell* **147,** 525–538 (Oct. 2011).

364. Ray, S. *et al.* Rare SOX2$^+$ Airway Progenitor Cells Generate KRT5$^+$ Cells that Repopulate Damaged Alveolar Parenchyma following Influenza Virus Infection. *Stem Cell Reports* **7,** 817–825 (Nov. 2016).

365. Zuo, W. *et al.* p63$^+$Krt5$^+$ distal airway stem cells are essential for lung regeneration. *Nature* **517,** 616–620 (Jan. 2015).

366. Wynn, T. A. & Vannella, K. M. Macrophages in Tissue Repair, Regeneration, and Fibrosis. *Immunity* **44,** 450–462 (Mar. 2016).

367. Hombrink, P. *et al.* Programs for the persistence, vigilance and control of human CD8$^+$ lung-resident memory T cells. *Nat Immunol* **17,** 1467–1478 (2016).

368. Ariotti, S. *et al.* T cell memory. Skin-resident memory $CD8^+$ T cells trigger a state of tissue-wide pathogen alert. *Science* **346,** 101–105 (Oct. 2014).

369. Nomiyama, H., Osada, N. & Yoshie, O. A family tree of vertebrate chemokine receptors for a unified nomenclature. *Developmental Comparative Immunology* **35,** 705–715 (2011).

370. Aguilar, S. V. *et al.* ImmGen at 15. *Nat Immunol* **21,** 700–703 (July 2020).

371. Bersudsky, M. *et al.* Non-redundant properties of IL-1α and IL-1β during acute colon inflammation in mice. *Gut* **63,** 598–609 (Apr. 2014).

372. Chen, C. J. *et al.* Identification of a key pathway required for the sterile inflammatory response triggered by dying cells. *Nat Med* **13,** 851–856 (July 2007).

373. Eckert, N., Werth, K., Willenzon, S., Tan, L. & Förster, R. B cell hyperactivation in an Ackr4-deficient mouse strain is not caused by lack of ACKR4 expression. *J Leukoc Biol* **107,** 1155–1166 (June 2020).

374. Ahlqvist, E. *et al.* High-resolution mapping of a complex disease, a model for rheumatoid arthritis, using heterogeneous stock mice. *Hum Mol Genet* **20,** 3031–3041 (Aug. 2011).

375. Kimura, I. *et al.* Maternal gut microbiota in pregnancy influences offspring metabolic phenotype in mice. *Science* **367** (Feb. 2020).

376. Al Nabhani, Z. *et al.* A Weaning Reaction to Microbiota Is Required for Resistance to Immunopathologies in the Adult. *Immunity* **50,** 1276–1288 (May 2019).

377. Gomez de Agüero, M. *et al.* The maternal microbiota drives early postnatal innate immune development. *Science* **351,** 1296–1302 (Mar. 2016).

378. Dubois, S., Mariner, J., Waldmann, T. A. & Tagaya, Y. IL-15Rα recycles and presents IL-15 In trans to neighboring cells. *Immunity* **17,** 537–547 (Nov. 2002).

379. Jelley-Gibbs, D. M. *et al.* Repeated stimulation of CD4 effector T cells can limit their protective function. *J. Exp. Med.* **201,** 1101–1112 (Apr. 2005).

380. Lim, K. *et al.* In situ neutrophil efferocytosis shapes T cell immunity to influenza infection. *Nat Immunol* (Aug. 2020).

381. Jain, A., Song, R., Wakeland, E. K. & Pasare, C. T cell-intrinsic IL-1R signaling licenses effector cytokine production by memory CD4 T cells. *Nat Commun* **9,** 3185 (Aug. 2018).

382. Deets, K. A. & Vance, R. E. Inflammasomes and adaptive immune responses. *Nat Immunol* **22,** 412–422 (Apr. 2021).

383. Jakubzick, C. V., Randolph, G. J. & Henson, P. M. Monocyte differentiation and antigen-presenting functions. *Nat Rev Immunol* **17,** 349–362 (June 2017).

384. Baumgarth, N. *et al.* B-1 and B-2 cell-derived immunoglobulin M antibodies are nonredundant components of the protective response to influenza virus infection. *J Exp Med* **192,** 271–280 (July 2000).

385. Waffarn, E. E. & Baumgarth, N. Protective B cell responses to flu–no fluke! *J Immunol* **186,** 3823–3829 (Apr. 2011).

386. Rangel-Moreno, J. *et al.* B cells promote resistance to heterosubtypic strains of influenza via multiple mechanisms. *J Immunol* **180,** 454–463 (Jan. 2008).

387. León, B., Ballesteros-Tato, A., Randall, T. D. & Lund, F. E. Prolonged antigen presentation by immune complex-binding dendritic cells programs the proliferative capacity of memory CD8 T cells. *J Exp Med* **211,** 1637–1655 (July 2014).

388. Allie, S. R. *et al.* The establishment of resident memory B cells in the lung requires local antigen encounter. *Nat Immunol* **20,** 97–108 (Jan. 2019).

389. Lee, B. O. *et al.* CD4 T cell-independent antibody response promotes resolution of primary influenza infection and helps to prevent reinfection. *J Immunol* **175,** 5827–5838 (Nov. 2005).

390. Ng, P. M. L. *et al.* Enhancing Antigen Cross-Presentation in Human Monocyte-Derived Dendritic Cells by Recruiting the Intracellular Fc Receptor TRIM21. *J Immunol* **202,** 2307–2319 (Apr. 2019).

391. Lenart, M. *et al.* Alterations of TRIM21-mRNA expression during monocyte maturation. *Immunobiology* **222,** 494–498 (Mar. 2017).

392. Fallet, B. *et al.* Interferon-driven deletion of antiviral B cells at the onset of chronic infection. *Sci Immunol* **1** (Oct. 2016).

393. Buch, T. *et al.* A Cre-inducible diphtheria toxin receptor mediates cell lineage ablation after toxin administration. *Nat. Methods* **2,** 419–426 (June 2005).

394. Gerner, M. Y., Kastenmuller, W., Ifrim, I., Kabat, J. & Germain, R. N. Histo-cytometry: a method for highly multiplex quantitative tissue imaging analysis applied to dendritic cell subset microanatomy in lymph nodes. *Immunity* **37,** 364–76 (2012).

395. Stoltzfus, C. R. *et al.* CytoMAP: A Spatial Analysis Toolbox Reveals Features of Myeloid Cell Organization in Lymphoid Tissues. *Cell Rep* **31,** 107523 (Apr. 2020).

396. Low, J. S. *et al.* Tissue-resident memory T cell reactivation by diverse antigen-presenting cells imparts distinct functional responses. *J. Exp. Med.* **217** (Aug. 2020).

397. Hendriks, J. *et al.* During viral infection of the respiratory tract, CD27, 4-1BB, and OX40 collectively determine formation of $CD8^+$ memory T cells and their capacity for secondary expansion. *J Immunol* **175,** 1665–1676 (Aug. 2005).

398. Janssen, E. M. *et al.* $CD4^+$ T-cell help controls $CD8^+$ T-cell memory via TRAIL-mediated activation-induced cell death. *Nature* **434,** 88–93 (Mar. 2005).

399. Halle, S. *et al.* Induced bronchus-associated lymphoid tissue serves as a general priming site for T cells and is maintained by dendritic cells. *J Exp Med* **206,** 2593–2601 (Nov. 2009).

400. Moyron-Quiroz, J. E. *et al.* Persistence and responsiveness of immunologic memory in the absence of secondary lymphoid organs. *Immunity* **25,** 643–654 (Oct. 2006).

401. Rangel-Moreno, J. *et al.* The development of inducible bronchus-associated lymphoid tissue depends on IL-17. *Nat Immunol* **12,** 639–46 (2011).